TESIS DE LA UNIVERSIDAD DE ZARAGOZA

2020

108

Andrés José Chueca López

Novel anda Highly Efficient Cycloplatinated NHC Complexes for the Generation of White Light

Departamento
Química Inorgánica

Director/es
Fuertes Lorda, Sara
Sicilia Martínez, Violeta

ISSN 2254-7606

Prensas de la Universidad
Universidad Zaragoza

ISSN 2254-7606

Universidad Zaragoza
1542

Tesis Doctoral

NOVEL ANDA HIGHLY EFFICIENT CYCLOPLATINATED NHC COMPLEXES FOR THE GENERATION OF WHITE LIGHT

Autor

Andrés José Chueca López

Director/es

Fuertes Lorda, Sara
Sicilia Martínez, Violeta

UNIVERSIDAD DE ZARAGOZA

Química Inorgánica

2018

Novel and Highly Efficient Cycloplatinated NHC Complexes for the Generation of White Light

Memoria presentada en la Facultad de Ciencias de la Universidad de Zaragoza para optar al grado de Doctor en Ciencias, Sección Químicas, por el Licenciado

Andrés José Chueca López

VIOLETA SICILIA MARTÍNEZ, Profesora Titular de Universidad del Departamento de Química Inorgánica de la Escuela de Ingeniería y Arquitectura de la Universidad de Zaragoza

SARA FUERTES LORDA, Doctora en Ciencias (Químicas) por la Universidad de Zaragoza en Octubre de 2007 y Contratada a través del Proyecto CTQ2015-67461-P en el Instituto de Síntesis Química y Catálisis Homogénea (ISQCH)

CERTIFICAN:

Que la presente Memoria titulada "Novel and Highly Efficient Cycloplatinated NHC Complexes for the Generation of White Light." ha sido realizada en el Departamento de Química Inorgánica de la Universidad de Zaragoza y en el Instituto de Síntesis Química y Catálisis Homogénea (ISQCH) bajo nuestra dirección, autorizando su presentación para que sea calificada como Tesis Doctoral.

Zaragoza, 09 de Mayo de 2018

Fdo. Dra. Violeta Sicilia Martínez

Fdo. Dra. Sara Fuertes Lorda

Cómo resumir en unas pocas palabras todo lo que este momento significa.

Me gustaría, en primer lugar, dar las gracias a la Dra. Violeta Sicilia por su dirección y dedicación en estos cuatro largos años. Por enseñarme no solo todo lo que es necesario saber, sino también lo que es bueno saber. Por su paciencia en los momentos difíciles, y por su confianza en los momentos buenos. Por ser un referente para mí en el cuidado y la atención al detalle que hay que poner en todo el trabajo que se lleve a cabo.

Además, este camino plagado de obstáculos habría sido tremendamente difícil de sortear sin la inestimable codirección de la Dra. Sara Fuertes, que en todo momento se ha volcado en la consecución de mis objetivos. Por enseñarme los entresijos de la investigación y la buena praxis. Gracias por la constante ayuda en el día a día y por no dejar que me duerma en los laureles.

Por supuesto, mi más sincero agradecimiento al Ministerio de Economía y Competitividad (MINECO) ya que este trabajo no podría haberse realizado sin la ayuda tanto por la concesión de la beca FPI (BES-2013-067193) dentro del proyecto CTQ2012-35251, como de la financiación del proyecto CTQ2015-67461-P. También agradecer al Gobierno de Aragón por su apoyo constante al Grupo Consolidado, Grupo E17_17R, *Química Inorgánica y de los Compuestos Organometálicos*).

Me gustaría hacer una mención especial al Prof. Juan Forniés, responsable con sus clases de que me picase el gusanillo que me llevó, unos años después, a comenzar mi andadura en la química inorgánica y organometálica.

Así mismo, me gustaría hacer patente mi agradecimiento al Dr. Babil Menjón y al Prof. José María Casas, que no sólo invirtieron su valioso tiempo en transmitirme su conocimiento, sino que depositaron su confianza en mi capacidad para ser un miembro útil del equipo.

Igualmente importante la mención al resto de miembros del Grupo *Química Inorgánica y de los Compuestos Organometálicos*. A los doctores Consuelo Fortuño, Irene Ara, Miguel Baya y Antonio Martín quienes, a pesar de no ser responsables directos de este trabajo, no dudaron en ningún momento en ayudarme a resolver las dudas y los problemas surgidos por el camino.

No es posible olvidar tampoco a los compañeros más jóvenes del grupo, con los que he compartido la mayor parte de mi andadura como doctorando. Lo que comenzó como la Generación A, y que al poco se convirtió en el grupo de las Folcloricas. Tampoco puedo dejar a un lado a los miembros que ya dejaron el grupo para proseguir con sus carreras, pero que fueron de vital importancia para mí como referencia y punto de apoyo en mis inicios, ni a todos aquellos que aunque de forma temporal han formado parte de esta familia. Alberto, Antonio, David, Daniel, Lorenzo, Mapi, Andersson, Úrsula, Sonia, M. Angeles, Hector, Elena... ¡Muchas gracias Platineros!

Por los buenos ratos, los limones de Murcia, los helados de alta tecnología, los dewárboles de cartón, los concursos tontos de puertas navideñas, las partidas de láser y otras tantas actividades que me han recordado que una Tesis Doctoral no trata sólo de sintetizar compuestos y realizar medidas, sino también de forjar amistades y de apoyarse los unos en los otros cuando las cosas se ponen feas. Alicia, Elisa, ¡mil gracias!

Muchas gracias al resto de compañeros del Departamento de Química Inorgánica, ya que sin ellos la tarea investigadora sería tremendamente aburrida. También a todos los compañeros del resto de la Facultad de Ciencias de la Universidad de Zaragoza, en especial a aquellos que un día te dicen que se van de estancia a la misma ciudad que tú, en las mismas fechas que tú, y que acaban convirtiéndose en amigos que te piden que les saques fotos de espaldas, mirando al infinito, al más puro estilo de Instagram.

Me gustaría tener presentes también a todos los técnicos del centro, gracias a los cuales podemos obtener los resultados que sustentan nuestras conclusiones.

Mi agradecimiento no quedaría completo sin recordar mis dos escapadas al Instituto de Ricerca en Energia de Catalunya (IREC) de Barcelona, donde la implicación de los doctores Mariano Perálvarez y Marc Torrell me permitió aprender lo difícil pero gratificante que es entenderse con científicos de otras ramas de conocimiento. Gracias a ellos y a los miembros de sus equipos por hacerme sentir menos marciano fuera de mi zona de confort.

Devo ringraziare anche tutta la gente che ho conosciuto nel Istituto per lo Studio delle Macromolecole (ISMAC) di Milano, dove tre mesi hanno trascorso come un fulmine. Grazie a Dr. Chiara Botta, Dr. Wojciech Mròz e Umberto Giovanella ho imparato tantissimo sulla chimica dei materiali. Ma sopratutto vi ringrazio a tutti per farmi sentire come a casa, per la paciencia quando non sapevo spiegare in italiano quello che pensavo, per insegnarmi un pò più della cultura italiana, e per l'interese quando il giallo è diventato rosso, e quando il blu era finalmente blu e non verde. Per tutti gli unicorni, l'amido di mais, tutte le "pausa pranzo", le "ma come vieni in Italia e non ti piace il caffè!"... Benedetta, Cristina, Claudio, Elisa, Francesco, Cecilia, Erika, Francesco, Silvia, Stefania…. Grazie Mille!!!

Por supuesto agradecer al "Cónclave Maligno" por estos últimos meses de presión en los que me han ayudado a mantener la sonrisa. Por esos cafés y vermuts en los que siempre había noticias jugosas que contar y que han conseguido hacerlo todo más llevadero.

Y qué mejor para sentirte como en casa que un "Gossip Group" que te entiende casi sin palabras, que te apoya y se preocupa. ¡¡¡Y que te lleva de viaje en Nochevieja consiguiendo que seas una de las tres únicas personas que comen uvas en una plaza abarrotada!!! Patri, Silvia, por más tardes de sofá viendo como sucumbís al peligroso mundo de los videojuegos, por más postureo en la salamandra de Parc Güell, por más restaurantes nuevos que probar, muchísimas gracias por estar siempre ahí aunque la distancia nos mantenga separados.

Uni II, tampoco me olvido de los momentos que hemos vivido todos juntos desde que nos conocimos en 2006. Doce años que nos convierten en una pequeña familia que comparte los éxitos y tropiezos, y que busca cualquier excusa para poder reunirse y ponerse al día. Que celebra cuando uno más de nosotros se une al club de los Doctores o encuentra trabajo. Por más cafés improvisados en mañanas de sábado y por más momentos como salir de fiesta y ser partícipe de un momento "Lluvia de Estrellas" cuando tu amiga va al baño y a los treinta segundos sale con otra ropa y otro peinado (sí María, ese momento en el Parros con tu hermana me marcó). Porque cuando salir a tomar algo significa disfrutar no solo de ese algo, sino de la mejor compañía que se puede tener. Alba, Elena, Esther, Isa, Jaime, Javi, Laura, María, Mel, Samuel, Silvia, Patri, Teresa, sois mi pequeña familia de (bio)químicos locos, muchas gracias por estar ahí.

Ni que decir tiene que aquella gente que forma parte de tu vida durante más de veinte años se convierte en familia por derecho propio. Aquellas personas que te lo ponen difícil cuando te conocen con ocho añitos, pero que lo luego te lo dan todo. Que te llaman para jugar una partida de canasta, para salir a dormir la siesta a la piscina, que te hacen partícipe de sus momentos especiales, que te abren las puertas de su casa por muy lejos que estén y te llevan al final del mundo. Por todos los recuerdos y vivencias que me han llevado a ser quien soy hoy, Actea, Adri, Alberto, Álvaro, Chris, Chus, Cindy, Cris, Diego, Elena, Guille, Irene, Laura, Luz, Patri, Raul y Sergio, ¡muchísimas gracias!

Gracias a la familia, la de sangre, la que no eliges pero te quiere porque le sale del corazón y no porque toque. La que forma parte de quién eres porque dedican su tiempo a enseñarte, la que incluso siendo más joven es capaz de darte alguna lección.

Por último, y por supuesto no por ello menos importante, quería dejar constancia de lo agradecido que estoy a las dos personas más valiosas de mi vida. M. Ángel y M. Jesús, más conocidos como papá y mamá, siempre ahí sin importar la situación. Guiándome en todas mis decisiones, pero dejándome cometer los errores de los que aprender, y ahorrándome una fortuna en consultas con psicólogos. Gracias por enseñarme los valores que creo que me hacen mejor persona, y por animarme a no rendirme. Gracias por los sacrificios hechos por mí, y por todas las alegrías que me dais. M U C H A S G R A C I A S.

RESUMEN

La tecnología LED y OLED ha irrumpido en el campo de la iluminación y actualmente se considera una alternativa para reemplazar a las ya prohibidas lámparas incandescentes y fluorescentes dado su menor consumo energético. Tanto los WLEDs como los WOLEDs, emisores de luz blanca empleados en iluminación, incorporan metales de tierras raras cuyo mercado está controlado en un 85% por China. Esto supone un elevado riesgo de abastecimiento y precio, lo que puede afectar dramáticamente a la industria mundial. En este sentido el uso de compuestos organometálicos de metales de transición como rutenio, osmio, iridio y platino con propiedades luminiscentes se considera una alternativa a los WLEDs y WOLEDs convencionales. La elevada constante de acoplamiento spin-orbita (ξ) en estos metales pesados permite la relajación de las reglas de selección que dictan las transiciones energéticas permitidas y prohibidas, de modo que los procesos de fosforescencia pueden tener lugar de forma eficiente. Como consecuencia, los máximos rendimientos cuánticos teóricos ascienden a la unidad, dando lugar a materiales funcionales con un mayor potencial para aplicaciones de bajo consumo energético.

Nuestro trabajo se ha centrado en la síntesis y caracterización de nuevos derivados luminescentes de Pt(II) y la implementación de alguno de ellos en dispositivos emisores de luz blanca. Los compuestos preparados contienen un cromóforo del tipo "Pt(R-C^C*)" dónde R-C^C* es un ligando carbeno N-heterocíclico ciclometalado. La presencia de dos enlaces Pt-C aumenta el desdoblamiento de los orbitales del metal respecto a los ligandos C,N-ciclometalados, más conocidos y estudiados, y aporta una gran estabilidad física y química a los compuestos.

Para desarrollar este trabajo, se prepararon los complejos [{Pt(μ-Cl)(R-C^C*)}$_2$] siguiendo un protocolo en varios pasos desarrollado y empleado exclusivamente en nuestro grupo de investigación; su descripción se recoge en el Capítulo 1 de esta Tesis. Los complejos [{Pt(μ-Cl)(R-C^C*)}$_2$] resultaron ser excelentes precursores de compuestos con diversas estequiometrías: [PtCl(NC-C^C*)L], [Pt(NC-C^C*)PPh$_3$L], [Pt(R-C^C*)(CNR')$_2$]PF$_6$, NBu$_4$[Pt(R-C^C*)(CN)$_2$], [Pt(R-C^C*)(P^P)]PF$_6$ y [Pt(R-C^C*)(acac)] que a su vez pueden servir de precursores de compuestos con enlaces metal-metal, como [{Pt(R-C^C*)(acac)}$_2$Tl]PF$_6$. Todos los compuestos preparados han sido exhaustivamente caracterizados por diferentes técnicas, siendo las más significativas: IR, RMN y difracción de rayos X. Se ha llevado a cabo también la determinación de las propiedades fotofísicas de todos los compuestos preparados y su estudio mediante cálculos teóricos DFT/TD-DFT. Todo ello se recoge en los Capítulos 2-4 de esta Tesis.

Tal y como planteamos este trabajo, la mayor parte de los compuestos preparados han resultado ser emisores de luz azul bastante eficientes. Teniendo en cuenta que la luz azul es el componente esencial de la luz blanca, se ha estudiado la potencial aplicación de varios de ellos en diversos dispositivos emisores de luz blanca, con resultados prometedores que se describen en el Capítulo 5 de esta Tesis Doctoral.

El conocimiento logrado acerca de estos sistemas puede facilitar un diseño racional de futuros materiales funcionales.

Abbreviations

GC: Gas Chromatography

IR: Infrared Spectroscopy

MS: Mass Spectrometry

NMR: Nuclear Magnetic Resonance

UV-vis: Ultravioleta-visible Spectroscopy

2-MeOEtOH: 2-Metoxyethanol

2-MeTHF: 2-Methyltetrahydrofuran

Adetone-d_6: Deuterated acetone

Methylene chloride-d_2/CH_2Cl_2-d_2/CD_2Cl_2: Deuterated dichloromethane

CH_3CN: Acetonitrile

$CHCl_3$-d/$CDCl_3$: Deuterated chloroform

DMSO(-d_6): (Deuterated) dimethylsulfoxide

Et_2O: Diethylether

MeOH: Methanol

THF: Tetrahydrofuran

NHC: N-heterocyclic carbene

acac: Acetylacetonate

Cl: Chloride

CN: Cyanide

CNtBu: *Tert*-butyl isocyanide

CNXyl: 2,6-Dimethylphenyl isocyanide

MMI: 2-Mercapto-1-methyl imidazole

PPh3: Triphenylphosphine

py: Pyridine

FO: Frontier Orbitals

MO: Molecular Orbitals

EL: Electroluminescence

PL: photoluminescence

ILCT: Intraligand Charge Transfer

LL'CT: Ligand-to-ligand Charge Transfer

MCCT: Metal-centered Charge Transfer

LMCT: Ligand-to-metal Charge Transfer

MLCT: Metal-to-ligand Charge Transfer

MMLCT: Metal-metal-to-ligand Charge Transfer

LMMCT: Ligand-to-metal-metal Charge Transfer

ITO: Indium tin oxide

IV: Ink vehicle

MoO_3: Molybdenum trioxide

OXD-7: 1,3-Bis[2-(4-*tert*-butylphenyl)-1,3,4-oxadiazo-5-yl]bencene

PBD: 2-(4-Biphenylyl)-5-(4-*tert*-butylphenyl)-1,3,4-oxadiazole

PEDOT:PSS: Poly(3,4-ethylenedioxythiophene)-poly(styrenesulfonate)

PMMA: Poly(methylmetacrilate)

PVK: Poly(N-vinylcarbazole)

TCTA: Tris(4-carbazoyl-9-ylphenyl)amine

TPBi: 1,3,5-Tris(1-phenyl-1H-benzimidazol-2-yl)bencene

ZnO: Zinc oxide

EIL: Electron Injection Layer

EML: Emissive Layer

ETL: Electron Transport Layer

HIL: Hole Injection Layer

HTL: Hole Transport Layer

*All supporting information (SI) files can be found in digital format.

Introduction

General lighting accounts for around 15% of the world's electricity consumption and it is expected that demand will rise 50% by 2030. In the light of this, it is widely accepted that corrective measures to minimize energy consumption had to be taken and the reason for the massive disruption of Solid-State Lighting (SSL) technology to replace the incandescent and fluorescent phase-out.[1] In SSL, the use of conventional *p–n* junctions represents the most common solution to highly efficient and durable optoelectronic devices, and gave birth to the well-known Light Emitting Diodes (LEDs). LEDs, with outstanding energy-conversion efficiency (up to 50%) together with their significant durability (around 25.000 hours) and sustainability, have the potential for inducing important energy savings. In recent years, Organic Light Emitting Diodes (OLEDs) have started to draw attention due to the possibility of fabricating larger and even flexible illumination systems (see Figure I.1).[2]

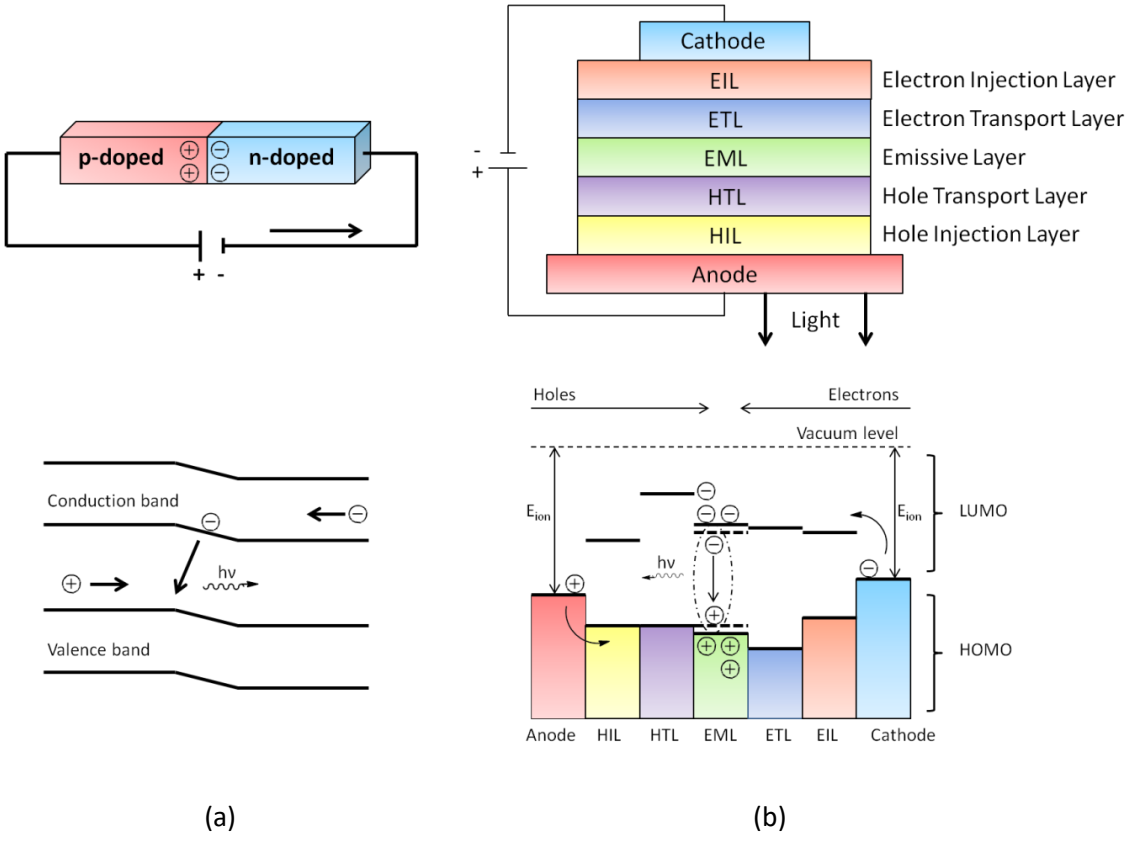

(a) (b)

Figura I.1. Typical p-n junction in conventional LEDs (a), structure and favorable energy diagram in OLEDs (b).

Although the first OLEDs consisted of a fluorescent organic material as EML, the reduced Internal Quantum Efficiency (IQE = 25%), due to the harvesting of only the singlet excitons, motivated the use of heavy metal complexes (mostly Eu) as dopants in order to collect both singlet and triplet excitons and achieve a theoretical IQE of 100%.[3] The use of

phosphors as dopants in the EML of OLEDs gave birth to the phosphorescent OLEDs (PHOLEDs).

Nowadays, two main strategies are available within state-of-the-art SSL to generate white luminescence. On one hand, the RGB (red, green and blue) approach is a device in which the three emitters (primary at around 455nm, 530nm and 630nm) are closely packaged forming a compact semiconductor light source (see Figure I.2).[4]

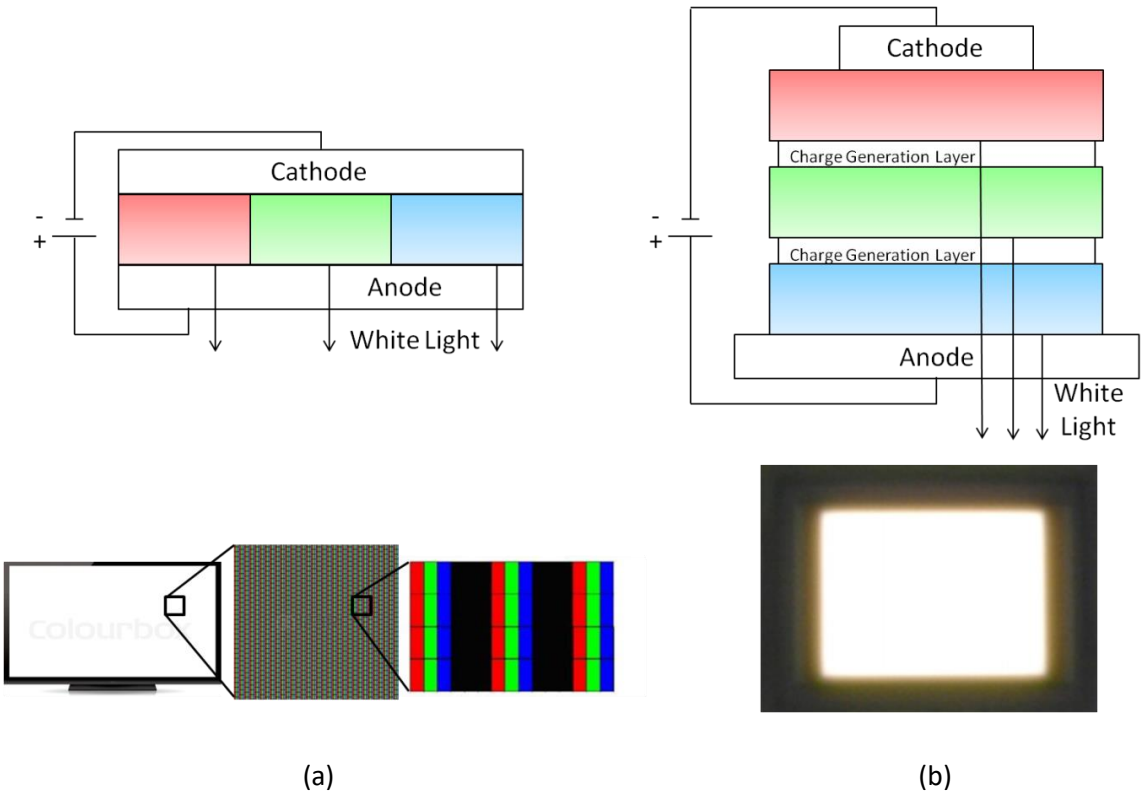

Figure I.2. White light generation in OLEDs with RGB subpixels (a) and multilayer architecture panels from Lumiotec (b).

The second approach is the so-called PC-LEDs (phosphor-converted LED) based on high efficiency blue LEDs combined with yellow and/or red phosphors. In these devices, the phosphor absorbs part of the blue light from the pumping LED which is partially downconverted. White light results then from the combination of the phosphors' re-emission and the non-absorbed light from the LED. PC-LEDs can be built in two different configurations, those being conformal and remote phosphor architectures (see Figure I.3).

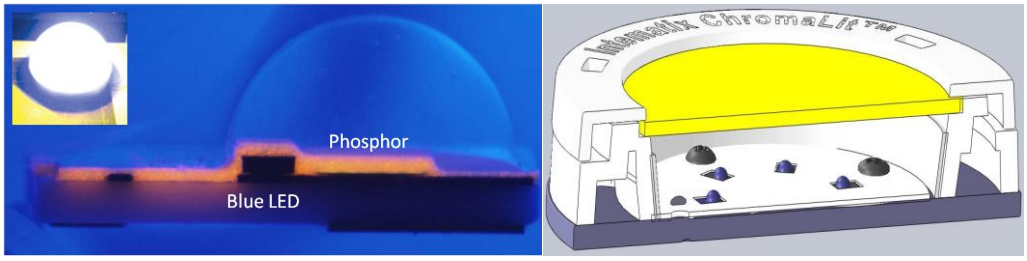

(a) (b)

Figure I.3. Philips Lumileds HB-LEDs with package level conformal coating (a) and Intematix ChromaLit light source with remote phosphor configuration (b).

There is a major difference between the two options. The conformal approach is based on integrating the active powder on the LED chip, i.e. into the package. In this configuration, the phosphor is subjected to the heat generated at the *p-n* junction, and relatively high temperatures can affect the phosphor performance thus inducing an efficiency drop. On the other hand, the concept of remote configurations, existing for more than ten years, is currently drawing renewed attention due to the sizeable gains with respect to the conformal option.[5] The phosphor is now applied as a separate 2D or 3D component optically pumped by an UV or blue LED rather than being included as a part of the package. Moreover, placing the emitting centers far from the LED pumping source, its operating temperature is lower and more stable thus providing improved lifetime (lower thermal degradation) and color stability. Apart from this, the remote phosphor, placed far away from the LED and incorporated into a highly efficient reflector system, reduces the chances of chip re-absorption as well as harvesting a notably percentage of the light emitted backwards, increasing the total output power, especially if compared to white conformal devices.

Concerning the chemical composition of phosphors used in PC-LEDs are generally based on rare-earth-doped inorganic compounds. Materials like aluminates, silicates, garnets or nitrides incorporate rare-earth elements, typically Ce^{3+} and Eu^{2+}, as activator ions. As an example of these systems we find the commonly used blue GaN or InGaN LEDs with the YAG:Ce^{3+} yellow emitter on top (Figure I.3 a). However, despite the extraordinary quantum efficiency of these compounds, as in the case of rare-earth doped PHOLEDs, some logistic problems are foreseen on the horizon. One of them is the dependency on China policies, responsible of about 85 % of the global production. The other is the relative scarcity of rare earth elements that leads to a long-term price rise.[6] In this framework, it becomes clear that new approaches are needed in order to minimize the dependence of the lighting market on rare-earth availability.

The production of high quality white light has been a constant challenge in the development of new illumination systems. Three parameters condition whether a light can be classified as white light or not, and they have to be thoroughly controlled in order to achieve optimal light.[7] These parameters are the Correlated Color Temperature (CCT), which is a value related to the appearance in color of the light to human eye, the Color Rendering Index (CRI), related to the reproducibility of the full gamut of colors in the objects irradiated by this light, and the distance to the Planckian Locus (Duv), which correlates the emission with the radiation from an ideal blackbody.

Although LEDs were responsible of an incredible reduction of energy consumption, they have some disadvantages, such as the poor quality white light obtained due to the narrow emission bands extracted from these architectures even when complex structures, such as the tunable RGB systems, are used (see Figure I.4 a). Despite the fact that the development of phosphors based on rare earth ions as dopants for PC-LEDs has rendered high light output and efficacies, the mixture of the remaining photons from the source and the lower energy ones emitted by the phosphor yields light with spectral shapes usually lacking in red component (see Figure I.4 b), and as a consequence poor CRI values and high CCT are commonly obtained.[8] To reduce the temperature of the emitted light and improve the CRI values, an additional red phosphor can be added to the configuration. This solution widens the emission spectrum towards the red region, although technical issues are usually addressed, such as an increment in the complexity of the device or reabsorption of the radiation by the lower energy emitting phosphors.

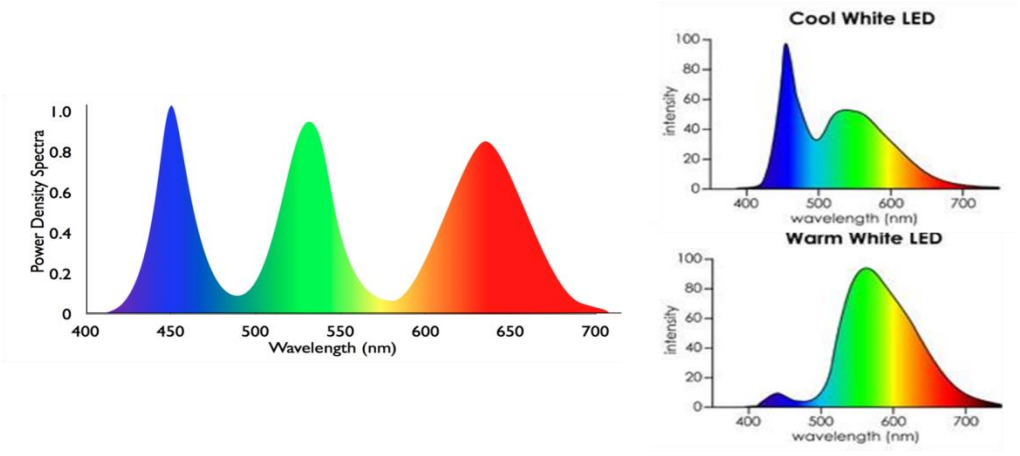

(a) (b)

Figure I.4. RGB conventional LED (a) and down-conversion of blue light from GaN or InGaN by different doping amounts of YAG:Ce^{3+} (b).

As an alternative to rare earth elements, organometallic compounds[9] containing heavy transition elements, such as gold(III),[10] ruthenium(II),[11] osmium (II),[12] iridium(III)[13] and

platinum(II),[14] are taking much interest in lighting applications. The presence of a metal from the third transition row, with a big spin-orbit coupling constant (ξ), results in an efficient intersystem crossing (ISC) which allows the population of the triplet states through the initial population of singlet states (Figure I.5). Within this illumination field, square planar platinum (II) complexes containing aromatic molecules with delocalized π electron density such as C^N cyclometallated (*ca.* benzoquinolinate and phenylpyridinate) derivatives are suitable systems for these purposes because of the nature of their emissive states.[15] Cyclometallated ligands display an additional advantage over purely N-donor ligands. The splitting of the *d* orbitals can be enhanced due to the strong ligand field induced by the electronic features of the C-σ bond (σ donor) and the aromatic fragment (π acceptor). Consequently, the energy of the metal centred (MC) (d-d) excited states raise, preventing non-radiative decay processes (see Figure I.6 a). According to this, the incorporation of strong field ligands to the metal coordination sphere is essential for the design of these demanded systems.

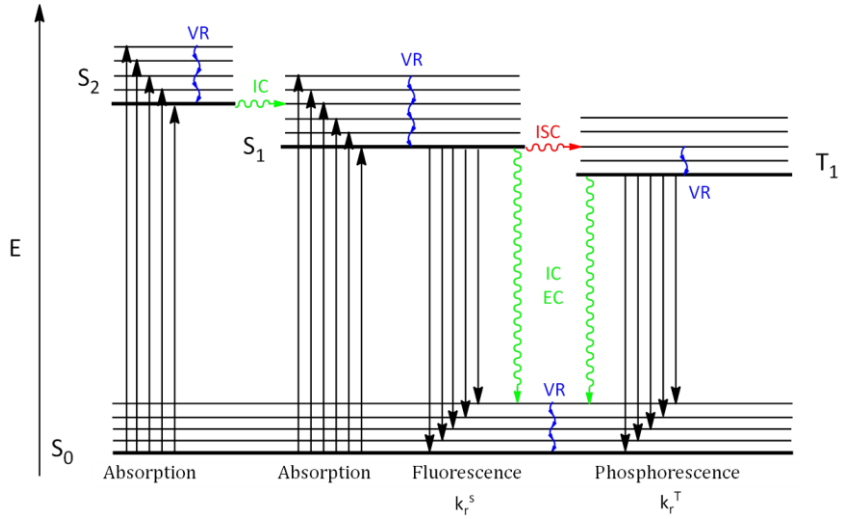

Figure I.5. Jablonski diagram of photoluminescent systems.

The MO diagram in these complexes is the represented in Figure I6 b, in such a way that the emission typically originates from intra-ligand (^{3}ILCT), metal-to-ligand (^{3}MLCT) or even ligand-to-ligand (^{3}LL'CT) charge transfer transitions. In addition, in complexes with sterically undemanding ligands, the molecules arrange into aggregates through Pt···Pt and/or π-π interactions, mostly in concentrated solutions or solid state. In these cases, Pt(II) compounds exhibit red-shifted phosphorescent emissions due to metal-metal-to-ligand charge transfer (^{3}MMLCT) and/or excimeric ππ* excited states with the absorption and emission being highly dependent on the extent of the interactions and therefore on the crystallization solvent, concentration, temperature or the nature of the counter ion (Figure I.7).

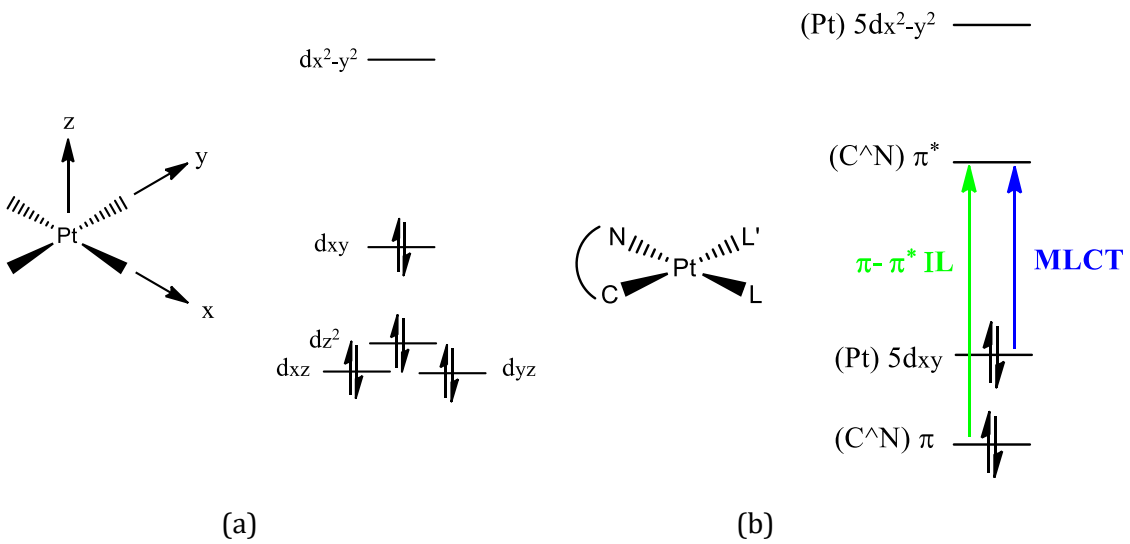

Figure I.6. Crystal-field splitting of the *d* orbitals of platinum (II) in square-planar complexes (a) and MOs diagram in cyclometalated C^N compounds of platinum (II) (b).

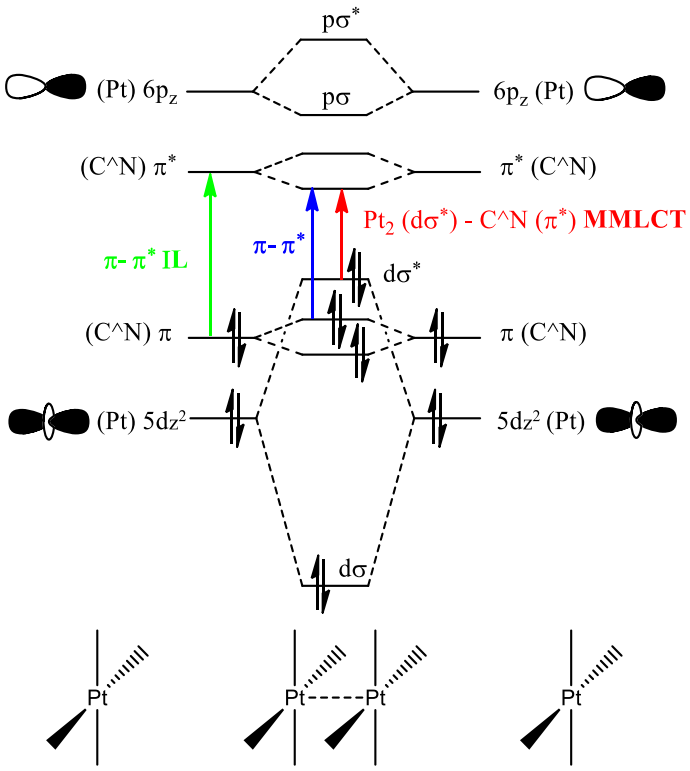

Figure I.7. MO diagram of dinuclear C^N cyclometalated Pt(II) complex with Pt···Pt and π···π interactions.

At the beginning of this work in 2014, just a few examples of Pt(II) complexes used as phosphorescent dopants in optoelectronic devices had been reported. In the late 1990s some red light emitting devices with low external quantum efficiencies (EQE < 5%) based on N^N^N^N tetradentate ligands such as porphirines were published.[16] The production

of red light underwent a relevant boost at the beginning of the 2000s with the incorporation of O^N^N^O and N^C^C^N ligands, that rendered devices with EQE as high as 17%.[17] It was at that moment that blue and green devices started to incorporate complexes with N^C^N cyclometalated ligands to achieve EQE higher than 10%.[18] However, examples of devices producing high energy emissions were still scarce, and it was not until the second decade of the 2000s that efficient blue emitters started to become important, since the production of white light continued to be a worldwide challenge.[14b, c] Although examples of Ir(III) complexes had been reported for this goal, usually containing fluorinated ligands,[19] the examples with Pt(II) were still focussed on tetradentate [14c, d, 20], pincer-type[14a-c, 14e, 18, 21] or C^N bidentate ligands,[22] since the aggregates arising from Pt-Pt and π-π interactions in blue emitters can give birth to a dual emission rendering white light (see Figure I.8).

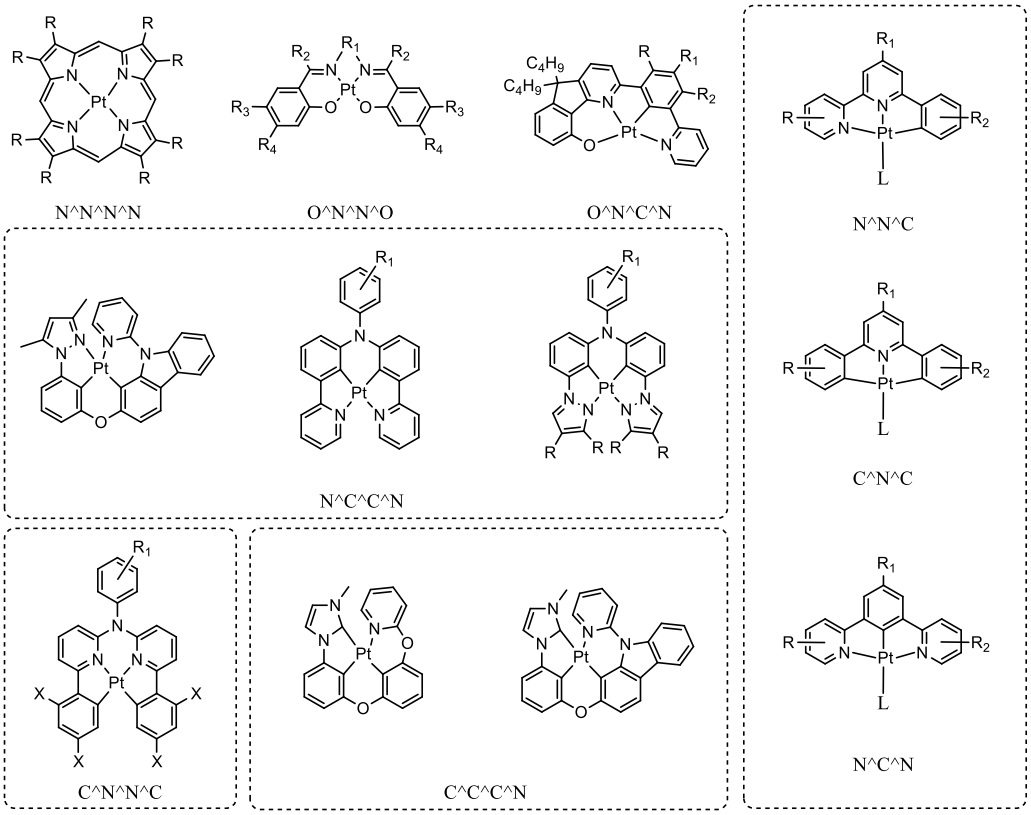

Figure I.8. Precedent Pt(II) complexes for electroluminescent devices.

Because of all that, we decided to focus on Pt(II) compounds containing cyclometalated N-heterocyclic carbenes (C^C*) as bidentate ligands aiming to get blue and efficient phosphorescent materials.

Carbene ligands in metal complexes were initially classified in two main groups, depending on their structure, the oxidation state of the metal and the observed reactivity: Schrock- and Fischer-type carbenes.[23]

Fischer-type metal-carbene complexes are generally formed with metals in low oxidation states from the late transition groups and π-donor R substituents at the carbene. The interaction can be understood as a two electron σ-donor contribution of the carbon atom and the π-backbonding from the metal to a *p* orbital of the carbon. Since the *d* orbitals of the metal have lower energies than the *p* orbital of the carbene, the π-backbonding is less effective than the σ contribution, this leading to a bond polarization (M^--C^+). On the other hand, Schrock-type metal-carbene complexes are usually formed with metals in high oxidation states from the first transition groups with H or alquil groups at the carbene. They present a triplet state for both the metal and the carbene, leading to a compensated electronic interaction. Since the *d* orbitals of the metal and the *p* orbitals of the carbene are closer in energy, the π-backbonding is more effective and the opposite polarization takes place (M^+-C^-) (see Figure I.9). In both cases, the electrophilic (Fischer) or nucleophilic (Schrock) character of the carbene makes these complexes very reactive towards nucleophiles and electrophiles respectively.

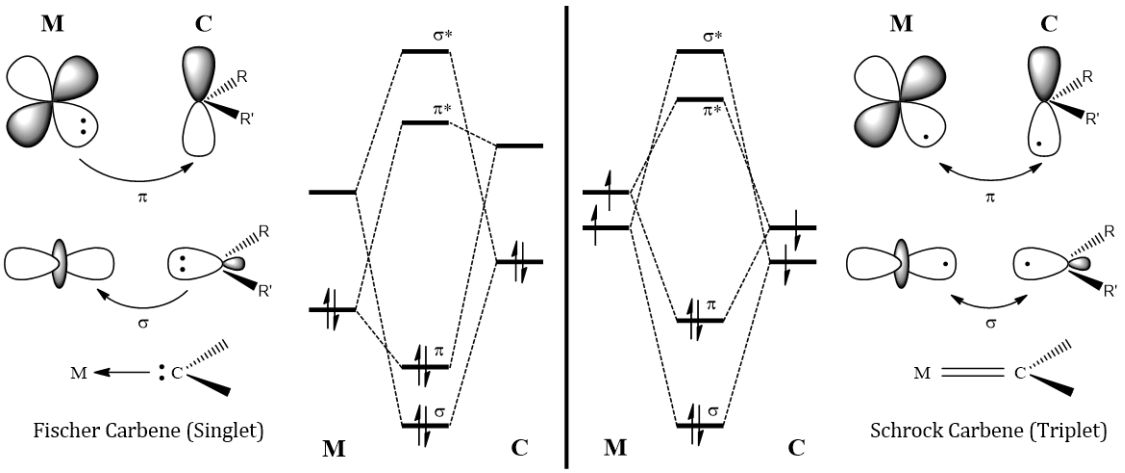

Figure I.9. Bond models and MO diagrams for Fischer (left) and Schrock (right) metal-carbene complexes.

At the beginning of the 1990s Arduengo et al. prepared the first stable and persistent N-heterocyclic carbene (NHC) (see Figure I.10).[24] This type of ligand has demonstrated to be very versatile in organometallic chemistry, and they have been widely used in catalysis and liquid crystals in the last decades. NHCs are considered a third kind of carbenes, with properties different to the Fischer and Schrock ones.[25] NHC are formally neutral two-electron donor ligands that can be described as purely σ–donors, in which the σ–donor character is even greater than in phosphine ligands. In addition, they present poor π–

acceptor ability, comparable to nitriles and pyridines, as a consequence of the internal π-backbonding from the nitrogen atoms. These characteristics translate into a low reactivity of the NHC-M bond towards nucleophiles and electrophiles.

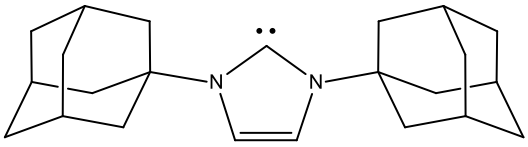

Figure I.10. Chemical structure of Arduengo's carbene.

Generation of high quality white light, which was planned as the final goal of this work, requires efficient materials able to contribute to the blue region of the visible spectrum. In the chemistry of Pt(II), population of a high energy excited states necessary for this efficient blue emission upon excitation competes with the photo- or thermal population of aforementioned high-lying metal dd* states, the latter leading to severe geometrical distortions of the molecules which result in non-radiative deactivation and degradation via bond-breaking processes.[21b] Therefore, a rational approach for the design of efficient and stable Pt(II) blue-phosphorescent systems is the incorporation of strong field ligands to the metal coordination sphere, such as C-deprotonated imines able to act as bidentate,[22] tridentate[14a-c, 14e, 18, 21] and even tetradentate[14c, d, 20] ligands. In this context, cyclometalated N-heterocyclic carbenes (C^C*) may surpass the high ligand field splitting capacity of the C^N-ligands, since they present two C-σ bonds, which open the door to blue and efficient phosphorescent compounds. Another consequence of the presence of strong carbon-metal bonds is the robustness and/or stability of the NHC complexes which may provide long-term functional materials.[26] In addition, the use of bidentate ligands has the advantage of the allowed electronic tunability of the Pt(II) complexes by varying the ancillary ligands, which contribute to the emission wavelength and decay lifetimes.[27]

At the moment we planned this PhD just some cyclometalated NHC Pt(II) compounds, most of them containing β–diketonates as ancillary ligands, had been reported.[26e, 28] Therefore, we decided to explore this research field and study the effect of the change of both, the C^C* and the ancillary ligands in the emissive properties of Pt(II) compounds. Although this introduction covers the research topic until the beginning of the PhD thesis, the field has undergone an impressive boost in the last years that must be highlighted.[29]

A major part of the research made during this PhD has been published in the following papers, which have been included at the end of this Memory:

1.- S. Fuertes; A. J. Chueca; A. Martin; V. Sicilia*. **Pt_2Tl Building Blocks for Two-Dimensional Extended solids: Synthesis, Crystal Structures, and Luminescence.** *Crystal Growth & Design,* **2017**, *17*, 4336-4346

2.- S. Fuertes; A. J. Chueca; L. Arnal; A. Martin; V. Sicilia*. **Heteroleptic NHC cycloplatinated complexes: a new approach to highly efficient blue-light emitters.** *Inorganic Chemistry*, **2017**, *56*, 4829-4839

3.- S. Fuertes, A. J.Chueca, M. Perálvarez, P. Borja, M. Torrell, J. Carreras, V. Sicilia*. **White Light Emission from Planar Remote Phosphor Based on NHC Cycloplatinated Complexes**. ACS *Applied Materials & Interfaces***, 2016**, *8*, 16160-16169

4.- S. Fuertes, A. J. Chueca, V. Sicilia*. **Exploring the Transphobia Effect on Heteroleptic NHC Cycloplatinated Complexes**. *Inorganic Chemistry*, **2015**, *54*, 9885-9895

However, some of the results have not been published yet. In order to include all the results and to show them in a coherent way we have organized this Memory in five chapters:

In Chapter 1, the step-by-step synthesis protocol to achieve complexes [{Pt(μ-Cl)(R-C^C*)}$_2$] (R-C^C* = Cyclometalated N-Heterocyclic carbene; R-HC^C* = 1-(naphthalen-2-yl)-3-methyl-1*H*-imidazol-2-ylidene (Naph^C*); 1-(4-ethoxycarbonylphenyl)-3-methyl-1*H*-imidazol-2-ylidene (EtO_2C-C^C*); 1-(4-cyanophenyl)-3-methyl-1*H*-imidazol-2-ylidene (NC-C^C*); 1-(3,5-dichlorophenyl)-3-methyl-1*H*-imidazol-2-ylidene (Cl-C^C*)) are described. They were used as starting materials to obtain new blue-emitting compounds of Pt(II) with different stoichiometries.

In Chapter 2, the synthesis of heteroleptic compounds such as [PtCl(NC-C^C*)L] (L = PPh_3, py, CNXyl, MMI) and *trans*-(C*, P)-[Pt(R-C^C*)(PPh_3)L']PF_6 (R-C = Naph, CO_2Et, L' = py; R = CN, L' = py, CNXyl, MMI) and how the small difference in the degree of transphobia T[C_{Ar}/L] and T[C*/L] limits the synthesis of these compounds as a unique isomer to those with PPh_3 are described.

In Chapter 3, compounds containing two isocyanide or cyanide ligands such as [Pt(R-C^C*)(CNR')$_2$]PF_6 (R′ = *tert*-butyl (^{t}Bu), 2,6-dimethylphenyl (Xyl)) and NBu_4[Pt(R-C^C*)$(CN)_2$] (R−C = Naph R = CO_2Et, CN, Cl) are described

In Chapter 4, compounds containing chelate ligands such as [Pt(R-C^C*)(P^P)]PF_6 (R-C = Naph, R = CN; P^P = dppm, dppe**,** dppbz) and [Pt(R-C^C*)(acac)] are described. In case of the acac derivatives, their ability to form Pt-Tl cluster such as [{Pt(R-C^C*)(acac)}$_2$Tl]PF_6 is also presented.

The luminescence of all of these compounds have been deeply studied and described conveniently in the corresponding chapter. As expected, most of our compounds resulted to be efficient blue-emitters. Therefore, we explored different ways of using them to generate white light. The potential applications of these compounds have been described all together in Chapter 5.

The realization of this work required the use of specific laboratory operation protocols, such as Schlenk techniques, glove box systems or separation techniques (GC). It also required the use of several spectroscopic and spectrometric techniques for the characterization of the new complexes (IR, MS, NMR, X-ray) and the study of their photophysical properties (UV-vis absorption, steady state emission, emission lifetime and quantum yield). In addition, several deposition techniques were used for the lighting applications (drop casting, screen printing, spin coating, high vacuum evaporation and Organic Molecular Beam Epitaxy). Full experimental work and data collection were made by the author of this PhD with the exception of MS spectra, CHNS elemental analysis, theoretical calculations and X-ray structures, the latter being performed by Dr. Sara Fuertes and Dr. Antonio Martín.

Many of the results shown in this Memory have been published in the aforementioned papers and presented in four national and international conferences, obtaining the “best poster award” in the Vth Spanish-Portuguese workshop on photochemistry organized by the Grupo Especializado de Fotoquímica (GRUFO) from the Real Sociedad Española de Quimica (RSEC) in Toledo, September 2016.

Chapter 1.

Starting materials

DISCUSSION

The dichloro-bridge compounds containing cyclometalated N-heterocyclic carbene ligands, [{Pt(μ-Cl)(R-C^C*)}$_2$] (R-C^C*: 1-(naphthalen-2-yl)-3-methyl-1*H*-imidazol-2-ylidene (Naph^C*, **4A**);[29e] 1-(4-ethoxycarbonylphenyl)-3-methyl-1*H*-imidazol-2-ylidene (EtO_2C-C^C*, **4B**);[30] 1-(4-cyanophenyl)-3-methyl-1*H*-imidazol-2-ylidene (NC-C^C*, **4C**);[31] 1-(3,5-dichlorophenyl)-3-methyl-1*H*-imidazol-2-ylidene (Cl-C^C*, **4D**);[32] have been used as starting materials to obtain new luminescent compounds of Pt(II). Their syntheses and characterization have been already reported in the references within this paragraph.

The preparation of [{Pt(μ-Cl)(R-C^C*)}$_2$] has been accomplished following the general synthetic pathway shown in Scheme 1.1. For that, four different substituted aryl bromides have been successfully coupled to imidazole via the Ullmann reaction, with adjustment of the base (KOH, K_2CO_3), the copper(I) catalysts (CuI, Cu_2O) and the solvent for the specific aryl bromide substrate.

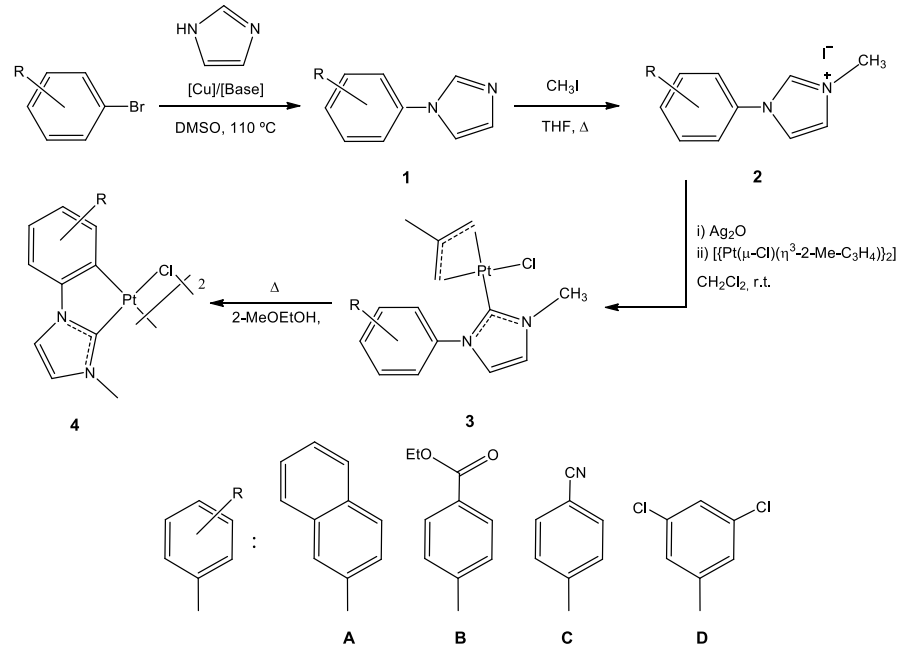

Scheme 1.1. Schematic route for the preparation of the starting materials.

As an example, the reaction of 1 equivalent of 4-bromobenzonitrile with 2 equivalents of imidazole, in the presence of K_2CO_3 and CuI in dimethylsulfoxide was carried out under argon atmosphere at 110ºC. After 70 hours the crude was studied by gas chromatography to assess the completion of the reaction, as can be deduced by the disappearance of the signal attributed to the limiting reagent 4-bromobenzonitrile (3.4 min), and the recording of a new major signal (6.1 min) assigned to the coupling product in the chromatogram (see Figure 1.1).

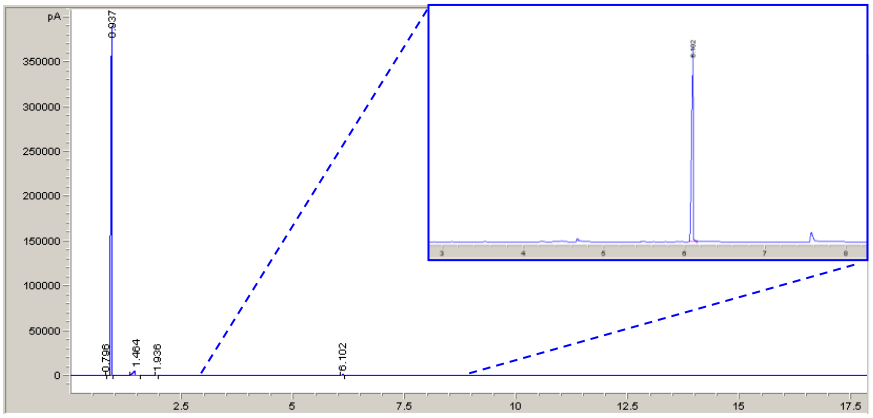

Figure 1.1. GC chromatogram of **1C** before the reaction work-up.

Once the crude was cooled down, extracted with ethyl acetate, it was washed with water and brine, dried with $MgSO_4$, evaporated to dryness and washed with hexane. Compound **1C** was thus obtained as a white solid in a high yield. As observed in the ^{1}H-NMR spectrum of **1C**,† the appearance of three different resonances for the hydrogen atoms in the imidazole moiety proved the successful C-N coupling (see Figure 1.2).

The reaction of the organic substrates (**1**) with iodomethane in refluxing tetrahydrofuran yielded white solids corresponding to the expected imidazolium salts (**2**), whose ^{1}H-NMR spectra showed an additional resonance at ca. 4 ppm, due to the new methyl group (see Figure 1.3 for **2C**).

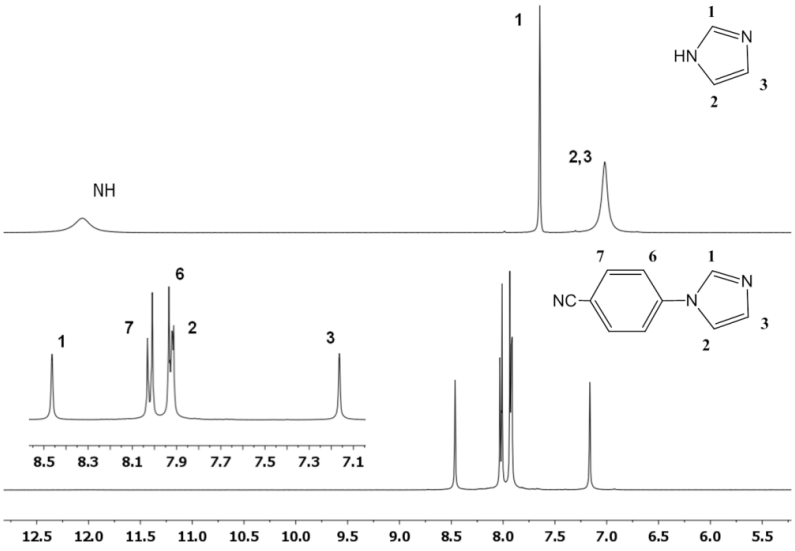

Figure 1.2. ^{1}H-NMR spectra of imidazole (up) and **1C** (down) in DMSO-d_6.

† Labeling of the hydrogen atoms was carried out following that of compound **2C** in order to facilitate a better comprehension for the reader.

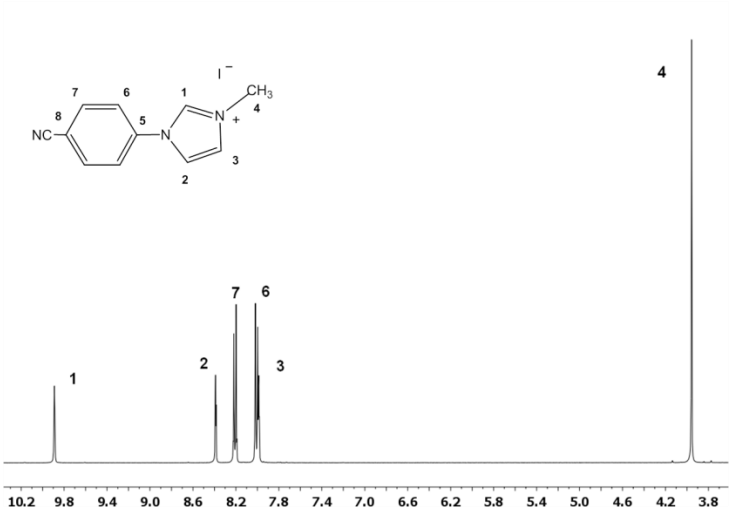

Figure 1.3. ^{1}H-NMR spectrum of **2C** in DMSO-d_6.

The formation of the platinum(II) N-heterocyclic carbenes (**3**) was achieved through the activation of the C1-H bond with Ag_2O to form the silver carbene, and the subsequent transmetalation reaction to platinum(II). The absence of a resonance at ca. 10 ppm in the ^{1}H-NMR spectra, corresponding to H1, the presence of a signal at 177.4 ppm in the ^{13}C{^{1}H} APT NMR, attributed to C1, and the presence of ^{195}Pt satellites in the signals due to H2, H3, C2 and C3 in the corresponding ^{1}H and ^{13}C NMR spectra (see Figure 1.4 and Figure 1.5 for **3C**) brought to light the successful coordination of the NHC to the platinum center through the C1 atom.

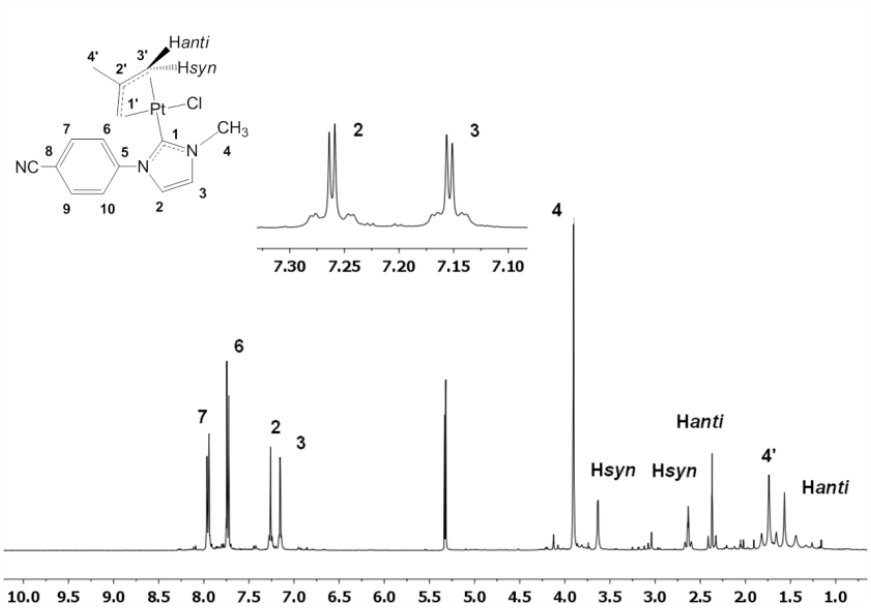

Figure 1.4. ^{1}H NMR spectrum of **3C** in CD_2Cl_2.

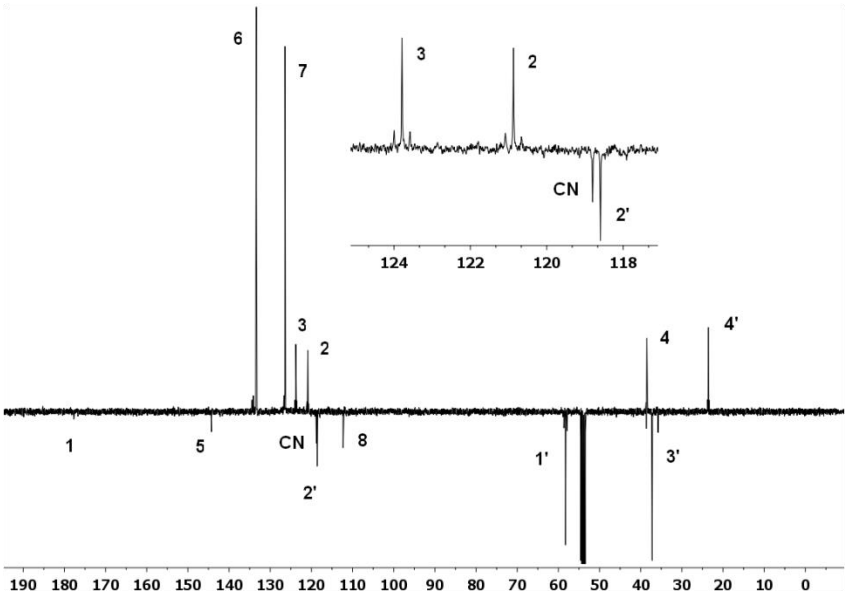

Figure 1.5. $^{13}C\{^{1}H\}$ APT NMR spectrum of **3C** in CD_2Cl_2.

The cyclometalation of **3** to give **4** was accomplished by refluxing a solution of complex **3** in 2-methoxyethanol. The recrystallization of the resulting solid in boiling acetonitrile was required to obtain **4** as pure species. Compound **4** is poorly soluble in common organic solvents but fairly soluble in dimethylsulfoxide (DMSO). Figure 1.6 illustrates the ^{1}H-NMR spectrum of **4C** in dmso-d_6. Evidence of how the activation of the C6-H6 bond led to the formation of the five-membered cycloplatinated complex is the lack of the H6 resonance and the presence of Pt satellites in the signal due to H7.

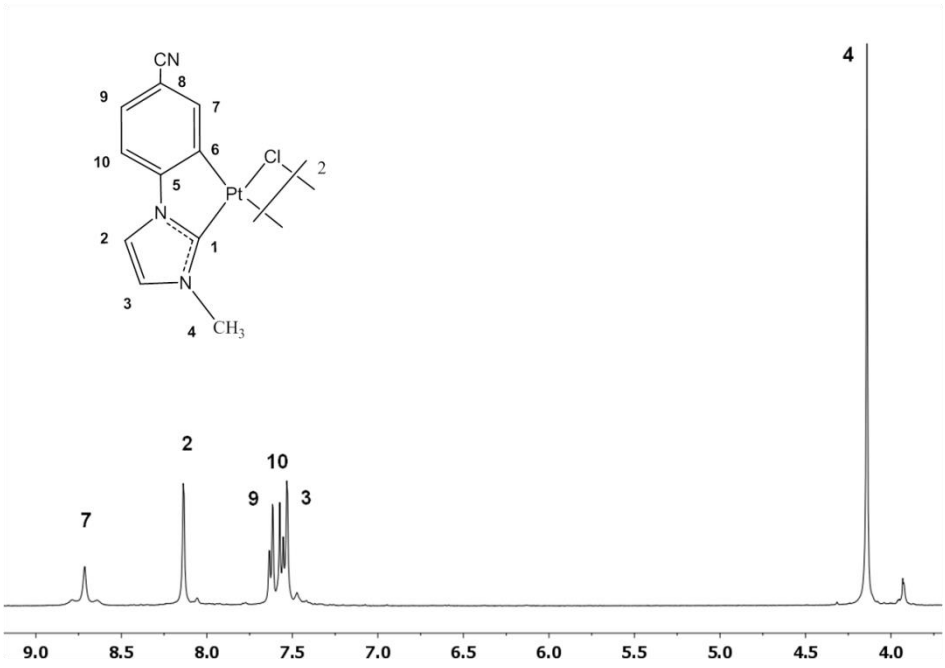

Figure 1.6. ^{1}H-NMR spectrum of **4C** in DMSO-d_6.

It should be noted the presence of two sets of signals. Giving the coordinating capacity of DMSO, they likely correspond to the *cis*-(C*, DMSO) and *trans*-(C*, DMSO) isomers of complex [PtCl(NC-C^C*)(DMSO)] resulting from the cleavage of the dichloro-bridged complex. The lack of selectivity of this process seems to be governed by the transphobia degree of pairs of ligands in trans positions. This fact will be tackled in chapter two.

Chapter 2.

Cleavage of the dichloro-bridge systems: heteroleptic compounds

2.1 SYNTHESIS AND CHARACTERIZATION OF NEW COMPLEXES

2.1.1. Synthesis and Characterization of [PtCl(NC-C^C*)L] (L = PPh_3, py, CNXyl, MMI)

As indicated at the end of Chapter 1, the dichloro-bridge complexes [{Pt(μ-Cl)(R-C^C*)}$_2$] (**4**) can undergo the cleavage of the bridging system *via* the reaction with a coordinating molecule, resulting in the formation of [PtCl(R-C^C*)(L)] as mixtures of the *cis*-(C*,L) and the *trans*-(C*,L) isomers.† This behavior has been investigated by testing this reaction on complex **4C** with a variety of σ-donor ligands (L) such as triphenylphosphine (PPh_3), pyridine (py), 2,6-dimethylphenylisocyanide (CNXyl) and 2-mercapto-1-methylimidazole (MMI) (see Scheme 2.1).

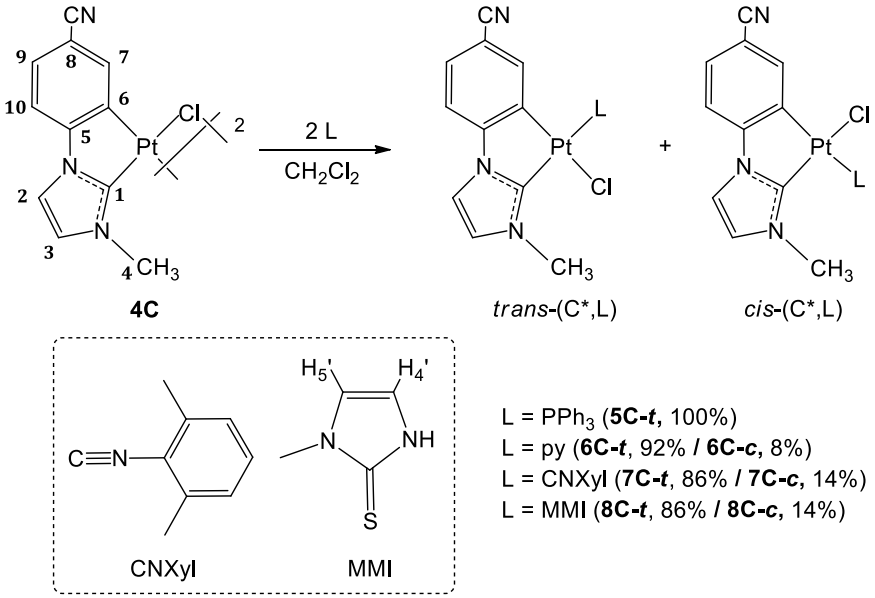

Scheme 2.1. Synthetic route for complexes **5C**-**8C**.

The dinuclear complex [{Pt(*μ*-Cl)(NC-C^C*)}$_2$] (**4C**) reacts with PPh_3, py, CNXyl and MMI in a 1:2 molar ratio at low temperature (–8ºC) (Scheme 2.1 and SI-2.1) to give the mononuclear complexes [PtCl(NC-C^C*)L] (L = PPh_3 (**5C**); py (**6C-*t*/ 6C-*c***), CNXyl (**7C-*t*/ 7C-*c***), MMI (**8C-*t*/ 8C-*c***)).‡ Relevant structural information was provided by multinuclear NMR spectra (see Table 2.1 and Experimental Section in SI-2-1). Compound **5C** was obtained as a pure solid with the *trans*-(C*, PPh_3) being the only isomer obtained. This could be deduced from the ^{1}H and ^{31}P{^{1}H} NMR spectra, where only one set of signals was

† As a simplification, in the following the *cis*-(C*,L) and *trans*-(C*,L) isomers are noted as *c* and *t* respectively.

‡ These compounds have been published (see SI-2.1, SI-2.2; compounds **5, 6, 7** and **8** in the article).

observed (see Figure 2.1), and confirmed by X-ray crystallography (see Figure 2.2, and full data analysis discussion in SI-2.1).

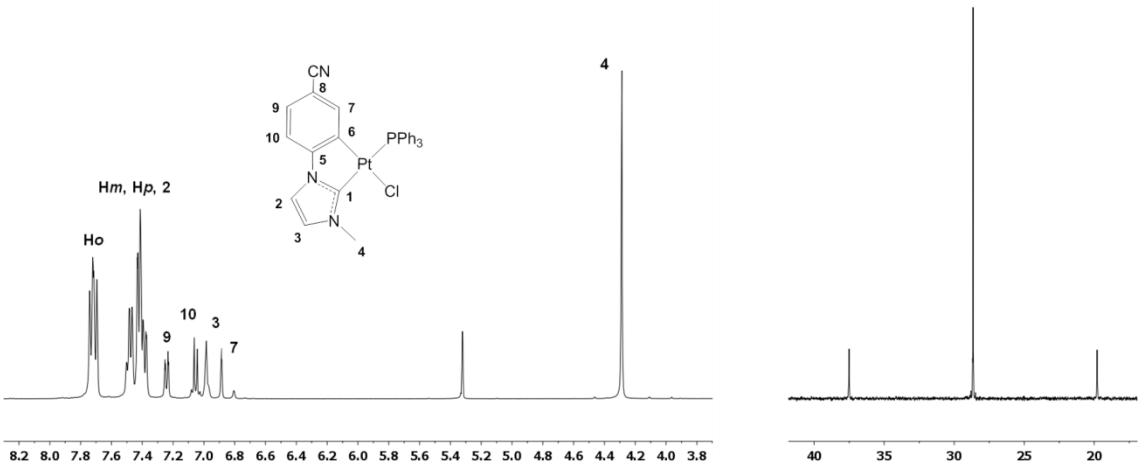

Figure 2.1. ^{1}H (left) and $^{31}P\{^{1}H\}$ NMR (right) spectra of **5C** in CD_2Cl_2.

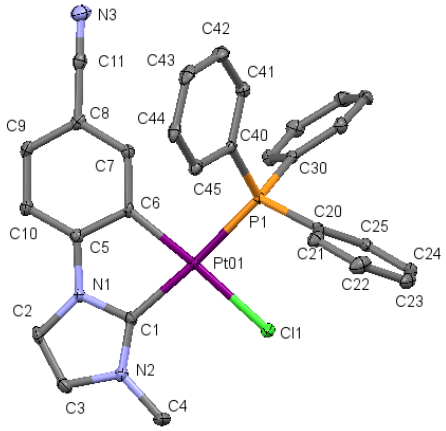

Figure 2.2. Molecular structure of complex **5C·MeOH**. Thermal ellipsoids are drawn at the 50% probability level. Solvent molecules and hydrogen atoms have been omitted for clarity.

By contrast, in all other cases (**6C**-**8C**), the cleavage of the bridging system rendered both isomers *cis*- and *trans*-(C*,L) with the trans isomer being the main one, especially when L is py (**6C**) (see the ^{1}H NMR spectra in Figure 2.3). Attempts to improve the selectivity of the process, by temperature control and reaction time were performed with L= CNXyl, resulting in cis/trans mixtures with the same ratios.

Concerning the ^{1}H NMR, especially sensitive to both, the nature of L and the geometric disposition of the ligands around the Pt centre, are the H7 and the H4 resonances. In all cases, as depicted in Figure 2.3, the H7 resonances of the *trans*-(C*,L) isomers appear more shielded than those of the cis-derivatives.

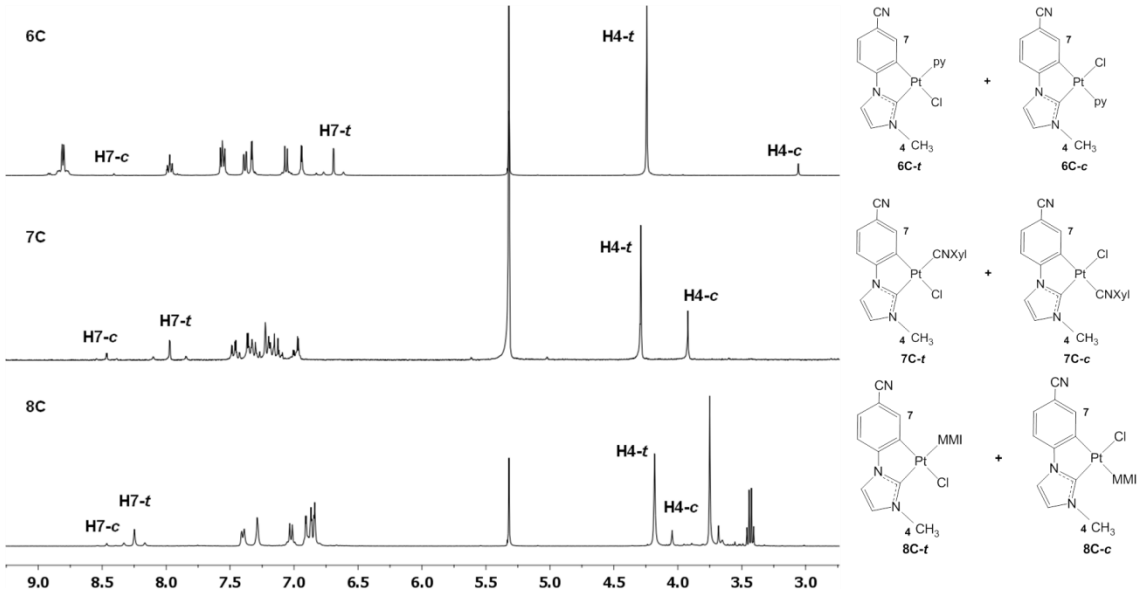

Figure 2.3. ^{1}H NMR spectra of compounds **6C** (up), **7C** (middle) and **8C** (down) in CD_2Cl_2.

Within the trans isomer complexes, in particular, when L = PPh_3 (**5C**) and py (**6C-*t***), the H7 resonance undergoes an important upfield shift comparing with that in complexes with L = CNXyl (**7C-*t***) and MMI (**8C-*t***) (Table 2.1). This effect has been associated with the anisotropic shielding effect caused by the proximity in space of the aromatic ring current of the phenyl (**5C**) and pyridine (**6C-*t***) groups to the H7.[33] This C–H7 ⋯ π interaction was also observed in the X-ray structure of **5C**, as discussed in SI-2.1. Likewise, in the *cis*-(C*,L) isomer of complexes **6C**–**8C**, the H4 resonance is the one that suffers the anisotropic shielding effect since it moves upfield in relation to that of the trans one, this effect being more intense when L is pyridine (3.06 **6C-*c***; 4.24 **6C-*t***). In both geometric isomers, the H7 signal appears accompanied by platinum satellites. The Pt-H7 coupling constants of the trans isomers are larger than those of the cis derivatives, which is in agreement with the higher trans influence of the L ligands comparing to the Cl one.[27e, 34]

As expected, the ^{195}Pt{^{1}H} NMR spectrum of **5C** exhibits only a doublet at -4227 ppm with a ^{195}Pt–^{31}P coupling constant of 2868 Hz, while two ^{195}Pt resonances were observed for complexes **6C**-**8C** (Figure 2.4). The main one corresponds to the trans isomer and appears less shielded than that of the cis one, in all three cases. The ^{195}Pt–^{31}P coupling constant value in **5C** is typical of a P–Pt–C trans arrangement[34b, 35] making evident the strong trans influence of the carbene atom (C*).

Table 2.1. Significant NMR data for compound characterization[a]

	$\delta^{1}H$ (J_{Pt-H})		$\delta^{13}C$ (J_{Pt-C})			$\delta^{31}P$ (J_{Pt-P}) [J_{P-P}]	$\delta^{195}Pt$
	H7	H4	C1	C7	C3		
5C[b]	6.88 (64.0)	4.29	170.1	141(57.0)	124.3 (26.0)	28.6 (2868.0)	- 4227.0
6C-*t*	6.69(61.8)	4.24	152.7	135.2 (37.8)	123.1 (38.4)		
6C-*c*	8.41 (55.1)	3.06					
7C-*t*	7.97 (77.3)	4.28	167.7	140.8 (72.4)	123.9 (30.9)		
7C-*c*	8.45 (47.2)	3.92					
8C-*t*	8.27 (65.9)	4.19	159.3	135.4 (37.1)	123.6 (37.3)		
8C-*c*	8.47 (57.5)	4.04					
9C[b]	6.85 (58.8)	2.87	171.2	142.9 (55.4)	124.6 (31.3)	28.2 (2881.6)	- 4274.6
10C[b]	7.02 (50.7)	3.91	169.3	143.5 (51.0)	125.3	19.3 (2585.2)	- 4697.0
11C[b]	6.97 (59.4)	4.08	170.7	142.6 (56.1)	126.7	26.1 (2786.3)	- 4533.7
12C	7.34 (50.6)	3.04	172.7	142.5 (54.0)	124.9 (29.0)	(*t*-C*): 50.2 (2673.8) [7.0] (*c*-C*): 43.1 (2014.6)	- 4996.0

[a] δ (ppm), J (Hz), [b] *trans*-(C*,P) isomer is the only one observed.

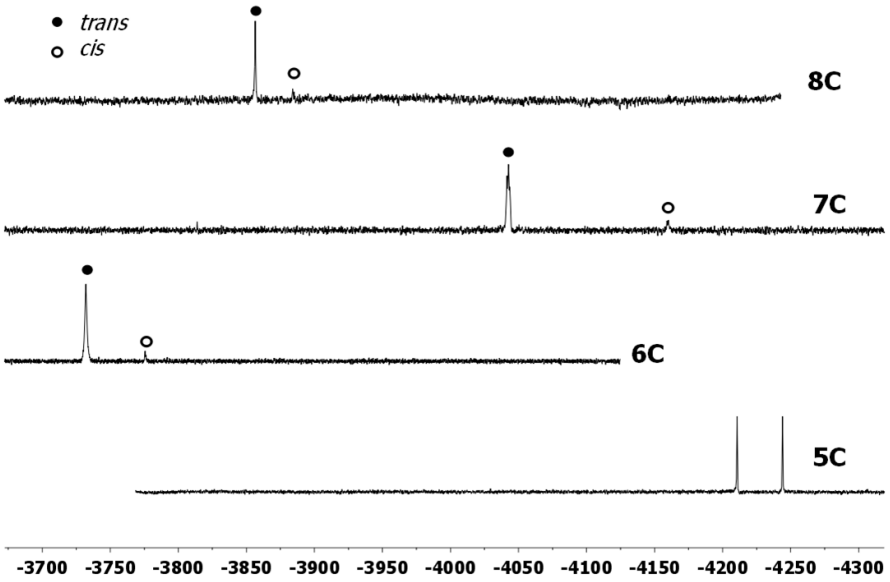

Figure 2.4. $^{195}Pt\{^{1}H\}$ spectra of **5C**-**8C** in CD_2Cl_2.

The mononuclear complexes [PtCl(R-C^C*)PPh_3] (R-C = Naph (**5A**); R = CO_2Et (**5B**)) were prepared later from **4A** and **4B** with the *trans*-(C*,PPh_3) being the only isomer† and their spectroscopic features matched with those of **5C**.

2.1.2. Synthesis and Characterization of the Cationic Complexes: *trans*-(C*, P)-[Pt(R-C^C*)(PPh_3)L']PF_6 (R-C = Naph, L' = py (9A); R = CO_2Et, L' = py (9B); R = CN, L' = py (9C), CNXyl (10C), MMI (11C)) and [Pt(NC-C^C*)(dppe)]PF_6 (12C)).

We aimed to prepare heteroleptic NHC cyclometalated compounds to explore the effect of different ancillary ligands on their photophysical properties. First of all we performed the synthesis and characterization of compounds labeled as **C** following pathways a and b in Scheme 2.2. The reaction of compound **5C** with 1 equivalent of L' (L' = py, CNXyl, MMI) in the presence of KPF_6 rendered compounds **9C**-**11C** with general formula [Pt(C^C*)(PPh_3)(L')]PF_6 (Scheme 2.2, path a). The X-ray crystal structures (see Figure 2.5; full data and discussion in SI-2.1), ^{1}H and $^{31}P\{^{1}H\}$ NMR spectra showed that the PPh_3 remains coordinated *trans* to the C*. Interestingly, compound **10C** could also be prepared by adding KPF_6 and PPh_3 to the mixture of cis/trans isomers of complex **7C** (see Scheme 2.2, path b). Therefore, in this case, the main fraction of this reaction does not proceed with stereoretention, since the CNXyl ligand, that is located trans to C* in **7C-*t***, migrates to the cis position by the coordination of the PPh_3.

† These compounds have been published (see SI-2.3, SI-2.4; compounds **1A** and **1B** in the article).

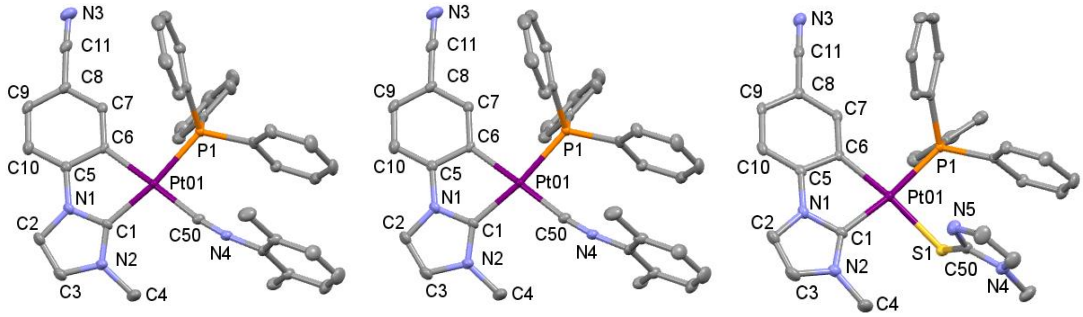

Figure 2.5. X-ray crystal structures of the cation complexes **9C** (left), **10C** (middle), **11C** (right).

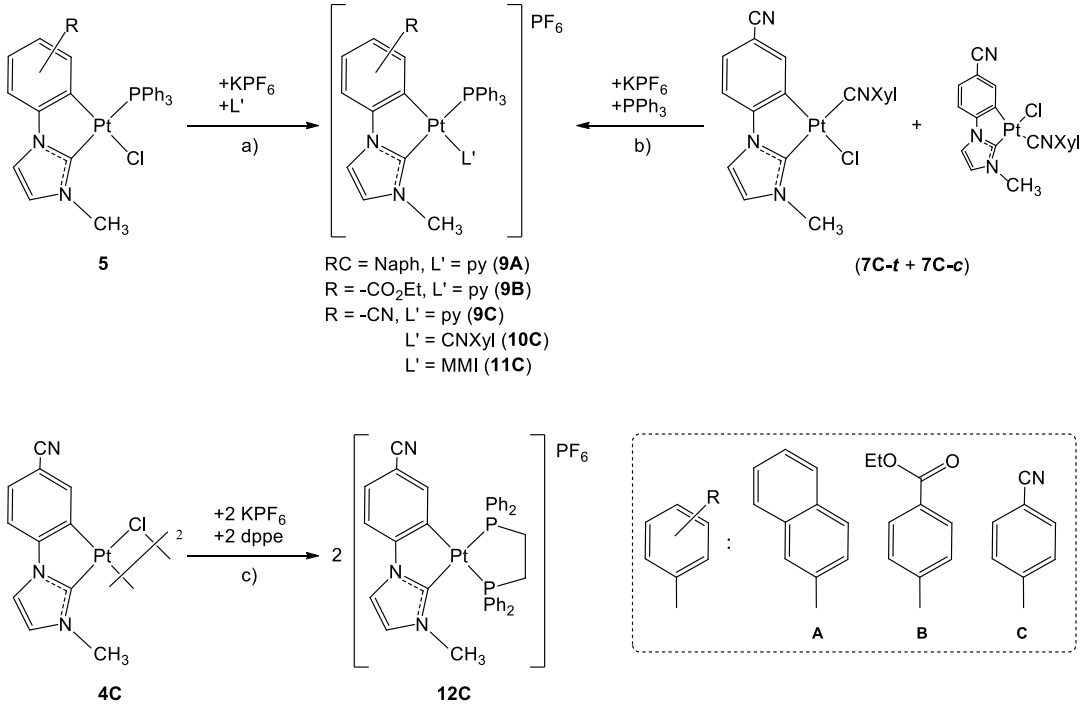

Scheme 2.2. Synthetic pathways to cationic complexes.

In addition, when a suspension of **4C** in acetone was treated with KPF_6 and dppe (1:2 molar ratio) compound **12C** was formed, a mononuclear species with the dppe acting as a chelate ligand (see Scheme 2.2, path c and X-ray and multinuclear NMR studies).†

Relevant structural information arises from the multinuclear NMR spectra (Table 2.1 and SI-2.1 and 2.2 for full data and Figures). The $^{31}P\{^{1}H\}$ NMR spectra of **9C-11C** show a singlet flanked by platinum satellites. The δP and ^{195}Pt-^{31}P coupling constants values are quite similar to those found in complex **5C**, in agreement with a *trans*-(C*, PPh_3) arrangement in

† This compound has also been published (see SI-2.1, SI-2.2; compound **12** in the article).

these complexes. In the $^{31}P\{^{1}H\}$ NMR spectrum of **12C**, the two different P atoms appear as two doublets accompanied by Pt satellites. The chemical shifts and the observed P-P coupling of 7 Hz confirm the chelating arrangement of the dppe around the platinum center.[36] Significant are also the $^{195}Pt\{^{1}H\}$ spectra (see Figure 2.6 and Table 2.1) which confirm the presence of a single isomer in each case. They exhibit a doublet for compounds **9C-11C** and a doublet of doublets for **12C** due to the coupling with two ^{31}P nuclei, these chemical shifts are ranging from – 4274 to – 4996 ppm.

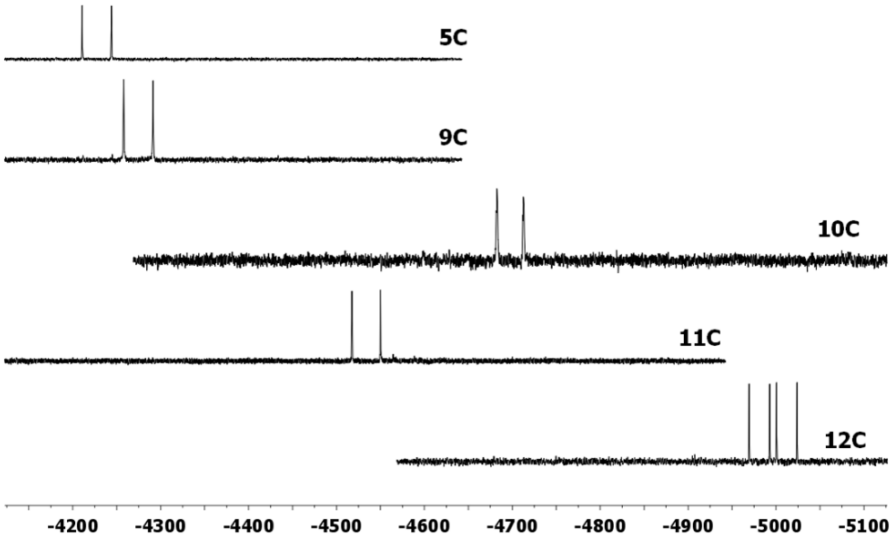

Figure 2.6. $^{195}Pt\{^{1}H\}$ spectra of **5C** and **9C-12C** in CD_2Cl_2.

According with the *trans*-(C*, PPh_3) arrangement of these compounds, H7 resonances appear in the range of 6.80 – 7.30 ppm due to the anisotropic shielding effect caused by the proximity in space of the phenyl groups of the PPh_3. When L' is pyridine (**9C**) and dppe (**12C**), the H4 resonance also suffers the anisotropic shielding effect, since it moves upfield (2.87 **9C**, 3.04 **12C**) comparing with that in complexes **10C** (3.91) and **11C** (4.08).

On view of the obtained results we expanded the work to the synthesis of **9A** and **9B** following path "a" in Scheme 2.2. Their molecular structures determined by single crystal X-ray diffraction studies confirmed the proposed structure for them.†

† Full data and discussion for compounds **2A** (**9A**) and **2B** (**9B**) in SI-2.3 and SI-2.4.

2.1.3. Discussion about the results shown in sections 2.1.1 and 2.1.2 for compounds 5C-12C.

As shown above, the cleavage of the chlorine-bridge system in [{Pt(μ-Cl)(NC-C^C*)}$_2$] (**4C**) by different ancillary ligands (L) led to the clean formation of *trans*-(C*, L)-[PtCl(C^C*)L] when L is PPh_3 (**5C**). If L is py, CNXyl and MMI, the bridge-splitting reaction gave mixtures of cis/trans isomers (**6C-8C**).

In an attempt to explain this behavior we have used the term transphobia degree (T) of pairs of trans ligands, which has been accepted by many authors to explain the geometries of stable square-planar complexes of d^8 transition metals. The degree of T has been assumed to be related to the trans influence, in such a way that the greater the trans influence of two ligands, the greater the transphobia, and the cis disposition of them will be the favored geometry. In this sense the heteroleptic complexes [PtCl(C^N)L] (HC^N = 3,8-dinitro-6-phenylphenanthridine, 2-(4-bromophenyl)imidazol[1,2-*a*]pyridine; L= PPh_3, tht, C≡NR (R = ^{t}Bu, 2,6-dimethylphenyl)) and [Pt(C^P)(C≡CPh)L] (C^P= $CH_2C_6H_4P$(o-tolyl)$_2$-κC,P; L = CO, py, tht) exist as the *trans*-(C,Cl) isomer as expected on the basis of the transphobia degree (T) of pairs of trans ligands.[33a, 34a] However, the steric requirements of the ligands involved can also play an important role in determining the geometries of these complexes. In this sense, complex [Pt(C^P)(C≡CPh)PPh_3], exhibits the *trans*- (C, C≡CPh) geometry instead of the expected one considering electronic preferences (*trans*-C,PPh_3), which was attributed to the crowding associated with the cis disposition of the P(o-tolyl)$_2$ and the PPh_3 group.[34a]

Therefore, we have tried to explain the preferred geometry for complexes [PtCl(NC-C^C*)L] (**5C-8C**) and [Pt(C^C*)(PPh_3)L]$^+$ (**9C-11C**) on the basis of the transphobia effect (T). With this purpose we have studied the relative trans influences of the two σ Pt-C bonds present in the Pt(C^C*) unit, both expected to have a great trans influence, and those of the auxiliary ligands (Cl, PPh_3, py, CNXyl, MMI), comparing the $^1J_{Pt\text{-}P}$, $^2J_{Pt\text{-}C}$ and $^3J_{Pt\text{-}H}$ values affected by the ligands located at their trans positions (see Table 2.1 and SI-2.1).

The $^1J_{Pt\text{-}P}$ values observed for complexes *trans*-(C*,P)-[PtCl(NC-C^C*)(PPh_3)] (**5C**), and [Pt(NC-C^C*)(PPh_3)L']PF_6 (L' = py (**9C**), CNXyl (**10C**), MMI (**11C**)) range from 2585.2 to 2881.6 Hz, which are typical of a P-Pt-C trans arrangement.[34b, 35] These values are also very similar to those observed in Q[Pt(CH_2-C_6H_4-P(o-tolyl)$_2$)(C≡CPh)$_2$] (Q = Li^+ (2746 Hz), NBu_4^+ (2603 Hz)) with the Pt-P bond trans to a Pt-$C_{acetylide}$ one.[34a] In addition, the $^1J_{Pt\text{-}P}$ corresponding to the P trans to C* (2673.8 Hz) in [Pt(NC-C^C*)(dppe)]PF_6 (**12C**), resulted to be similar to that observed in complexes with phosphine ligands located in the trans

position, such as [Pt(C^P)(dppe)]$^+$[C^P = {(R)-1-[1-diphenylphosphino]ethyl}naphthyl-C,P; $J_{Pt\text{-}P\ (transP)}$=2770Hz],[36c] or [Pt(dppe)(PAn-H)]$^+$ [PAn = 9-diphenylphosphinoanthracene; $J_{Pt\text{-}P\ (transP)}$=2796],[37] indicating that the C* displays a great trans influence, similar to alkynyl or phosphine ligands.

Then, we focused again on complex [Pt(C^C*)(dppe)]PF_6 (**12C**) and we observed the $^1J_{Pt\text{-}P}$ values for the P trans to C_{Ar} and C* are 2014.6 and 2673.8 Hz respectively. These values indicate that the trans influence of C_{Ar} is slightly greater than that of C*. The same assessment was inferred from the $^3J_{Pt\text{-}Ho(py)}$ in complex **6C** which exhibits different values when pyridine is facing C_{Ar} (**6C-*c*,** 20.7 Hz) or C* (**6C-*t*,** 28.0 Hz). Moreover, an evaluation of the electronic effects of the different L ligands can be undertaken by comparison of the spectroscopic and crystallographic data of complexes with the same stoichiometry and configuration, such as *trans*-(C*, P) [Pt(NC-C^C*)(PPh_3)L]$^{0,+}$ (L = Cl (**5C**), py (**9C**), CNXyl (**10C**), MMI (**11C**)) or *cis*-(C*,L) [PtCl(NC-C^C*)L] (L = py (**6C-*c***), CNXyl (**7C-*c***), MMI (**8C-*c***)) (Table 2.1). On the basis of the observed $^3J_{Pt\text{-}H7}$ (64.0 **5C**, 58.8 **9C,** 50.7 **10C**, and 59.4 Hz, **11C**) and $^2J_{Pt\text{-}C7}$ (57.0 **5C,** 55.4 **9C**, 51.0 **10C** and 56.1 Hz **11C**) in the *trans*-(C*, P) named complexes, the trans influence order seems to be CNXyl > py ~ MMI > Cl.

An additional comparison of the values of δC1 (170.1 ppm **5C**, 152.7 **6C-*t***; 167.7, **7C-*t*;**159.3, **8C-*t***) and $^3J_{Pt\text{-}C3}$ (26.0 Hz **5C**, 38.4 **6C-*t***; 30.9, **7C-*t*;** 37.3, **8C-*t***) in complexes *trans*-(C*,L)-[PtCl(NC-C^C*)L] (L = PPh_3 (**5C**), py (**6C-*t***), CNXyl (**7C-*t***), MMI (**8C-*t***)) indicates that the trans influence of PPh_3 is even greater than that of CNXyl. Finally, the X-ray data analysis of **5C** and **9C-12C** (SI-2.1) indicate that the longest Pt-C6 distances correspond to those of **12C** and **10C**, with the dppe and CNXyl located at the trans position. Therefore, the trans influence of all the used ancillary ligands seems to follow the order: PPh_3 / dppe > CNXyl > py ~ MMI > Cl.

Taking into account all these assumptions the T[C_{Ar}/L] > T[C*/L] and T[C_{Ar}/PPh_3] > T[C_{Ar}/CNXyl] > T[C_{Ar}/py] ~ T[C_{Ar}/MMI] > T[C_{Ar}/Cl]. Therefore, the T[C_{Ar}/PPh_3] should be greatest one and the experimental results seem to indicate that the difference between T[C_{Ar}/PPh_3] and T[C*/PPh_3] is big enough to direct the clean formation of *trans*-(C*, PPh_3) complexes **5C**, **9C-11C**.

However, the difference between T[C_{Ar}/L] and T[C*/L] (L = py, CNXyl, MMI, Cl) is, in each case, not big enough to avoid the formation of mixtures of isomers. Based on the order of T[C_{Ar}/L] named above, the cleavage of the chlorine-bridge system in [{Pt(μ-Cl)(C^C*)}$_2$] (**4C**) by py to give complex **6C** was expected to be no more stereoselective than that with CNXyl or MMI, but it is. Other factors to promote the greater stability of **6C-*t***, such as the

steric hindrance between py and the imidazol fragment of C^C* in the cis isomer can be excluded. Given that the H7 and H4 resonances in **6C-*t*** and **6C-*c*** suffer a great anisotropic shielding effect, which was discussed in the NMR section, we considered the C–H···π (py) interactions to be involved in it. C–H···π interactions have been known to play a key role in the stereoselectivity of coordination compounds amongst other fields in chemistry.[38] It has been widely reported that intramolecular C–H···π hydrogen bonds can induce the formation of single linkage isomers.[39] In both isomers of **6C**, a CH···π interaction could be possible: Csp^3–H4 (Me) ··· π (py) in **6C-*c*** and a T-shaped Csp^2–H7 (Ar) ··· π (py) in **6C-*t***. As reported before, the interaction energy involving a T-shaped aromatic CH is somewhat stronger than that of the aliphatic ones.[38a, 40] So, we would expect **6C-*t*** to be more stable than **6C-*c***. DFT calculations for models of **6C-*c*/-*t*** in solution of CH_2Cl_2 were carried out (see Figure 2.7). In effect, isomer **6C-*t*** with the C–H7 pointing at the pyridine ring is 1.01 Kcal mol^{-1} more stable than **6C-*c***. This subtle difference in energy added to the bigger T[C_{Ar}/py)] vs T[C*/py] results to be reasonably determining for the high stereoselectivity of isomers in **6C**.

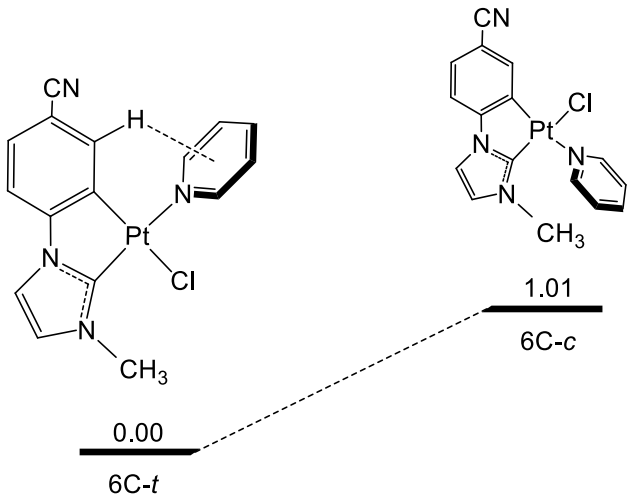

Figure 2.7. DFT- computed energies for the **6C-*c*/-*t*** isomers (ΔE, kcal mol^{-1}).

In complexes **5C** , **9A**, **9B**, and **9C-11C**, their X-ray structures and NMR data also show the presence of Csp^2–H7 (Ar) ··· π interactions, which will contribute together with the difference of T[C_{Ar}/L] vs T[C*/L] to the selective formation of the *trans*-(C*, PPh_3) isomer, as experimentally observed.

2.2 Optical properties and DFT/TD-DFT calculations.

Absorption spectra and DFT/TD-DFT calculations. Compounds [PtCl(R-C^C*)L] (R-C = Naph, L = PPh_3 (**5A**); R= CO_2Et, L = PPh_3 (**5B**); R= CN, L = PPh_3 (**5C**), py (**6C**), CNXyl (**7C**), MMI (**8C**)) resulted to be scarcely emissive. By contrast, the heteroleptic ionic compounds [Pt(R-C^C*)(PPh_3)L']PF_6 (R-C = Naph, L' = py (**9A**); R = CO_2Et, L' = py (**9B**); R = CN, L' = py (**9C**), CNXyl (**10C**), MMI (**11C**)) showed a bright emission and were thoroughly investigated (all the information can be seen in SI-2.3 and SI-2.4). The photophysical features of two sets compounds **9A**-**9C** and **9C**-**11C** were studied in order to establish the influence of both the cyclometalated NHCs and the ancillary ligands on their absorption and emission properties.

UV-vis spectra of compounds **9A**-**9C** in diluted CH_2Cl_2 solutions show high energy (HE) absorption bands at $\lambda_{abs} \leq 300$ nm ($\varepsilon > 10^4$ M^{-1} cm^{-1}), attributable to singlet intraligand (^{1}IL) transitions of the NHC moiety. Spectra of **9B** and **9C** are rather similar, pointing out the similarities of the electronic features of the two substituents at the phenyl ring of the NHC ligand (R = CN, CO_2Et), and different from the naphthyl counterpart, **9A** (see Figure 2.8). The latter exhibits an additional low-energy (LE) band at $\lambda_{abs} \sim 350$ nm ($\varepsilon > 10^3$ M^{-1} cm^{-1}), which is very similar to that observed in complexes with the same cyclometalated NHC ligand (Naph^C*).[29e, 30] It appears to be slightly shifted to higher energies compared to the isocyanide derivatives, [(Naph^C*)Pt(CNR')$_2$]PF_6 (R' = *t*-Bu, Xyl),[30] described in Chapter 3, which indicates participation of the ancillary ligands in it.

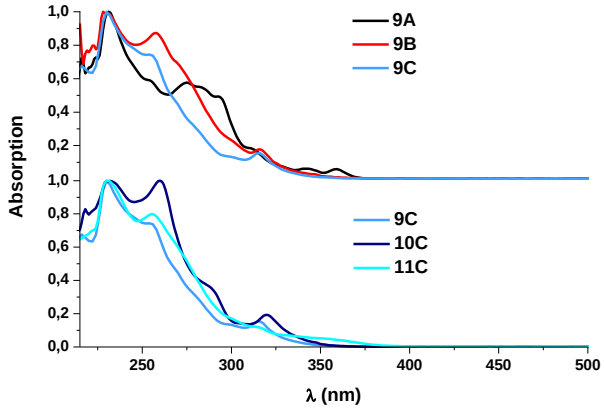

Figure 2.8. Absorption spectra in CH_2Cl_2 ($5x10^{-5}$ M) at r.t.

The involvement of the auxiliary ligands in the lowest energy absorptions can also be noticed for complexes **9C**–**11C**. The one corresponding to the isocyanide derivative, **10C** (λ = 320 nm), is shown to be clearly red-shifted with respect to the pyridine one, **9C** (λ = 316 nm), while that of **11C**, becomes a less intense shoulder (λ = 314 nm) accompanied by

an additional band at λ = 352 nm. This lowest-energy absorption of **11C** (352 nm) obeys Beer's Law, suggesting that it is due to transitions in the molecular species and that no significant aggregation occurs within the concentration range from 10^{-3} to 10^{-6} M (see Figure S9 in SI-2.4). UV-vis spectra of all complexes were recorded in different solvents (Table S2 in SI-2.4) showing no significant solvatochromism, except for compound **9A** (see Figure S10 in SI-2.4). It presents a slightly negative solvatochromism in the lower energy spectral region (λ > 340 nm), which indicates the existence of charge-transfer (CT) transitions.[15a]

Solid state diffuse-reflectance spectra (see Figure S11 in SI-2.4) show no particular differences compared to those observed in solution of CH_2Cl_2. Therefore, the weak intermolecular π-π and C-H···F interactions observed in their X-ray structures (at ca. 100 K) seem to have no important effects in the absorption at room temperature.

DFT and TD-DFT calculations in a solution of CH_2Cl_2 for **9A–9C** and **11C** have been carried out to provide correct assignments for the UV-vis absorptions and also to evaluate the effect of both cyclometalated R–C^C* and ancillary ligands (L) on the photophysical properties. Full data corresponding to these calculations can be seen in SI-2.3 and SI-2.4. The relative compositions of the frontier molecular orbitals (FOs) in the ground state are reported in Table 2.2. As can be seen, the composition of the FOs of **9B** and **9C** are practically identical, which confirm the similarities of the electronic features of the R-C^C* (R = CN, CO_2Et) cyclometalated groups. In these cases, the highest occupied molecular orbitals (HOMOs) are mainly constructed from π-orbitals of the C^C* ligand (ca. 75%) and dπ-orbitals of the Pt center (25 %) and the lowest unoccupied molecular orbitals (LUMOs) are similar to the HOMOs but with some contribution of the ancillary ligands: 20% Pt, ca. 65% C^C*, 8% PPh_3, and 7% py. However, in case of **9A**, the HOMO is almost entirely localized on the Naph^C* fragment (90%) while the LUMO is mostly centered on the pyridine (70%) with small contributions of Naph^C*(15%) and Pt (10%) orbitals. By a comparison of **9C** and **11C**, it can be observed that in **11C** the presence of MMI instead of py in the coordinating sphere of platinum leads to a HOMO mainly based on the auxiliary ligand (MMI, 85%) with only a low contribution of Pt and R-C^C*orbitals, while no significant changes are induced in the LUMO composition with respect to that in **9C**, which is mostly centered on the R-C^C* orbitals. Thus, by modification of both ligands, either the R-C (C^C*) or L, the nature and composition of the FOs, and therefore the nature of the lowest energy singlet transition, change considerably. The calculated S_1 in CH_2Cl_2 (Table 2.3) arises from HOMO to LUMO transition for **9B**, **9C** and **11C,** while for **9A**, it arises mainly from H→L (39%) and H→L+1 (36%) transitions.

Considering that the calculated allowed absorptions are in good qualitative agreement with the experimental UV-vis spectra (Figure 2.9 and Figures S13-S15 in SI-2.4) the lowest-energy absorption bands can be attributed to mixed transitions: ILCT [π(NHC)] → π*(NHC)/LL'CT [π(NHC) → π*(L')] for **9B** and **9C** and LL'CT [π(NHC) → π*(py)]/ ILCT [π(NHC) → π*(NHC)]/LMCT [π(NHC) → 5d(Pt)] for **9A** and L'LCT [π*(MMI) → π*(NHC)]/L'MCT [π*(MMI) → 5d(Pt)] for **11C**. Complex **11C** shows also a very weak calculated absorption at 336 nm (S_2, see Figure 2.9) that implicates the H–1→L (95%) transition. Its energy and electronic nature are very similar to the calculated S_1 transition in complexes **9B** and **9C**.

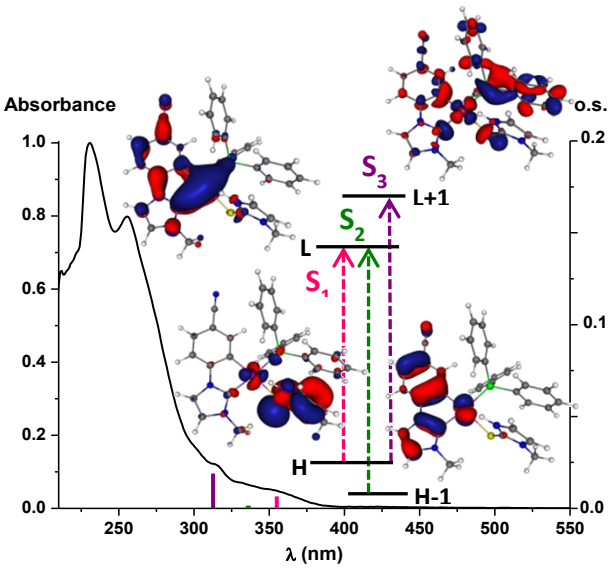

Figure 2.9. Normalized UV–vis absorption spectrum of **11C** in CH_2Cl_2, calculated transitions in CH_2Cl_2 (colored bars) with the diagrams of the frontier orbitals.

Emission spectra. The phosphorescence of complexes **9A-C**, **10C** and **11C** in CH_2Cl_2 (10^{-5} M, 298 K) is quenched, even under an argon atmosphere, which may be due to thermal nonradiative processes,[41] but they show intense phosphorescence in rigid matrix (see Table 2.4). In CH_2Cl_2 solution at 77 K all compounds show well resolved vibronic emissions, and their excitation profiles mimic the corresponding UV-Vis absorptions. In the case of **9A,** containing a Naph^C* cyclometalated group, the phosphorescence appears at λ_{max} ~ 474 nm with a substantially long monoexponential decay (~ 480 μs).

Table 2.2. Population analysis (%) of frontier MOs in the ground state for **9A—9C** and **11C** in solution of CH_2Cl_2

MO	eV				Pt				R-C^C*				PPh_3				L			
	9A	**9B**	**9C**	**11C**	**9A**	**9B**	**9C**	**11C**	**9A**	**9B**	**9C**	**11C**	**9A**	**9B**	**9C**	**11C**	**9A**	**9B**	**9C**	**11C**
L+1	-1.57	-1.66	-1.72	-1.37	26	5	5	23	34	7	4	25	14	1	1	46	26	87	90	6
L	-1.72	-1.89	-1.99	-2.00	11	20	20	23	15	64	69	67	4	8	7	7	70	8	4	3
H	-6.28	-6.72	-6.88	-6.46	9	25	24	9	90	74	75	3	1	1	1	3	0	0	0	85
H-1	-6.60	-7.16	-7.24	-6.85	18	61	56	24	80	8	4	74	1	30	39	1	1	1	1	1

Table 2.3. Selected singlet excited states calculated by TD-DFT for **9A—9C** and **11C** in solution of CH_2Cl_2

Comp	λ_{exc} (calc.)/nm	o.s.	Transition (% contribution)*	Assignment
9A	S_1: 335.92	0.0942	H → L (39%); H → L+1 (36%)	^{1}LL'CT,^{1}ILCT,^{1}LMCT
9B	S_1: 337.30	0.0066	H → L (93%)	^{1}ILCT, ^{1}LL'CT
9C	S_1: 331.8	0.0047	H → L (94%)	^{1}ILCT, ^{1}LL'CT
11C	S_1: 355.3	0.0066	H → L (92%)	^{1}L'LCT, ^{1}L'MCT
	S_2: 336.4	0.0015	H–1 → L (95%)	^{1}ILCT, ^{1}LL'CT
	S_3: 312.7	0.0190	H → L+1 (76%)	^{1}L'L'CT, ^{1}L'LCT, ^{1}L'MCT

* Transitions with contributions < 10% were not included

Table 2.4. Photophysical data for complexes **9A–9C**, **10C** and **11C**.

Com.	Media (T/K)	λ_{ex} (nm)	λ_{em} (nm)	τ (μs)[d]	ϕ[e]
9A	CH_2Cl_2[a](77)	355	474_{max}, 511, 551, 598	481	
	CH_2Cl_2[b] (77)	357	474_{max}, 511, 551, 598	478	
	PMMA Film	340	476_{max}, 511, 600_{sh}		0.87
	Solid (298)	368	557, 600_{max}, 650	35	0.06
	Solid (77)	361	541_{sh}, 552, 581_{sh}, 597_{max}, 648_{sh}	65	
9B	CH_2Cl_2[a](77)	315	444_{max}, 475, 506, 545_{sh}	23	
	CH_2Cl_2[b] (77)	360	447_{max}, 477, 509, 545_{sh}	24	
	PMMA Film	330	448, 476_{max}, 503, 543_{sh}		0.68
	Solid (298)	360	455, 474_{max}, 501	2.6	0.19
	Solid (77)	364	455, 474_{max}, 505	15	
9C	CH_2Cl_2[a](77)	314	444_{max}, 474, 505, 538_{sh}	23	
	CH_2Cl_2[b] (77)	355	447_{max}, 477, 509, 538_{sh}	22	
	PMMA Film	320	446, 472_{max}, 500, 540_{sh}		0.93
	Solid (298)	350	446, 472_{max}, 500, 540_{sh}	17	0.35
	Solid (77)	355	447, 469_{max}, 500, 540_{sh}	25	
10C	CH_2Cl_2[a](77)	320	449_{max}, 480, 513, 543	26.9	
	CH_2Cl_2[b] (77)	350	450, 483_{max}, 515, 545, 615	24	
		400	545_{max}, 615_{sh}	1.6	
		450	545_{sh}, 615_{max}	2.0	
	PMMA Film	340	453, 480_{max}, 511, 550_{sh}		0.87
	Solid (298)	465	590	1.2	0.11
	Solid (77)	350	465, 488_{max}, 524	20	
		390	465, 488, 545_{max}	1.8	
		460	545_{sh}, 615_{max}	2.2	
11C[c]	CH_2Cl_2[a](77)	314, 355	444_{max}, 474, 506, 543_{sh}	19	
	CH_2Cl_2[b] (77)	320, 375	449_{max}, 479, 512, 548_{sh}	14	
		450	558	4	
	Solid (298)	370	449, 474_{max}, 505, 538_{sh}	2.6	0.11
	Solid (77)	370	444, 474_{max}, 506, 538_{sh}	12.7	

a = 10^{-5}M; *b* = 10^{-3}M; *c* = not soluble to prepare PMMA films in CH_2Cl_2 10^{-2} M; *d*= measurements at λ_{max}; *e* = PMMA films in Ar atmosphere.

The analogous complexes, **9B**, **9C**, as well as **10C** and **11C**, all of them containing R-C^C* (R = CN, CO_2Et) cyclometalated groups, exhibit a phosphorescent emission (λ_{max} ~ 450 nm) blue-shifted with respect to **9A** (see Figure 2.10) and shorter decays (about 20 μs). Among those complexes containing the NC-C^C* cyclometalated group, **9C–11C**, the Xyl derivative (**10C**) produces an emission slightly shifted to lower energies with respect to those of **9C** and **11C**.

The emissive behavior (emission energy and lifetime) of **9A** in CH_2Cl_2 rigid matrix is very similar to that observed in other compounds containing the same "(Naph^C*)Pt" fragment.[29e, 30] Thus, taking into account all these data and the TD-DFT calculations, the phosphorescent emissions of **9A** can be mainly assigned to ^{3}ILCT [π(NHC) → π*(NHC)] transitions mixed with some, if any, ^{3}LL'CT [π(NHC) → π*(L)]/^{3}LMCT [π(NHC) → 5d(Pt)]

character. The emission bands of **9B** and **9C–11C** are tentatively ascribed to transitions of monomeric species derived from ^{3}ILCT [π(NHC) → π*(NHC)]/^{3}LL'CT [π(NHC) → π*(L')] excited states. It is worth noting that the LE absorption (S_1) of **11C** was attributed in the UV-Vis Section to mixed transitions L'LCT [π*(MMI) → π*(NHC)]/L'MCT [π*(MMI) → 5d(Pt)]. However, the emission features are identical with those observed for **9B**, **9C** and **10C**, which correspond to the assignment of the S_2-calculated absorption. In fact, if assuming the lowest energy absorption (S_1) as the emissive state, the geometry of the first excited state (T_1) should show a decrease of the Pt-S bond distance with respect to that of the ground state (S_0) (see Table S11 in SI-2.4) because an electron would be promoted from a dπ*[Pt/S(MMI)] antibonding orbital in the excitation process (see the HOMO in Figure 2.9).

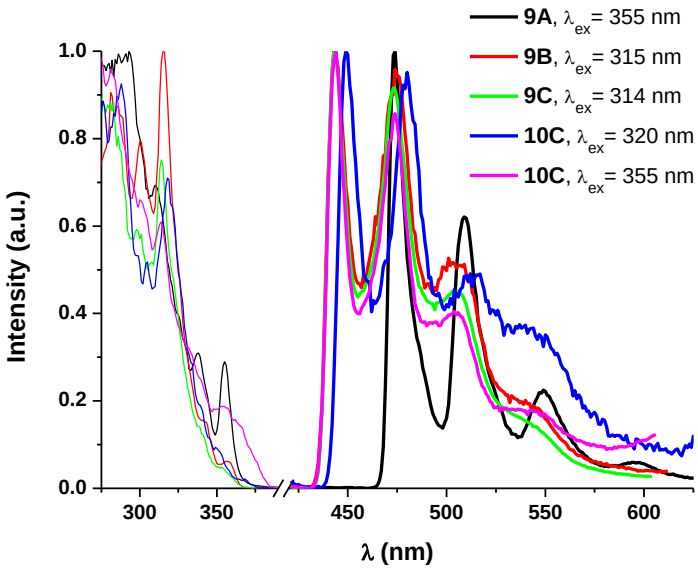

Figure 2.10. Normalized excitation (—) and emission (**—**) spectra in rigid matrix of CH_2Cl_2 (10^{-5} M) at 77 K.

However, this is not observed, and the Pt-S distance remains invariable (Δ= 0.01). Nonetheless, there is a shortening of the Pt-C6 and Pt-C1 distances in the T_1 structure compared to those of the S_0 one, which may be attributed to promoting an electron from a dπ*(Pt/NHC) antibonding orbital (see the HOMO-1 in Figure 2.9) in the excitation process. This same shortening is also detected in the T_1 structures of **9B** and **9C**. Thus, the emissive behavior of **9B**, **9C,** and **11C** is practically identical and seems to arise from the S_1 (**9B** and **9C**) and S_2 (**11C**) low-lying absorptions.

At higher concentration (10^{-3} M), the pyridine complexes **9A**–**9C** display the same emission profiles and lifetimes than those obtained in diluted solution (10^{-5} M), whereas

for **10C** and **11C**, the emission profile depends on the excitation wavelength. In complex **10C**, upon monitoring the spectra at λ_{ex} = 400 nm, an unstructured (LE) band at 545 nm becomes the predominant one, while one emission at 615 nm can be selectively tuned by exciting at λ_{ex} = 450 nm. In complex **11C**, a LE emission band at 558 nm is observed upon excitation at 450 nm (see Figure S16 in SI-2.4). The excitation maxima of these LE bands appearing in the LE spectral region (~ 400 and 450 nm) and their lifetime decays (in the order of 2–4 μs) are shorter than those of the monomer emissions. As a result of taking all of this into consideration, we tentatively ascribe these LE bands to $^3\pi\pi^*$ transitions from aggregates formed by intermolecular interactions. This wavelength-dependent behavior was formerly observed in some of the isocyanide derivatives $[Pt(C\hat{}C^*)(CNR)_2]PF_6$.[30]

The spectra of poly(methyl methacrylate) (PMMA) films of all of these complexes perfectly match with those in rigid matrix of CH_2Cl_2 (see Figure 2.11 and Table 2.4). Thus, the origin of the emissions for all complexes in PMMA seems to be the same as those in rigid matrix. Quantum yield (QY) measurements revealed that all complexes are very good blue-emitters at room temperature. To the best of our knowledge, the QY values (Φ_{em} : 68% – 93%) are among the highest ones for blue emitters of platinum(II).[26e, 28a, b, 41-42]

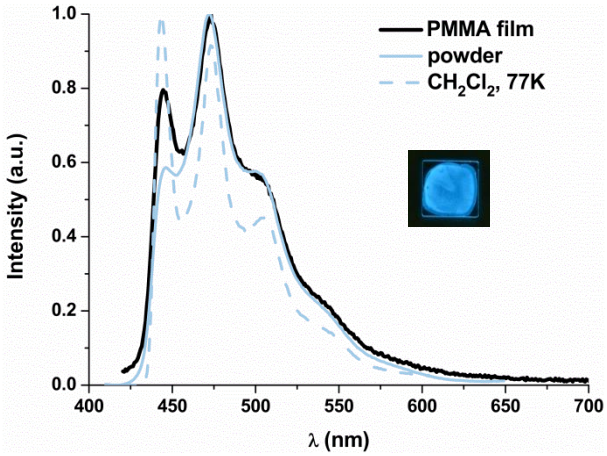

Figure 2.11. Normalized emission spectra of **9C**. Picture taken under UV light (λ_{ex} = 365 nm).

Experiments with pure powders showed that, at 298 K and 77 K, complexes **9B**, **9C,** and **11C** exhibit a phosphorescent blue emission (see Figure 2.12) with patterns and lifetimes very similar to those in rigid matrix of CH_2Cl_2. Hence, their emissions most likely originate from the same excited states. However, the naphthyl derivative, **9A**, shows an orange emission with maximum at ca. 600 nm either at 298 K or at 77 K (see Figures 2.12 and S17 in SI-2.4) instead of the blue one displayed in PMMA and rigid matrix of CH_2Cl_2. Its apparent vibronic spacings (1286 cm^{-1}), which match the skeletal vibrational frequency of

the NHC ligand, and the lifetime values allow it to be ascribed to $^3\pi\pi^*$ transitions from aggregates formed by intermolecular π···π interactions among the "Naph^C*" moieties.[29e, 30, 42a]

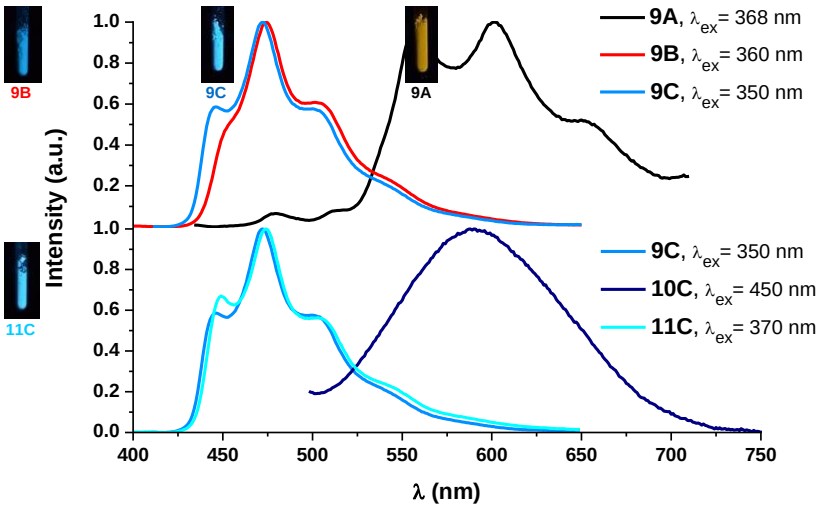

Figure 2.12. Normalized emission spectra in solid state at 298 K. Pictures under UV light (λ_{ex} = 365 nm).

Complex **10C** shows at 298 K an unstructured broad band with a maximum at 590 nm that fits a short monoexponential decay (τ= 1.2μs). Upon cooling to 77 K, the emissive behavior resembles to the wavelength-dependent one registered in a rigid matrix of CH_2Cl_2 (10^{-3} M) (see Figure S18 in SI-2.4). QY measurements carried out on neat solid powders (6% – 35%) revealed that the emissions are generally quenched because of the presence of dioxygen in the measuring chamber. The QY value results particularly low for complex **9A**, which could be attributed to the low efficiency of the emissive $^3\pi\pi^*$ excited states.

Chapter 3.

New NHC cycloplatinated complexes with cyanide and isocyanide ligands

As inferred from Chapter 2, the synthesis of heteroleptic compounds [Pt(R-C^C*)LL']PF_6 is very challenging, since *cis*- and *trans*-(C*,L) isomers can be obtained. To avoid this problem, we have carried out the synthesis of several complexes with general formula [Pt(R-C^C*)L_2]$^{+/-}$. In this Chapter we describe those with L being strong-field monodentate ligands, such as cyanide (CN^-) or isocyanides (CNR').

3.1 ISOCYANIDE COMPOUNDS

3.1.1. Synthesis and Characterization of [Pt(R-C^C*)(CNR')$_2$]PF_6 (R' = ^{t}Bu, Xyl)

The reaction of a suspension of the dichloro-bridge complexes [{Pt(μ-Cl)(R-C^C*)}$_2$] (R–C = Naph (**4A**); R = -CO_2Et (**4B**), -CN (**4C**)) with 2 equiv of KPF_6 and 4 equiv of CNR′ in acetone rendered compounds [Pt(R-C^C*)(CNR')$_2$]PF_6 (R′ = *tert*-butyl (^{t}Bu) (**13A**-**13C**), 2,6-dimethylphenyl (Xyl) (**14A**-**14C**))† (see Scheme 3.1). After removing the KCl, all compounds were obtained from their corresponding solutions as pure solids in good yields (77–88%). All the information can be seen in SI-3.1 and SI-3.2.

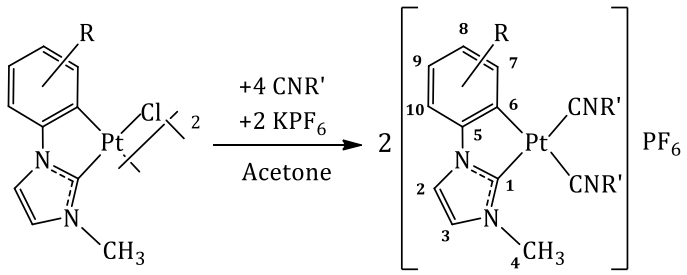

4A (R-C = Naph)
4B (R = -CO_2Et)
4C (R = -CN)

R-C = Naph; R' = ^{t}Bu (**13A**), Xyl (**14A**)
R = -CO_2Et; R' = ^{t}Bu (**13B**), Xyl (**14B**)
R = -CN; R' = ^{t}Bu (**13C**), Xyl (**14C**)

Scheme 3.1. Synthesis of compounds **13A**-**13C** and **14A**-**14C**.

Their IR spectra showed two absorptions at ~2200 cm^{-1} due to ν(C≡N) assignable to terminal isocyanide ligands.[27d, 33a, b, 43] The MALDI(+) mass spectra showed the corresponding [Pt(R–C^C*)(CNR')$_2$]$^+$ peaks and the conductivity measurements confirmed their behavior as 1:1 electrolytes. The ^{1}H NMR spectra of **13A**-**13C** and **14A**-**14C** showed the expected signals for the NHC moieties, with the resonance of H7 flanked by platinum satellites ($^3J_{Pt-H7}$ ca. 60 Hz), and two inequivalent isocyanide ligands, with intensity ratios corresponding to the proposed stoichiometry (see Figure 3.1 left for **14C**, and SI-3.2 for **13B** and **14B**).

† In SI-3.1 and 3.2 these compounds appear labeled as **5** (**13B**), **6** (**14B**), **7** (**13C**), **8** (**14C**), **9** (**13A**), and **10** (**14A**).

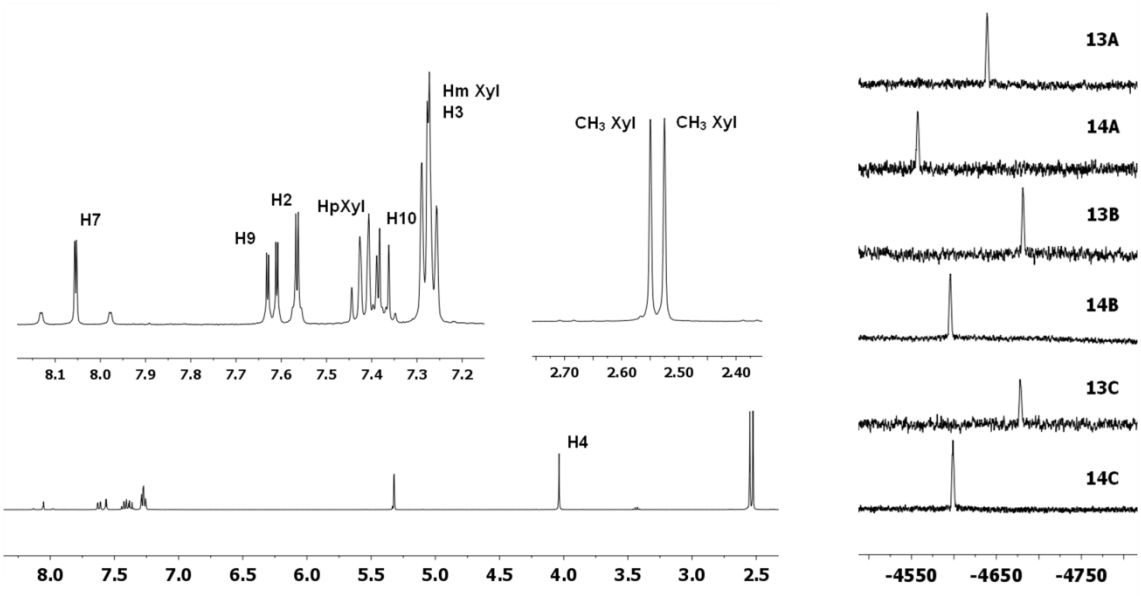

Figure 3.1. ^{1}H NMR spectrum of **14C** (left) and ^{195}Pt{^{1}H} spectra of **13A**-**13C** and **14A**-**14C** (right) in CD_2Cl_2.

^{195}Pt{^{1}H} NMR spectra of **13A**-**13C** and **14A**-**14C** exhibit the corresponding singlets at about −4600 ppm with those of the Xyl derivatives (**14A**-**14C**) being less shielded (~ 80 ppm) than those of the ^{t}Bu ones (**13A**-**13C**) (Figure 3.1 right). This may be related to the presence of the electron withdrawing Xyl ring.[27e] Also, as inferred from the ^{195}Pt chemical shifts of **13A**-**13C** (or **14A**-**14C**) the CN and CO_2Et groups present electronic features rather similar, while the larger π system due to the extra aromatic ring in the naphthyl derivatives withdraw more electron density from the platinum center causing the downfield shift (~ 40 ppm) of the ^{195}Pt NMR signals for **13A** and **14A** when compared to those of **13B**, **13C**, **14B** and **14C**. The molecular structures, as determined by single crystal X-ray crystallography of **13A** and **14A**-**14C** (Figures 3.2 and S5-S8 in SI-3.2) confirmed the structures proposed for these compounds on the basis of the spectroscopic data discussed above. Full data and discussion for them can be found in SI 3.1 and 3.2.

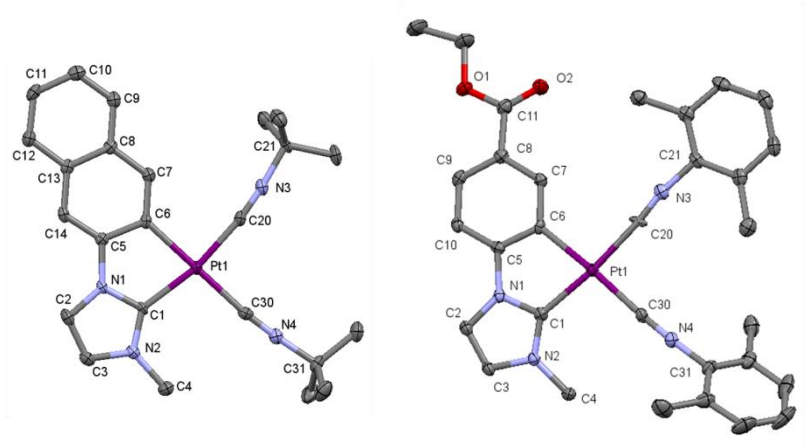

(a) (b)

Figure 3.2. Molecular structures of the cations of **13A·Me$_2$CO** (a) and **14B** (b). Thermal ellipsoids are drawn at the 50% probability level. Hydrogen atoms, PF_6^- anions and solvent molecules have been omitted for clarity.

3.1.2. Optical properties and DFT/TD-DFT calculations of [Pt(R-C^C*)(CNR')$_2$]PF$_6$ (R' = ^{t}Bu, Xyl) .

Absorption Spectra and DFT/TD-DFT Calculations. UV−vis spectra data of compounds **13A**-**13C** and **14A**-**14C** are summarized in Table S3 (SI-3.2). As shown in Figure 3.3, they all display strong absorption bands at ~ 260 (**13B**-**13C** and **14B**-**14C**) and 290 nm (**13A** and **14A**) ($\varepsilon > 10^4$ $M^{-1}cm^{-1}$) which are normally attributed to the ^{1}IL or metal-perturbed IL transitions of the NHC ligand. Complexes **13B**-**13C** and **14B**-**14C** also show less intense ($\varepsilon \approx 10^3$ $M^{-1}cm^{-1}$) lowest energy absorption bands at λ around 320 nm. The similitude of the UV−vis spectra of compounds **13B** and **14B** with those of **13C** and **14C**, indicates that the electronic features of the R-groups (CN and CO_2Et) of the C^C* ligands are rather similar. For complexes **13A** and **14A**, the lowest energy absorption band appears at λ > 360 nm, which may be due to the presence of a more extended conjugation in the R−C^C* ligand. The LE absorptions (λ > 300 nm) appear slightly shifted to the red when R' is Xyl with respect to those when R' = ^{t}Bu, thus suggesting a certain contribution of the ancillary ligands to the FOs. UV−vis spectra of **13A**-**13C** and **14A**-**14C** present a moderate negative solvatochromism (see Figure S9 in SI-3.2) in the lower energy spectral region (λ > 350 nm), which is characteristic of charge transfer (CT) transitions.[15a] The solid-state diffuse reflectance UV−vis spectra (Figure S10 in SI-3.2) show no particular differences with respect to those observed in dichloromethane solution.

For a correct assignment of the absorption bands and to better analyze the effect of the R and R′-substituents on the photophysical properties, we have carried out DFT and TD-DFT calculations in CH_2Cl_2 solution for **13A** and **14A**-**14C** (Tables 3.1 and 3.2 and Figure 3.4, and also Tables S4-S7 and Figures S11-S13 in SI-3.2).

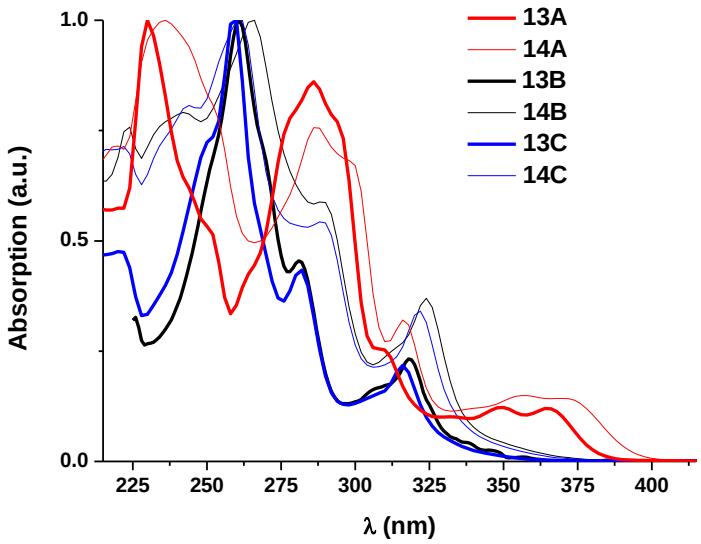

Figure 3.3. Absorption spectra of **13A**-**13C** and **14A**-**14C** in CH_2Cl_2 (5×10^{-5} M).

The highest occupied molecular orbitals HOMOs are mainly constructed from π-orbitals of the C^C* ligand (85–96%) with a small contribution of the platinum (dπ) (3–12%) and the isocyanide ligands (1–4%). In particular, in **13A** and **14A**, the HOMO is almost entirely localized on the naphthyl fragment (>90%). By contrast, the LUMOs are distributed over the platinum center (23–30%), the C^C* (37–49%) and CNR′ (26–35%) ligands. The calculated allowed transitions are in good agreement with the experimentally observed absorption maxima (Figures 3.4 and S13 in SI-3.2). The major contribution (>94%) to the lowest energy calculated absorptions (S_1) for **13A** and **14A**-**14C** is the HOMO→LUMO transition (Table 3.2). Therefore, they can be attributed to mixed LL′CT [π(NHC) → π*(CNR′)]/LMCT [π(NHC) → 5d(Pt)] transitions, with an important ILCT [(NHC)] character for complexes **13A** and **14A**.

The major contribution (>91%) to the S_2 excited state for **13A** and **14A**-**14C** is the H-1→LUMO transition which has a mixed L′MCT [π(CNR′) → 5d(Pt)]/L′LCT [π(CNR′) → π* (NHC)] character for **14B** and **14C** while LMCT [π(NHC) → 5d(Pt)]/LL′CT [π(NHC) → π*(CNR′)] for **13A** and **14A**. From these data it is also evident that the electronic features of the R-groups (CN and CO_2Et) of the C^C* ligands are rather similar and quite different from the Naph^C* one, in which the presence of a more extended conjugation in the R-C^C* ligand increases the contribution of R-C fragment to the HOMO and H-1 at the expense of the imidazole fragment and the isocyanide ligands. Because of that, the HOMO–LUMO and H-1–LUMO energy gaps result smaller for complexes **13A** and **14A** with respect to those of **14B** and **14C**.

Table 3.1. Population analysis (%) of frontier MOs in the ground state for **13A** and **14A-14C** in solution of CH_2Cl_2

MO	eV				Pt				Imidazole (C*)				Ar (R-C)				CNR'			
	14B	**14C**	**13A**	**14A**	**14B**	**14C**	**13A**	**14A**	**14B**	**14C**	**13A**	**14A**	**14B**	**14C**	**13A**	**14A**	**14B**	**14C**	**13A**	**14A**
L+1	-1.78	-1.83	-1.47	-1.77	4	5	1	5	1	1	10	1	0	0	87	0	95	94	2	94
L	-2.51	-2.60	-2.20	-2.33	23	25	30	30	21	23	24	22	21	26	16	15	35	26	30	33
H	-6.70	-6.85	-6.14	-6.17	12	10	4	3	31	33	3	3	53	55	92	93	4	2	1	1
H-1	-7.10	-7.20	-6.49	-6.53	13	8	9	8	7	1	20	20	20	1	70	71	60	90	1	1

Table 3.2. Selected singlet excited states calculated by TD-DFT for complexes **13A** and **14A**–**14C** in solution of CH_2Cl_2

	λ_{exc} **(calc.)/nm**	**o.s.**	**Transition (Percentage contribution)**	**Assignment**[a]
			[(Naph-C^C*)Pt(CN^{t}Bu)$_2$] (13A)	
S1	365.8	0.2138	H → L (94%); H-1→ L+1 (4%)	ILCT / LL'CT / LMCT
S2	347	0.0038	H-1→ L (96%)	LL'CT / LMCT
			[(Naph-C^C*)Pt(CNXyl)$_2$] (14A)	
S1	375.5	0.2410	H → L (95%); H-1 → L+3 (3%)	ILCT / LL'CT / LMCT
S2	355.2	0.0085	H-1→ L (97%)	LL'CT / LMCT
			[(EtOOC-C^C*)Pt(CNXyl)$_2$] (14B)	
S1	363.1	0.0079	H → L (97%)	LL'CT / LMCT
S2	316.6	0.3257	H-1→ L (91%)	L'LCT / L'MCT
			[(NC-C^C*)Pt(CNXyl)$_2$] (14C)	
S1	352.7	0.0006	H → L (97%)	LL'CT / LMCT
S2	314.8	0.0004	H-1→ L (96%)	L'LCT / L'MCT

a: L = NHC; L' = CNR'

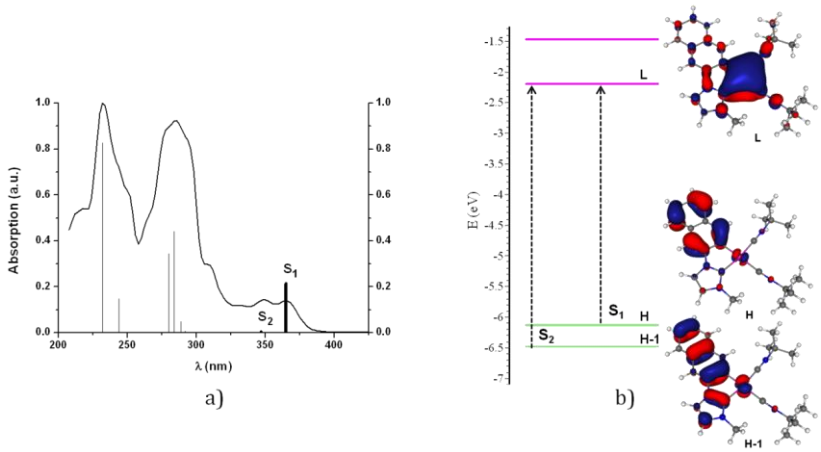

Figure 3.4. (a) UV−vis absorption spectrum of **13A** in CH_2Cl_2, calculated transitions in CH_2Cl_2 (bars); (b) Calculated molecular orbitals for **13A**.

Additionally, calculations for complexes **13A** and **14A** also show the red shift of the lowest-lying absorption when R′ is Xyl with respect to that when R′ = ^{t}Bu in line with the experimental UV−vis data.

Emission Spectra. Emission data for **13A**-**13C** and **14A**-**14C** are summarized in Table 3.3. All complexes do not display phosphorescence in solution of CH_2Cl_2 (10^{-5} M) under Ar atmosphere at rt, which may be due to the thermal quenching by solvent molecules.[41] However, in a rigid matrix (CH_2Cl_2 solution at 77 K), these molecules show bright and long life luminescence. Compounds **13B**-**13C** and **14B**-**14C** show highly structured emissions with maxima at λ ∼ 460 nm (see Figure 3.5) and apparent vibronic spacings [1345−1401 cm^{-1}] corresponding to the C=C/C=N stretches of the cyclometalated NHC ligand. The excitation spectra exhibit identical profiles to the corresponding UV−vis absorption spectra. Lifetime measurements fit to one component (14−26 μs).

Therefore, from these data and considering the TD-DFT calculations, these phosphorescent emissions can be assigned to mixed ^{3}LL′CT [π(NHC) → π*(CNR′)]/^{3}LMCT [π(NHC) → 5d(Pt)] transitions of monomeric species. As stated in the UV−vis and TD-DFT sections, the emission bands of the Xyl derivatives (**14B**, **14C**) are red-shifted with respect to those of the ^{t}Bu ones (**13B**, **13C**).

At higher concentration (10^{-3} M) complexes **13B**, **14B**, and **14C**, show an additional unstructured LE band when exciting at longer wavelengths λex > 450 nm (see Figure S14 in SI-3.2), although it is rather weak for complex **13B**. The excitation maxima of this LE band appear red-shifted, and their lifetime decays (in the order of 2−4 μs) are shorter than those of the monomer emissions. Thus, taking into account all this and their crystal

packing, we tentatively ascribe this LE band to $^3\pi\pi^*$ transitions from aggregates formed by intermolecular interactions.

Neat solid samples of **13B**-**13C** and **14B**-**14C** display bright blue emissions (see Figure 3.6) with band profiles and lifetimes that resemble those obtained in rigid matrix of CH_2Cl_2, which can be assigned to the same excited states.

Table 3.3. Photophysical Data for complexes **13A**-**13C** and **14A**-**14C**.

Comp	Media (T/K)	λ_{ex} (nm)	λ_{em} (nm)	τ (μs)[c]	ϕ
13A	Solid (298)	360	540_{max}, 586, 635	75.0	0.40
	Solid (77)	360	540_{max}, 586, 635	86.0	
	CH_2Cl_2[a,b](77)	365	481_{max}, 518, 553, 597, 652_{sh}	296 (481, 518) 52 (553, 597)	
14A	Solid (298)	383	481_{max}, 513, 561,609, 661_{sh}	88.0	0.17
		440	481, 514, 565_{max}, 609, 661_{sh}	79.0	
	Solid (77)	402	476_{max}, 511, 559, 607, 664_{sh}	173.0	
	CH_2Cl_2[a] (77)	360	479_{max}, 517, 557, 601	178.0	
	CH_2Cl_2[b] (77)	360	478_{max}, 515, 563, 609		
		450	564_{max}, 612	30.0	
13B	Solid (298)	365	455, 483_{max}, 513, 550_{sh}	19.5	0.41
		465	643	2.6	
	Solid (77)	365	454, 472, 487_{max}, 502, 520_{sh}	21.5	
	CH_2Cl_2[a] (77)	326	455_{max}, 486, 520	26.5	
	CH_2Cl_2[b] (77)	340, 365	454_{max}, 486, 520, 538_{sh}	26.6	
		485	665	4.0	
14B	Solid (298)	370	464, 492_{max}, 528, 567	5.1	0.15
		475	620	2.1	
	Solid (77)	370	462, 492_{max}, 528, 567	16.8	
	CH_2Cl_2[a] (77)	325	464_{max}, 495, 531, 600_{sh}	14.5	
	CH_2Cl_2[b] (77)	370	464_{max}, 495, 531, 625	16.4	
		450	464, 495, 531, 625_{max}	2.5	
13C	Solid (298)	360	449, 477_{max}, 510, 550_{sh}, 590	4.5	0.17
		450	477, 510, 550, 590_{max}	3.8	
	Solid (77)	360	454, 487_{max}, 510, 538_{sh}	30.0	
	CH_2Cl_2[a,b](77)	320	451, 482, 517	25.0	
14C	Solid (298)	375	458, 488_{max}, 520, 570_{sh}	2.3	0.21
	Solid (77)	375	463, 495_{max}, 530, 570_{sh}	14.8	
	CH_2Cl_2[a] (77)	323	461_{max}, 494, 528, 569_{sh}	20.0	
	CH_2Cl_2[b] (77)	365	461_{max}, 494, 529, 569_{sh}, 609_{sh}	18.0	
		450	494, 529, 569_{sh}, 609_{max}	2.0	

a = 10^{-5}M; *b* = 10^{-3}M; c = Lifetime measured at the λ_{max} if not specified

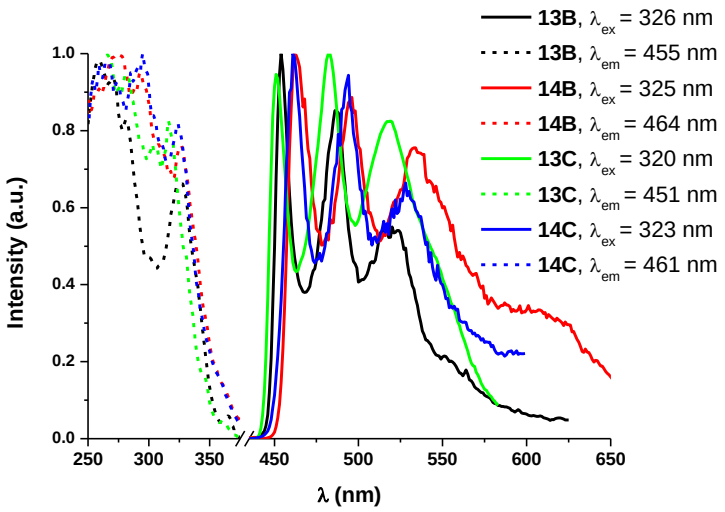

Figure 3.5. Normalized excitation and emission spectra of **13B**, **13C**, **14B**, and **14C** at 77 K in rigid matrix of CH_2Cl_2 (10^{-5} M).

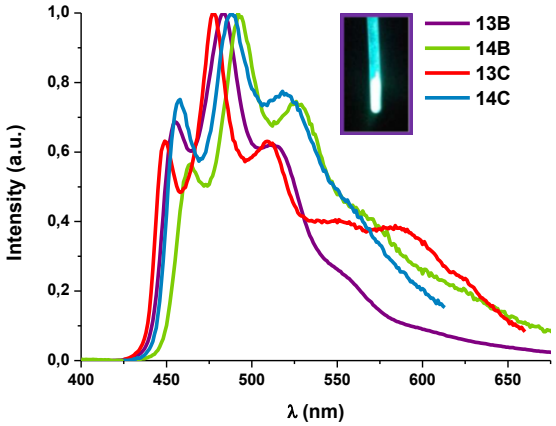

Figure 3.6. Normalized emission spectra of **13B**, **13C**, **14B**, and **14C** in solid state at 298 K. Picture of **13B** under UV light (λex = 365 nm).

For complexes **13B**, **14B** and **13C**, the LE band (λmax = 643 nm **13B**, 620 nm **14B**, 590 nm **13C**) attributable to $^3\pi\pi^*$ transitions can be selectively obtained upon excitation at λex > 450 nm (see Figure S15 in SI-3.2). Complexes **13A** and **14A** exhibit a rather different emissive behavior to that observed for complexes **13B**-**13C** and **14B**-**14C**. In the solid state, compound **13A** displays a yellow emission band with maximum at 540 nm (see Figure 3.7) either at 298 or at 77 K. However, in rigid matrix of CH_2Cl_2 (10^{-3} and 10^{-5} M, 77 K), a highly structured band is observed at 481 nm. The intricate emission profile is not dependent on the excitation wavelength.

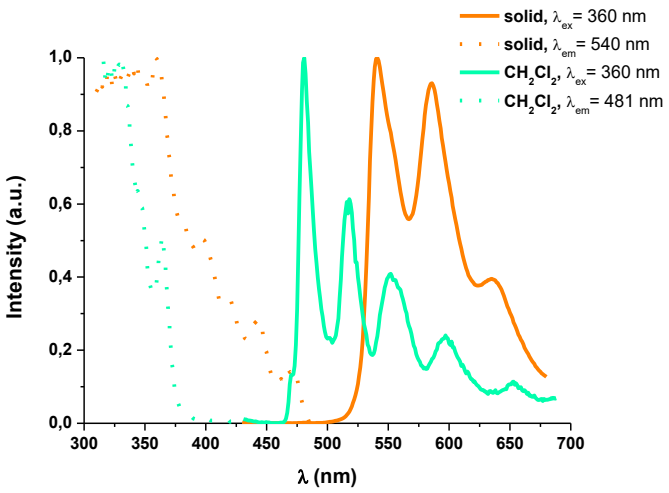

Figure 3.7. Normalized excitation and emission spectra of **13A** in solid state and in rigid matrix of CH_2Cl_2 (10^{-5} M, 77 K).

The decay lifetimes suggest the contribution of two different bands: HE band (481 and 518 nm) and LE band (553 and 597 nm). As shown in Figures S16 and S17 in SI-3.2, this emissive pattern was also observed in **14A** but in this case, the emission spectrum can be tuned by using different excitation wavelengths. In rigid matrix of CH_2Cl_2 (10^{-3} M, 77K), the HE band completely disappears when exciting upon 450 nm. In the light of its long lifetime and DFT calculations, the HE band can be assigned to ^{3}ILCT [(NHC)] transitions with some, if any, ^{3}LL'CT [π(NHC) → π*(CNR')]/^{3}LMCT [π(NHC) → 5d(Pt)] character. On the other hand, the structured LE band which exhibits shorter decay lifetime and red-shifted excitation profile compared to those of the HE band can be tentatively assigned to a mixed LL'CT [π(NHC) → π*(CNR')]/LMCT [π(NHC) → 5d(Pt)] transition with some ^{3}ππ* character. The LE emission band of **14A** does appear 11 nm (352 cm^{-1}) shifted to the red when compared to that of **13A**, suggesting the participation of the ancillary ligand (CNR') in the excited state.

Quantum yield (ϕ) measurements carried out on neat solid samples of **13A**-**13C** and **14A**-**14C** reveal that complexes **13A**, **13B**, and **14C** are very good emitters at r.t. with values of 40%, 41% and 21%, respectively (see Table 3.3).

3.2 CYANIDE COMPOUNDS

3.2.1. Synthesis and Characterization of Complexes NBu_4 [Pt(R-C^C*)$(CN)_2$]

KCN was added to a freshly prepared suspension of [Pt(R-C^C*)$(NCCH_3)_2$]ClO_4 in methanol in a molar ratio (2:1) (see Scheme 3.2 paths a and b). After 2 hours of reaction, the solvent was removed under reduced pressure and an exchange of the cation was accomplished by reaction of the residue with 1 equiv. of NBu_4ClO_4 in acetone (see Scheme 3.2 path c). The solvent was evaporated to dryness and the residue was washed with water. Then, it was recrystallized from CH_2Cl_2/Et_2O to give the corresponding compound NBu_4[Pt(R-C^C*)$(CN)_2$] (R−C = Naph (**15A**); R = CO_2Et (**15B**), CN (**15C**); R' = Cl (**15D**)) as pure solids in good yields (45-67%) (see details of synthesis and characterization in SI-3.3, Figures S1-S4).

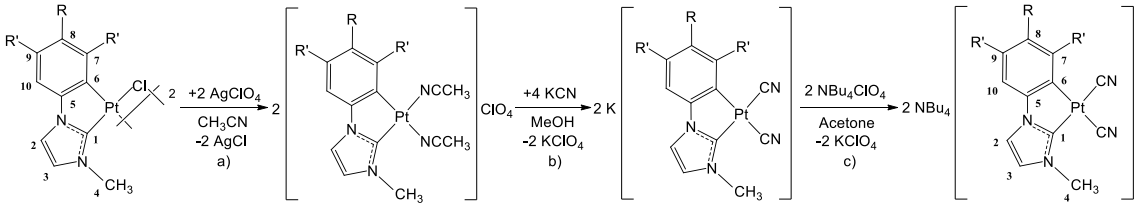

Scheme 3.2. Synthetic route for compounds **15A**-**15D**.

Two absorptions in the range of 2125-2107 cm^{-1} were observed in the IR spectra of compounds **15A**-**15D**, as expected from the *cis* configuration of two inequivalent cyanide ligands.[27c, 44] Compound **15B** presents an additional absorption at 1696 cm^{-1} attributed to the (C=O) bond in the ethoxycarbonyl fragment, while the nitrile group in **15C** is responsible of an absorption band at 2218 cm^{-1}. The MALDI(-) spectra of **15A**-**15D** showed peaks corresponding to [Pt(R-C^C*)$(CN)_2$]$^-$ and their ^{1}H NMR spectra showed the expected resonances for the NHC moiety and the NBu_4^+ cation, according to the proposed stoichiometry. Compounds NBu_4[Pt(R-C^C*)$(^{13}CN)_2$] (**15A'**-**15D'**) were prepared following the same method but using K^{13}CN and their ^{13}C{^{1}H} NMR spectra showed two doublets for the two inequivalent cyanides flanked by platinum satellites (see Figure 3.8 for **15A, 15A'** and Table 3.4). The $^1J_{Pt\text{-}13C}$ values for *trans*-($C_{Ar}/^{13}CN$) are of the same order than those corresponding to *trans*-($C_{Ar}/^{13}CN$) for [Pt(C^N)$(CN)_2$]$^-$ (C^N = phenylpyridinate, benzoquinolate).[27c, 44] The $^1J_{Pt\text{-}13C}$ values in *trans*-(C*/^{13}CN) are just a little bigger than those of *trans*-($C_{Ar}/^{13}CN$) but clearly smaller than those of the *trans*-(N/^{13}CN) in complexes [Pt(C^N)$(CN)_2$]$^-$ (C^N = phenylpyridinate, benzoquinolate),[44] in agreement with the high trans influence of the carbenic atom.

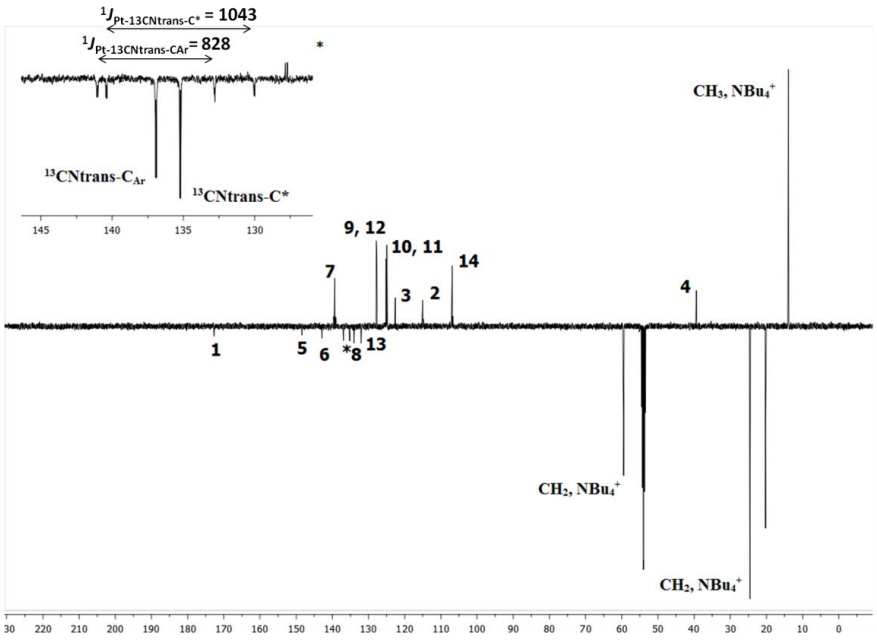

Figure 3.8. $^{13}C\{^1H\}$ NMR of **15A** and **15A'** (inset).

The $^1J_{Pt\text{-}13C}$ value for the *trans*-(C*/CN) in all four compounds **15A**-**15D** undergoes small variations of no more than 18 Hz, while the coupling constant in the *trans*-(C_{Ar}/CN) arrangement present greater differences (up to 64 Hz) depending on the substituents at the cyclometalated (Ar) fragment. $^{195}Pt\{^1H\}$ NMR spectrum of each of **15A**-**15D** shows a singlet at ca. -4500 ppm (see Figure 3.9). The similarity of δ in compounds **15B** and **15C** confirmed, once again, the rather similar electronic properties of the cyclometalated NHC ligands **B** and **C**.[30, 32, 45]

Table 3.4. Significant NMR data for compounds **15A**-**15D**[a]

Δ		**15A**	**15B**	**15C**	**15D**
^1H ($J_{Pt\text{-}H}$)	H7	8.56 (57.8)	8.74 (55.7)	8.40 (54.8)	-
	H4	4.15	4.16	4.13	4.05
^{13}C ($J_{Pt\text{-}C}$)	C1	172.7	172.2	172.0	170.2
	C7	139.3 (60.8)	141.5 (64.8)	143.4 (65.7)	-
	$^{13}CN_{trans\text{-}C^*}$	135.2 (1043)	134.5 (1037)[b]	133.9 (1044)	131.8 (1025)
	$^{13}CN_{trans\text{-}CAr}$	136.9 (828)	136.4 (840)	135.4 (850)	130.7 (892)
^{195}Pt		-4501.3	-4543.6	-4539.6	-4498.5

[a] δ (ppm), J (Hz), CD_2Cl_2; [b] performed at 193K

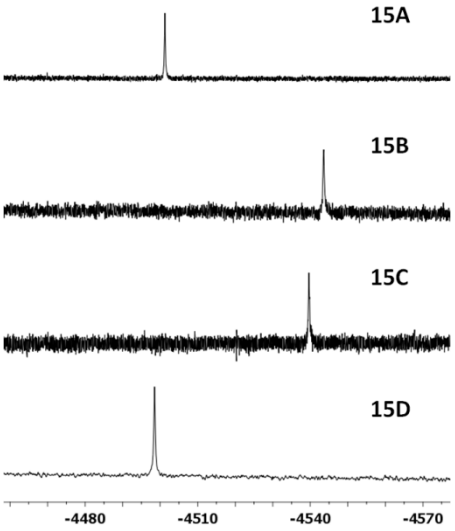

Figure 3.9. $^{195}Pt\{^{1}H\}$ NMR spectra of **15A**-**15D** in CD_2Cl_2.

X-ray diffraction studies were performed on a single-crystal of **15B**, **15C** and **15D**. In the mononuclear anionic complexes the Pt atom shows a distorted square-planar environment, because of the small bite angle of the cyclometalated ligand [C(1)-Pt-C(6) angle of *ca.*79º] (Figure 3.10, Table 3.5 and Tables S1 and S2).

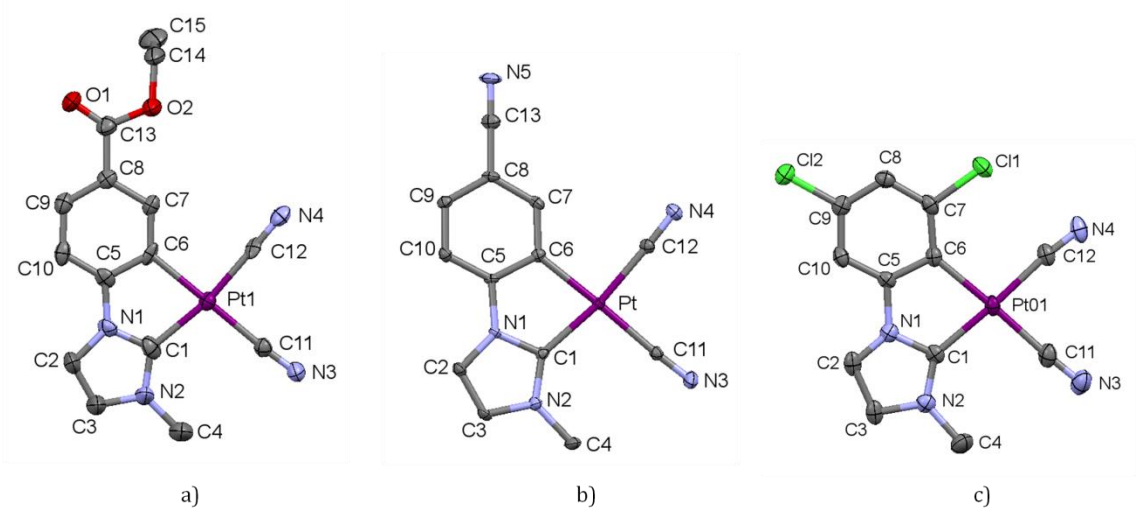

Figure 3.10. Molecular structure of the anion in compounds **15B** (a), **15C** (b) and **15D** (c). Thermal ellipsoids are drawn at the 50% probability level. Hydrogen atoms, NBu_4^+ cations and solvent molecules have been omitted for clarity.

Bond distances and angles in the Pt(C^C*) metalocycle are similar to those found in other cyclometalated NHC complexes.[29e, 30-32, 45] The Pt-C and C-N bond lengths of the two CN ligands, are similar one to another, as expected from the not so different trans influence of the two carbon atoms of the C^C* ligand, already observed in compounds [Pt(R-C^C*)(CNR')$_2$]PF_6.[30] They are also similar to those observed in the bis-cyanide complex in the double salt [Pt(bzq)(CNXyl)$_2$][Pt(bzq)(CN)$_2$] (bzq = benzoquinolate).[44]

Table 3.5. Selected bond lengths (Å) and angles (°) for **15B–15D**

	15B·CH_2Cl_2[a]	**15C·$CHCl_3$**	**15D·0.5H_2O**
Pt-C(1)	2.034(13)	2.010(4)	2.022(4)
Pt-C(6)	2.072(11)	2.043(4)	2.073(4)
Pt-C(11)	2.031(12)	2.013(4)	2.003(5)
Pt-C(12)	1.947(12)	1.992(4)	1.997(4)
C(11)-N(3)	1.147(15)	1.150(6)	1.158(6)
C(12)-N(4)	1.171(15)	1.153(5)	1.139(5)
C(1)-Pt-C(6)	78.8(5)	79.34(16)	79.67(16)
C(1)-Pt-C(11)	100.8(5)	98.54(16)	98.08(18)
C(6)-Pt-C(12)	91.4(5)	92.23(17)	97.79(16)
C(11)-Pt-C(12)	89.0(4)	89.88(17)	84.65(18)
Pt-C(11)-N(3)	176.3(10)	176.0(4)	176.4(5)
Pt-C(12)-N(4)	177.3(11)	177.9(4)	172.4(4)

[a]Compound **15B** exhibits two molecules of complex and two molecules of CH_2Cl_2 in the asymmetric unit (see SI-3.3, Table S2).

The complex anions of **15B** and **15C** adopt a zig-zag arrangement in a layer, with the NBu_4^+ cations intercalated between each two layers, thus avoiding π···π and Pt···Pt interactions among them (see Figure 3.11). In compound **15D**, the presence of water molecules from the crystallization solvent allow the formation of hydrogen interactions between one molecule of water and four complex anions through two O-H···NC (ca. 2.2 Å) and two C-H···O interactions (ca. 2.4 Å) (see Figure 3.12 a). On the other hand, the chlorine atoms in the phenyl ring allow the molecules to arrange themselves in pairs via C-H···Cl interactions (Figure 3.12 b), yielding chains separated by intercalation of the NBu_4^+ counterions, as in **15B** and **15C**.

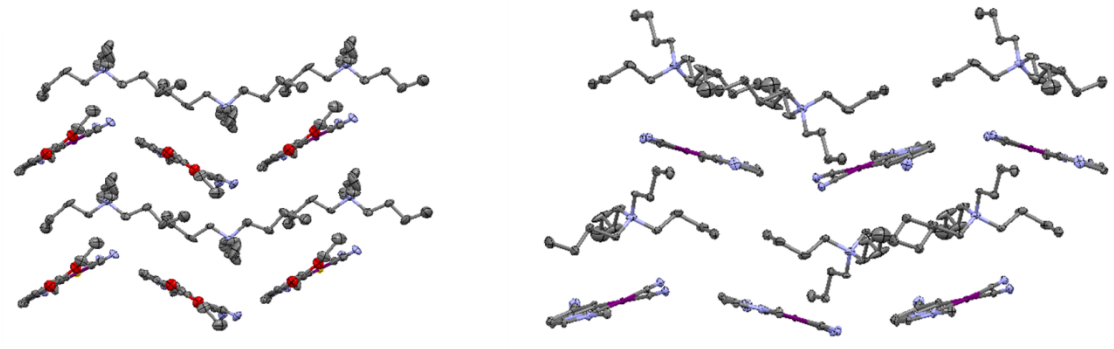

(a) (b)

Figure 3.11. Molecular packing view of **15B** (a) and **15C** (b).

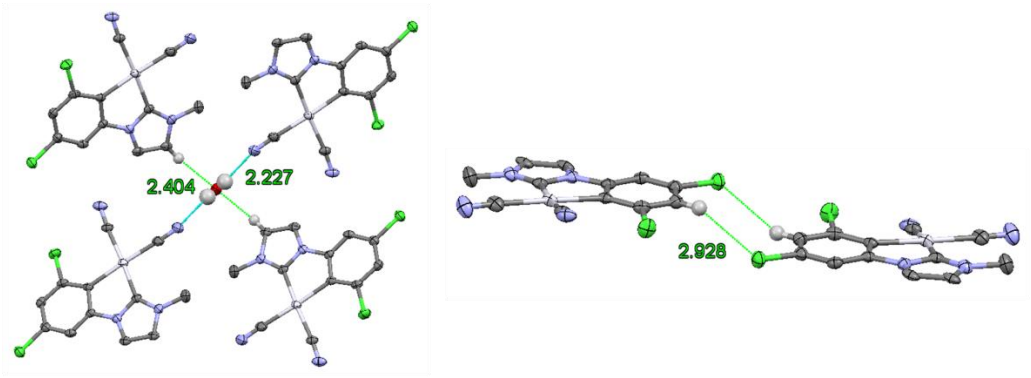

Figure 3.12. Intermolecular interactions in the crystal structure of **15D**.

3.2.2. Optical properties and DFT/TD-DFT calculations of $NBu_4[Pt(R\text{-}C\hat{}C^*)(CN)_2]$

Absorption spectra and DFT/TD-DFT calculations. Absorption data are summarized in Table 3.6, Figures 3.13 and 3.14, and Figures S5 and S6 in SI-3.3). As observed in Figure 3.13, solutions (10^{-4} M) of all four compounds **15A**-**15D** in dichloromethane show strong absorption bands in the high energy (HE) region at $\lambda < 300$ nm ($\varepsilon > 10^4$ M^{-1} cm^{-1}), commonly assigned to singlet intraligand (^{1}IL) transitions of the cyclometalated NHC ligand. As inferred from the similar absorption spectra, **15B** and **15C** are a new example of the similarities of the electronic features of **B** and **C**, as previously reported in Pt(II) complexes with these two cyclometalated NHC ligands.[30, 32, 45] All three compounds **15B**-**15D** show an intense low-energy absorption at $\lambda \sim 320$ nm ($\varepsilon \approx 10^4$ M^{-1} cm^{-1}) and their lowest-energy one at *ca.* 340 nm ($\varepsilon \approx 10^3$ M^{-1} cm^{-1}), with just little blue-shift of the absorption bands of **15D** with respect to those of **15B** and **15C**; this behavior was already observed in compounds [Pt(R-C^C*)(acac)][32] which will be discussed in Chapter 4.2. On the other hand compound **15A** presents a different spectrum profile, with the lowest-energy absorption band located at $\lambda \sim 356$ nm ($\varepsilon \approx 10^3$ M^{-1} cm^{-1}).

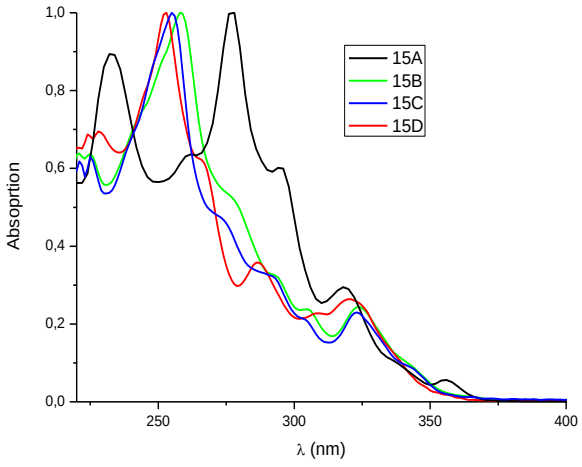

Figure 3.13. Absorption spectra of compounds **15A**-**15B** in CH_2Cl_2 (10^{-4}M).

In all the four compounds **15A-15D**, the lowest energy absorption obey Beer's Law, suggesting that in each case it corresponds to a transition in the molecular species with no significant aggregation in concentration up to $5 \cdot 10^{-4}$M (see Figure S6 in SI-3.3). The UV-vis spectra of powdery solid samples (Figure 3.14) show no significant differences with those in dichloromethane solution.

Table 3.6. Absorption Data in 10^{-4} M solution for compounds **15A-15D** at rt

Comp	λ abs / nm ($10^3\varepsilon$ $M^{-1}cm^{-1}$)
15A	232 (35.2), 262 (25.0), 278 (39.3), 294 (23.7), 318 (11.6), 334 (4.6), 356 (2.2) ***CH_2Cl_2***
	226 (36.7), 252 (22.6), 260 (24.9), 274 (38.3), 292 (22.8), 313 (10.0), 336 (3.6), 354 (2.7) ***MeOH***
	238 (26.4), 262 (22.1), 276 (33.6), 296 (18.1), 320 (9.9), 334 (4.3), 356 (1.5) ***THF***
	228, 276, 284, 292, 313, 337, 355 ***Solid***
15B	245 (24.0), 252 (28.0), 258 (31.6), 275 (17.0), 293 (10.3), 305 (7.5), 324 (7.7), 342 (3.1) ***CH_2Cl_2***
	240 (16.3), 256 (24.3), 273 (14.6), 290 (7.9), 303 (5.5), 320 (5.8), 338 (2.1) ***MeOH***
	245 (11.6), 252 (13.1), 259 (15.0), 277 (7.0), 294 (4.2), 305 (3.3), 326 (3.3), 344 (1.7) ***THF***
	259, 274, 321, 362 ***Solid***
15C	249 (29.1), 255 (32.9), 273 (15.7), 291 (10.9), 304 (7.2), 323 (7.8), 342 (3.3) ***CH_2Cl_2***
	252 (31.9), 270 (15.0), 284 (10.9), 291 (9.2), 302 (6.1), 319 (7.5), 337 (2.7) ***MeOH***
	256 (29.5), 273 (19.5), 291 (13.5), 303 (8.9), 324 (7.1), 330 (5.8), 343 (3.4) ***THF***
	251, 273, 289, 321 ***Solid***
15D	246 (19.9), 253 (24.5), 265 (15.3), 286 (8.8), 309 (5.6), 320 (6.5), ***CH_2Cl_2***
	251 (22.6), 264 (18.4), 282 (14.5), 305 (5.3), 317 (4.7) ***MeOH***
	246 (17.9), 252 (21.1), 265 (12.7), 287 (6.9), 293 (6.2), 306 (5.0), 319 (5.6), 326 (5.2), 335 (3.7) ***THF***
	257, 286, 321, 400 ***Solid***

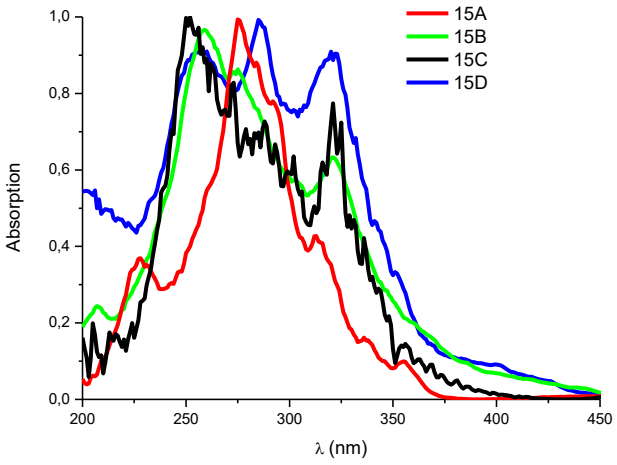

Figure 3.14. Solid-state diffuse reflectance UV-vis spectra of **15A-15D**.

DFT and TD-DFT calculations for compounds **15C** and **15D** were carried out in CH_2Cl_2 solution for a correct assignment of the transitions (see Figure 3.15, Tables 3.7 and 3.8, and Tables S3 and S4 in SI-3.3).

Since **B** and **C** have already demonstrated similar features, we assumed the same behavior for **15B** as for **15C**. The highest occupied molecular orbitals (HOMOs) are mainly built from π orbitals of the NHC ligand and dπ orbitals of the platinum center in all cases, with a very small contribution of π orbitals of the CN^- ligands (5-6%).

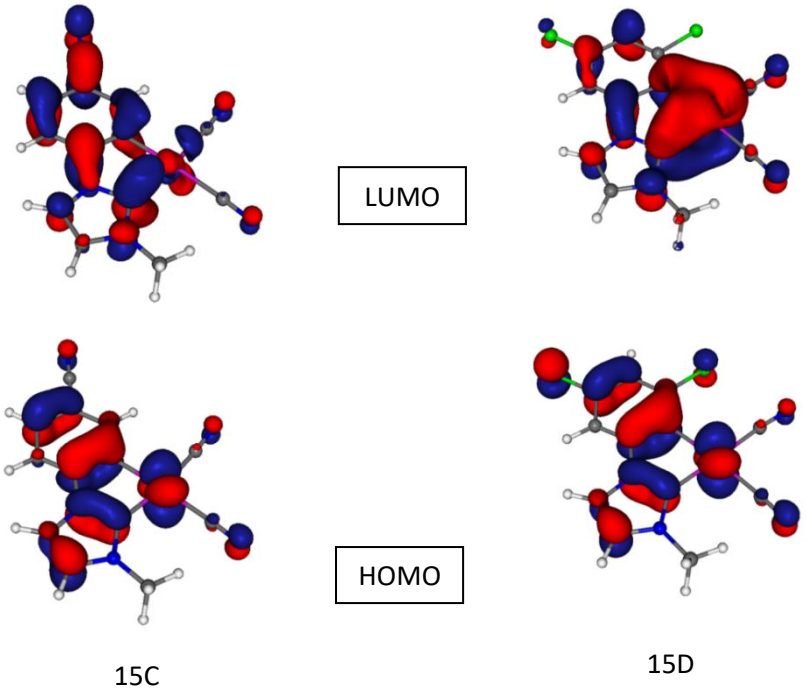

Figure 3.15. FOs of compounds **15C** and **15D** calculated in CH_2Cl_2 solution.

Table 3.7. Population Analysis (%) of Frontier MOs in the Ground State for **15C** and **15D** in solution of CH_2Cl_2

MO	eV		Pt		C*		R-C		CN	
	15C	**15D**	**15C**	**15D**	**15C**	**15D**	**15C**	**15D**	**15C**	**15D**
L+1	-0.42	-0.32	20	5	13	14	60	79	7	2
L	-1.32	-1.06	14	26	25	31	56	34	5	9
H	-5.71	-5.69	32	30	23	20	40	44	6	5
H-1	-6.08	-6.02	45	37	24	22	17	29	14	12
H-2	-6.09	-6.01	96	97	0	1	2	1	2	1

The lowest unoccupied molecular orbitals (LUMOs) still show a small contribution of the ancillary ligands (5-9%) but differ from the HOMOs in the distribution of the electronic density between Pt and both halves of the NHC ligand. The lowest-energy absorption calculated (S_1) in dichloromethane solution show that, for both the two compounds it corresponds mainly to the HOMO to LUMO transitions (>95%) and it can be attributed to ^{1}MLCT [5d(Pt) → π*(NHC)] in compound **15C (** and **15B)** and ^{1}ILCT [π(NHC) → π*(NHC)] with some ^{1}MLCT [5d(Pt) → π*(NHC)] character for **15D**. In case of **15A**, the lowest energy absorption band (λ ~ 356 nm) match well with that for compound [Pt(Naph-C*)(acac)][29e] and a similar origin can be presumed, that is ^{1}LL'CT [π(NHC) → π*(CN)] with some ^{1}ML'CT [5d(Pt) → π*(CN)] character.

Table 3.8. Selected singlet excited states calculated by TD-DFT for **15C** and **15D** in solution of CH_2Cl_2

States	λ_{exc} (calc.)/nm	o.s.	Transition (% contribution)*	Assignment
[(NC-C^C*)Pt(CN)$_2$] (15C)				
S1	342.50	0.0031	H → L (95%)	^{1}MLCT
S2	315.56	0.0275	H-2→ L (98%)	
S3	303.06	0.1746	H-1→ L (94%)	
[(Cl-C^C*)Pt(CN)$_2$)] (15D)				
S1	327.33	0.0133	H → L (97%)	^{1}ILCT/^{1}MLCT
S2	298.98	0.0431	H-2→ L (99%)	
S3	293.42	0.1705	H-1→ L (92%)	

*Transitions with contributions < 10% were not included

Emission Spectra. Compounds **15A**-**15C** are emissive in solid state, in PMMA films and in CH_2Cl_2 glassy solutions, while **15D** is barely emissive even at low temperatures. Emission data for **15A**-**15C** are summarized in Table 3.9. As can be seen in Figure 3.16 upon excitation in the low-lying absorption region (λ: 320-350 nm) compounds **15B** and **15C** display a phosphorescent high energy (HE) structured emission band with maxima at λ_{max} ~ 470 nm in solid state and 5% (w/w) PMMA films which undergo a blue shift to λ_{max} ~ 445 nm in glassy CH_2Cl_2 solution due to the change in the relative intensity of the emission maxima. This phosphorescent HE emission, assigned as ^{3}MLCT [5d(Pt) → π*(NHC)] on the light of the theoretical calculations and absorption data aforementioned, reaches a high PLQY (Φ = 0.62) in a 5% (w/w) PMMA film for **15C**.

Some differences can be observed in the emissive behavior of **15A**. In diluted solution of CH_2Cl_2 (10^{-5} M) at 77 K it displays a phosphorescent structured emission in the blue region of the spectrum. This HE emission with long decay lifetimes (*ca*. 460 μs) can been explained by a high contribution of ^{3}ILCT [π(NHC) → π*(NHC)] transitions in the monomeric species.

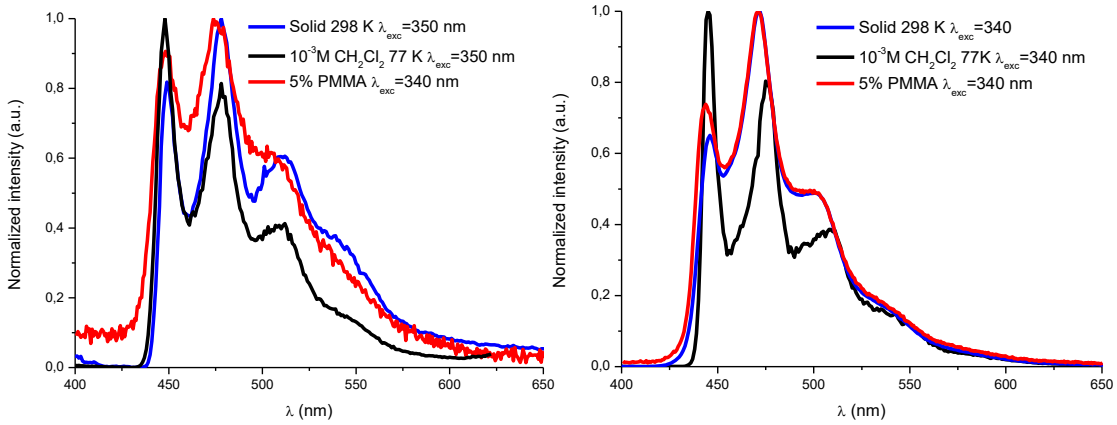

(a) (b)

Figure 3.16. Normalized emission spectra of **15B** (a) and **15C** (b)

As observed in other compounds containing the Naph^C* moiety, higher concentrations of them lead to the formation of aggregates through π···π stacking.[29e, 30, 45] This is reflected in the emission features of compound **15A** even in CH_2Cl_2 solution at 10^{-3} M, where an additional low energy (LE) emission band with maxima at 531, 577 and 627 nm and decay lifetime of *ca*. 80 μs is observed (see Figure 3.17 a). Powdery samples of **15A** revealed the LE band as the only contribution to the emission, regardless of the excitation wavelength (320-400 nm). The lower energy excitation (λ_{ex}> 350 nm) and the emission lifetimes, are in agreement with the formation of emissive aggregates through π···π interactions and has been tentatively ascribed to excimeric π···π* transitions.[30, 45]

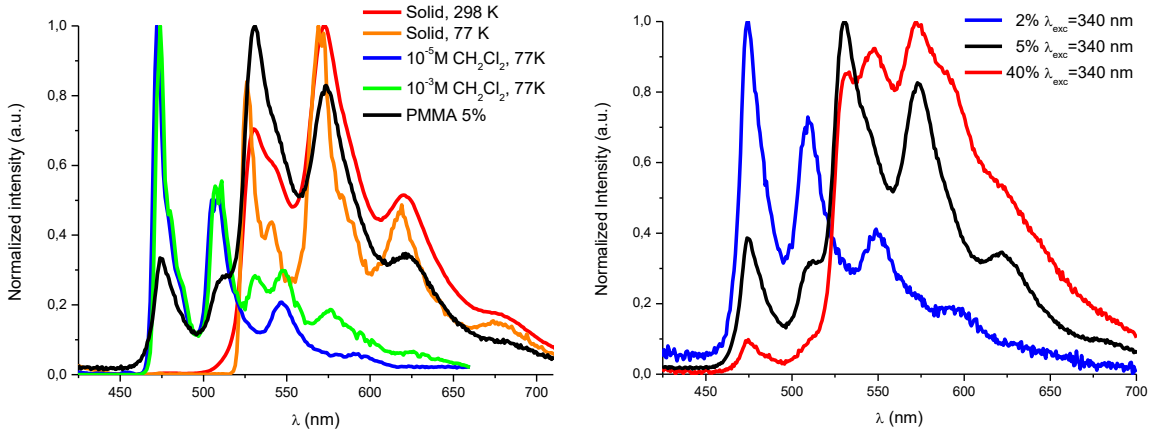

(a) (b)

Figure 3.17. Normalized emission spectra of **15A** in different matrix (a) and in PMMA at different doping concentrations (b).

Table 3.9. Emission Data for Complexes **15A**-**15C**.

	Medium (T/K)	λ_{ex} **(nm)**	λ_{em} **(nm)**	τ **(μs)**[a]	ϕ[b]
15A	PMMA (298) 2%	340	474_{max}, 510, 549, 594_{sh}		0.36
	5%	340	474, 513, 530_{max}, 574, 622, 677_{sh}		0.83
	40%	340	474, 511_{sh}, 532, 548, 573_{max}, 590, 619_{sh}		0.58
	Solid (298)	350	530, 541, 573_{max}, 620, 677_{sh}	78.2	
	Solid (77)	350	526, 541, 571_{max}, 619, 674_{sh}	84.3	
	CH_2Cl_2 (77) [c]	350	472_{max}, 509, 531, 548, 576		
	CH_2Cl_2 (77) [d]	350	474_{max}, 509, 546, 592_{sh}	466.1	
15B	PMMA (298)	340	448, 474_{max}, 505		0.10
	Solid (298)	350	454, 478_{max}, 507, 537_{sh}	11.3	
	Solid (77)	350	449, 478_{max}, 510, 539_{sh}	13.7	
	CH_2Cl_2(77) [c]	350	449_{max}, 480, 513, 543_{sh}	15.7	
15C	PMMA (298)	340	444, 472_{max}, 500, 532_{sh}		0.62
	Solid (298)	340	446, 471_{max}, 501, 530_{sh}	12.9	
	Solid (77)	340	442, 471_{max}, 501, 530_{sh}	16.0	
	CH_2Cl_2 (77) [c]	340	445_{max}, 475, 509, 535_{sh}	19.9	

a = Lifetime measured at the λ_{max}. b = measured under argon. c = 10^{-3} M. For **15B** and **15C** the same results at 10^{-5} M were found. d = 10^{-5} M.

A PMMA film doped with 5% (w/w) of complex **15A** showed an efficient yellow phosphorescence (Φ= 0.83), similar to that found in solid samples, but still with some contribution of the HE band due to monomeric species.

A study carried out at different concentrations confirmed the aforementioned assignment of the emission bands, since at lower concentration (2% w/w in PMMA) the HE structured band is the only one observed, while by increasing it to 40% (w/w), the HE band disappears being the LE emissions attributed to excimeric π···π* transitions the only ones observed (see Figure 3.17 b).

Chapter 4.

New NHC cycloplatinated complexes with diphosphine and β-diketonate ligands

4.1 DIPHOSPHINE COMPOUNDS

4.1.1. Synthesis and Characterization of [Pt(R-C^C*)(P^P)]PF_6

Compounds [Pt(R-C^C*)(P^P)]PF_6 (R-C = Naph, P^P = dppm **16A**, dppe **17A,** dppbz **18A**; R = CN, P^P = dppm **16C**, dppe **17C** (see Chapter 2, compound **12C**), dppbz **18C**) were prepared in high yields, 72% **16A** – 93% **16C**, following the procedure indicated in Scheme 4.1† and fully characterized (see Experimental section in SI-4.1). Their IR features corresponding to PF_6^-, and the conductivity of their solutions agree with their ionic formulation, but the most relevant structural information came from the multinuclear NMR spectra (see Table 4.1 Figures 4.1 and 4.2, and Figures S1-S6 in SI-4.1) and the X-ray diffraction study on single crystals of **16A**, **18A**, **16C** and **17C** (see below Figure 4.3).

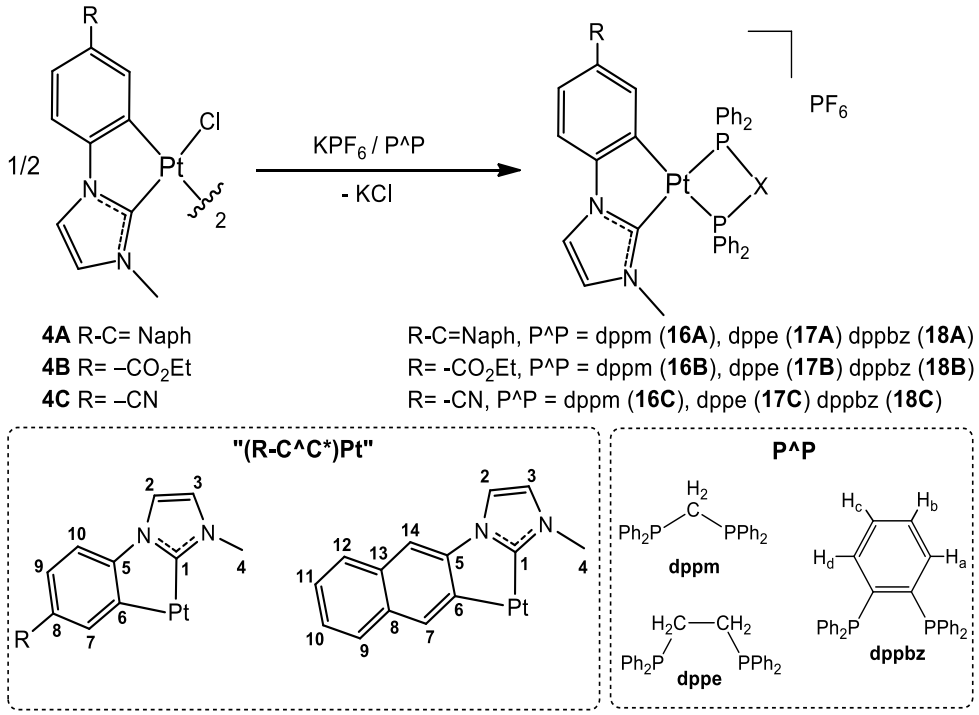

Scheme 4.1. Synthetic route for the preparation of **16A**-**18A**, **16B**-**18B** and **16C**-**18C**.

The $^{31}P\{^1H\}$ NMR spectra of dppm derivatives (**16A** and **16C**) (Figure 4.1 a for **16C**) exhibit one AB system ($J_{P,P} \approx 40$ Hz) flanked by two sets of ^{195}Pt satellites. The larger $^1J_{Pt,P}$ value corresponds to the P atom located trans to the N-Heterocyclic carbene (C1), whose trans influence is big but smaller than that of the aromatic C atom (C6).[31] For dppe (**17A**, **17C**†)

† Compounds **16B**-**18B** were synthesized in a simultaneous undergraduate research project by Lorenzo Arnal Vallés, under the title Compounds of Pt(II) with N-heterocyclic carbene: from molecules to phosphors, with deposit number TAZ-TFG-2016-2095 (University of Zaragoza).
† Although compound **17C** was presented in Chapter 2 as **12C**, it was renamed in this chapter to facilitate the reader the comparison of the properties.

and dppbz (**18A**, **18C**) derivatives, the two inequivalent P atoms (Table 4.1, Figure 4.1 b for **17A**) appear as an AX system, with the $J_{P,P}$ value being quite smaller than that observed for the dppm complexes (**16A** and **16C**).[35a] In complexes **16A** and **16C**, the signals of the two P atoms appear upfield shifted with respect to that of free dppm (δ = -23.8 ppm), while for **17A**, **17C** and **18A**, **18C** they appear highly downfield shifted with respect to that of the corresponding free diphosphine (dppe = -12.5 ppm, dppbz = -13.8 ppm) with positive and quite similar chemical shifts for all the four complexes. The shielding effect of the incorporation of phosphorus in a four-membered ring, with respect to the free diphosphine, and the deshielding one when phosphorus takes part of a five-membered metalocycle have been observed in many cases.[36b]

Table 4.1: Relevant ^{31}P, ^{195}Pt NMR data (δ(ppm), J(Hz))

	δ Pt	$^1J_{Pt,Ptrans\text{-}C1}$	$^1J_{Pt,Ptrans\text{-}C6}$	$\delta P_{trans\text{-}C1}$	$\delta P_{trans\text{-}C6}$	$J_{P,P}$
16A	-4384.0	2398.6	1526.1	-36.9 (ν_A)	-37.5 (ν_B)	39.8
17A	-4991.0	2715.1	1925.9	50.6	43.6	6.0
18A	-4906.0	2671.6	1915.4	47.6	39.3	4.1
16C	-4426.7	2345.3	1611.9	-38.5 (ν_A)	-39.0 (ν_B)	44.0
17C	-4996.0	2673.8	2014.6	50.2	43.1	7.0
18C	-4939.6	2634.7	2001.4	46.4	39.3	5.2

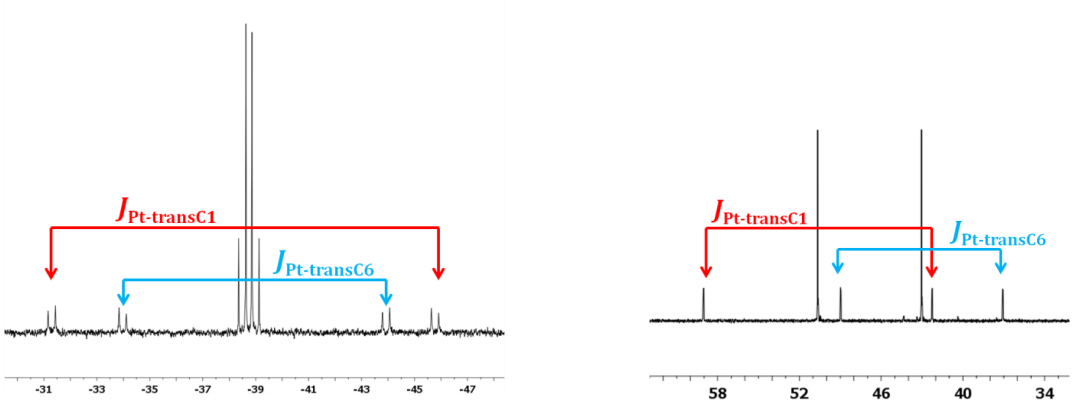

(a) (b)

Figure 4.1. $^{31}P\{^1H\}$ NMR spectra in CD_2Cl_2 of **16C**, AB system (a) and **17A** (b).

It is worth to be noticed the downfield shift of the ^{195}Pt resonances of the dppm complexes (**16A**, **16C**) when compared to those of the dppe (**17A**, **17C**) and dppbz (**18A**, **18C**) counterparts, which can be attributed to the great strain in the 4-membered ring (see Figures 4.2 and Table 4.1).[35a, 36b]

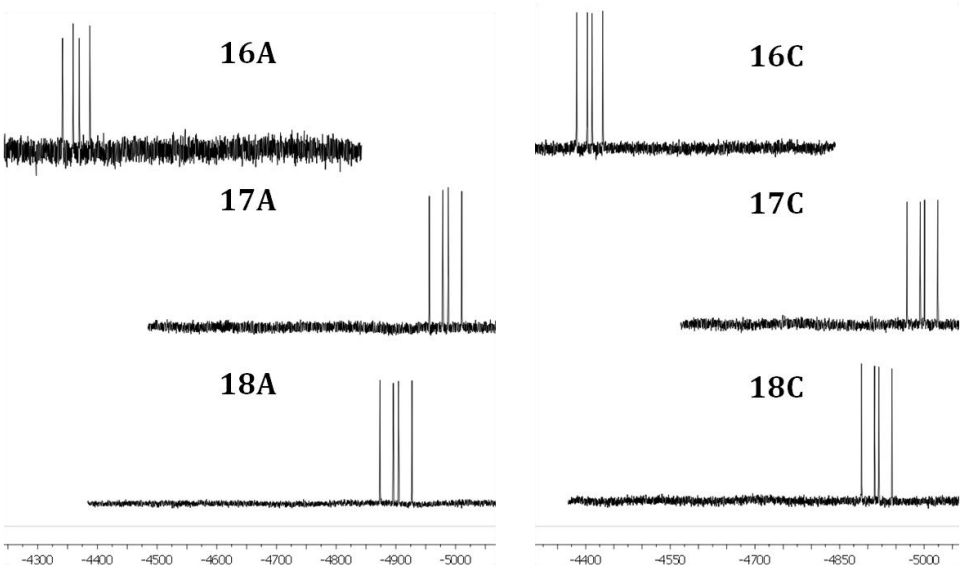

(a) (b)

Figure 4.2. $^{195}Pt\{^{1}H\}$ NMR spectra of **16A**-**18A** (a) and **16C-18C** (b) in CD_2Cl_2 at r.t.

The X-ray diffraction study on single crystals of **16A**, **18A, 16C** and **17C** (Figure 4.3 and Table 4.2, and Figures S7-S10 and Table S1 in SI-4.1) confirmed that in these complexes the platinum center exhibits a distorted square-planar environment as a consequence of the small bite angles of both chelate ligands (R-C^C* and P^P). Bond distances and angles concerning the "Pt(C^C*)" moiety are similar to those observed for other five-membered metalacycles of Pt(II) with the N-heterocyclic carbenes.[28b, 29e, 30-32, 45] Regarding the "Pt(P^P)" fragment, the Pt–P1 bond lengths [2.3209(6) - 2.3284(9) Å] are slightly longer than those of the Pt-P2 ones [2.2787(13) - 2.2922(10) Å], complying with the C_{Ar} atom (C6) atom having a higher trans influence than that of the C* one (C1).[31] The P-Pt-P bite angle in **16A** and **16C** (~71°) is smaller than that in **18A** and **17C** (~ 83°) and significantly smaller than 90°, implying that the four-membered chelate ring is under great strain. In the cationic complex of **18A** the benzene ring (C38-C43) is not coplanar with the Pt (II) coordination plane (Pt, C1, C6, P1, P2), forming a dihedral angle of 18.99º.

In their crystal structure packings, there are no Pt-Pt contacts (Figures S7-S10). However, rather weak intermolecular interactions were observed. The molecules arrange themselves in pairs in a head-to-tail fashion (**16A** and **18A**) supported by C_{Ar}-H···π (2.80 – 2.91 Å) and π···π (3.35 Å for **18A**) intermolecular contacts between the C^C* fragments and aromatic rings from the P^P ligand. In case of **16C** and **17C**, they show head-to-tail distribution supported by π···π (3.32 – 3.37 Å) intermolecular contacts between the C^C*

fragments. Also, in all four crystal structures there are some weak C-H···F contacts (d C-F= 2.97 - 3.32 Å; d H-F= 2.32 - 2.60 Å) between the complex cation and the PF_6^- anion [27e, 46]

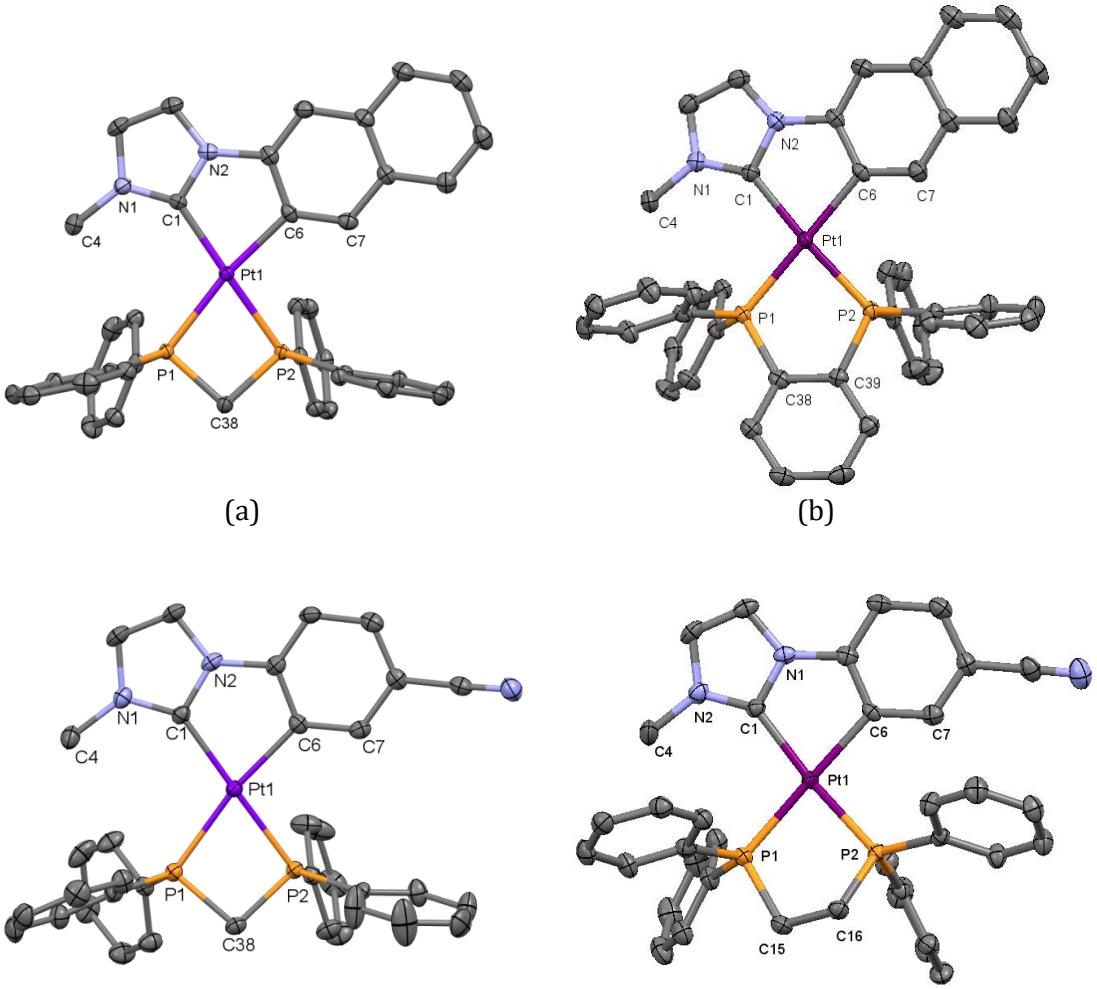

Figure 4.3: Molecular structures of the cation complexes **16A** (a) **18A** (b), **16C** (c) and **17C** (d). Thermal ellipsoids are drawn at the 50% probability level. Hydrogen atoms, PF_6 and solvent molecules have been omitted for clarity. Labeling of the P atoms in **17C** (d) was changed with respect to that of **12C** in Chapter 2 and SI-2 for comparison purposes.

This cation-anion association seems to occur in acetone solutions, which substantiates the low conductivity values observed for them (Λ_M: 62.9- 69.0 Ω^{-1} cm^2 mol^{-1} in a $5 \cdot 10^{-4}$ M acetone solution) compared with the expected ones for 1:1 electrolytes (100-120 Ω^{-1} cm^2 mol^{-1}).[47]

Table 4.2: Selected bond lengths (Å) and angles (°).

	16A·CH_2Cl_2	**18A·0.5 CH_2Cl_2**	**16C**	**17C· CH_2Cl_2**
Pt(1)-C(1)	2.030(2)	2.0602(3)	2.041(3)	2.055(4)
Pt(1)-C(6)	2.047(2)	2.086(3)	2.054(3)	2.080(4)
Pt(1)-P(1)	2.3209(6)	2.3020(11)	2.3284(9)	2.3218(13)
Pt(1)-P(2)	2.2831(6)	2.2886(10)	2.2922(10)	2.2787(13)
C(1)-Pt(1)-C(6)	79.66(9)	79.30(12)	79.36(11)	79.05(17)
C(6)-Pt(1)-P(2)	100.08(7)	97.55(9)	100.25(8)	96.00(12)
C(1)-Pt(1)-P(1)	108.65(6)	100.66(9)	109.28(8)	101.91(13)
P(1)-Pt(1)-P(2)	71.72(2)	82.83(3)	71.17(4)	83.15(5)

4.1.2. Optical properties and DFT/TD-DFT calculations of [Pt(R-C^C*)(P^P)]PF_6

Absorption spectra and DFT/TD-DFT calculations. The absorption spectra of **16A**–**18A** and **16C**–**18C** in CH_2Cl_2 at low concentration ($5\cdot10^{-5}$ M) show the lower energy absorption onsets at $\lambda \geq 350$ (**16A**–**18A**) and ≈ 320 nm (**16C**–**18C**) (see Figure 4.4 and Table S2). These transitions obey the Beer's law in the range $5\cdot10^{-4}$ M – 10^{-6} M (see Figure S11) indicating the absence of significant aggregation within this concentration range.

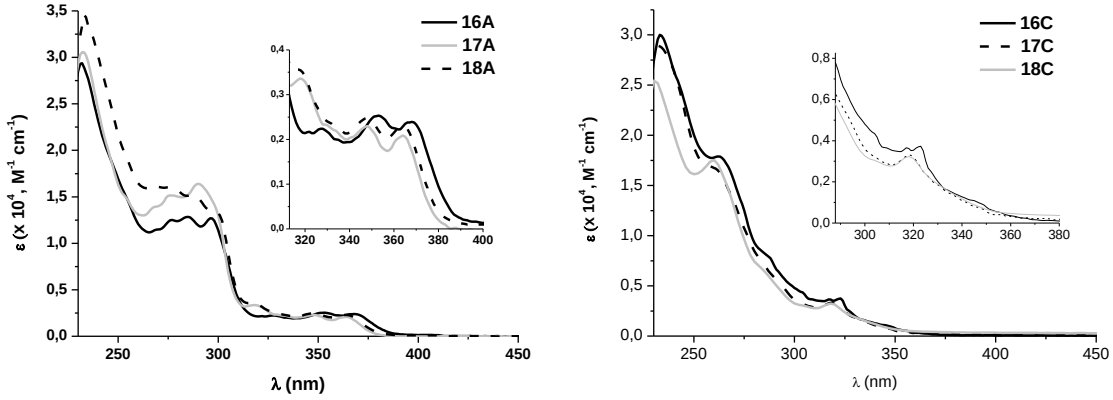

Figure 4.4. UV-vis spectra of **16A–18A** (left) and **16C–18C** (right) in CH_2Cl_2 ($5\cdot10^{-5}$ M).

The electronic features of the NC-C^C* derivatives (**16C–18C**) differ from those of the naphthyl counterpart (**16A–18A**), as previously stated.[30, 45] Regarding the ancillary ligands (P^P), the low energy bands of the dppm derivatives (**16A** and **16C**) appear red shifted with respect to the corresponding dppe and dppz ones (see insets Figure 4.4). It seems clear that both, R-C^C* and P^P, ligands are involved in the lowest energy spin-allowed

transition. Diffuse reflectance spectra of powdery samples of **16A**–**18A** and **16C**–**18C** are quite similar to those observed in solution of CH_2Cl_2 (Figure S12). Therefore, the same origin of the lower energy absorption can be assumed.

According to DFT and TD-DFT calculations carried out on **16A**, **18A**, **16B** and **18B**† (see SI-4.1: full discussion, Tables S3-S8, Figures S13-S16), the origin of the lowest energy absorption can be ascribed to mixed LL'CT [π(NHC) → π*(P^P)] / LMCT [π(NHC) → 5d(Pt)] / ILCT [π(NHC) → π*(NHC)] transitions for the Naph^C* derivatives (**16A** and **18A**), and mainly LL'CT [π(NHC) → π*(P^P)]/ ILCT [π(NHC) → π*(NHC)] for the EtO_2C-C^C* ones (**16B** and **18B**) and therefore for **16C** and **18C**.

Emission spectra. Emission data for **16A**–**18A** and **16C**–**18C** are summarized in Table 4.3. In rigid matrix (10^{-5} M CH_2Cl_2 solution at 77 K) and in PMMA films, all complexes show blue and highly structured emissions with vibronic spacings [~ 1474 cm^{-1}] corresponding to the C=C / C=N stretches of the cyclometalated NHC ligands (see Figure 4.5 and S17). The emission lifetimes fit to one rather long component for **16A**–**18A** (286-563 μs) and **16C**–**18C** (17-28 μs), indicating the emission from a triplet state. These values are in line with those observed for other compounds containing these same "(R-C^C*)Pt" (R-C = Naph, R = CN) moieties.[29e, 30, 45]

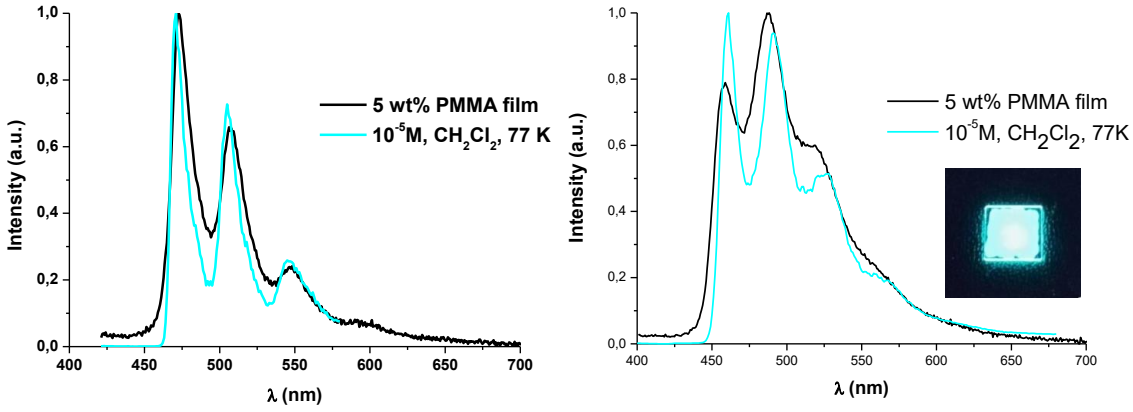

(a) (b)

Figure 4.5. Normalized emission spectra of **16A** (a) and **16C** (b). Picture under UV-light (365nm).

† Given the similarities in the electronic properties of the two NHC ligands **B** and **C**, the studies carried out for TAZ-TFG-2016-2095 have been used for a proper assignment in **16C** and **18C**.

Table 4.3. Photophysical Data for complexes **16A**-**18A** and **16C**-**18C**.

Comp.	Media (T/K)	λ_{ex} (nm)	λ_{em} (nm)	τ (μs)[c]	ϕ[d]
16A	CH_2Cl_2[a](77)	367	470_{max}, 505, 546, 598_{sh}	286.1	
	CH_2Cl_2[b] (77)	380	473_{max}, 509, 556, 606, 656_{sh}	211.0	
		418	473, 509, 560_{max}, 608, 658_{sh}	72.5	
	PMMA Film	340	473_{max}, 508, 547, 592_{sh}		0.75
	Solid (298)	400	560, 605_{max}, 654, 718_{sh}	34.7	0.21
17A	CH_2Cl_2[a](77)	362	471_{max}, 506, 547, 593_{sh}	541.0	
	CH_2Cl_2[b] (77)	367	475_{max}, 509, 552, 603_{sh}	435.3	
		400	475, 509, 567_{max}, 612, 663_{sh}	73.9	
	PMMA Film	340	476_{max}, 510, 550, 597_{sh}		0.53
	Solid (298)	361	560, 601_{max}, 649	47.4	0.24
18A	CH_2Cl_2[a](77)	363	473_{max}, 508, 548, 594_{sh}	563.9	
	CH_2Cl_2[b] (77)	373	475_{max}, 510, 552, 603_{sh}	419.0	
		395	475, 510, 570_{max}, 617, 669_{sh}	110.4	
	PMMA Film	340	476_{max}, 511, 551, 598_{sh}		0.89
	Solid (298)	375	476, 510, 578_{max}, 613	21.8	0.06
		400	476, 510, 582, 615_{max}		
16C	CH_2Cl_2[a](77)	323	456_{max}, 487, 521, 557_{sh}	21.2	
	CH_2Cl_2[b] (77)	350	460_{max}, 491, 524, 558_{sh}	17.5	
	PMMA Film	340	459, 487_{max}, 516, 554_{sh}		0.75
	Solid (298)	340	459, 489_{max}, 520, 555_{sh}	6.5	0.15
17C	CH_2Cl_2[a](77)	317	446_{max}, 477, 508, 540_{sh}	28.0	
	CH_2Cl_2[b] (77)	340	449_{max}, 480, 512, 546_{sh}		
	PMMA Film	340	450, 478_{max}, 503, 544_{sh}		0.73
	Solid (298)	325	460_{sh}, 489_{max}, 517_{sh}	31.3	0.20
18C	CH_2Cl_2[a](77)	317	445, 475_{max}, 507, 540_{sh}	26.2	
	CH_2Cl_2[b] (77)	367	448, 470_{max}, 505, 544, 589_{sh}	23.7	
	PMMA Film	340	450, 478_{max}, 503, 544_{sh}		0.61
	Solid (298)	328	448, 476_{max}, 504, 540_{sh}	10.9	0.07

a = 10^{-5} M; *b* = 10^{-3} M; *c*= data at λ_{max}; *d* = 5 wt% PMMA films in Ar atmosphere.

The excitation spectra corresponding to these emissions match with the UV-vis absorption ones but contrary to what can be expected from the UV-vis and TD-DFT calculations, the emission of **16A** is not red-shifted with respect to those of **17A** and **18A**. This and the big difference in the emission lifetimes of the **A** and **C** derivatives suggest that their emissions arise from different excited states. Therefore the phosphorescent emissions have been assigned to mainly ^{3}ILCT [π(NHC) → π*(NHC)] for **16A**–**18A** and mixed ^{3}LL'CT [π(NHC) → π*(P^P)]/ ^{3}ILCT [π(NHC) → π*(NHC)] transitions for **16C**–**18C**.

At higher concentration (10^{-3} M) in CH_2Cl_2 at 77K or in the solid state, the emissions of compounds **16C**–**18C** do not differ much from those obtained in diluted solution (10^{-5} M) of CH_2Cl_2 at 77K, and can be assigned to the same excited state (see Table 4.3). However, compounds **16A**–**18A**, at higher concentration (10^{-3} M) display wavelength-dependent emissions, similarly to those observed in related complexes [(Naph^C*)Pt(CNR')$_2$]PF_6 (R' = *t*-Bu, Xyl).[30] Upon excitation at λ ≤ 380 nm, they show a high energy (HE) band identical to

the one in diluted solution, but at longer excitation wavelengths (λex ~ 400 nm) the intensity of this HE band decreases and a low energy (LE) band with maximum at *ca*. 565 nm becomes predominant (Figure 4.6 a for **16A**). This LE emission presents shorter lifetimes (≤ 100 μs) but a vibronic pattern with spacings [~ 1343 cm^{-1}] typical of the C=C / C=N stretches of the cyclometalated NHC ligands.

The solid state spectra of compounds **16A**–**18A** show this structured LE emission with maximum at ~ 610 nm when exciting at 360-375 nm; just in compound **18A**, a significant contribution of HE emission is also observed, but the LE band can be almost selectively obtained if the excitation wavelength increases to 400 nm (see Figure 4.6 b). This LE band is tentatively ascribed to $^3\pi\pi^*$ due to the formation of aggregates in the ground state, since it appears at high concentration (10^{-3} M), as aforementioned. The excitation spectra features (see Figure 4.6 a) and the π–π contacts described by X-ray diffraction studies support this assignment. Quantum yield (QY) measurements in PPMA films revealed that all complexes are very good blue and green-cyan emitters at room temperature. To the best of our knowledge, the QY values (53% – 89%) are amongst the highest ones for blue and green-cyan emitters of platinum(II) in PMMA film: [Pt(C^C*)(acac)] (Φ = 0.86,[26e] 0.90[28b], [Pt(C*^C^C*)Cl] (Φ = 0.32[14b] and [Pt(C^X-L^L')] [C^X = phenyl methyl imidazole; L^L' = phenoxy pyridine, Φ = 0.58; L^L' = carbazolyl pyridine, Φ = 0.89; C^X = phenyl pyrazole; L^L' = carbazolyl pyridine, Φ = 0.85].[14c]

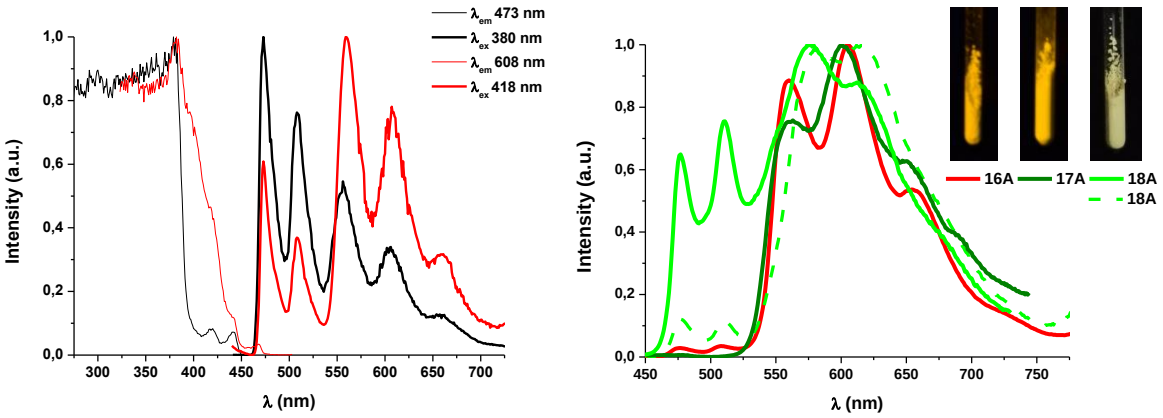

(a) (b)

Figure 4.6. Normalized excitation and emission spectra of **16A** in rigid matrix of CH_2Cl_2 (10^{-3} M, 77 K) (a) and **16A**–**18A** in solid state at r.t. (—, λex= 375 nm and ---, λex= 400 nm, for **18A**) (b). Pictures taken with UV light (λ_{ex} = 365 nm).

4.2 ACETYLACETONATE COMPOUNDS

4.2.1. Synthesis and Characterization of [Pt(R-C^C*)(acac)]

The β-diketonate compounds [Pt(R-C^C*)(acac)] (**19B–19D**) were synthesized by reaction of the corresponding chlorine bridged compounds [{Pt(μ-Cl)(R-C^C*)}$_2$] (R = CO_2Et **4B**, CN **4C**, Cl **4D**) with Tl(acac) in a 1:2 molar ratio (see Experimental Section and Scheme 4.2 path a),† following the same procedure than that reported previously by our group for compound [Pt(Naph^C*)(acac)].[29e]

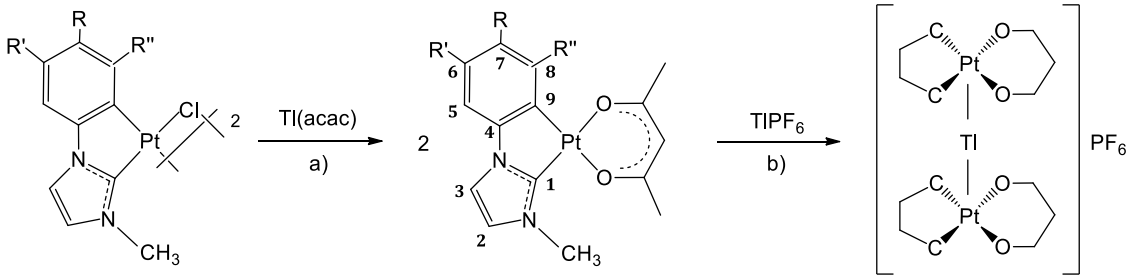

4B (R = CO_2Et; R', R'' = H)
4C (R = CN; R', R'' = H)
4D (R = H; R', R'' = Cl)

19B (R = CO_2Et; R', R'' = H)
19C (R = CN; R', R'' = H)
19D (R = H; R', R'' = Cl)

20B (R = CO_2Et; R', R'' = H)
20C (R = CN; R', R'' = H)
20D (R = H; R', R'' = Cl)

Scheme 4.2. Synthetic pathway for the preparation of compounds **19B**-**19D** and **20B**-**20D**.

Compound **19C** was already reported by Egen et al. following a different method.[48] The synthetic procedure of **19B–19D** requires the availability of the dichloro bridged complexes **4B–4D**. Then, compound **4D** was prepared following the step-by-step method used previously for **4B–4C**[30-31] (see Supporting Information 4.3: description, Scheme S1 and Figures S1–S4). The IR spectra of compounds **19B–19D** show two υ(C=O) stretching vibrations at significantly lower energies than those found for the free ligand (ca. 1720 cm^{-1}) which are indicative of the diketonate chelation to the metal center.[29e] Their ^{1}H and ^{13}C NMR spectra show the expected signals for the cyclometalated NHC group and evidence the nonequivalence of the two halves of the β-diketonate ligand, as correspond for a chelate coordination (see NMR data and Figure S5 in SI-4.3).

† Compounds **19B**, **19C** and **19D** appeared labeled as **1B**, **1A** and **1C** respectively in SI-4.2 and 4.3. Atom labeling for NMR purposes according to SI-4.2 and 4.3.

The ^{195}Pt NMR spectra show a singlet at about −3400 ppm for **19B** and **19C** and at −3167 ppm for **19D**, which seems to suggest a less electron-donor character of the Cl-C^C* with respect to the other R-C^C* fragments.

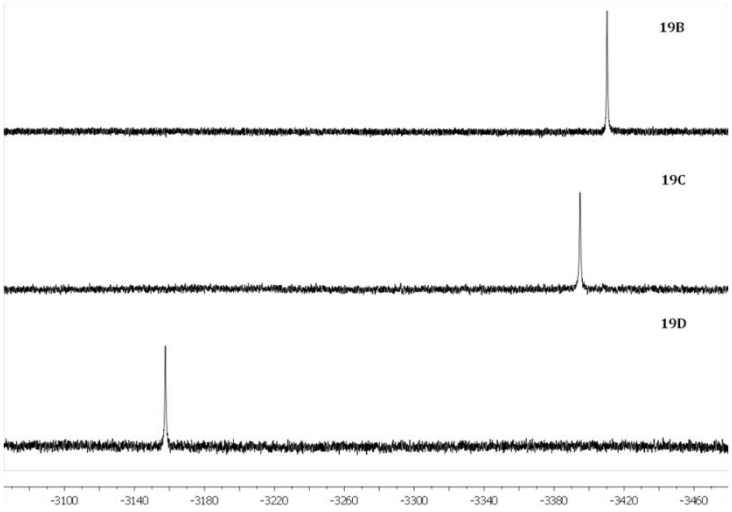

Figure 4.7. ^{195}Pt {^{1}H} NMR spectra of compounds **19B**–**19D** in CD_2Cl_2.

The molecular structures of **19B** and **19D** (Figures 4.8 a–c), determined by single-crystal X-ray diffraction (full description in SI-4.2), showed that in both complexes, the platinum(II) center exhibits a distorted square-planar environment. In the solid state, complex **19B** arranges together in pairs in a head-to-tail fashion through intermolecular Pt···Pt (3.370 Å) and π–π (~3.43 Å) interactions between the NHC ligand and the acac (see Figure 4.8 b).[29e] However, in **19D**, neither Pt···Pt nor π···π intermolecular interactions were observed in the crystal, although C–H···Cl short contacts were found, as can be seen in Figure S8 in SI-4.3.

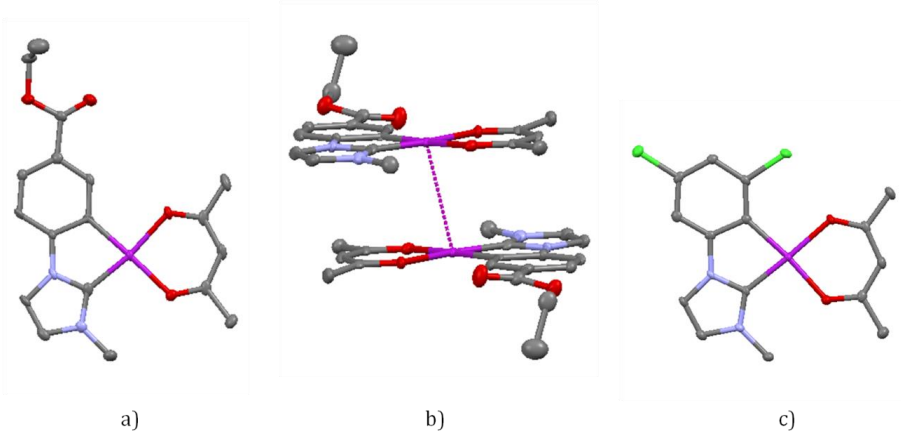

Figure 4.8. Molecular structures of **19B** (a) and **19D** (c), and dimer-like stacking view of **19B** (b).

4.2.2. Synthesis and Characterization of the clusters [{Pt(R-C^C*)(acac)}$_2$Tl]PF$_6$

Previous work in our research group in the field of intermetallic interactions showed that "Pt-M" (M = Ag(I), Au(I), Tl(I))[49] clusters are often luminescent, and also that these Pt-M and M···M interactions can increase the emission efficiency of these species. As other neutral Pt(II) complexes,[49] compounds [Pt(R-C^C*)(acac)] (**19B**–**19D**) are expected to be basic enough towards acid metal centers to give clusters containing Pt → M donor–acceptor bonds. Therefore we decided to explore the reactivity of **19B**–**19D** towards $TlPF_6$.

Treatment of the β-diketonate compounds [Pt(R-C^C*)(acac)] (R = CO_2Et **19B**, CN **19C**, Cl **19D**) with $TlPF_6$ (2:1 molar ratio) in CH_2Cl_2/acetone led to the clusters [{Pt(R-C^C*)(acac)}$_2$Tl]PF$_6$ (R = CO_2Et **20B**, CN **20C**, Cl **20D**),† which were obtained as analytical pure solids in good yield and characterized by ^{1}H NMR, IR, mass spectrometry (see Scheme 4.2 path b and Supporting Information 4.3) and X-ray crystallography. Their MALDI(+) spectra show the molecular peaks associated with [{Pt(R-C^C*)(acac)}$_2$Tl]$^+$ and [Pt(R-C^C*)(acac)Tl]$^+$, which might suggest the integrity of the trimetallic species. However, in solution at room and low (−80 °C) temperatures, the ^{1}H and ^{195}Pt{^{1}H} NMR spectra of **20B**–**20D** fit those of their corresponding starting materials (see ^{195}Pt{^{1}H} NMR spectra of **20C** in Figure S9 in SI-4.3), indicating the breakdown of the Pt–Tl bonds. The photophysical data (see below) of all of these compounds were investigated and are in agreement with the rupture of the Pt–Tl bonds in solution.

The X-ray crystal structures of **20B**, **20C** and **20D** were performed on single crystals obtained from solutions of them in acetone (**20B**, **20C**) or CH_2Cl_2 (**20D**). As can be seen, compounds **20B**–**20D** display a "Pt_2Tl" sandwich structure (Figures 4.9 and 4.10), where two slightly distorted square planar "Pt(R-C^C*)(acac)" subunits are bonded to a Tl(I) center through Pt–Tl bonds. In each complex, the two Pt–Tl bonds exhibit intermetallic distances in the range of those observed in complexes containing Pt(II)–Tl(I) donor–acceptor bonds with no bridging ligands between the metal centers.[50] In case of **20C** and **20B**, the Pt-Tl vectors are almost perpendicular to the Pt coordination planes (angles with the normal: 18.9(1)º Pt1A, 5.7(1)º Pt1B, **20C**; 11.4(2)º Pt1A, 10.8(1)º Pt1B, **20B**), which reveal an almost square pyramidal environment around the platinum center with the thallium atom being located on the apical position shared by both the two pyramids with a Pt-Tl-Pt angle of 169.813(9)º **20C** and 144.512(18)º **20B**.

† Compounds **20B**, **20C** and **20D** appeared labeled as **2B**, **2A** and **2C** respectively in SI-4.2 and 4.3

In these compounds the platinum coordination planes are almost parallel (interplanar angle: 14.8(1)º **20C**, 34.8(2)º **20B**) but lie somewhat staggered [torsion angle O1A-Pt1A-Pt1B-O1B: 40.6º **20C**, 90.7º **20B**]. In case of **20C** an additional acetone molecule interacts with the Tl(I) center through a weak Tl-O bond (2.7692(42) Å). The Tl-O separation is comparable to those in other complexes[50-51] but significantly longer than the sum of the covalent radii (2.21 Å).[52]

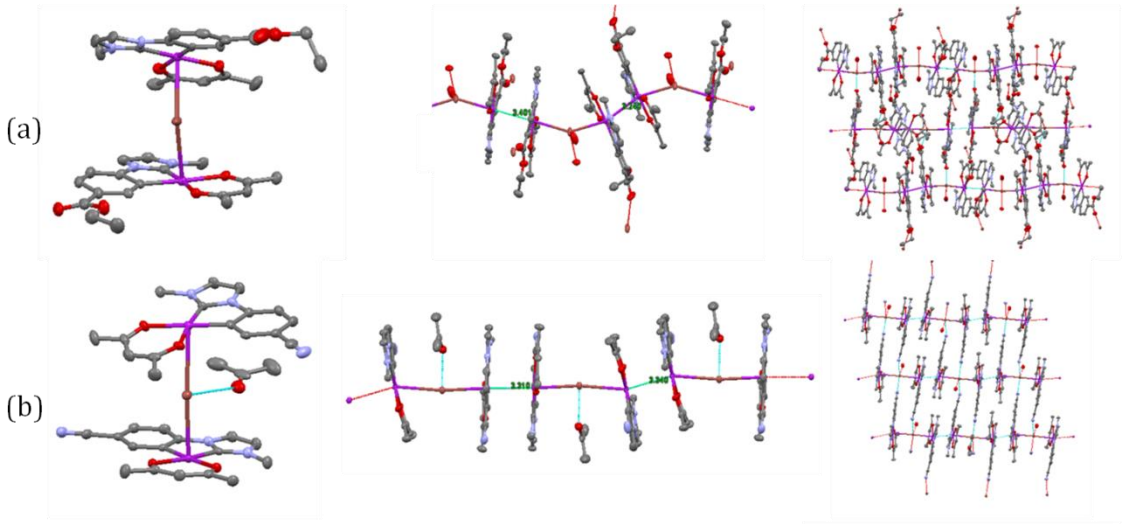

Figure 4.9. Molecular and supramolecular structure views of **20B** (a) and **20C** (b).

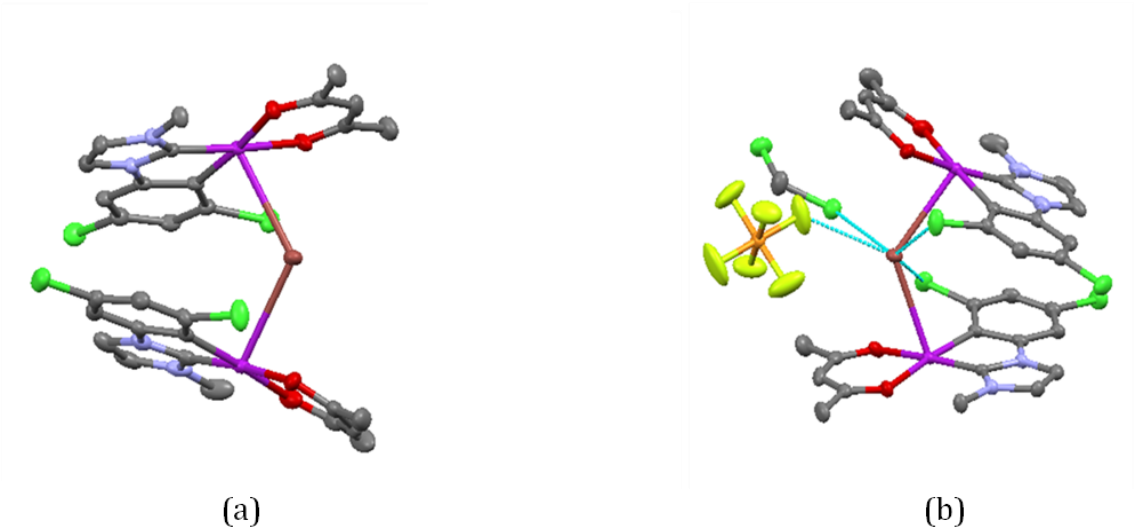

Figure 4.10. Molecular structure of **20D** (a) and structure view of the Tl···E interactions (b).

The trinuclear "Pt_2Tl" units rearrange in the crystal generating two-dimensional (2D) networks through additional stabilizing contacts. On one hand, the "Pt_2Tl" units stack through intermolecular Pt···Pt (3.340 Å, 3.310Å **20C**; 3.401 Å, 3.240Å **20B**) interactions[27d,

[53] and weak π−π contacts between the NHC and the acac ligands[29e], giving rise to almost linear PtB−Tl−PtA··PtA−Tl−PtB···PtB wires in **20C** [angles: PtB-Tl-PtA: 169.813º, Tl-PtA··PtA: 158.77º, Tl-PtB···PtB: 165.32º] and zig-zag chains in **20B** [angles: PtB-Tl-PtA: 145.512º, Tl-PtA··PtA: 177.80º, Tl-PtB···PtB: 160.07º] (see Figure 4.9).

These chains appear linked together through two additional Tl-E (E') (E, E' = N **20C**, O **20B**) bonds with the R substituents of the R-C^C* groups (R= CN **20C**, CO_2Et **20B**) belonging to the two adjacent chains (see Figure 4.9). The Tl-N (NC-C^C*) and Tl-O (CO_2Et-C^C*) distances are longer than expected for covalent bonds but shorter than the sum of the covalent radii of Tl(I) (1.55 Å) and the van der Waals radii of N (1.55 Å) and O (1.52 Å).[54] The Tl···N separations are comparable to those found in derivatives containing Tl···N interactions, such as $[PtTl(C^N)(CN)_2]$(C^N = 7,8-benzoquinolinate (bzq), 2-phenylpyridinate (ppy)) or $[\{PtTl(bzq)(CC\text{-}C_5H_4N\text{-}2)_2\}_2]$[27b] and [trans,trans,trans-$Tl_2\{Pt(C_6F_5)_2(CN)_2\}$ $(CH_3COCH_3)_2]_n$.[51b] Then, the five-coordinated Tl(I) center in **20C** is located in the middle of the base of a square-pyramid with bond angles around the Tl(I) center close to 90º [angles: Pt1A-Tl-N3B: 92.0º, Pt1B-Tl-N3B: 95.0º, Pt1A-Tl-N3A: 81.2º, Pt1B-Tl-N3A: 93.3º, O3-Tl-N3B: 89.5º, O3-Tl-N3A: 101.6º, Pt1A-Tl-O3: 86.2º, Pt1B-Tl-O3: 86.5º]. Single crystals of **20B** were also obtained from an acetone solution, however in this case the Tl(I) center does not coordinate any acetone molecule and exhibits a distorted tetrahedral coordination environment [angles: Pt1A-Tl-O3A: 108.5.0º, Pt1A-Tl-O3B: 110.8º, Pt1B-Tl-O3A: 93.1º, Pt1B-Tl-O3B: 87.8º, O3A-Tl-O3B: 107.6º].

Compound **20D**, unlike **20B** and **20C**, is a discrete molecule and not a 2D lattice, because of the absence of intermolecular or packing interactions (see Figure 4.10 a, Figure S10 in SI-4.3). In compound **20D**, the Tl(I) in addition to the two Pt−Tl bonds (*d* Pt-Tl: 3.0230(2) Å, 2.9962(2) Å; Pt-Tl-Pt: 119.475(8)º), establishes two intramolecular Tl···Cl contacts (*d* Tl···Cl = 3.3237(1) and 3.5717(4) Å), one with each of the "Pt(Cl-C^C*)(acac)" fragments, a Tl···F contact (*d* Tl···F = 3.063 Å) with the anion and a Tl···Cl contact (*d* Tl··Cl = 3.497 Å) with a CH_2Cl_2 molecule, to complete a distorted octahedral coordination environment (Figure 4.10 b). All the Tl-E (E = Cl, F) distances are rather long, but lower than the sum of the van der Waals radii of Tl(I) (1.96 Å), and F (1.47 Å) or Cl (1.75Å).[54] In this molecule, the Pt-Tl vectors are further away from the perpendicular to the Pt coordination planes (angles: 25.2(1)º Pt1A, 19.6(1)º Pt1B) than in compounds **20C** and **20B** and the angle Pt-Tl-Pt (119.475(8)º) is far away from the ones observed in **20C** and **20B**, probably forced by the existence of the two intramolecular Tl···Cl contacts (Figure 4.10 b).

It should be noted that in **19B,** the molecules arrange themselves in dimers through Pt···Pt interactions, not giving rise to 1D wires, as observed in **20B** and **20C**. Presumably, the Pt-Tl donor acceptor bond decreases the electron density on the platinum, playing a similar role to that of π-acceptor ligands, thereby reducing electronic repulsions between the Pt centers and favoring the 1D chain formation through Pt···Pt interactions.[55]

4.2.3. Optical properties and DFT/TD-DFT calculations of compounds [Pt(R-C^C*)(acac)] and the corresponding clusters [{Pt(R-C^C*)(acac)}$_2$Tl] PF_6

Absorption spectra and DFT/TD-DFT calculations. Full data and Figures can be found in SI-4.3. UV−vis spectroscopic data of compounds **19B**−**19D** and **20B**−**20D** have been listed in Table S1. The spectra of **19B**−**19D** in CH_2Cl_2 solution (see Figure S11) display low intensity absorptions (ε > 103 M^{-1} cm^{-1}) at low energies (λ > 290 nm). In the case of **19D**, they appear clearly shifted to higher energies with respect to those of **19B** and **19C**, indicating the participation and the effect of the R-C^C* (R = CN, CO_2Et, Cl) group in these absorptions. In the case of **19C**, these absorptions are very similar to those of **19B** in energy and profile, in agreement with the similar electronic features observed previously for the R-C^C* (R = CN, CO_2Et) groups.[45] The solid-state diffuse reflectance UV−vis spectra (Figure S12) show additional broad bands at low energy when compared with those observed in dichloromethane solution, which can be tentatively attributed to the existence of intermolecular Pt−Pt interactions, on the light of the X-ray structure of **19B** and those of other related complexes.[29e]

DFT and TD-DFT calculations in solution of CH_2Cl_2 for **19B** and **19D** have been carried out to provide correct assignments for the UV−vis absorptions and also to evaluate the effect of the cyclometalated R-C^C* group (see full data and discussion in SI-4.3). Considering the composition of the frontier molecular orbitals (FOs), the calculated allowed absorptions, which are in good agreement with the experimental UV−vis spectra (Figure S14), and the origin of calculated S_1, which arises mainly from a HOMO to LUMO transition (79% **19B**, 62% **19D**), the lowest energy absorption band can be attributed basically to L'LCT [π(acac) → π*(NHC)] transitions for **19D**, and mixed L'LCT [π(acac) → π*(NHC)]/MLCT [5d(Pt) → π*(NHC)] transitions for **19B**. Although S_2 arises mainly from an H-1 to LUMO transition, it is very similar in nature to S_1. Taking into account the similarities in the electronic features of the R-C^C* (R = CN, CO_2Et) groups observed in the absorption spectra of **19B** and **19C**, as well as in those of other compounds reported previously,[45] the nature of the lowest energy absorption of **19C** is expected to be quite similar in nature to that of **19B**.

The absorption spectra of complexes **20B**–**20D** in 2-MeTHF solutions (10^{-4} M) are all identical to those of their respective precursors, **19B**–**19D** (see Figure S15 in SI-4.3), which match with the rupture of the Pt–Tl bonds in solution, as deduced from their NMR spectra. Similar behavior was previously observed in related extended structures with M–Tl bonds [M(C^N)$(CN)_2$Tl] (M = Pt,[27b] Pd,[56] C^N = 7,8-benzoquinolinate, 2-phenylpyridinate).

The absorption spectra of powdery solid samples of **20B**–**20D** basically fit with those of the starting materials (Figure S16). In the low-energy region just **20B** displays an additional absorption with respect to its precursor, with λ_{max} at 400 nm (see Figure 4.11). Keeping in mind the shorter Pt–Tl and Pt···Pt distances in the network of **20B** compared to those of **20C**, this absorption could be attributed to metal–metal-to-ligand charge transfer (^{1}MMLCT) [dσ*(Pt–Pt) → π*(NHC)] transitions likely to have been affected by the Pt–Tl bonds.

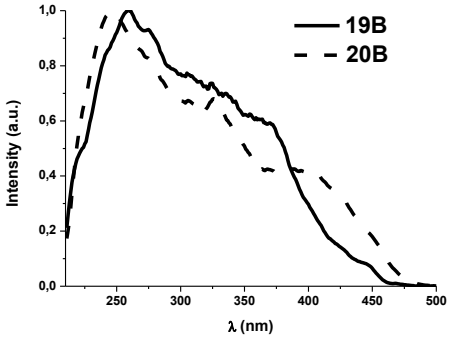

Figure 4.11. Normalized diffuse reflectance spectra of powdery solids samples of **19B** and **20B** at r.t.

Emission Spectra. Emission data are summarized in Table 4.4†. In diluted glassy solutions of 2-MeTHF (10^{-5} M, 77 K), compounds **19B**–**19D** show blue well resolved vibronic emissions (see Figure S17) that do not change at higher concentration (10^{-3} M, Figure S18). Their vibrational spacings [1367–1406 cm^{-1}] correspond to the C=C/C=N stretches of the cyclometalated NHC ligand (C^C*), suggesting their involvement in the excited state. The emissions of **19B** and **19C** (λmax ≈ 440 nm) are red-shifted with respect to that of **19D** (λmax = 417 nm), probably due to the participation of the R-substituent in the stabilization of the LUMO, as revealed by the DFT studies. Emissions and lifetime decays of **19B** and **19C** are identical to those observed in [Pt(R-C^C*)(py)(PPh_3)]PF_6[45] and very similar [Pt(R-C^C*)$(CNR')_2$]PF_6[30] which contain the same "(R-C^C*)Pt" fragments. Thus, taking into account all this and the TD-DFT calculations, the phosphorescent emissions of

† Figures S17-S25 can be found in SI-4.3.

19B–19D can be mainly ascribed to transitions of monomeric species derived from ^{3}ILCT [(NHC)] transitions mixed with some, if any, ^{3}L'LCT [π(acac) → π*(NHC)]/^{3}MLCT [5d(Pt) → π*(NHC)] in the case of **19B** and **19C** and with ^{3}L'LCT [π(acac) → π*(NHC)] for **19D**. Emission spectra for the 5 wt % films of complexes **19B–19D** in (PMMA) are wavelength dependent, as can be shown in Figure 4.12. Upon excitation at λ = 330 nm, all the three compounds show a phosphorescent emission in the blue to green region of the visible spectrum, like in glassy 2-MeTHF, with quantum yields up to 0.93 (**19B**), very similar to that of **19C** (0.98), while just 0.04 for **19D** (Table 4.4).

Table 4.4. Emission data for Complexes **19B-19D** and **20B-20D**.

C.	Medium (T/K) [wt %]	λ_{ex}/nm	λ_{em}/nm	τ/μs [λ_{max}][a]	ϕ
19B	PMMA film [5 wt %][b]	330	446, 474$_{max}$, 502, 536$_{sh}$		0.93
		390	452, 484$_{sh}$, 532$_{max}$		0.59
	PMMA film [40 wt %][b]	330	452, 484$_{sh}$, 532$_{max}$		0.82
	solid (298 K)	400	485$_{max}$, 519, 550	2.1 (60%), 1.0 (40%) [485] 1.5 (83%), 2.8 (17%) [519]	0.48
	solid (77 K)	400	461, 495, 554$_{max}$	2.6 [461], 3.8 [554]	
	2-MeTHF (77 K)[c]	332	442, 472, 502, 536$_{sh}$	16.9	
19C	PMMA film [5 wt %][b]	330	441, 470$_{max}$, 503, 536$_{sh}$		0.98
		390	443, 474, 535$_{max}$		0.72
	PMMA film [40 wt %][b]	330	443, 474, 535$_{max}$		0.46
	solid (298 K)	400	462$_{sh}$, 479$_{max}$, 513, 555	0.28 (77%), 0.65 (23%)	0.04
	solid (77 K)	400	451, 477, 512$_{max}$	0.78 (70%), 3.1 (30%) [451]	
	2-MeTHF (77 K)[c]	332	439$_{max}$, 468, 500, 523$_{sh}$	17.1	
19D	PMMA film [5 wt %][b]	330	425, 450$_{max}$, 475		0.04
		400	540		0.09
	solid (298 K)	380	433, 452$_{max}$, 476, 516	3	0.07
	solid (77 K)	380	432, 456$_{max}$, 482, 515$_{sh}$	11.6	
	2-MeTHF (77 K)[c]	320	417$_{max}$, 443, 472, 500$_{sh}$	15.6	
20B	solid (298 K)	474	580	0.31 (67%), 1.15 (33%)	0.02
	solid (77 K)	474	561	0.95	
	2-MeTHF (77 K)[c]	332	443$_{max}$, 473, 505, 534$_{sh}$	16.7	
20C	solid (298 K)	380	450, 478$_{max}$, 506	0.64 [450] 0.43 (80%), 1.44 (20%) [478] 0.44 (77%), 1.8 (23%) [506]	0.17
	solid (77 K)	380	500	1.7	
	2-MeTHF (77 K)[c]	330	439$_{max}$, 469, 500, 524$_{sh}$	16.5	
20D	solid (298 K)	351	425, 450$_{max}$, 480, 514	1.3 (54%), 2.4 (46%) [450] 1.8 [480], 1.9 [514]	0.10
	solid (77 K)	343	421$_{sh}$, 448$_{sh}$, 494$_{max}$	3.3 (44%), 8.6 (56%) [494]	
	2-MeTHF (77 K)[c]	320	417$_{max}$, 444, 472, 501$_{sh}$	13.2	

[a]Lifetime measured at the $\lambda_{max.}$ [b]298 K. [c]10^{-5} M; at 10^{-3} M, the same emission and τ were obtained.

However, upon excitation at λ > 390 nm, there is a dramatic change in the emission profiles whereby a low-energy (LE) structureless band with maxima at ca. 540 nm becomes predominant, while the HE is still observed but as a low intensity shoulder.

Intrigued by this behavior, we carried out further experiments only focused on **19B** and **19C** since **19D** is barely emissive.

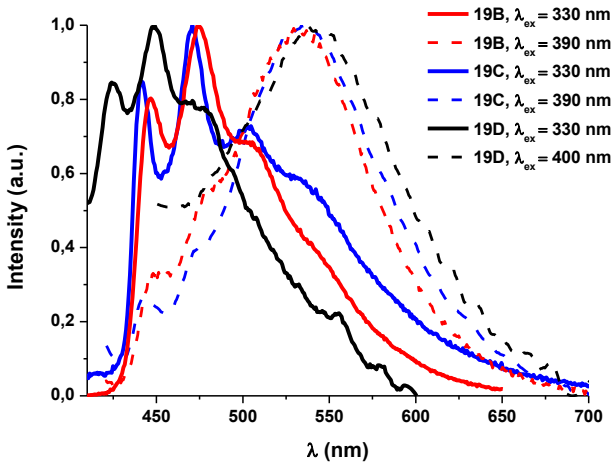

Figure 4.12. Normalized emission spectra of **19B**-**19D** in 5 wt % PMMA film.

Therefore, their emission spectra were registered in PMMA coated films at different weight concentrations ranging from 0.5 wt % to 40 wt %. As can be seen in Figure 4.13 (**19B**) and Figure S19 (**19C**), pure highly structured emissions were found at a concentration of 0.5 wt %. When increasing the weight percentage of the complex in the PMMA film, the intensity of the LE increases and that of the HE band decreases, resulting in a green emission as much for 20 wt % as for 40 wt % films. At 40 wt %, the green emission shows no dependence with the λex (see Figure S20). At 40 wt % concentration the QY values of the green emission kept fairly high for **19B** (0.82), while the emission of **19C** (QY = 0.46) became slightly self-quenched. In all likelihood, the LE bands can be attributed to metal–metal-to ligand charge transfer (^{3}MMLCT) [dσ*(Pt–Pt) → π*(NHC)] transitions, generated by the existence of aggregates in the ground state through Pt–Pt interactions, as observed in the X-ray structure of **19B**. The excimeric nature of this LE emission is discarded since the excitation spectrum of **19B** in PMMA film at 40 wt % is very similar to that obtained for the solid state one (see Figure S21). Therefore, the dual emission observed in PMMA films of **19B**–**19D** is likely due to a relatively slow internal conversion between the two emissive states ^{3}ILCT(NHC)/^{3}MMLCT at 298 K.[57]

In the solid state, powdery samples of **19B**–**19D** display bright blue and greenish blue emissions (λmax ≈ 480 nm for **19B** and **19C**; λmax= 452 nm for **19D**) with the emission of compound **19D** located further into the blue region of the spectrum than the others (Figure S22). Upon cooling to 77 K, the emission of **19D** appears a bit more structured and with a longer lifetime, being quite similar to the one obtained in 2-MeTHF solution (Figure 4.14).

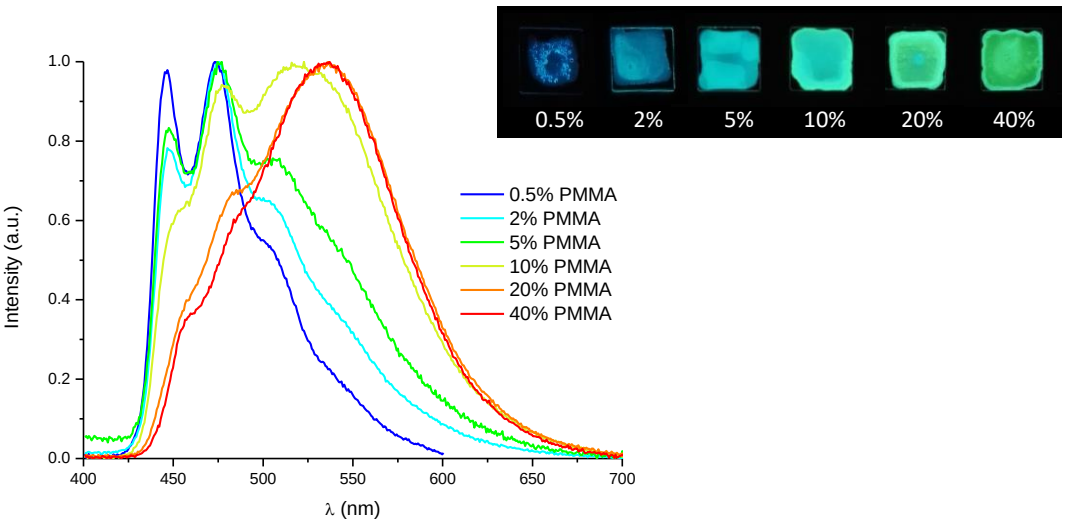

Figure 4.13. Normalized emission spectra of **19B** at λ_{ex} = 360 nm. Pictures under UV lamp (λ_{ex} = 365 nm).

However, both **19B** and **19C** (see Figure 4.14), regardless the excitation wavelength (350 to 450 nm), display broad bands with λmax = 512 and 554 nm, respectively, accompanied by high energy (HE) structured emissions at 461 (**19B**) nm and 451 (**19C**).

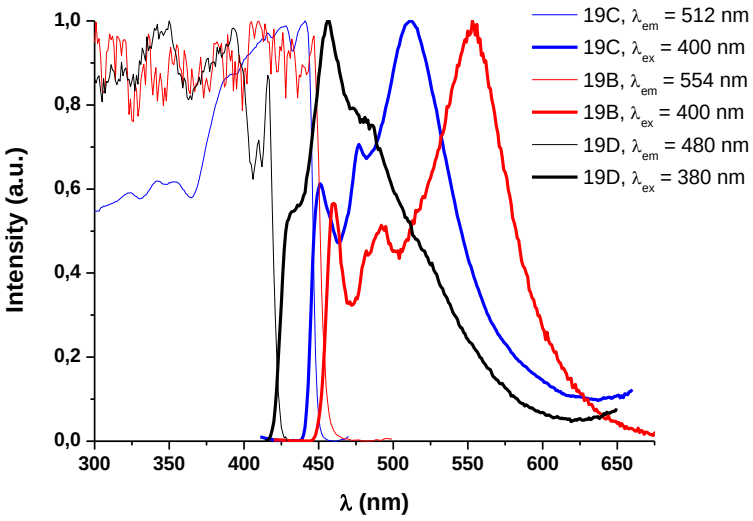

Figure 4.14. Normalized excitation (–) and emission (---) spectra of **19B**-**19D** in solid state at 77 K.

These HE bands resemble to those obtained in PMMA films with a low doping concentration (<5 wt %) and in solution of 2-MeTHF. Likewise, the LE bands of **19B** (554 nm) and **19C** (512 nm) are closely related to those obtained in PMMA films (>10 wt % and λex >360 nm). Therefore, these dual emissions (HE and LE bands) may come from the excited states discussed above (^{3}ILCT [(NHC)] and ^{3}MMLCT, respectively).

The emissive behavior of the "Pt_2Tl" clusters, **20B–20D**, was investigated to compare it with that of **19B–19D**. As expected, in glassy solutions of 2-MeTHF compounds **20B–20D** give the same emission bands and lifetime decays than **19B–19D** either at diluted (10^{-5} M) or concentrated solutions (10^{-3} M), which once again, evidence the rupture of the M–Tl bonds in solution even at 77 K (Figure S23). Emission spectra of **20B–20D** in 5 wt % PMMA films closely resemble those of their corresponding precursors, (see Figure S24), which pointed us to consider that in PMMA films the Pt–Tl bonds, if present, are negligible. In solid state at room temperature, the "Pt_2Tl" complexes display vibronic bands like their corresponding starting materials except **20B**, which shows a structureless broad band considerably shifted to lower energies (Figures 4.15 and 4.16), in line with the features observed in the absorption spectra of powdery samples (Figures 4.11 and S16).

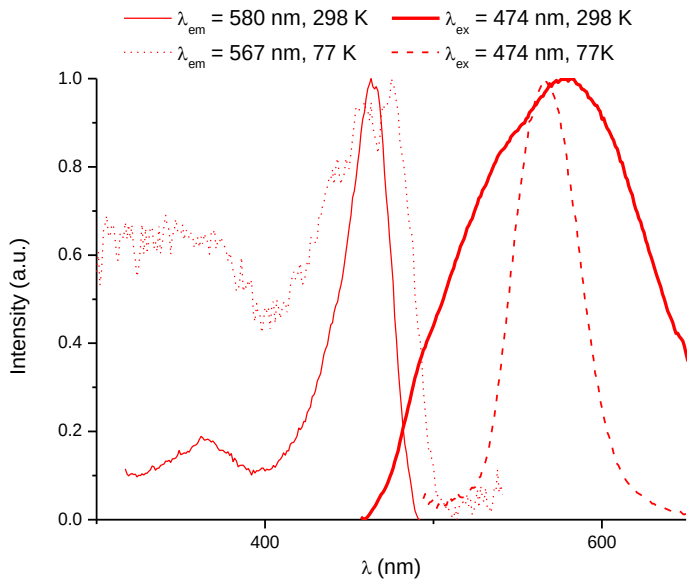

Figure 4.15. Normalized excitation (-) and emission (–) spectra of **20B** in the solid state.

At 77 K the emission of **20B** becomes a narrow unstructured band at 561 nm (Figure 4.15). Considering that the excitation spectra match the absorption one and the short lifetime decay, and keeping in mind the X-ray structure, the emission of **20B** could be mainly attributed to ^{3}MMLCT [dσ*(Pt–Pt) → π*(NHC)] transitions somewhat disturbed by the Pt–Tl bonds.

Upon cooling to 77 K the emission profile of **20C** retains a minor contribution of the HE band but displays a predominant unstructured LE emission band at ca. 500 nm (Figure 4.16). This LE band appears just slightly blue-shifted with respect to the LE band of **19C**, but it shows similar lifetime and excitation spectra, so the same ^{3}MMLCT nature can be presumed for it. It should be stressed that even though the crystal structures obtained for

20B and **20C** show similar 2D networks, in **20C**, the presence of an extended metallic [Pt–Pt–Tl–Pt–Pt–] chain is not reflected in its absorption or emissive properties at room temperature (see Figure S25). However, at 77 K the emission of **20C** also depends on the intermolecular Pt···Pt interactions.

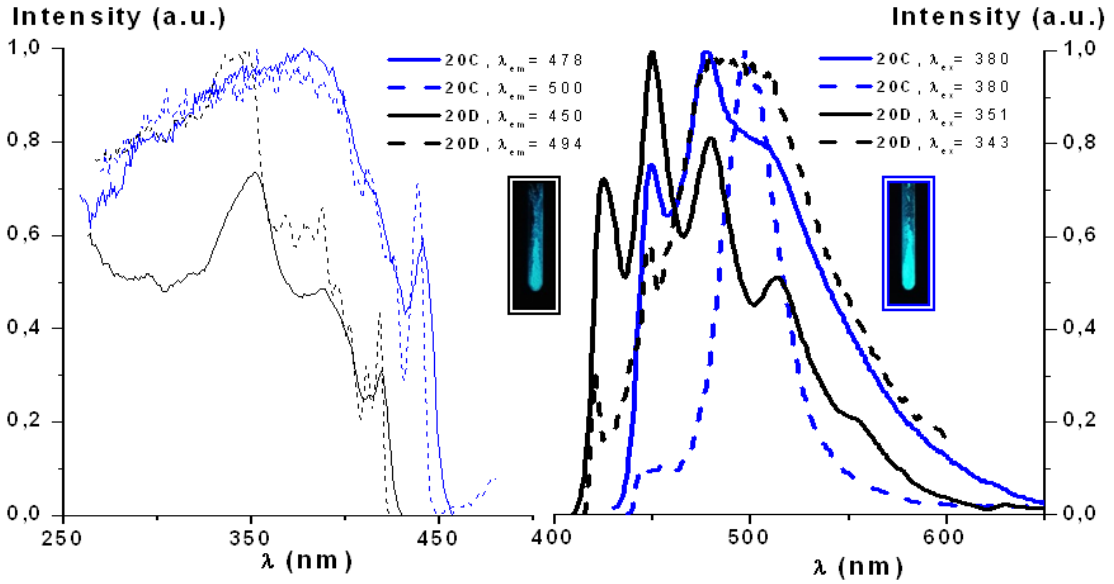

Figure 4.16. Normalized excitation (left) and emission (right) spectra of **20C** and **20D** in the solid state at 298 K (–) and 77 K (---). Pictures under UV light (λ_{ex} = 365 nm) at 298 K.

For **20D**, consisting of "Pt_2Tl" discrete molecules, the emission profile and its biexponential decay differ from those of the starting complex as much at 298 K as at 77 K, indicating that it is affected by the Pt–Tl bonds. At 77 K the mayor LE band appears slightly red-shifted in relation to those of other trinuclear derivatives $(NBu_4)_3[\{Pt(C_6F_5)_4\}_2Tl]$ (450 nm, 298 K; 445 nm, 77 K),[58] $[Tl_2Pt(CN)_4]$ (448 nm),[59] which were attributed to a metal-centered phosphorescence process [Pt(5dz²) → Tl(6pz)] (^{3}MM'CT) within the trinuclear entity. The observed shift in **20D** might be attributed to the contribution of the planar and low-lying C^C* and acac ligands to the frontier orbitals, which likely reduces the gap of the transition, more than to the existence of stronger Pt–Tl bonds, as deduced by comparing intermetallic distances (2.9962(2), 3.0230(2) Å, **20D** – vs 2.9777(4), 3.0434(4) Å $[\{Pt(C_6F_5)_4\}_2Tl]_3$). Therefore, the emission can be tentatively ascribed to charge transfer from the platinum fragments to the thallium [^{3}(L+L')MM'CT],[50] with some contribution of ^{3}MM'LCT/^{3}IL [dσ*(Pt–Tl) → π*(C^C*)] excited states. For powdery samples of **20D** at 77 K the existence of close excited states generated by small differences in the molecular arrangement cannot be excluded, which could explain the huge width of the emission band.

Chapter 5.

Lighting applications

5.1 OLEDs CONTAINING [Pt(R-C^C*)(PPh_3)(L')]PF_6

Lighting devices described in Sections 5.1 and 5.2 have already been published and full information can be found in SI-2.3 and 2.4 (for Section 5.1) and SI-3.1 and 3.2 (for Section 5.2). In the supporting information, the numbering of the compounds corresponds to that in the publications. For those devices described in Section 5.3 the corresponding supplementary data can be found in SI-5.

5.1.1 Fabrication of devices

Compounds [Pt(NC-C^C*)(PPh_3)(py)]PF_6 (**9C**) and [Pt(NC-C^C*)(PPh_3)(CNXyl)]PF_6 (**10C**), described in Chapter 2, were chosen to fabricate Organic Light Emitting Diodes (OLEDs) with blue (**9C**), yellow-orange (**10C**) and white light (mixtures of **9C** and **10C**) emission. OLEDs were fabricated by a full solution process technology with a non-doped emitting layer (EML) thanks to the good processability of the compounds. Most of the works on Pt based OLEDs deals with devices fabricated with vacuum evaporation techniques[17b, 60] due to the low solubility and/or poor ability of these compounds to form thin homogeneous films when deposited from solution. To the best of our knowledge, solution processed devices reported so far have been obtained with emissive layer (EML) composed by host-guest systems where the Pt emitter is blended in either polymeric or molecular hosts in order to reduce aggregation quenching processes and to increase the film homogeneity, both for molecular[20a, 61] and dendrimeric emitters.[62] For these reasons all the devices reported so far with non-doped EML have been obtained by using vacuum processed technologies.[29d, 63] On the other hand, non-doped devices offer many advantages, as the higher color stability and simpler device structure. Moreover, for blue emitting devices, the use of blends imposes strict requirements on the host triplet energy levels, whose energy must be high enough to prevent back-transfer processes. To the best of our knowledge, the results reported here represent the first example of solution processed Pt-based devices obtained with non-doped EML. With this very simple approach, by mixing two compounds at different ratios, we are able to tune the OLEDs emission from blue to yellow-orange, passing through white. All the information can be found in SI-2.3 and 2.4. Despite the conventional approach used for solution-processable organometallic platinum complex, i.e., dispersion in a conjugated host matrix with proper additives to achieve good charge-carrier balancing, we explore here a simpler bilayer structure consisting of a hole injection layer covered with a neat compound as the EML, thanks to its good film-forming ability. As the hole injection layer, a film of poly(vinylcarbazole) (PVK) is deposited onto the ITO/ PEDOT:PSS-coated glass by following the procedure reported elsewhere.[64]

Afterwards, a neat film of **9C** or **10C** is deposited by spin coating from a $CHCl_3$ solution. The experimental work and the corresponding discussion were made by Dr. Chiara Botta and Umberto Giovanella at the Istituto per lo Studio delle Macromolecole (ISMAC).

5.1.2 Electroluminescence (EL) results

This simple and unconventional, for organometallic phosphors, device architecture exhibited an unexpectedly good electrooptical performance. The EL spectra of **9C** and **10C** and of four mixtures of them at different weight ratios are shown in Figure 5.1 (left). The EL spectrum of **9C** well corresponds to its photoluminescence (PL) spectrum with structured blue emission at 452 and 478 nm (see Figure S19 in SI-2.4).

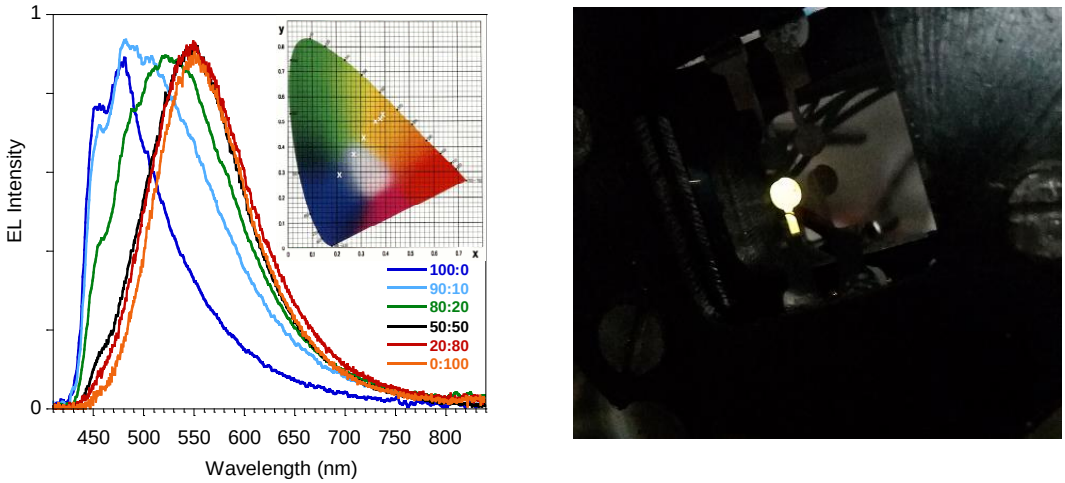

Figure 5.1. EL spectra of ITO/PEDOT:PSS/PVK/EML/Ba/Al devices with an EML of spin-coated **9C** (navy blue line), **10C** (orange line), and **9C**/**10C** at different weight ratios, driven at 5 V. The CIE 1931 chromaticity diagram is reported with the (x, y) positions of the OLED emission (left). Picture of OLED ITO/PEDOT: PSS/PVK/2C:3C (90:10)/Ba/Al with white light emission (right).

The EL spectrum of **10C** displays the broad band at 550 nm associated with its excimer emission (see Figure S20). The EL spectra of the **9C**/**10C** mixtures with a **10C** content of 50% or higher display mainly the emission of **10C**, while a balanced emission from the two compounds is obtained for the device with a **10C** content of 10–20%, giving nearly white-light emission (see Figure 5.1). The situation is quite different in the corresponding PL spectra, whose dominant emission comes from the **9C** compound (see Figure S22). The different behaviors of the PL and EL spectra of the **9C**/**10C** mixtures are mainly related to the higher efficiency of the **10C**-based device compared to the **9C** one (see Table 5.1). These observations suggest a more favorable energy barrier for carrier injection in **10C**, in agreement with the positions of their HOMO–LUMO energy levels (see Figure S23). Despite the fact that the devices are not optimized in terms of the platinum complex layer

thickness and charge-carrier regulation, they display encouraging good performance (see Table 5.1 and Figure S24) and stability, considering the simple and unusual bilayer device architecture unexplored for organometallic complexes processed by solution methods.

Table 5.1. OLEDs performances

weight ratio		EQE (%)[a]	L_{MAX} (cd/m²)[b]	CIE 1931 (x, y)
9C	10C			
0	100	0.3	50	(0.39;0.53)
20	80	0.2	101	(0.38:0.51)
50	50	0.1	9	(0.36;0.50)
80	20	0.02	5	(0.31;0.44)
90	10	0.007	6	(0.27;0.37)
100	0	0.01	4	(0.21;0.29)

a = External Quantum Efficiency. b = Maximum Luminance.

This makes our devices the first example of platinum-based OLEDs fabricated by a fully solution-processed technology with a nondoped EML. This approach allowed us to tune the OLED emission from blue (**9C**) to yellow-orange (**10C**), passing through white (mixtures of **9C** and **10C**).

5.2 REMOTE PHOSPHOR DEVICES CONTAINING [Pt(R-C^C*)(CNR')$_2$]PF$_6$

5.2.1 Fabrication of devices

In view of the luminescent properties of compounds described in Chapter 3.1 our goal was to achieve white light with high CRI and reasonable CCT by using compounds [Pt(R-C^C*)(CNR')$_2$]PF$_6$ (RC= Naph, R'= ^{t}Bu **13A**; R = CO_2Et, R' = ^{t}Bu **13B**; R = NC, R' Xyl, **14C**) and [Pt(bzq)(CN)(CN^{t}Bu)] (**R1**) as phosphors, which were selected as blue (**13B**, **14C**), yellow (**13A**) and red (**R1**) (full information can be found in SI-3.1 and 3.2). Several devices for remote operation were prepared by depositing the active materials on common glass disks. The interest of the remote phosphor scheme lies in the fact that far from the LED−dye, the emitters gain in stability and reliability. Concerning our particular case, we have observed that placing the phosphors far from the pumping source (i.e., LED−dye), in a remote configuration and avoiding direct contact between them, the degradation of the emission is notably reduced by compared to the conformal option. In normal operation, the junction of the LED can reach temperatures in the range of 70−100 °C (depending on the operation current and dissipation strategies). In the conformal option, phosphor is subjected to the heat generated by the junction that affects to both phosphor efficiency and stability. Furthermore, if the phosphor's efficiency is not high, sizable part of the pump energy absorbed is transformed into heat, increasing even further

the temperature of the LED-junction and the phosphor. This translates into faster degradation of the system (see Figure S18 in SI-3.2). To combine the luminescence from the different components and control the final chromatic properties of the device, different slurries have been sequentially deposited. Keeping in mind the objective of high CRI luminescence, the thickness and concentration of each individual layer have been calculated accordingly to their respective quantum efficiencies.

The deposition of the phosphors was carried out via screen printing using suspensions of the blue (**13B**, **14C**), yellow (**13A**) and red (**R1**) components on a commercial transparent terpineol based ink vehicle, on top of a glass disc of 1.6 mm thick and 27 mm diameter. Each layer deposited contained a total weight of 1.5 mg. Complexes with different ancillary ligands such as **13A** and **14C** are not compatible because ligand exchange processes have been observed to occur and they should be deposited in different layers and with ink vehicle layers in between to avoid the contact. However, complexes **13A** and **13B** containing the same ancillary ligand, ^{t}BuNC, could be mixed together in the same suspension. Besides, complex **R1** was suspended together with the ink vehicle and deposited as red layer. In practice, this was correlated to the number of sublayers of each suspension deposited and the proportion of the platinum complexes in the suspensions. In general, all the compounds are deposited by successive steps (multiple sublayers), except the red one (**R1**) that is obtained by a single deposition. The order of the compounds on the glass substrate has been established according to the energy of their respective emissions, aiming to minimize the reabsorption of the light emitted by previous phosphors. Therefore, the first layer to be deposited will be that with the shorter emission wavelength.

After a meticulous optimization of the samples, devices **DEV1–DEV3** were selected because of their suitability for general lighting applications (CRI, CCT, etc.). Their composition and architecture is described in SI-3.2 and summarized in Table 5.2.

Table 5.2. Composition and architecture of **Devices 1-3.**

	Blue (B)	Yellow (Y)	Red (R)	Composition
DEV1	**13B**: 28%; Ink Vehicle: 60%	**13A**: 12%	**R1**: 10% IV: 90%	15 sublayers BY, 3 sublayers IV, 1 sublayer R
DEV2	**13B**: 33% Ink Vehicle: 60%	**13A**: 7%	**R1**: 10% IV: 90%	26 sublayers BY, 3 sublayers IV, 1 sublayer R
DEV3	**14C**: 40% IV: 60%	**13A**:40% IV:60%	**R1**: 10% IV: 90%	3 sublayers B, 3 sublayers IV 4 sublayers Y, 3 sublayers IV 1 sublayer R

This work was performed by the pre-doctoral student Andrés Chueca López at IREC under the supervision of Dr. Mariano Perálvarez

5.2.2 Results

The phosphor disks were introduced in the holder structure shown in Figure 5.2 and mounted with the coating facing the pump source for their study under UV illumination.

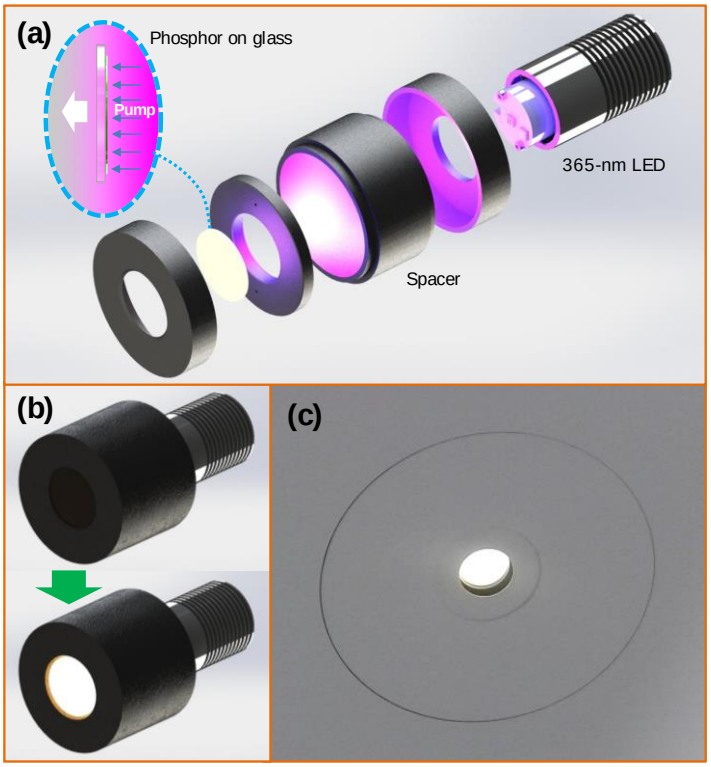

Figure 5.2. (a) Explosion of the sample holder used to pump the phosphors and coupling the resulting emission into the integrating sphere. (b) Sequence of the emission triggering. (c) Photo of the resulting white emission from **DEV2**.

Luminescence spectra of the different devices are represented in Figure 5.3 left. At glance, it is observed how the variations of the relative compositions aforementioned have a direct influence on the luminescence spectral shape. The analysis of the spectra allowed us to extract different photometric and chromatic parameters, which appear summarized in Table 5.3. This chart shows that the luminous fluxes and efficiencies of the different samples are, in general, relatively low, especially if compared to conventional devices. However, in spite of this, the values of luminous efficacy of the radiation are very promising, kept in all cases within the optimum range for general lighting.[7a] CRI, CCT, and CIE (see Figure 5.3 right) parameters are also very appealing. CRI values are relatively high, around 80, whereas the correlated color temperatures fall within the suitable range for lighting.[7b, c]

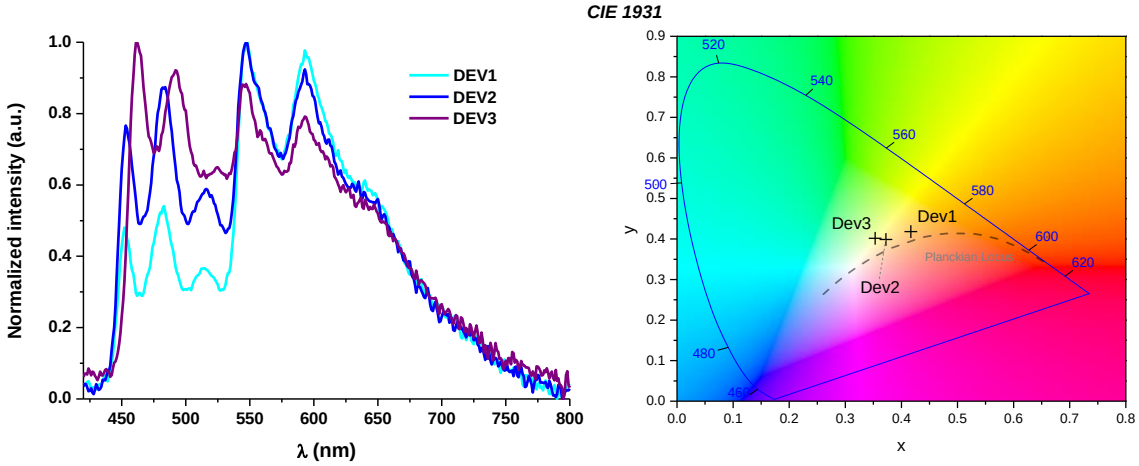

Figure 5.3. Normalized emission spectra (left) and CIE coordinates of devices **DEV1**–**DEV3** (right).

Table 5.3. Key Performance Data of Devices.

Device	LF (lm)[a]	WPE (%) [b]	LE (lm/W)[c]	LER (lm/W)[d]	CRI[e]	CCT[f]	CIE [x,y][g]
DEV1	1.49	0.85	0.27	317.2	77.0	3477	0.4168, 0.4183
DEV2	1.68	1.00	0.30	304.6	82.6	4356	0.3724, 0.3988
DEV3	1.26	0.76	0.23	300.9	81.3	4897	0.3532, 0.4018

[a]Luminous flux. [b]Wall-plug efficiency. [c]Luminous efficacy. [d]Luminous efficacy of the radiation. [e]Color rendering index. [f]Correlated color temperature. [g]CIE coordinates.

For more details, **DEV1** exhibits an emission with a CCT (3477 K) in the warm/neutral range. The CRI is the lowest among the three samples (77.0). As previously stated, the delivered light output is low (1.49 lm) but in consonance with the rest of the samples. In spite of this, the spectral power distribution is compensated (LER 317.2 lm/W) turning this sample into suitable for general lighting.

The results of **DEV2** reveal that, by addition of complex **13B**, with emission in the blue/green range, the white luminescence becomes "colder" (blue-shifted) than the one observed in **DEV1** (4356 K). The CRI and total light output are the best among all the devices (82.6 and 1.68 lm, respectively). In agreement to the LER (304.6 lm/W), also in this case the light is suitable for general lighting applications.

Concerning **DEV3**, the use of compound **14C** instead of **13B** makes the emission more bluish (4897K) but always within the suitable ranges. The luminous flux is the poorest

among the three structures analyzed (1.26 lm) but, the CRI is reasonable good (81.3) and the LER value is very promising and adequate for its implementation in lighting systems.

In light of the results, it becomes clear that the method reported here has proven to be effective in controlling the spectral power distribution of the emitting devices and their colorimetric properties. Nevertheless, it was observed that under a CW incident flux of about 92 mW at 365 nm, which is equivalent to a CW irradiance of 187.4 W/m2, the emission of all the structures rapidly decreases. Figure 5.4 shows the reduction of the luminescence intensity of **DEV3** with time. As observed, the total flux drops down to 50% in approximately 8 min. In this case, the fastest degeneration corresponds to compound **14C** (blue/green), as supported by the red–shift of the emission shown in the lower insert.

It is expected that the low light power delivered and fast degradation of the emission in these devices could be improved by following two particular strategies: (a) implementing a high reflectance mixing chamber (painted in barium sulfate, for example) to harvest part of the light emitted backward by the excited phosphor (approximately 50% of the total) and (b) the use of pulsed excitation as opposed to CW operation. With an adequate modulation of the pump light, fast enough to not be perceived by the human eye and slow enough to respect phosphor emission fall- and rise-times, a 50% duty-cycle square wave would be able to roughly induce 50% degradation reduction.

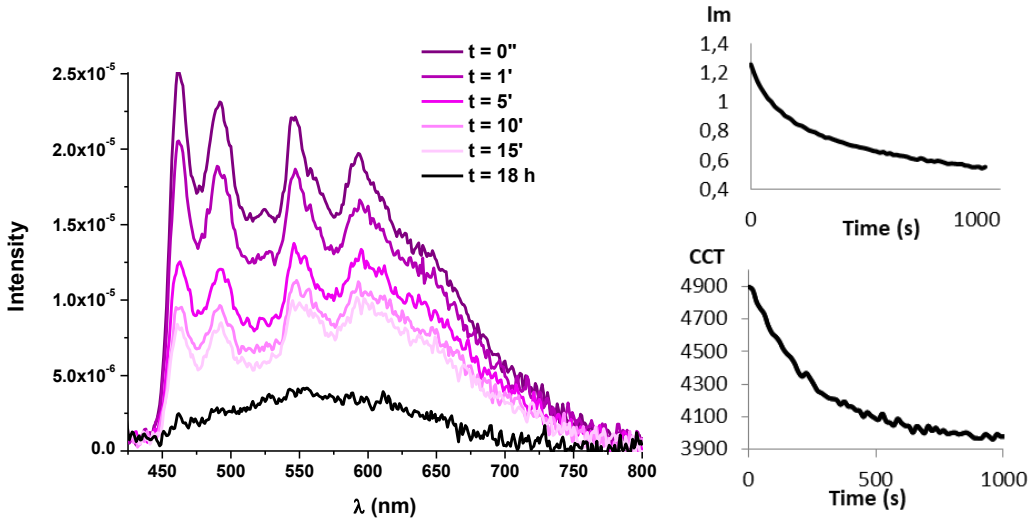

Figure 5.4. Emission spectra of the degradation studies of **DEV3**. Inset: Evolution of the luminous flux (up) and evolution of the CCT (down) with time upon irradiation at 365 nm.

5.3. LIGHTING DEVICES CONTAINING [Pt(R-C^C*)(P^P)]PF_6

This work was performed by the pre-doctoral student Andrés Chueca López at IREC under the supervision of Dr. Mariano Perálvarez (5.3.1) and at ISMAC under the supervision of Dr. Chiara Botta (5.3.2) but are still unpublished.

5.3.1 Remote phosphor devices

Complexes [Pt(R-C^C*)(P^P)]PF_6 (R-C = Naph, P^P = dppm **16A**; R = CO_2Et, P^P = dppm **16B**, dppbz **18B**)† described in Chapter 4.1 were selected as blue (**16B**, **18B**) and orange (**16A**) phosphors for white-light remote-phosphor devices. As red component, [Pt(bzq)(CN)(CNXyl)] (**R2**)[27a] was used. Several devices were prepared *via* screen printing following the same procedure stated in Chapter 5.2 (see SI-5). To achieve the high quality CCT and CRI values required in devices for indoor solid state lighting applications, as stated in the ANSI C8-78.377-2015 for commercial light sources, combination of the luminescence from different phosphors was required. Several remote-phosphor devices with two-component architectures (**D1**-**D10**) were prepared by sequential deposition of individual suspensions of the active materials. The different emitters were deposited in separated layers, keeping in mind that the emitter with the lowest energy emission must be the closest to the pumping source. The final parameters of the devices were controlled by variations in the relative amount (number of layers) of each phosphor (Table 5.3).

Table 5.3. Composition of devices indicated in amount of layers of each emitter.

	Devices									
	D1	**D2**	**D3**	**D4**	**D5**	**D6**	**D7**	**D8**	**D9**	**D10**
16A	3	3								
16B	2		4						3	4
18B		2		4	3	4	2	2		
R2			2	2	1	1	4	3	1	1

The phosphor stacks were studied under 365-nm UV LED light illumination. This wavelenght provides efficient excitation of all the bands of the different compounds. To do that, the disk was introduced in the holder structure (see Figure S2 a in SI-5) with the coating facing the pump source (see Figure S2 b in SI-5). Photometric and colorimetric parameters corresponding to **D1**-**D10** can be seen in Table 5.4 and Figure 5.5.

†Although **16B** and **18B** were prepared in a different project, as previously stated, they present really good emission quantum yields in PMMA films (Φ = 0.74 and 0.95 respectively) which make them promising candidates for applications. Data of their optical properties can be found in Tables S1 and S2 and Figure S1 in SI-5.

Table 5.4. Performance of remote phosphor devices **D1-D10**.

Devices (*)	CRI[a]	CCT[b]	D_{uv}	LF[c] (mlm)	LER[d] (lm/W)	LE[e] (lm/W)	WPE[f] (%)	CIE 1931 (x,y)[g]
D1$_{(16B/16A)}$	57.7	3292	0.019	237.2	379.5	0.86	0.41	0.4431, 0.4576
D2$_{(18B/16A)}$	62.4	3586	0.015	242.9	360.4	0.88	0.45	0.4158, 0.4313
D3$_{(16B/R)}$	94.3	2532	0.0031	173.1	239.8	0.63	0.56	0.4801, 0.4231
D4$_{(18B/R)}$	92.5	2570	0.0037	197.2	226.7	0.72	0.52	0.4641, 0.4014
D5$_{(18B/R)}$	83.6	3706	0.0057	179.6	227.9	0.65	1.53	0.3894, 0.3700
D6$_{(18B/R)}$	81.7	3938	0.0024	214.1	228.7	0.78	1.18	0.3815, 0.3722
D7$_{(18B/R)}$	85.7	1918	0.00097	140.6	209.9	0.51	0.46	0.5380, 0.4146
D8$_{(18B/R)}$	92.3	2176	0.0039	157.7	217.2	0.57	0.59	0.4998, 0.4032
D9$_{(16B/R)}$	93.7	3078	0.0065	183.1	249.1	0.67	0.99	0.4409, 0.4222
D10$_{(16B/R)}$	90.2	3355	0.0064	168.1	247.9	0.61	1.44	0.4214, 0.4138

[a] Color rendering index, [b] Correlated color temperature, [c] Luminous flux, [d] Luminous efficacy of the radiation, [e] Luminous efficacy, [f] Wall-plug efficiency, [g] CIE coordinates. * Components

Devices **D1** and **D2**, both containing compound **16A** as warm component, present rather low CRI and non-convenient high LER values,[65] the latter attributed to the excessive overlay of the emission bands of the cool (**16B**, **18B**) and warm (**16A**) components, resulting in an increase of the intensity at the green region of the visible spectrum (Figure S3 in S.I.-5). Also the CIE coordinates reveal that **D1** and **D2** are not suitable in the current configuration for white light applications, since they are far from the ideal Planckian locus ($|D_{uv}| > 0.006$) (Table 5.4, Figure 5.5). To solve these problems, the warm contribution was changed to compound [Pt(bzq)(CN)(CNXyl)] (**R2**), with a less pronounced overlay of the emission band with those of **16B** and **18B**.

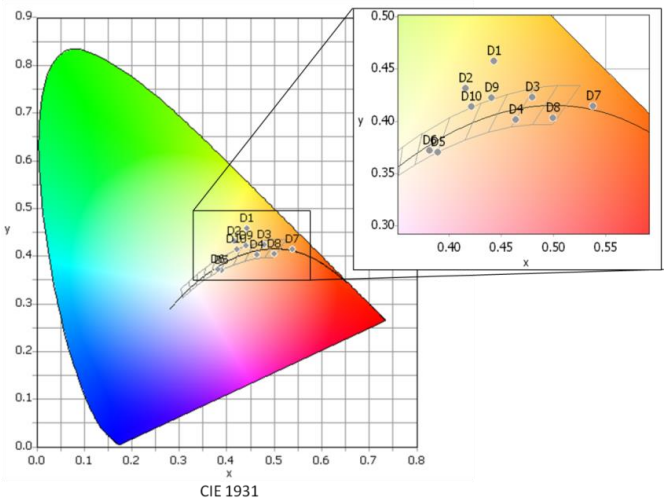

Figure 5.5. Distribution of the different devices in the CIE 1931 color space according to their respective color coordinates **D1**-**D10**.

Comparison of devices **D3** and **D4**, which just differ in the nature of blue phosphor (**16B** in **D3**, **18B** in **D4**), seems to indicate that both, **16B** and **18B**, combined with the **R2** component in 2:1 ratio, lead to devices with very similar photometric and colorimetric parameters; in both cases with excellent CRI values (94.3, 92.5) and CIE coordinates along the Planckian locus ($|D_{uv}|< 0.006$). The spectral shape of devices **D3** and **D4** resembles that obtained from incandescent lamps (CRI 100) (Figure 5.6 a). However, when the ratio blue:red is 3:1 or 4:1 the use of **18B** as blue component lead to a much colder light (CCT = 3706 K **D5**, 3938 K **D6**) than when **16B** was used (3078 K **D9**, 3355 K **D10**) and to CIE coordinates along the Planckian locus ($|D_{uv}|< 0.006$) although the CRI becomes clearly lower (*ca* 83).

If we compare those devices (**D4-D8**) containing the same active components, **18B** as blue and **R2** as red, it seems clear that modifications in the relative number of layers of each phosphor (**18B**: **R2** ratio: 0.5:1 **D7**, 0.66:1 **D8**, 2:1 **D4**, 3:1 **D5**, 4:1 **D6**) lead to a fine control of the CCT values (Figure 5.6 b) with no dramatical change in the rest of the parameters. In the light of the above sequence, it becomes clear the amount of **R2** contributes to make the emission warmer, being possible to achieve devices with high CRI (81.7- 92.5), CCT values ranging from 1918 K (**D7**) to 3938 K (**D6**) and CIE coordinates along the Planckian locus ($|D_{uv}|\sim 0.00097 - 0.0057$).

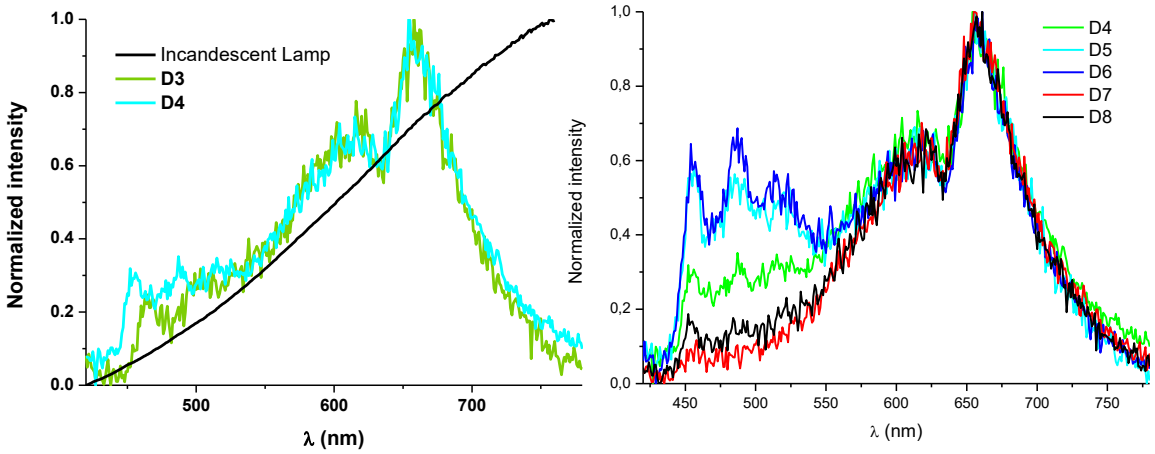

(a) (b)

Figure 5.6. Normalized emission spectra of devices **D3** and **D4** and a typical incandescent lamp in the visible region of the spectrum (a) and devices **D4-D8** (b).

In the case of those devices containing, **16B** (see Figure 5.7) as blue and **R2** as red in different ratios (**16B**: **R2**: 2:1 **D3**, 3:1 **D9**, 4:1 **D10**) the increase of the **R2** amount produces warmer light (2532 K in **D3**) with higher CRI (94.3 in **D3**) and lower D_{uv} values than in those devices using **18B** (**D4-D8**).

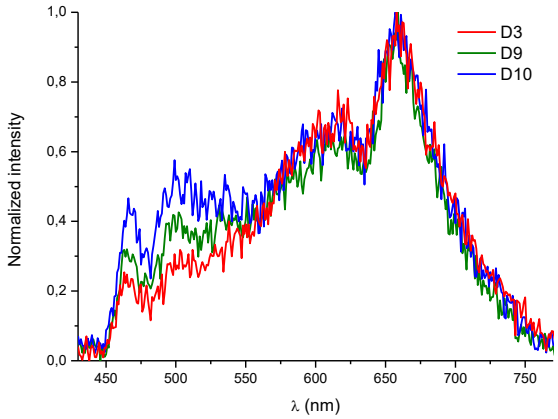

Figure 5.7. Normalized emission spectra of devices **D3**, **D9** and **D10**

Therefore, this approach allows the fabrication of devices with optimal CRI and D_{uv} values and a great range of nominal CCT values: 4000 K (**D6**), 3500 K (**D5** and **D10**), 3000 K (**D9**) and 2500 K (**D3** and **D4**). Although only a few examples of WLEDs emitting warm light with high CRI values have been reported.[66] This approach opens the gate to even very- or ultrawarm devices as **D7** and **D8** operating in the "firelight" range of CCTs with values of 1918 K and 2176 K respectively,[67] within optimal CRI and D_{uv} values.

5.3.2 OLEDs

Complexes [Pt(Naph^C*)(dppbz)]PF_6 (**18A**) and [Pt(CO_2Et-C^C*)(dppm)]PF_6 (**16B**) were chosen as yellowish-orange and blue emitters respectively for the fabrication of OLEDs, since mixtures of the two emitters in different proportions showed to be a good approach for the preparation of white emitting devices with tunable parameters such as CRI and CCT. Also several materials were tested on the fabrication of solution processed OLEDs in order to achieve the optimal configuration (see SI-5).

A common problem in the construction of efficient blue OLEDs is the choice of the appropriate host for the doping material. The large HOMO-LUMO gap of the blue phosphorescent emitters usually implies a deep HOMO and a high LUMO, resulting in a poor overlap with the FOs of the matrix and an inefficient transference of the carriers to the dopant. In addition, the host material must present a triplet state (T_1) at higher energies than those of the phosphors, thus avoiding the backwards energy transfer from the dopant to the host.[68] Taking all this into account the election of commercially available host materials can be troublesome.

A theoretical study of the T_1 energy levels of the selected blue emitter for OLED applications reveals that the commonly used hole transport layer (HTL) poly(vinylcarbazole) (PVK, $T_1 \sim 2.5$ eV) should not be the optimal choice for blue OLEDs containing **16B,** with a higher triplet state ($T_1 \sim 2.73$ eV) (see Tables S3-S5 in SI-5). However, TCTA, with $T_1 \sim 2.83$ eV, seems to be a more reasonable choice for the optimization of monochromatic devices (see Figure 5.8).

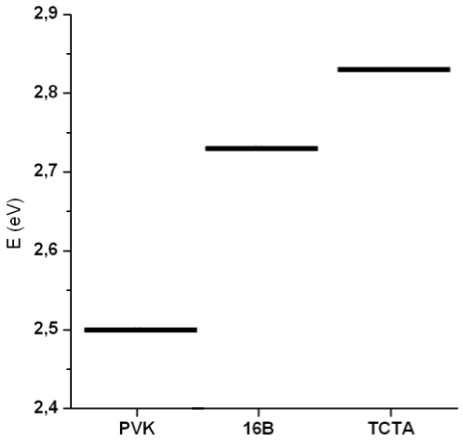

Figura 5.8. Energy of the T_1 in selected materials.

First, we optimized those devices containing **16B** in the EML. Devices **D1**-**D3** were prepared with a simple ITO/PEDOT:PSS/TCTA-**16B**-PBD/Ba/Al configuration (see Figure

5.9 a), where a solution of the host materials and the emitter in $CHCl_3$ was deposited by spin coating with different doping concentrations (see Table 5.5). The EL spectra of these three devices do not match the PL of the pure Pt(II) complex in PMMA film (see Figure 5.10 a for **D1**). The relatively high HOMO of TCTA in comparison to that of **16B** (see Figure 5.9) can result in a poor confinement of exciton at the dopant sites thus facilitating the radiative recombination in the host materials. Taking this into account, the green emission observed can be attributed to the electroplex of the matrix,[69] which is characterized by a very low EQE.

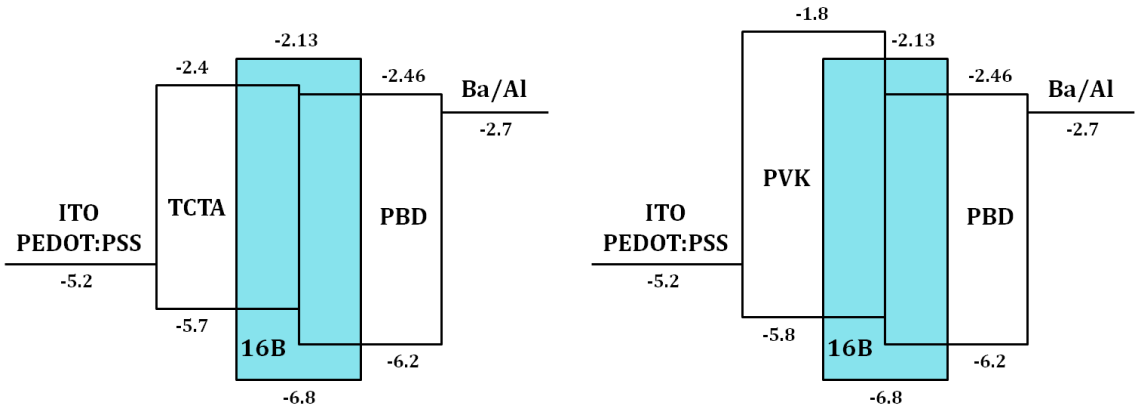

(a) (b)

Figure 5.9. Device architectures and flatband energy levels of the different materials in **D1**-**D3** (a) and **D4**-**D6** (b).

Table 5.5. Composition and EQE of **D1**-**D6**.

	16B (%)	HTL (%)	ETL (%)	EQE (%)
D1	5	47.5	47.5	0.02
D2	10	45	45	0.02
D3	20	40	40	0.02
D4	10	63	27	0.1
D5	15	59	26	<0.01
D6	20	57	23	0.02

Devices **D4**-**D6** were prepared following the architecture shown in Figure 5.9 b, in which TCTA was substituted by PVK. Although the T_1 of PVK is much lower than the one of **16B**, the higher LUMO of PVK favors electron trapping at the dopant and, as a consequence, a higher probability of forming excitons at the emitter sites. As a consequence, a better transport of both holes and electrons to the doping material results in an increased EQE (see Table 5.5). Contrary to the emission observed for **D1**-**D3**, in the case of **D4**-**D6**, as can be observed in Figure 5.10 b, the emission arises from the dopant Pt(II) complex (**16B**). However, some contribution of the blue emission of PVK to the EL is detected in the device

with the lowest proportion of **16B** (**D4**). The concentration study carried out in the three devices (**D4**-**D6**) reveals that, although higher concentrations avoid the emission of PVK, they induce a drastic reduction of the EQE. Thus, 10 w% was found to be the most appropriate doping concentration.

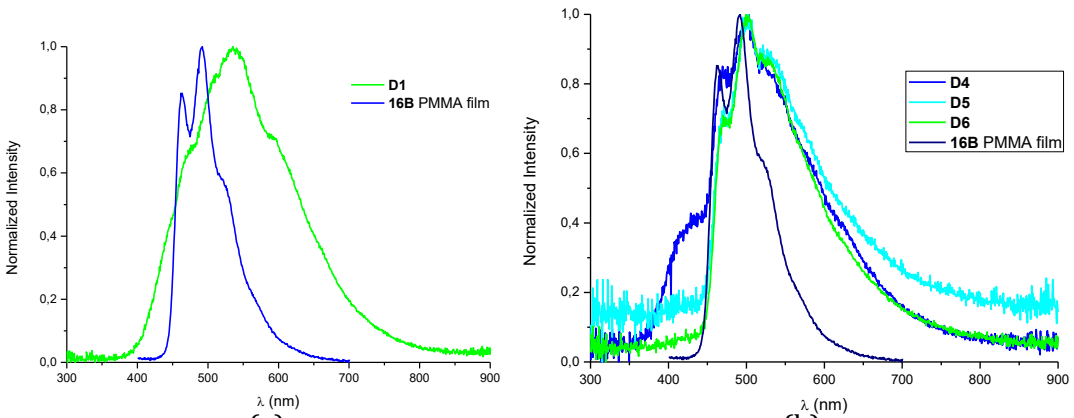

Figure 5.10. EL spectrum of **D1** (a) and **D4**-**D6**(b) compared to the PL spectrum of **16B** in PMMA.

Three new devices, **D7**-**D9**, with improved architectures were prepared at the optimum doping concentration (see Figure 5.11 and Table 5.6).

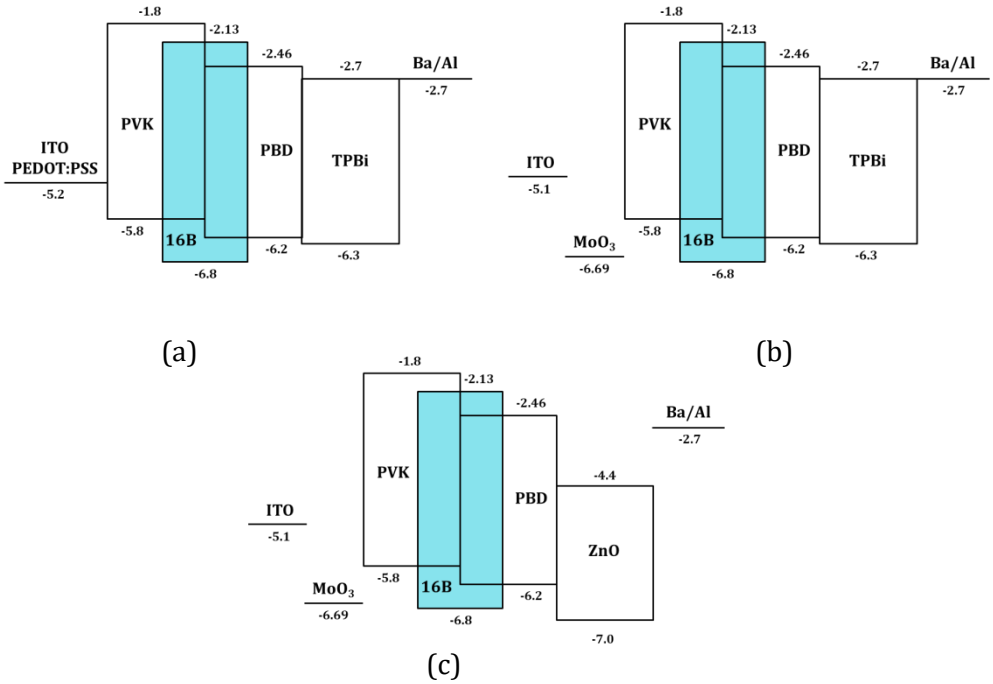

Figure 5.11. Device architectures and flatband energy levels of the different materials in **D7** (a), **D8** (b) **and D9** (c).

Table 5.6. Composition and EQE of **D7**-**D9**.

	16B (%)	HTL (%)	ETL (%)	EQE (%)
D7	10	63	27	0.1
D8	10	63	27	0.12
D9	10	63	27	0.08

Device **D7** was built with TPBi as additional EIL (Figure 5.11 a), which facilitates the injection of electrons into the system. As can be seen in Figure 5.12, the EL spectrum has a great contribution of the PVK to the emission. This is in good agreement with the recombination of charges taking place in the HTL, as observed in the EL spectrum of **D4**.

To improve the hole injection in the device, PEDOT:PSS was substituted in **D8** and **D9** by MoO_3, with a much lower work function (-6.69 eV). As expected, the closer match of energy levels of MoO_3 and **16B** facilitate the transport of the holes into the dopant, thus increasing the EQE of **D8** (Table 5.6).

Device **D9** was constructed using ZnO as EIL (Figure 5.11 c). The deep HOMO orbital (-7.0 eV) can act as a hole-blocking layer, allowing the holes to be trapped inside the emissive layer and thus no blue emission from PVK is detected.

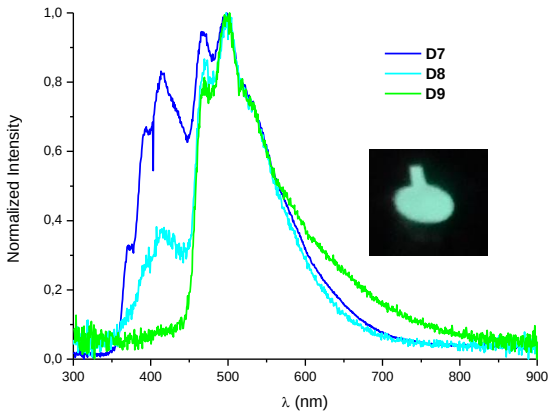

Figure 5.12. EL spectra of **D7**-**D9**; picture of **D8**.

Since both cool (blue) and warm (orange) components are necessary for the fabrication of white light emitting devices, **18A**, showing a dual emission (see Figure 4.6 b), was studied under the conditions aforementioned. Devices **D10**-**D12** were prepared with the same architectures of **D7**-**D9**, using a mixture of PVK and PBD as host material (see Table 5.7). The $I_{photodiode}$/V curves can be found in SI-5 (Figure S5 for **D7**-**D9** and Figure S6 for **D10**-**D12**).

Table 5.7. Composition and EQE of **D10**-**D12**.

	18A (%)	HTL (%)	ETL (%)	EQE (%)
D10	10	63	27	0.3
D11	10	63	27	0.4
D12	10	63	27	0.015

Device **D10** was built using the same ITO/PEDOT:PSS/PVK+Pt+PBD/TPBi/Ba/Al configuration used for **D7**. As can be expected from a more favorable injection of charges into emitters with smaller HOMO-LUMO gaps, due to a better overlap of the electrode work functions and the MO of the dopant, the EQE of **D10** is considerably higher than its blue homologous **D7**. However, the EQE is still very low, which can be understood once considered that also **18A** presents a very deep HOMO (see theoretical calculations in SI-4.1). The EL spectrum of **D10** (see Figure 5.13 a) reveals three contributions to the final spectrum: the blue emission from PVK (λ_{max} ~ 420 nm), two small maxima (λ ~ 477, 510 nm) corresponding to the HE emission band of **18A** (see Chapter 4.1) and a major contribution corresponding to the LE emission band of **18A**.

In order to reduce the relative contribution of the matrix, as observed in **D8**, PEDOT:PSS was substituted by MoO_3. The same three components were still observed in the EL spectrum of **D11**. However, in this case the contribution of the two blue components was reduced by half, thus obtaining a purer orange emission with slightly higher EQE (see Table 5.7).

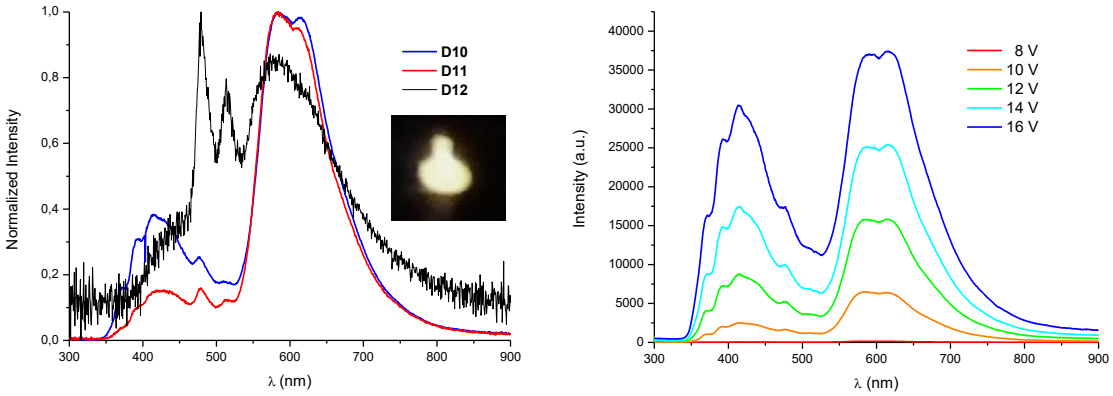

(a) (b)

Figure 5.13. EL spectra of devices **D10**-**D12** driven at 10 V; picture of **D11** (a) and variation of the intensity and the spectral profile of **D10** with the applied voltage (b).

As observed in the blue OLED **D9**, the use of ZnO as EIL increases the contribution of the HE band arising from **18A**, but severely reduces the EQE of **D12**. As can be seen in Figure 5.13 b for **D10**, the expected increment in the EL intensity with the applied voltage is observed, but no difference in the relative contributions was detected.

Taking into account these data, we proposed the fabrication of devices containing the two different dopants (**18A** and **16B**) for the generation of white light with two different architectures (see Table 5.8). Device **D13** was built with the optimized ITO/MoO_3/PVK+Pt+PBD/TPBi/Ba/Al configuration used for **D8** and **D11**. For the preparation of the EML, the two emitters were dissolved at a 10 wt% each, together with PVK and PBD.

Table 5.8. Composition, EQE and lighting parameters of **D13** and **D14**.

	18A/16B	HTL (%)	ETL (%)	EQE_{max} (%) [V]	CRI	CCT	CIE (x, y)	Duv
D13	10/10	57	23[a]	0.32 [11]	65.8	2592	0.4697, 0.4137	0.0004
D14	10/10	57	23[b]	0.2 [14]	75.7	5281	0.3408, 0.4138	0.0298

a = PBD; b = OXD-7

The EL spectrum of **D13** (see Figure 5.14 a) shows a major contribution corresponding to the LE band of **18A** with very small contributions of PVK and **16B**. Although the white light produced has a very appealing warm temperature of 2592 K within the Planckian locus (see Figure 5.14 b and Table 5.8), the small contribution of the blue components renders a rather poor CRI (65.8). Successively, for device **D14**, PBD was replaced by OXD-7 (HOMO = -6.5 eV; LUMO = -2.8 eV), as a further optimization step. Thus, the final configuration of **D14** consists of ITO/MoO_3/PVK+Pt+OXD-7/TPBi/Ba/Al. The EL spectrum (see Figure 5.14 a) reveals that the blue emission arising from **16B** becomes relevant, while there is still a big contribution of the LE band of **18A**. The change of the spectral shape leads to white light with a much cooler CCT (5281 K) and an increased CRI (75.7), both within commercial ranges.

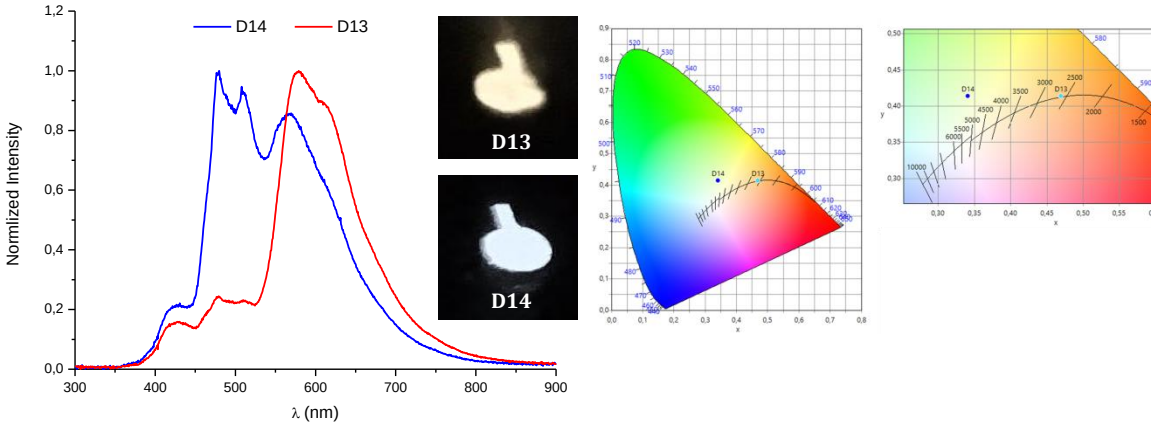

(a) (b)

Figure 5.14. EL spectra at 12 V (a) and CIE 1931 diagram (b) of **D13** and **D14**.

Both devices present a very high turn-on voltage (~11 V, Figure 5.15), probably due to the aforementioned high potential barriers for charge injection that should be further optimized. In addition, after achieving the maximum EQE, they undergo a roll-off (Figure 5.15, insets), a process due to triplet-triplet annihilation typical of long lived excited triplet states, as already reported in this kind of devices.[70] Irreversible degradation of the OLEDs was detected at high voltage (21 V for **D13**, 19 V for **D14**) (see Figure S7).

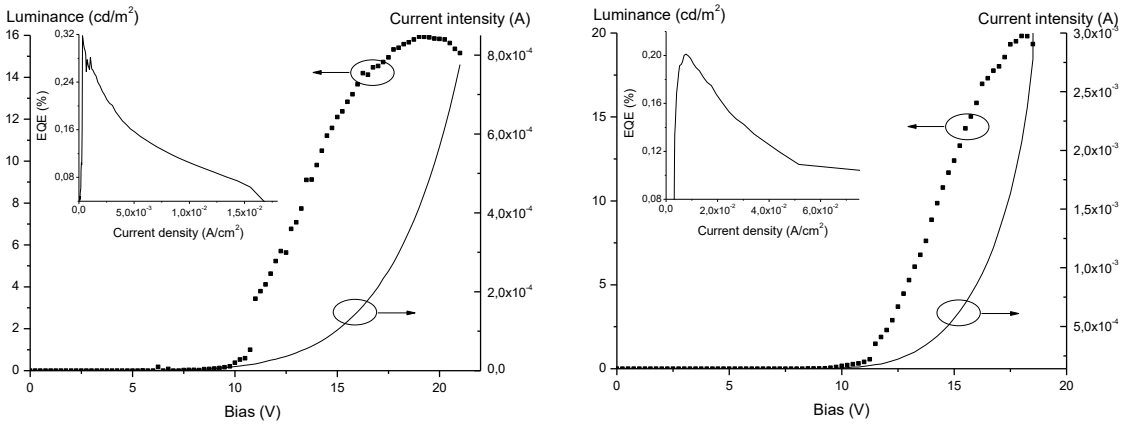

(a) (b)

Figure 5.15. I/V and Luminance/V (inset: EQE/J) curves of **D13** (a) and **D14** (b).

As observed in Figure 5.15, the maximum luminance values obtained[71] in **D13** and **D14** are very low (~16 cd/m^2 for **D13**; ~20 cd/m^2 for **D14**), which is in good agreement with the problems associated with a poor carrier balance.

Conclusions.

1.- We have been able to stablish a general step-by-step-pathway to prepare four dichloro-bridge compounds containing cyclometalated N-heterocyclic carbene ligands, [{Pt(μ-Cl)(R-C^C*)}$_2$] (R-C^C*:1-(naphthalen-2-yl)-3-methyl-1*H*-imidazol-2-ylidene (Naph^C*, **4A**); 1-(4-ethoxycarbonylphenyl)-3-methyl-1*H*-imidazol-2-ylidene (EtO_2C-C^C*, **4B**); 1-(4-cyanophenyl)-3-methyl-1*H*-imidazol-2-ylidene (NC-C^C*, **4C**); 1-(3,5-dichlorophenyl)-3-methyl-1*H*-imidazol-2-ylidene (Cl-C^C*, **4D**)). They have been revealed as very valuable starting materials to get new luminescent compounds of Pt(II) containing the "Pt(R-C^C*)" moiety.

2.- Based on the NMR data of heteroleptic compounds [Pt(C^C*)LL'], it could be inferred that the trans influence of the carbene atom (C*) is smaller than that of the metallated one (C_{Ar}), but not significantly. Also the trans influence of the ligands used seems to follow the order PPh_3 > CNXyl > py ~MMI > Cl. Therefore the transphobia degree (T) of pairs of trans ligands, resulted to be: T[C_{Ar}/L] >T[C*/L] and T[C_{Ar}/PPh_3] >T[C_{Ar}/CNXyl] >T[C_{Ar}/py] ~T[C_{Ar}/MMI] >T[C_{Ar}/Cl].

The difference between T[C_{Ar}/L] and T[C*/L] (L = py, CNXyl, MMI) is not enough to avoid the formation of mixtures of *cis*/*trans* isomers during the splitting of the chlorine-bridge by L to give the heteroleptic complexes [PtCl(C^C*)L]. However in all cases the *trans*-(C*, L)-[PtCl(C^C*)L] isomer is the major species, especially when L is py. In this case, the intramolecular T-shaped C_{Ar}–H··· π (py) interaction seems to contribute to the stabilization of this isomer, as proven by DFT calculations.

In case of complexes with PPh_3 the greatest T[C_{Ar}/PPh_3] together with the intramolecular T-shaped C_{Ar}–H··· π (Ph) interactions present in the *trans*-(C*, PPh_3)-[Pt(NC-C^C*)(PPh_3)L] complexes (L = Cl **5C,** py **9C**, CNXyl **10C**, MMI **11C**) would account for the stereo-selective formation of this isomer in each case.

3.- Compounds with stoichiometries [Pt(R-C^C*)(CNR')$_2$]PF_6 (R-C= Naph, R = CO_2Et, CN; R' = ^{t}Bu, Xyl), NBu_4[Pt(R-C^C*)(CN)$_2$] (R-C= Naph, R = CO_2Et, CN, Cl), [Pt(C^C*)(P^P)]PF_6 (R-C= Naph, R = CN, P^P = dppm, dppe, dppbz), [Pt(R-C^C*)(acac)] (R = CO_2Et, CN, Cl) have been prepared in high yield by elimination of Cl from the corresponding complex [{Pt(μ-Cl)(R-C^C*)}$_2$].

4.- The spectroscopic data (NMR, UV-vis and luminescence) of all the compounds and DFT/TD-DFT calculations bring to light the practically identical electronic features of the Et O_2C-C^C* and NC-C^C* moieties.

5.- Most compounds behave as very bright blue-emitters in PMMA films (5 wt%). That is, compounds *trans*-(C*, P)-[Pt(R-C^C*)(PPh_3)L]PF_6 (R-C = Naph, L = py **9A**; R = CN, L = py **9C**, CNXyl **10C**) showed QY of 87%, 93% and 87% respectively; in compounds NBu_4[Pt(C^C*)$(CN)_2$] the QY ranges from 62% to 83%; in compounds [Pt(C^C*)(P^P)]PF_6 from 53% to 89% and for compounds [Pt(R-C^C*)(acac)](R =CO_2Et, CN) the QY is 93% and 98%.

6.- In complexes containing the naphthyl moiety (R-C = Naph), the larger π system due to the extra aromatic ring lead to a more extended assembly of the complexes through π–π contacts. As a result, some of these compounds display bright yellow to orange luminescence in powdery samples or high concentration. By contrast, complexes with a less extended π system (EtO_2C-C^C*, NC-C^C*) do not show, in most cases, luminescence due to significant aggregation, being complexes [Pt(R-C^C*)(acac)] (R = CO_2Et **19B**, CN **19C**) the only examples.

7.- The mononuclear complexes [Pt(R-C^C*)(acac)] (R = CO_2Et **19B**, CN **19C**, Cl **19D**) reacted with TlPF6 in a 2:1 molar ratio to give the corresponding trinuclear cluster [{Pt(R-C^C*)(acac)}$_2$Tl]$^+$ (**20B**, **20C**, **20D**) containing donor–acceptor Pt–Tl bonds. These results confirmed the ability of this kind of Pt(II) complexes to act as Lewis bases for this kind of interactions. The Pt–Tl bonds present in the solid state, break down in solution even at low temperatures (- 80 ºC).

8.-The crystallographic, spectroscopic and photophysical study of **19B**–**19D** and their corresponding "Pt_2Tl" clusters discovered that electron withdrawing substituents, such as CN and CO_2Et, in the 4-position of the cyclometalated ring enable the "Pt_2Tl" clusters to self-assemble in 2D extended lattice through intermolecular Pt–Pt, π–π, Tl–N or Tl–O interactions. By contrast, Cl substituents in the positions 3 and 5 of the cyclometalated ring lead to discrete "Pt_2Tl" cluster (**20D**) because it allows the Tl center to satisfy its electronic demand through intramolecular Tl-Cl contacts.

9.- Complexes **19B** and **19C** show in 5wt% films in PMMA dual emissions, blue (HE) and green-yellow (LE) bands, attributed to ^{3}ILCT and ^{3}MMLCT excited states, respectively. By controlling the excitation wavelength and the concentration of the complex in the film the blue or green emissions could be finely tuned with very high PLQY (98%–72%). The inclusion of Tl into these systems does not improve the quantum efficiency. Instead, the emission of **20B** resulted to be quenched because of the existence of weakly emissive ^{3}MMLCT [dσ*(Pt-Pt) → π*(NHC)] excited states, due to the strong Pt···Pt interactions in the extended metallic [–Pt–Pt–Tl–Pt–Pt–] chain.

10.- Compounds trans-(C*,P) [Pt(NC-C^C*)(PPh_3)L]PF_6 (L = py **9C**, CNXyl **10C**) were chosen to fabricate OLEDs. Thanks to the good processability of these compounds, this is the first example of Pt-based devices fabricated by a full solution process technology with a non-doped emitting layer (EML). This very simple approach allowed us to tune the OLEDs emission from blue (**9C**) to yellow-orange (**10C**), passing through white (mixtures of **9C**: **10C**).

11.- Complexes [Pt(CO_2Et-C^C*)($CN^tBu)_2$]PF_6 **13B** and [Pt(NC-C^C*)(CNXyl)$_2$]PF_6 **14C,** were tested as blue, [Pt(Naph^C*)($CN^tBu)_2$]PF_6 **13A** as yellow and [Pt(bzq)(CN)(CN^tBu)] (**R1**) as red components of remote phosphors for white light illumination. To explore that, the phosphor stacks were constructed by depositing the higher energy emitter closer to the glass and the stacks were placed with the red layer facing the UV-pumping source. In this way, through the control of the composition, it is possible to control the spectral power distribution and the colorimetric features of the light to achieve white light with CCT, CRI and LER values within acceptable margins for general light applications.

12.- Complexes [Pt(CO_2Et-C^C*)(P^P)]PF_6 (P^P = dppm **16B**, dppbz **18B**) and [Pt(bzq)(CN)(CNXyl)] (**R2**) were selected as blue and red emitters for white-light remote-phosphor devices with two-component architectures. By changing the nature of the blue component and the blue: red ratio we were able to fabricate devices with optimal CRI and D_{uv} values and a great range of nominal CCT values: 4000 K, 3500 K, 3000 K and 2500 K.

13.- Compounds [Pt(CO_2Et-C^C*)(dppm)]PF_6 (**16B**) and [Pt(Naph^C*)(dppbz)]PF_6 (**18A**) were selected for the fabrication of two-component OLEDs. The optimization process brought to light the importance of carrier balance, which was found to be problematic since the FOs of the dopants are placed far away from those of the matrix, thus resulting in a difficult hole and electron injection and transport. As a consequence, low EQE for the white light emitting devices in the order of 0.3% were obtained. The problems observed with these molecules allow us to focus on the development of emitting molecules with more adequate FOs for future work.

However, with the development of new matrices with deeper HOMOs and higher LUMOs, these compounds can result in perfect dopants for OLEDs since they have intrinsic emission quantum yields close to unity and a proven ability to achieve outstanding CRI, CCT and Duv values.

Conclusiones

1.- Hemos sido capaces de establecer una ruta general paso-a-paso para preparar cuatro compuestos con cloros puente que contienen ligandos carbeno N-heterocíclico, [{Pt(μ-Cl)(R-C^C*)}$_2$] (R-C^C*: 1-(naftalen-2-il)-3-metil-1*H*-imidazol-2-ilideno (Naph^C*, **4A**); 1-(4-etoxicarbonilfenil)-3-metil-1*H*-imidazol-2-ilideno (EtO_2C-C^C*, **4B**); 1-(4-cianofenil)-3-metil-1*H*-imidazol-2-ilideno (NC-C^C*, **4C**); 1-(3,5-diclorofenil)-3-metil-1*H*-imidazol-2-ilideno (Cl_2C-C^C*, **4D**)), que han resultado ser valiosos materiales de partida para la obtención de nuevos compuestos luminiscentes de Pt(II) con el fragmento "Pt(R-C^C*)".

2.- Basándonos en los datos de RMN de los compuestos heterolépticos [Pt(C^C*)LL'], se ha podido deducir que la influencia trans del átomo carbenico (C*) es menor que la del átomo metalado (C_{Ar}), pero no excesivamente diferente. Además, la influencia trans de los ligandos utilizados parece seguir el orden PPh_3 > CNXyl > py ~MMI > Cl. Así pues, el grado de transfobia (T) de los pares de ligandos en posiciones trans resultó ser: T[C_{Ar}/L] > T[C*/L] and T[C_{Ar}/PPh_3] > T[C_{Ar}/CNXyl] > T[C_{Ar}/py] ~ T[C_{Ar}/MMI] > T[C_{Ar}/Cl].

La diferencia entre T[C_{Ar}/L] y T[C*/L] (L = py, CNXyl, MMI) no es suficiente para evitar la formación de mezclas de isómeros cis/trans durante la ruptura del sistema de cloros puente por L para dar los complejos heterolépticos [PtCl(C^C*)L]. Sin embargo en todos los casos el isómero trans-(C*, L)-[Pt(R-C^C*)L] es la especie mayoritaria, especialmente cuando L es py. En este caso, las interacciones intramoleculares T–shaped C_{Ar}–H···π (py) parecen contribuir a la estabilización de este isómero, como demuestran los cálculos DFT.

En el caso de complejos con PPh_3, el mayor T[C_{Ar} /PPh_3] junto con las interacciones intramoleculares T–shaped C_{Ar}–H···π (Ph) presentes en los complejos trans-(C*, PPh_3)-[Pt(NC-C^C*)(PPh_3)L] (L = Cl **5C**, py **9C**, CNXyl **10C**, MMI **11C**) justificarían en la formación estereoselectiva de este isómero en cada caso.

3.- Complejos con estequiometrías [Pt(R-C^C*)(CNR')$_2$]PF_6 (R-C= Naph, R = CO_2Et, CN; R' = ^{t}Bu, Xyl), NBu_4[Pt(R-C^C*)(CN)$_2$] (R-C= Naph, R = CO_2Et, CN, Cl; [Pt(C^C*)(P^P)]PF_6 (R-C= Naph, R = CO_2Et, CN, P^P = dppm, dppe, dppbz), [Pt(C^C*)(acac)] (R = CO_2Et, CN, Cl) han sido preparados con buen rendimiento por eliminación del Cl de los correspondientes complejos de partida [{Pt(μ-Cl)(R-C^C*)}$_2$].

4.- Los datos espectroscópicos (RMN, UV-vis y luminiscencia) de todos los compuestos y los cálculos DFT/TD-DFT demuestran las características electrónicas casi idénticas de las unidades EtO_2C-C^C* y NC-C^C*.

5.- La mayoría de los compuestos se comportan como emisores azules brillantes en películas de PMMA (5 wt%). Así, los complejos trans-(C*, P)-[Pt(R-C^C*)(PPh_3)L]PF_6 (R-C

= Naph, L = py **9A**; R = CN, L' = py **9C**, CNXyl **10C**) mostraron QY de 87%, 93% y 87% respectivamente; en compuestos $NBu_4[Pt(R\text{-}C\hat{}C^*)(CN)_2]$ los QY van del 62% al 83%; en compuestos $[Pt(R\text{-}C\hat{}C^*)(P\hat{}P)]PF_6$ van de 53% a 89% y para compuestos [Pt(R-C^C*)(acac)] (R = CO_2Et, CN) el QY es de 93% y 98%.

6.- En complejos con la unidad naftilo (R-C = Naph), el sistema π de mayor tamaño debido al anillo aromático adicional conlleva la organización de los complejos a través de contactos π–π. Como resultado, algunos de estos compuestos presentan una intensa luminiscencia amarilla-naranja en muestras pulverulentas o en disolución a altas concentraciones. Por el contrario, complejos con un sistema π menor (EtO_2C-C^C*, NC-C^C*, Cl-C^C*) no muestran, en la mayoría de los casos, luminiscencia debido a la formación de agregados, siendo los complejos [Pt(R-C^C*)(acac)] (R = CO_2Et **19B**, CN **19C**) los únicos ejemplos.

7.- Los complejos mononucleares [Pt(R-C^C*)(acac)] (R = CO_2Et **19B**, CN **19C**, Cl **19D**) reaccionaron con $TlPF_6$ en relación molar 2:1 para dar los correspondientes clústeres trinucleares $[\{Pt(R\text{-}C\hat{}C^*)(acac)\}_2Tl]^+$ (**20B**, **20C**, **20D**) con enlaces Pt–Tl de tipo dador-aceptor. Estos resultados confirman la capacidad de este tipo de complejos de Pt(II) para actuar como bases de Lewis en este tipo de interacciones. Los enlaces Pt–Tl presentes en estado sólido desaparecen en disolución incluso a baja temperatura (-80 ºC).

8.- El estudio cristalográfico, espectroscópico y fotofísico de **19B**-**19D** y sus correspondientes clústeres "Pt_2Tl" puso de manifiesto que sustituyentes electroatractores, como CN y CO_2Et, en la posición 4 del anillo ciclometalado permiten a los clústeres "Pt_2Tl" organizarse en redes extendidas 2D a través de interacciones intermoleculares Pt–Pt, π–π, Tl–N o Tl–O. Por el contrario, sustituyentes Cl en posiciones 3 y 5 en el anillo ciclometalado conduce a clústeres discretos "Pt_2Tl" (**20D**) ya que permite al centro de Tl satisfacer la demanda electrónica por contactos intramoleculares Tl–Cl.

9.- Los complejos **19B** y **19C** muestran emisiones duales, azul (HE) y verde-amarilla (LE), en películas de PMMA al 5 wt%, atribuidas a estados excitados ^{3}ILCT y ^{3}MMLCT respectivamente. Controlando la longitud de onda de excitación y la concentración del complejo en el film las emisiones azul y verde pueden ser reguladas con QY muy elevados (98%-72%). La inclusión del Tl en estos sistemas no mejora la eficiencia quántica. En su lugar, la emisión de **20B** queda casi anulada debido a la existencia de estados excitados ^{3}MMLCT [dσ*(Pt-Pt)→π*(NHC)] poco emisores, debido a las interacciones fuertes Pt···Pt en la cadena metálica [–Pt–Pt–Tl–Pt–Pt–].

10.- Los compuestos trans-(C*, P)-[Pt(NC-C^C*)(PPh_3)L]PF_6 (L = py **9C**, CNXyl **10C**) fueron elegidos para la fabricación de OLEDs. Gracias a la buena procesabilidad de estos compuestos, este es el primer ejemplo de dispositivos basados en Pt fabricados totalmente mediante tecnología de procesado de disoluciones con una capa emisora (EML) no dopada. Esta aproximación tan simple nos permitió modular la emisión de los OLEDs desde azul (**9C**) hasta amarillo-naranja (**10C**), pasando por el blanco (mezclas **9C**:**10C**).

11.- Los complejos [Pt(CO_2Et-C^C*)($CN^tBu)_2$]PF_6 **13B** y [Pt(NC-C^C*)($CNXyl)_2$]PF_6 **14C**, se probaron como componentes azul, [Pt(Naph^C*)($CN^tBu)_2$]PF_6 **13A** amarilla y [Pt(bzq)(CN)(CN^tBu)] (**R1**) roja en fósforos remotos para conseguir luz blanca. Para ello, los apilamientos de emisores se prepararon depositando el emisor de más alta energía más cerca del vidrio, y se colocaron con el emisor rojo más cerca de la fuente de bombeo UV. A través del control de la composición, es posible controlar la distribución espectral y las propiedades colorimétricas de la luz y conseguir así luz blanca con valores de CCT, CRI y LER dentro de los estándares para aplicaciones de iluminación general.

12.- Se seleccionaron los complejos [Pt(R-C^C*)(P^P)]PF_6 (R = CO_2Et, P^P = dppm **16B**, dppbz **18B**) and [Pt(bzq)(CN)(CNXyl)] (**R2**) como emisores azules y rojo para dispositivos emisores de luz blanca de tipo fósforo remoto con arquitectura de dos componentes. Cambiando la naturaleza de la componente azul y la proporción azul:rojo fuimos capaces de fabricar dispositivos con valores óptimos de CRI y D_{uv} en un gran rango de valores nominales de CCT: 4000K, 3500K, 3000K y 2500K.

13.- Se seleccionaron los complejos [Pt(CO_2Et-C^C*)(dppm)]PF_6 (**16B**) y [Pt(Naph^C*)(dppbz)]PF_6 (**18A**) para la fabricación de OLEDs de dos componentes. El proceso de optimización puso de manifiesto la importancia de un buen balance de transportadores de carga, que se demostró problemático ya que los Orbitales Frontera (OF) de los dopantes están situados demasiado lejos de los de la matriz, resultando así en difícil inyección y transporte de huecos y electrones. Como consecuencia, se obtuvieron valores bajos de EQE del orden de 0.3% para los dispositivos emisores de luz blanca. Los problemas observados con estas moléculas nos permiten focalizar futuros trabajos en el desarrollo de moléculas emisoras con OF más adecuados.

Sin embargo, con el desarrollo de nuevas matrices con HOMOs más profundos y LUMOs más elevados, estos compuestos pueden llegar a ser dopantes perfectos para OLEDs, dado su elevado QY intrínseco cercano a la unidad, y su demostrada capacidad para proporcionar a la luz producida valores adecuados de CRI, CCT, D_{uv} y LER.

References.

1. Lighting Research and Development. *Multi-Year Program Plan* **2013,** *U. S. Department of Energy*, DOE/EERE-0961.

2. (a) Tang, L.; Edman, S.; Light-Emitting Electrochemical Cells: A Review on Recent Progress. *Top. Curr. Chem.* **2016,** *374*, 40; (b) Chamorro-Posada, P.; Martín-Gil, J.; Martín-Ramos, P.; Navas-Gracia, L.-M., Fundamentos de la Tecnología LED. *Universidad de Valladolid- Departamento de Teoría de la Señal e Ingeniería Telemática-Departamento de Ingeniería Agrícola y Forestal.* **2008**.

3. Fang, J.; Ma, D., Efficient Red Organic Light-Emitting Devices Based on a Europium Complex. *Appl. Phys. Lett.* **2003,** *83*, 4041-4043.

4. (a) Sun, L.; Huang, Q.; Feng, C.; Li, W.; Wang, C., Visual color matching system based on RGB LED light source. *Proc. SPIE 10616, International Conference on Optical Instruments and Technology: Optical Systems and Modern Optoelectronic Instruments, 106161C (10 January 2018); doi: 10.1117/12.2295274* **2017**; (b) Li, Y.-C.; Chang, Y.-H.; Singh, P.; Chang, L.-B.; Yeh, D.-H.; Chao, T.-Y.; Jian, S.-Y.; Li, Y.-C.; Tan, C.-M.; Lai, C.-S.; Chow, L.; Ying, S.-P., RGB-Stack Light Emitting Diode Modules with Transparent Glass Circuit Board and Oil Encapsulation. *Materials* **2018,** *11*, 365.

5. Narendran, N.; Gu, Y.; Freyssinier-Nova, J. P.; Zhu, Y., Extracting Phosphor-Sattered Photons to Improve White LED efficiency. *Phys. Status Solidi A* **2005,** *202*, R60-R62.

6. Department of Energy, U. S., Critical Materials Strategy 2011. *U. S. Department of Energy* **2012**, DOE/PI-0009.

7. (a) Erdem, T.; Demir, H. V., Color Science of Nanocrystal Quantum Dots for Lighting and Displays. *Nanophotonics* **2013,** *2*, 57-81; (b) D'Andrade, B. W.; Forrest, S. R., White Organic Light-Emitting Devices for Solid-State Lighting. *Adv. Mater.* **2004,** *16*, 1585-1595; (c) Gather, M. C.; Köhnen, A.; Meerholz, K., White Organic Light-Emitting Diodes. *Adv. Mater.* **2011,** *23*, 233-248.

8. (a) Sun, Z.; Zhang, Q.; Li, Y.; Wang, H., Thermal Stable $La_2Ti_2O_7:Eu^{3+}$ Phosphors for Blue-Chip White LEDs with High Color Rendering Index. *J. Alloy. Compd.* **2010,** *506*, 338-342; (b) Sai, Q.; Zhao, Z.; Xia, C.; Xu, X.; Wu, F.; Di, J.; Wang, L., Ce-Doped Al_2O_3–YAG Eutectic and its Application for White LEDs. *Opt. Mater.* **2013,** *35*, 2155-2159.

9. (a) Xu, H.; Chen, R.; Sun, Q.; Lai, W.; Su, Q.; Huang, W.; Liu, X., Recent Progress in Metal-Organic Complexes for Optoelectronic Applications. *Chem. Soc. Rev.* **2014,** *43*, 3259-3302; (b) Xiao, L.; Chen, Z.; Qu, B.; Luo, J.; Kong, S.; Gong, Q.; Kido, J., Recent Progresses on Materials for Electrophosphorescent Organic Light-Emitting Devices. *Adv. Mater.* **2010,** *23*, 926-952.

10. (a) Tang, M.-C.; Chan, A. K.-W.; Chan, M.-Y.; Yam, V. W.-W., Platinum and Gold Complexes for OLEDs. *Top. Curr. Chem.* **2016,** *374*, 46; (b) Wong Ben, Y. W.; Wong, H. L.;

Wong, Y. C.; Chan, M. Y.; Yam Vivian, W. W., Versatile Synthesis of Luminescent Tetradentate Cyclometalated Alkynylgold(III) Complexes and Their Application in Solution-Processable Organic Light-Emitting Devices. *Angew. Chem. Int. Ed.* **2016,** *56*, 302-305; (c) Wong, B. Y.-W.; Wong, H.-L.; Wong, Y.-C.; Au, V. K.-M.; Chan, M.-Y.; Yam, V. W.-W., Multi-Functional Bis(alkynyl)gold(III) N^C Complexes with Distinct Mechanochromic Luminescence and Electroluminescence Properties. *Chem. Sci.* **2017,** *8*, 6936-6946; (d) Tang, M.-C.; Lee, C.-H.; Lai, S.-L.; Ng, M.; Chan, M.-Y.; Yam, V. W.-W., Versatile Design Strategy for Highly Luminescent Vacuum-Evaporable and Solution-Processable Tridentate Gold(III) Complexes with Monoaryl Auxiliary Ligands and Their Applications for Phosphorescent Organic Light Emitting Devices. *J. Am. Chem. Soc.* **2017,** *139*, 9341-9349.

11. (a) Zhu, Y.; Ma, Y.; Zhu, J., The Counter Anion Effect of Ion-Type Phosphorescent Dye Tris(4,7-diphenyl-1,10-phenanthroline)ruthenium(II) Complexes as Dopant for Light-Emitting Diodes. *J. Lumin.* **2013,** *137*, 198-203; (b) Ma, D.; Zhang, C.; Qiu, Y.; Duan, L., Sustainable Phosphorescence Based on Solution-Processable and Vacuum-Sublimable Cationic Ruthenium(II) Complexes Achieved by Counter-Ion Control. *Org. Electron.* **2017,** *42*, 194-202.

12. (a) Du, B. S.; Liao, J. L.; Huang, M. H.; Lin, C. H.; Lin, H. W.; Chi, Y.; Pan, H. A.; Fan, G. L.; Wong, K. T.; Lee, G. H.; Chou, P. T., Os(II) Based Green to Red Phosphors: A Great Prospect for Solution-Processed, Highly Efficient Organic Light-Emitting Diodes. *Adv. Funct. Mater.* **2012,** *22*, 3491-3499; (b) Chang, S.-H.; Chang, C.-F.; Liao, J.-L.; Chi, Y.; Zhou, D.-Y.; Liao, L.-S.; Jiang, T.-Y.; Chou, T.-P.; Li, E. Y.; Lee, G.-H.; Kuo, T.-Y.; Chou, P.-T., Emissive Osmium(II) Complexes with Tetradentate Bis(pyridylpyrazolate) Chelates. *Inorg. Chem.* **2013,** *52*, 5867-5875; (c) Liao, J.-L.; Chi, Y.; Yeh, C.-C.; Kao, H.-C.; Chang, C.-H.; Fox, M. A.; Low, P. J.; Lee, G.-H., Near Infrared-Emitting Tris-Bidentate Os(II) Phosphors: Control of Excited State Characteristics and Fabrication of OLEDs. *J. Mater. Chem. C* **2015,** *3*, 4910-4920; (d) Chou, P. T.; Chi, Y., Phosphorescent Dyes for Organic Light-Emitting Diodes. *Chem. - Eur. J.* **2007,** *13*, 380-395; (e) Lee, T. C.; Hung, J. Y.; Chi, Y.; Cheng, Y. M.; Lee, G. H.; Chou, P. T.; Chen, C. C.; Chang, C. H.; Wu, C. C., Rational Design of Charge-Neutral, Near-Infrared-Emitting Osmium(II) Complexes and OLED Fabrication. *Adv. Funct. Mater.* **2009,** *19*, 2639-2647.

13. (a) Henwood, A. F.; Zysman-Colman, E., Luminescent Iridium Complexes Used in Light-Emitting Electrochemical Cells (LEECs). *Top. Curr. Chem.* **2016,** *374*, 36; (b) Henwood, A. F.; Zysman-Colman, E., Lessons Learned in Tuning the Optoelectronic Properties of Phosphorescent Iridium(III) Complexes. *Chem. Commun.* **2017,** *53*, 807-826; (c) Ma, D.; Tsuboi, T.; Qiu, Y.; Duan, L., Recent Progress in Ionic Iridium(III) Complexes for Organic Electronic Devices. *Adv. Mater.* **2016,** *29*, 1603253; (d) Henwood, A.-F.; Pal, A.-K.;

Cordes, D.-B.; Slawin, A. M.-Z.; Rees, T.-W.; Momblona, C.; Babaei, A.; Pertegás, A.; Ortí, E.; Bolink, H.-J.; Baranoff, E.; Zysman-Colman, E., Blue-Emitting Cationic Iridium(III) Complexes Featuring Pyridylpyrimidine Ligands and their Use in Sky-Blue Electroluminescent Devices. *J. Mater. Chem. C* **2017,** *5*, 9638-9650.

14. (a) Tam, A. Y.-Y.; Tsang, D. P.-K.; Chan, M.-Y.; Zhu, N.; Yam, V. W.-W., A Luminescent Cyclometalated Platinum(II) Complex and its Green Organic Light Emitting Device with High Device Performance. *Chem. Commun.* **2011,** *47*, 3383-3385; (b) Fleetham, T.; Wang, Z.; Li, J., Efficient Deep Blue Electrophosphorescent Devices Based on Platinum(II) Bis(*N*-methyl-imidazolyl)benzene Chloride. *Org. Electron.* **2012,** *13*, 1430-1435; (c) Hang, X. C.; Fleetham, T.; Turner, E.; Brooks, J.; Li, J., Highly Efficient Blue-Emitting Cyclometalated Platinum(II) Complexes by Judicious Molecular Design. *Angew. Chem. Int. Ed.* **2013,** *52*, 6753-6756; (d) Kui, S. C. F.; Chow, P. K.; Tong, G. S. M.; Lai, S. L.; Cheng, G.; Kwok, C. C.; Low, K. H.; Ko, M. Y.; Che, C. M., Robust Phosphorescent Platinum(II) Complexes Containing Tetradentate O^N^C^N Ligands: Excimeric Excited State and Application in Organic White-Light-Emitting Diodes. *Chem. - Eur. J.* **2013,** *19*, 69-73; (e) Yan, B. P.; Cheung, C. C. C.; Kui, S. C. F.; Xiang, H. F.; Roy, V. A. L.; Xu, S. J.; Che, C. M., Efficient White Organic Light-Emitting Devices Based on Phosphorescent Platinum(II)/Fluorescent Dual-Emitting Layers. *Adv. Mater.* **2007,** *19*, 3599-3603; (f) Ma, B.; Djurovich, P. I.; Garon, S.; Alleyne, B.; Thompson, M. E., Platinum Binuclear Complexes as Phosphorescent Dopants for Monochromatic and White Organic Light-Emitting Diodes. *Adv. Funct. Mater.* **2006,** *16*, 2438-2446.

15. (a) Williams, J. A. G., Photochemistry and Photophysics of Coordination Compounds: Platinum. *Top. Curr. Chem.* **2007,** *281*, 205-268; (b) Williams, J. A. G.; Develay, S.; Rochester, D. L.; Murphy, L., Optimising the Luminescence of Platinum(II) Complexes and their Application in Organic Light Emitting Devices (OLEDs) *Coord. Chem. Rev.* **2008,** *252*, 2596-2611; (c) Williams, J. A. G., Molecular Organometallic Materials for Optics. In *Top. Organomet. Chem.*, Bozec, H.; Guerchais, V., Eds. Springer: New York, 2009; Vol. 28; (d) Yang, C. L.; Zhang, X. W.; You, H.; Zhu, L. Y.; Chen, L. Q.; Zhu, L. N.; Tao, Y. T.; Ma, D. G.; Shuai, Z. G.; Qin, J. G., Tuning the Energy Level and Photophysical and Electroluminescent Properties of Heavy Metal Complexes by Controlling the Ligation of the Metal with the Carbon of the Carbazole Unit. *Adv. Funct. Mater.* **2007,** *17*, 651-661; (e) Ionkin, A. S.; Marshall, W. J.; Wang, Y., Syntheses, Structural Characterization, and First Electroluminescent Properties of Mono-cyclometalated Platinum(II) Complexes with Greater than Classical π−π Stacking and Pt−Pt Distances. *Organometallics* **2005,** *24*, 619-627; (f) Berenguer, J. R.; Lalinde, E.; Moreno, M. T.; Sánchez, S.; Torroba, J., Facile Metalation of Hbzq by [cis-Pt(C_6F_5)$_2$(thf)$_2$]: A Route to a Pentafluorophenyl

Benzoquinolate Solvate Complex That Easily Coordinates Terminal Alkynes. Spectroscopic and Optical Properties. *Inorg. Chem.* **2012,** *51*, 11665-11679; (g) Díez, Á.; Lalinde, E.; Moreno, M. T., Heteropolynuclear Cycloplatinated Complexes: Structural and Photophysical Properties. *Coord. Chem. Rev.* **2011,** *255*, 2426-2447; (h) Berenguer, J. R.; Lalinde, E.; Moreno, M. T., Luminescent Cyclometalated-Pentafluorophenyl Pt^{II}, Pt^{IV} and Heteropolynuclear Complexes. *Coord. Chem. Rev.* **2018,** *366*, 69-90; (i) Lalinde, E.; Lara, R.; López, I. P.; Moreno, M. T.; Alfaro-Arnedo, E.; Pichel, J. G.; Piñeiro-Hermida, S., Benzothiazole-Based Cycloplatinated Chromophores: Synthetic, Optical, and Biological Studies. *Chem. - Eur. J.* **2018,** *24*, 2440-2456; (j) Berenguer, J. R.; Pichel, J. G.; Gimenez, N.; Lalinde, E.; Moreno, M. T.; Pineiro-Hermida, S., Luminescent Pentafluorophenyl-Cycloplatinated Complexes: Synthesis, Characterization, Photophysics, Cytotoxicity and Cellular Imaging. *Dalton Trans.* **2015,** *44*, 18839-18855.

16. (a) O'Brien, D. F.; Baldo, M. A.; Thompson, M. E.; Forrest, S. R., Improved Energy Transfer in Electrophosphorescent Devices. *Appl. Phys. Lett.* **1999,** *74*, 442-444; (b) Baldo, M. A.; O'Brien, D. F.; You, Y.; Shoustikov, A.; Sibley, S.; Thompson, M. E.; Forrest, S. R., Highly Efficient Phosphorescent Emission from Organic Electroluminescent Devices. *Nature* **1998,** *395*, 151; (c) Kwong, R. C.; Sibley, S.; Dubovoy, T.; Baldo, M.; Forrest, S. R.; Thompson, M. E., Efficient, Saturated Red Organic Light Emitting Devices Based on Phosphorescent Platinum(II) Porphyrins. *Chem. Mater.* **1999,** *11*, 3709-3713.

17. (a) Che, C. M.; Kwok, C. C.; Lai, S. W.; Rausch, A. F.; Finkenzeller, W. J.; Zhu, N.; Yersin, H., Photophysical Properties and OLED Applications of Phosphorescent Platinum(II) Schiff Base Complexes. *Chem. - Eur. J.* **2010,** *16*, 233-247; (b) Kavitha, J.; Chang, S. Y.; Chi, Y.; Yu, J. K.; Hu, Y. H.; Chou, P. T.; Peng, S. M.; Lee, G. H.; Tao, Y. T.; Chien, C. H.; Carty, A. J., In Search of High-Performance Platinum(II) Phosphorescent Materials for the Fabrication of Red Electroluminescent Devices. *Adv. Funct. Mater.* **2005,** *15*, 223-229; (c) Fukagawa, H.; Shimizu, T.; Hanashima, H.; Osada, Y.; Suzuki, M.; Fujikake, H., Highly Efficient and Stable Red Phosphorescent Organic Light-Emitting Diodes Using Platinum Complexes. *Adv. Mater.* **2012,** *24*, 5099-5103 and references therein.

18. (a) Cocchi, M.; Virgili, D.; Fattori, V.; Rochester, D. L.; Williams, J. A. G., N^C^N-Coordinated Platinum(II) Complexes as Phosphorescent Emitters in High-Performance Organic Light-Emitting Devices. *Adv. Funct. Mater.* **2007,** *17*, 285-289; (b) Yang, X.; Wang, Z.; Madakuni, S.; Li, J.; Jabbour, G. E., Efficient Blue- and White-Emitting Electrophosphorescent Devices Based on Platinum(II) [1,3-Difluoro-4,6-di(2-pyridinyl)benzene] Chloride. *Adv. Mater.* **2008,** *20*, 2405-2409.

19. (a) He, L.; Duan, L.; Qiao, J.; Dong, G.; Wang, L.; Qiu, Y., Highly Efficient Blue-Green and White Light-Emitting Electrochemical Cells Based on a Cationic Iridium Complex with

a Bulky Side Group. *Chem. Mater.* **2010,** *22*, 3535-3542; (b) Yang, C.-H.; Mauro, M.; Polo, F.; Watanabe, S.; Muenster, I.; Fröhlich, R.; De Cola, L., Deep-Blue-Emitting Heteroleptic Iridium(III) Complexes Suited for Highly Efficient Phosphorescent OLEDs. *Chem. Mater.* **2012,** *24*, 3684-3695; (c) Chang, C.-H.; Chen, C.-C.; Wu, C.-C.; Chang, S.-Y.; Hung, J.-Y.; Chi, Y., High-Color-Rendering Pure-White Phosphorescent Organic Light-Emitting Devices Employing Only Two Complementary Colors. *Org. Electron.* **2010,** *11*, 266-272.

20. (a) Cheng, G.; Chow, P. K.; Kui, S. C. F.; Kwok, C. C.; Che, C. M., High-Efficiency Polymer Light-Emitting Devices with Robust Phosphorescent Platinum(II) Emitters Containing Tetradentate Dianionic O^N^C^N Ligands. *Adv. Mater.* **2013,** *25*, 6765-6770; (b) Feng, K.; Zuniga, C.; Zhang, Y.-D.; Kim, D.; Barlow, S.; Marder, S. R.; Brédas, J. L.; Weck, M., Norbornene-Based Copolymers Containing Platinum Complexes and Bis(carbazolyl)benzene Groups in Their Side-Chains. *Macromolecules* **2009,** *42*, 6855-6864; (c) Turner, E.; Bakken, N.; Li, J., Cyclometalated Platinum Complexes with Luminescent Quantum Yields Approaching 100%. *Inorg. Chem.* **2013,** *52*, 7344-7351.

21. (a) Williams, J. A. G.; Beeby, A.; Davies, E. S.; Weinstein, J. A.; Wilson, C., An Alternative Route to Highly Luminescent Platinum(II) Complexes: Cyclometalation with N∧C∧N-Coordinating Dipyridylbenzene Ligands. *Inorg. Chem.* **2003,** *42*, 8609-8611; (b) Rausch, A. F.; Murphy, L.; Williams, J. A. G.; Yersin, H., Improving the Performance of Pt(II) Complexes for Blue Light Emission by Enhancing the Molecular Rigidity. *Inorg. Chem.* **2012,** *51*, 312-319.

22. (a) Shigehiro, T.; Yagi, S.; Maeda, T.; Nakazumi, H.; Fujiwara, H.; Sakurai, Y., Photo- and Electroluminescence from 2-(Dibenzo[b,d]furan-4-yl)pyridine-Based Heteroleptic Cyclometalated Platinum(II) Complexes: Excimer Formation Drastically Facilitated by an Aromatic Diketonate Ancillary Ligand. *J. Phys. Chem. C* **2013,** *117*, 532-542; (b) Tan, G.; Chen, S.; Siu, C.-H.; Langlois, A.; Qiu, Y.; Fan, H.; Ho, C.-L.; Harvey, P. D.; Lo, Y. H.; Liu, L.; Wong, W.-Y., Platinum(II) Cyclometallates Featuring Broad Emission Bands and their Applications in Color-Tunable OLEDs and High Color-Rendering WOLEDs. *J. Mater. Chem. C* **2016,** *4*, 6016-6026; (c) Fleetham, T.; Li, G.; Li, J., Phosphorescent Pt(II) and Pd(II) Complexes for Efficient, High-Color-Quality, and Stable OLEDs. *Adv. Mater.* **2017,** *29*, 1601861; (d) Zhao, J.; Feng, Z.; Zhong, D.; Yang, X.; Wu, Y.; Zhou, G.; Wu, Z., Cyclometalated Platinum Complexes with Aggregation-Induced Phosphorescence Emission Behavior and Highly Efficient Electroluminescent Ability. *Chem. Mater.* **2018,** *30*, 929-946; (e) Brooks, J.; Babayan, Y.; Lamansky, S.; Djurovich, P. I.; Tsyba, I.; Bau, R.; Thompson, M. E., Synthesis and Characterization of Phosphorescent Cyclometalated Platinum Complexes. *Inorg. Chem.* **2002,** *41*, 3055-3066; (f) Huo, S.; Carroll, J.; Vezzu Dileep, A. K., Design, Synthesis, and

Applications of Highly Phosphorescent Cyclometalated Platinum Complexes. *Asian J. Org. Chem.* **2015,** *4*, 1210-1245.

23. Elschenbroich, C., Organometallics. Third, Completely Revised and Extended Ed. *Wiley-VCH Verlag Gmbh & Co. KGaA Wiesbaden* **2005**.

24. Arduengo, A. J.; Harlow, R. L.; Kline, M., A Stable Crystalline Carbene. *J. Am. Chem. Soc.* **1991,** *113*, 361-363.

25. Nolan, S. P., N-Heterocyclic Carbenes, Effective Tools for Organometallic Synthesis. *Wiley-VCH Verlag Gmbh & Co. KGaA Weinheim* **2014**.

26. (a) Li, K.; Guan, X.; Ma, C.-W.; Lu, W.; Chen, Y.; Che, C.-M., Blue Electrophosphorescent Organoplatinum(II) Complexes with Dianionic Tetradentate Bis(carbene) Ligands. *Chem. Commun.* **2011,** *47*, 9075-9077; (b) Li, K.; Cheng, G.; Ma, C.; Guan, X.; Kwok, W.-M.; Chen, Y.; Lu, W.; Che, C.-M., Light-Emitting Platinum(II) Complexes Supported by Tetradentate Dianionic Bis(N-Heterocyclic Carbene) Ligands: towards Robust Blue Electrophosphors. *Chem. Sci.* **2013,** *4*, 2630-2644; (c) Zhang, Y.; Garg, J. A.; Michelin, C.; Fox, T.; Blacque, O.; Venkatesan, K., Synthesis and Luminescent Properties of cis Bis-N-Heterocyclic Carbene Platinum(II) Bis-Arylacetylide Complexes. *Inorg. Chem.* **2011,** *50*, 1220-1228; (d) Uesugi, H.; Tsukuda, T.; Takao, K.; Tsubomura, T., Highly Emissive Platinum(II) Complexes Bearing Carbene and Cyclometalated Ligands. *Dalton Trans.* **2013,** *42*, 7396-7403; (e) Hudson, Z. M.; Sun, C.; Helander, M. G.; Chang, Y.-L.; Lu, Z.-H.; Wang, S., Highly Efficient Blue Phosphorescence from Triarylboron-Functionalized Platinum(II) Complexes of N-Heterocyclic Carbenes. *J. Am. Chem. Soc.* **2012,** *134*, 13930-13933.

27. (a) Fornies, J.; Sicilia, V.; Borja, P.; Casas, J. M.; Diez, A.; Lalinde, E.; Larraz, C.; Martin, A.; Moreno, M. T., Luminescent Benzoquinolate-Isocyanide Platinum(II) Complexes: Effect of Pt···Pt and π···π Interactions on their Photophysical Properties. *Chem - Asian J.* **2012,** *7*, 2813-2823; (b) Forniés, J.; Fuertes, S.; Martín, A.; Sicilia, V.; Gil, B.; Lalinde, E., Extended Structures Containing Pt(II)–Tl(I) Bonds. Effect of these Interactions on the Luminescence of Cyclometalated Pt(II) Compounds. *Dalton Trans.* **2009**, 2224-2234; (c) Forniés, J.; Fuertes, S.; López, J. A.; Martín, A.; Sicilia, V., New Water Soluble and Luminescent Platinum(II) Compounds, Vapochromic Behavior of $[K(H_2O)][Pt(bzq)(CN)_2]$, New Examples of the Influence of the Counterion on the Photophysical Properties of d^8 Square-Planar Complexes. *Inorg. Chem.* **2008,** *47*, 7166-7176; (d) Díez, A.; Fornies, J.; Larraz, C.; Lalinde, E.; López, J. A.; Martin, A.; Moreno, M. T.; Sicilia, V., Structural and Luminescence Studies on π···π and Pt···Pt Interactions in Mixed Chloro-Isocyanide Cyclometalated Platinum(II) Complexes. *Inorg. Chem.* **2010,** *49*, 3239-3259; (e) Diez, A.; Fornies, J.; Fuertes, S.; Lalinde, E.; Larraz, C.; Lopez, J. A.; Martin, A.; Moreno, M. T.; Sicilia,

V., Synthesis and Luminescence of Cyclometalated Compounds with Nitrile and Isocyanide Ligands. *Organometallics* **2009,** *28*, 1705-1718; (f) Fernandez, S.; Fornies, J.; Gil, B.; Gomez, J.; Lalinde, E., Synthesis, Structural Characterisation and Photophysics of Anionic Cyclometalated Bis(alkynyl)(benzo[h]quinolinate)platinate(II) species. *Dalton Trans.* **2003,** 822-830.

28. (a) Tronnier, A.; Risler, A.; Langer, N.; Wagenblast, G.; Münster, I.; Strassner, T., A Phosphorescent C^C* Cyclometalated Platinum(II) Dibenzothiophene NHC Complex. *Organometallics* **2012,** *31*, 7447-7452; (b) Unger, Y.; Meyer, D.; Molt, O.; Schildknecht, C.; Münster, I.; Wagenblast, G.; Strassner, T., Green–Blue Emitters: NHC-Based Cyclometalated [Pt(C^C*)(acac)] Complexes. *Angew. Chem. Int. Ed.* **2010,** *49*, 10214-10216; (c) Strassner, T.; Unger, Y.; Meyer, D.; Molt, O.; Münster, I.; Wagenblast, G., The "Enders Triazole": A Well Known Molecule, but still a New Ligand!! *Inorg. Chem. Commun.* **2013,** *30*, 39-41; (d) Tronnier, A.; Strassner, T., (C^C*) Cyclometalated Binuclear N-Heterocyclic Biscarbene Platinum(II) Complexes - Highly Emissive Phosphorescent Emitters. *Dalton Trans.* **2013,** *42*, 9847-9851; (e) Tenne, M.; Metz, S.; Münster, I.; Wagenblast, G.; Strassner, T., Phosphorescent Platinum(II) Complexes Based on C^C* Cyclometalating Aryltriazol-5-ylidenes. *Organometallics* **2013,** *32*, 6257-6264.

29. (a) Leopold, H.; Strassner, T., 4,5-Substituted C^C* Cyclometalated Thiazol-2-ylidene Platinum(II) Complexes - Synthesis and Photophysical Properties. *Dalton Trans.* **2017,** *46*, 7800-7812; (b) Pinter, P.; Pittkowski, R.; Soellner, J.; Strassner, T., The Chameleonic Nature of Platinum(II) Imidazopyridine Complexes. *Chem. - Eur. J.* **2017,** *23*, 14173-14176; (c) Strassner, T., Phosphorescent Platinum(II) Complexes with C^C* Cyclometalated NHC Ligands. *Acc. Chem. Res.* **2016,** *49*, 2680-2689; (d) Tseng, C.-H.; Fox, M. A.; Liao, J.-L.; Ku, C.-H.; Sie, Z.-T.; Chang, C.-H.; Wang, J.-Y.; Chen, Z.-N.; Lee, G.-H.; Chi, Y., Luminescent Pt(II) Complexes Featuring Imidazolylidene-pyridylidene and Dianionic Bipyrazolate: From Fundamentals to OLED Fabrications. *J. Mater. Chem. C* **2017,** *5*, 1420-1435; (e) Fuertes, S.; García, H.; Perálvarez, M.; Hertog, W.; Carreras, J.; Sicilia, V., Stepwise Strategy to Cyclometallated Pt^{II} Complexes with N-Heterocyclic Carbene Ligands: A Luminescence Study on New β-Diketonate Complexes. *Chem. - Eur. J.* **2015,** *21*, 1620-1631.

30. Fuertes, S.; Chueca, A. J.; Perálvarez, M.; Borja, P.; Torrell, M.; Carreras, J.; Sicilia, V., White Light Emission from Planar Remote Phosphor Based on NHC Cycloplatinated Complexes. *ACS Appl. Mater. Interfaces* **2016,** *8*, 16160-16169.

31. Fuertes, S.; Chueca, A. J.; Sicilia, V., Exploring the Transphobia Effect on Heteroleptic NHC Cycloplatinated Complexes. *Inorg. Chem.* **2015,** *54*, 9885-9895.

32. Fuertes, S.; Chueca, A. J.; Martín, A.; Sicilia, V., Pt2Tl Building Blocks for Two-Dimensional Extended Solids: Synthesis, Crystal Structures, and Luminescence. *Cryst. Growth Des.* **2017,** *17*, 4336-4346.

33. (a) Sicilia, V.; Fuertes, S.; Martin, A.; Palacios, A., N-Assisted C-Ph-H Activation in 3,8-Dinitro-6-phenylphenanthridine. New C,N-Cyclometalated Compounds of Platinum(II): Synthesis, Structure, and Luminescence Studies. *Organometallics* **2013,** *32*, 4092-4102; (b) Fornies, J.; Sicilia, V.; Larraz, C.; Camerano, J. A.; Martin, A.; Casas, J. M.; Tsipis, A. C., One-Pot and Step-by-Step N-Assisted C-Ph-H Activation in 2-(4-Bromophenyl)imidazol[1,2-a]pyridine: Synthesis of a New C,N-Cyclometalated Compound [{Pt((CN)(μ-Cl)}$_2$] as Precursor of Luminescent Platinum(II) Compounds. *Organometallics* **2010,** *29*, 1396-1405; (c) Edwards, G. L.; Black, D. S. C.; Deacon, G. B.; Wakelin, L. P. G., In Vitro and In Vivo Studies of Neutral Cyclometallated Complexes against Murine Leukaemias. *Can. J. Chem.* **2005,** *83*, 980-989; (d) Newman, C. P.; Casey-Green, K.; Clarkson, G. J.; Cave, G. W. V.; Errington, W.; Rourke, J. P., Cyclometallated Platinum(II) Complexes: Oxidation to, and C-H Activation by, Platinum(IV). *Dalton Trans.* **2007,** 3170-3182; (e) Perez, S.; Lopez, C.; Caubet, A.; Solans, X.; Font-Bardia, M., Factors Affecting the Lability of the σ(M-X) Bond in Cycloplatinated and Cyclopalladated Complexes Containing C(sp^2, ferrocene),N,X$^-$ or C(sp^2, phenyl),N,X$^-$ (X = S, N) Terdentate Ligands. *J. Organomet. Chem.* **2004,** *689*, 3184-3196.

34. (a) Casas, J. M.; Fornies, J.; Fuertes, S.; Martin, A.; Sicilia, V., New Mono- and Polynuclear Alkynyl Complexes Containing Phenylacetylide as Terminal or Bridging Ligand. X-ray Structures of the Compounds NBu$_4$[Pt(CH$_2$C$_6$H$_4$P(o-tolyl)$_2$-κC,P)(C≡CPh)$_2$], Pt(CH$_2$C$_6$H$_4$P(o-tolyl)$_2$-κC,P)(C≡CPh)(CO), {Pt(CH$_2$C$_6$H$_4$P(o-tolyl)$_2$-κC,P)(μC≡CPh)}$_2$, and { Pt(CH$_2$C$_6$H$_4$P(o-tolyl)$_2$-κC,P)(C≡CPh)$_2$Cu}$_2$. *Organometallics* **2007,** *26*, 1674-1685; (b) Zucca, A.; Maidich, L.; Carta, V.; Petretto, G. L.; Stoccoro, S.; Agostina Cinellu, M.; Pilo, M. I.; Clarkson, G. J., Cyclometalated Complexes of Platinum(II) with 2-Vinylpyridine. *Eur. J. Inorg. Chem.* **2014,** *2014*, 2278-2287.

35. (a) Maidich, L.; Zuri, G.; Stoccoro, S.; Cinellu, M. A.; Zucca, A., Assembly of Symmetrical and Unsymmetrical Platinum(II) Rollover Complexes with Bidentate Phosphine Ligands. *Dalton Trans.* **2014,** *43*, 14806-14815; (b) Minghetti, G.; Zucca, A.; Stoccoro, S.; Cinellu, M. A.; Manassero, M.; Sansoni, M., Six-Membered Cyclometallated Derivatives of Platinum(II) Derived from 2-Benzylpyridines. Crystal and Molecular Structure of [Pt(L)(Ph$_3$P)Cl] (HL = 2-(1-methylbenzyl)pyridine). *J. Organomet. Chem.* **1994,** *481*, 195-204.

36. (a) Haghighi, M. G.; Rashidi, M.; Nabavizadeh, S. M.; Jamali, S.; Puddephatt, R. J., Cyclometalated Organoplatinum(II) Complexes: First Example of a Monodentate Benzo[h]quinolyl Ligand and a Complex with Bridging Bis(diphenylphosphino)ethane.

Dalton Trans. **2010,** *39*, 11396-11402; (b) Garrou, P. E., ΔR-ring Contributions to Phosphorus-31 NMR Parameters of Transition-Metal-Phosphorus Chelate Complexes. *Chem. Rev.* **1981,** *81*, 229-266; (c) Jia, Y.-X.; Li, B.-B.; Li, Y.; Pullarkat, S. A.; Xu, K.; Hirao, H.; Leung, P.-H., Stereoelectronic and Catalytic Properties of Chiral Cyclometalated Phospha-Palladium and -Platinum Complexes. *Organometallics* **2014,** *33*, 6053-6058.

37. Hu, J.; Lin, R.; Yip, J. H. K.; Wong, K.-Y.; Ma, D.-L.; Vittal, J. J., Synthesis and Electronic Spectroscopy of Luminescent Cyclometalated Platinum–Anthracenyl Complexes. *Organometallics* **2007,** *26*, 6533-6543.

38. (a) Nishio, M.; Umezawa, Y.; Honda, K.; Tsuboyama, S.; Suezawa, H., CH/π Hydrogen Bonds in Organic and Organometallic Chemistry. *CrystEngComm* **2009,** *11*, 1757-1788; (b) Saigo, K.; Kobayashi, Y., The Role of CH/π Interaction in the Stabilization of Less-Soluble Diastereomeric Salt Crystals. *Chem. Rec.* **2007,** *7*, 47-56; (c) Nishio, M.; Umezawa, Y., *Top. Stereochem.* **2006,** *25*, 255-302.

39. (a) Yamanari, K.; Nozaki, T.; Fuyuhiro, A.; Kushi, Y.; Kaizaki, S., Important Role of CH-π Interaction in Linkage Isomers of Bis(2,2'-bipyridine)ruthenium(II) Complexes with Pyrimidine-2-thione and Related Ligands. *J. Chem. Soc., Dalton Trans.* **1996,** 2851-2856; (b) Nakamura, M.; Okawa, H.; Kida, S., Substituent Effect on Stereoselectivity for Ccobalt(III), Chromium(III), and Manganese(III) Complexes of Ring-Substituted 1-l-menthyloxy-3-benzoylacetones. *Bull. Chem. Soc. Jpn.* **1985,** *58*, 3377-3378; (c) Onaka, S.; Furuta, H.; Takagi, S., (η-5-$CH_3C_5H_4$)Mn(CO)(dppfe): 2 Isomers Distinguished by their Characteristic CO Stretching Frequencies, which Differ only in Rotation of the Methylcyclopentadienyl Ligand - Evidence for an Intramolecular M-CO···H-C Interaction. *Angew. Chem. Int. Ed.* **1993,** *32*, 87-88; (d) Chowdhury, S. K.; Joshi, V. S.; Samuel, A. G.; Puranik, V. G.; Tavale, S. S.; Sarkar, A., Conformational Preferences in Molybdenum(II) π-Allyl Complexes - Role of CH/π Interaction. *Organometallics* **1994,** *13*, 4092-4096.

40. Tsuzuki, S.; Honda, K.; Uchimaru, T.; Mikami, M.; Tanabe, K., Origin of Attraction and Directionality of the π/π Interaction: Model Chemistry Calculations of Benzene Dimer Interaction. *J. Am. Chem. Soc.* **2002,** *124*, 104-112.

41. Ko, S.-B.; Park, H.-J.; Gong, S.; Wang, X. N.; Lu, Z.-H.; Wang, S. N., Blue Phosphorescent N-Heterocyclic Carbene Chelated Pt(II) Complexes with an α-Duryl-β-diketonato Ancillary Ligand. *Dalton Trans.* **2015,** *44*, 8433-8443.

42. (a) Tronnier, A.; Wagenblast, G.; Münster, I.; Strassner, T., Phosphorescent Platinum(II) Complexes with C^C* Cyclometalated NHC Dibenzofuranyl Ligands: Impact of Different Binding Modes on the Decay Time of the Excited State. *Chem. - Eur. J.* **2015,** *21*, 12881-12884; (b) Tronnier, A.; Metz, S.; Wagenblast, G.; Münster, I.; Strassner, T., Blue Phosphorescent Nitrile Containing C^C* Cyclometalated NHC Platinum(II) Complexes.

Dalton Trans. **2014,** *43*, 3297-3305; (c) Tenne, M.; Metz, S.; Wagenblast, G.; Munster, I.; Strassner, T., C^C* Cyclometalated Platinum(II) N-Heterocyclic Carbene Complexes with a Sterically Demanding β-Diketonato Ligand - Synthesis, Characterization and Photophysical Properties. *Dalton Trans.* **2015,** *44*, 8444-8455; (d) Tronnier, A.; Pöthig, A.; Herdtweck, E.; Strassner, T., C^C* Cyclometalated Platinum(II) NHC Complexes with β-Ketoimine Ligands. *Organometallics* **2014,** *33*, 898-908; (e) Soellner, J.; Tenne, M.; Wagenblast, G.; Strassner, T., Phosphorescent Platinum(II) Complexes with Mesoionic 1H-1,2,3-Triazolylidene Ligands. *Chem. - Eur. J.* **2016,** *22*, 9914-9918.

43. (a) Lai, S. W.; Lam, H. W.; Lu, W.; Cheung, K. K.; Che, C. M., Observation of Low-Energy Metal-Metal-to-Ligand Charge Transfer Absorption and Emission: Electronic Spectroscopy of Cyclometalated Platinum(II) Complexes with Isocyanide Ligands. *Organometallics* **2002,** *21*, 226-234; (b) Vicente, J.; Arcas, A.; Fernández-Hernández, J. M.; Aullón, G.; Bautista, D., Acetonyl Platinum(II) Complexes†. *Organometallics* **2007,** *26*, 6155-6169.

44. Forniés, J.; Fuertes, S.; Larraz, C.; Martín, A.; Sicilia, V.; Tsipis, A. C., Synthesis and Characterization of the Double Salts $[Pt(bzq)(CNR)_2][Pt(bzq)(CN)_2]$ with Significant Pt···Pt and π···π Interactions. Mechanistic Insights into the Ligand Exchange Process from Joint Experimental and DFT Study. *Organometallics* **2012,** *31*, 2729-2740.

45. Fuertes, S.; Chueca, A. J.; Arnal, L.; Martín, A.; Giovanella, U.; Botta, C.; Sicilia, V., Heteroleptic Cycloplatinated N-Heterocyclic Carbene Complexes: A New Approach to Highly Efficient Blue-Light Emitters. *Inorg. Chem.* **2017,** *56*, 4829-4839.

46. (a) Graber, S.; Doyle, K.; Neuburger, M.; Housecroft, C. E.; Constable, E. C.; Costa, R. D.; Orti, E.; Repetto, D.; Bolink, H. J., A Supramolecularly-Caged Ionic Iridium(III) Complex Yielding Bright and Very Stable Solid-State Light-Emitting Electrochemical Cells. *J. Am. Chem. Soc.* **2008,** *130*, 14944-14945; (b) Jude, H.; Rein, F. N.; White, P. S.; Dattelbaum, D. M.; Rocha, R. C., Synthesis, Structure, and Electronic Properties of a Dimer of $Ru(bpy)_2$ Doubly Bridged by Methoxide and Pyrazolate. *Inorg. Chem.* **2008,** *47*, 7695-7702.

47. Geary, W. J., Use of Conductivity Measurements in Organic Solvents for Characterisation of Coordination Compounds. *Coord. Chem. Rev.* **1971,** *7*, 81-122.

48. Schildknecht, C.; Ginev, G.; Kammoun, A.; Riedl, T.; Kowalsky, W.; Johannes, H.-H.; Lennartz, C.; Kahle, K.; Egen, M.; Geßner, T.; Bold, M.; Nord, S.; Erk, P., Novel Deep-Blue Emitting Phosphorescent Emitter. *Proc. SPIE 5937, Organic Light-Emitting Materials and Devices IX, 59370E (October 08, 2005); doi:10.1117/12.614331* **2005,** *5937*.

49. (a) Belío, Ú.; Fuertes, S.; Martín, A., Synthesis and Characterization of a "Pt_3Tl" Cluster Containing an Unprecedented Trigonal Environment for Thallium(I). *Inorg. Chem.* **2013,** *52*, 5627-5629; (b) Martín, A.; Belío, Ú.; Fuertes, S.; Sicilia, V., Luminescent Pt–Ag

Clusters Based on Neutral Benzoquinolate Cyclometalated Platinum Complexes. *Eur. J. Inorg. Chem.* **2013,** *2013*, 2231-2247; (c) Baya, M.; Belío, Ú.; Fernández, I.; Fuertes, S.; Martín, A., Unusual Metal–Metal Bonding in a Dinuclear Pt–Au Complex: Snapshot of a Transmetalation Process. *Angew. Chem. Int. Ed.* **2016,** *55*, 6978-6982; (d) Belio, U.; Fuertes, S.; Martin, A., Preparation of Pt-Tl clusters showing new geometries. X-ray, NMR and luminescence studies. *Dalton Trans.* **2014,** *43*, 10828-10843; (e) Fornies, J.; Sicilia, V.; Casas, J. M.; Martin, A.; Lopez, J. A.; Larraz, C.; Borja, P.; Ovejero, C., Pt-Ag Clusters and their Neutral Mononuclear Pt(II) Starting Complexes: Structural and Luminescence Studies. *Dalton Trans.* **2011,** *40*, 2898-2912.

50. Forniés, J.; Giménez, N.; Ibáñez, S.; Lalinde, E.; Martín, A.; Moreno, M. T., An Extended Chain and Trinuclear Complexes Based on Pt(II)−M (M = Tl(I), Pb(II)) Bonds: Contrasting Photophysical Behavior. *Inorg. Chem.* **2015,** *54*, 4351-4363 and references therein.

51. (a) Jamali, S.; Ghazfar, R.; Lalinde, E.; Jamshidi, Z.; Samouei, H.; Shahsavari, H. R.; Moreno, M. T.; Escudero-Adán, E.; Benet-Buchholz, J.; Milic, D., Cyclometalated heteronuclear Pt/Ag and Pt/Tl complexes: a structural and photophysical study. *Dalton Trans.* **2014,** *43*, 1105; (b) Forniés, J.; García, A.; Lalinde, E.; Moreno, M. T., Luminescent One- And Two-Dimensional Extended Structures and a Loosely Associated Dimer Based on Platinum(II)−Thallium(I) Backbones. *Inorg. Chem.* **2008,** *47*, 3651-3660; (c) Catalano, V. J.; Bennett, B. L.; Muratidis, S.; Noll, B. C., Unsupported Pt(0)−Tl(I) Bonds in the Simple $[Pt(PPh_2Py)_3Tl]+$ Complexes. *J. Am. Chem. Soc.* **2001,** *123*, 173-174.

52. Chen, W.; Liu, F.; Xu, D.; Matsumoto, K.; Kishi, S.; Kato, M., Luminescent Amidate-Bridged One-Dimensional Platinum(II)-Thallium(I) Coordination Polymers Assembled via Metallophilic Attraction. *Inorg. Chem.* **2006,** *45*, 5552-5560.

53. (a) Yam, V. W. W.; Wong, K. M. C.; Zhu, N., Solvent-Induced Aggregation through Metal···Metal/π···π Interactions: Large Solvatochromism of Luminescent Organoplatinum(II) Terpyridyl Complexes. *J. Am. Chem. Soc.* **2002,** *124*, 6506-6507; (b) Kato, M.; Kosuge, C.; Morii, K.; Ahn, J. S.; Kitagawa, H.; Mitani, T.; Matsushita, M.; Kato, T.; Yano, S.; Kimura, M., Luminescence Properties and Crystal Structures of Dicyano(diimine)platinum(II) Complexes Controlled by Pt···Pt and π−π Interactions. *Inorg. Chem.* **1999,** *38*, 1638-1641; (c) Buss, C. E.; Mann, K. R., Synthesis and Characterization of $Pt(CN\text{-}p\text{-}(C_2H_5)C_6H_4)_2(CN)_2$, a Crystalline Vapoluminescent Compound That Detects Vapor-Phase Aromatic Hydrocarbons. *J. Am. Chem. Soc.* **2002,** *124*, 1031−1039; (d) Dylla, A. G.; Janzen, D. E.; Pomije, M. K.; Mann, K. R., A Comparison of Isomers: trans- and cis-Dicyanobis(para-ethylisocyanobenzene)Platinum. *Organometallics* **2007,** *26*, 6243-6247; (e) Sun, Y.; Ye, K.; Zhang, H.; Zhang, J.; Zhao, L.; Li, B.; Yang, G.; Yang, B.; Wang, Y.; Lai, S. W.;

Che, C. M., Luminescent One-Dimensional Nanoscale Materials with $Pt^{II}\cdots Pt^{II}$ Interactions. *Angew. Chem. Int. Ed.* **2006,** *45*, 5610-5613; (f) Holland, L.; Shen, W.-Z.; von Grebe, P.; Sanz Miguel, P. J.; Pichierri, F.; Springer, A.; Schalley, C. A.; Lippert, B., A Neutral Pt_3 Stack Unsupported by any Bridging Ligand. *Dalton Trans.* **2011,** *40*, 5159-5161.

54. Bondi, A., van der Waals Volumes and Radii. *J. Phys. Chem.* **1964,** *68*, 441-451.

55. (a) Connick, W. B.; Marsh, R. E.; Schaefer, W. P.; Gray, H. B., Linear-Chain Structures of Platinum(II) Diimine Complexes. *Inorg. Chem.* **1997,** *36*, 913-922; (b) Charmant, J. P. H.; Forniés, J.; Gómez, J.; Lalinde, E.; Merino, R. I.; Moreno, M. T.; Orpen, A. G., Unprecedented Pt–Pt Bonded Trimer $\{[Pt_2Cu_4(C{:}CPh)_8]\}_3$ Showing Unusual Near-Infrared Luminescence. *Organometallics* **1999,** *18*, 3353-3358; (c) Aullón, G.; Alvarez, S., Chain Conformation and Metal⋯Metal Contacts in Dimers and Stacks of d^8-ML_4 Complexes: Electronic Effects. *Chem. - Eur. J.* **2006,** *3*, 655-664.

56. Sicilia, V.; Forniés, J.; Fuertes, S.; Martín, A., New Dicyano Cyclometalated Compounds Containing Pd(II)–Tl(I) Bonds as Building Blocks in 2D Extended Structures: Synthesis, Structure, and Luminescence Studies. *Inorg. Chem.* **2012,** *51*, 10581-10589.

57. Berenguer, J. R.; Lalinde, E.; Martín, A.; Moreno, M. T.; Sánchez, S.; Shahsavari, H. R., Binuclear Complexes and Extended Chains Featuring Pt^{II}–Tl^{I} Bonds: Influence of the Pyridine-2-Thiolate and Cyclometalated Ligands on the Self-Assembly and Luminescent Behavior. *Inorg. Chem.* **2016,** *55*, 7866-7878.

58. Falvello, L. R.; Forniés, J.; Garde, R.; García, A.; Lalinde, E.; Moreno, M. T.; Steiner, A.; Tomás, M.; Usón, I., Tri-$[Pt_2Tl]^{3-}$ and Polynuclear Chain $[Pt–Tl]_\infty^-$ Complexes Based on Nonbridged Pt^{II}–Tl^{I} Bonds: Solid State and Frozen Solution Photophysical Properties. *Inorg. Chem.* **2006,** *45*, 2543-2552.

59. Nagle, J. K.; Balch, A. L.; Olmstead, M. M., $Tl_2Pt(CN)_4$: A Non-Columnar, Luminescent Form of $Pt(CN)_4^{2-}$ Containing Platinum-Thallium Bonds. *J. Am. Chem. Soc.* **1988,** *110*, 319-321.

60. (a) Lu, W.; Mi, B.-X.; Chan, M. C. W.; Hui, Z.; Che, C.-M.; Zhu, N.; Lee, S.-T., Light-Emitting Tridentate Cyclometalated Platinum(II) Complexes Containing σ-Alkynyl Auxiliaries: Tuning of Photo- and Electrophosphorescence. *J. Am. Chem. Soc.* **2004,** *126*, 4958-4971; (b) Mydlak, M.; Mauro, M.; Polo, F.; Felicetti, M.; Leonhardt, J.; Diener, G.; De Cola, L.; Strassert, C. A., Controlling Aggregation in Highly Emissive Pt(II) Complexes Bearing Tridentate Dianionic N^N^N Ligands. Synthesis, Photophysics, and Electroluminescence. *Chem. Mater.* **2011,** *23*, 3659-3667.

61. (a) Cebrián, C.; Mauro, M.; Kourkoulos, D.; Mercandelli, P.; Hertel, D.; Meerholz, K.; Strassert, C. A.; De Cola, L., Luminescent Neutral Platinum Complexes Bearing an Asymmetric N^N^N Ligand for High-Performance Solution-Processed OLEDs. *Adv. Mater.*

2013, *25*, 437-442; (b) Li, H.; Li, J.; Ding, J.; Yuan, W.; Zhang, Z.; Zou, L.; Wang, X.; Zhan, H.; Xie, Z.; Cheng, Y.; Wang, L., Design, Synthesis, and Optoelectronic Properties of Dendrimeric Pt(II) Complexes and Their Ability to Inhibit Intermolecular Interaction. *Inorg. Chem.* **2014,** *53*, 810-821; (c) Mroz, W.; Botta, C.; Giovanella, U.; Rossi, E.; Colombo, A.; Dragonetti, C.; Roberto, D.; Ugo, R.; Valore, A.; Williams, J. A. G., Cyclometallated Platinum(II) Complexes of 1,3-Di(2-pyridyl)benzenes for Solution-Processable WOLEDs Exploiting Monomer and Excimer Phosphorescence. *J. Mater. Chem.* **2011,** *21*, 8653-8661; (d) Li, H.; Ding, J.; Xie, Z.; Cheng, Y.; Wang, L., Synthesis, Characterization and Electrophosphorescent Properties of Mononuclear Platinum(II) Complexes Based on 2-Phenylbenzoimidazole Derivatives. *J. Organomet. Chem.* **2009,** *694*, 2777-2785.

62. (a) Kong, F. K.-W.; Tang, M.-C.; Wong, Y.-C.; Chan, M.-Y.; Yam, V. W.-W., Design Strategy for High-Performance Dendritic Carbazole-Containing Alkynylplatinum(II) Complexes and Their Application in Solution-Processable Organic Light-Emitting Devices. *J. Am. Chem. Soc.* **2016,** *138*, 6281-6291; (b) Li, H.; Yuan, W.; Wang, X.; Zhan, H.; Xie, Z.; Cheng, Y., Enhancement of Luminescence Performance from the Alteration of Stacking Patterns of Pt(II) Dendrimers. *J. Mater. Chem. C* **2015,** *3*, 2744-2750.

63. Hsu, C.-W.; Ly, K. T.; Lee, W.-K.; Wu, C.-C.; Wu, L.-C.; Lee, J.-J.; Lin, T.-C.; Liu, S.-H.; Chou, P.-T.; Lee, G.-H.; Chi, Y., Triboluminescence and Metal Phosphor for Organic Light-Emitting Diodes: Functional Pt(II) Complexes with Both 2-Pyridylimidazol-2-ylidene and Bipyrazolate Chelates. *ACS App. Mater. Interfaces* **2016,** *8*, 33888-33898.

64. Giovanella, U.; Betti, P.; Botta, C.; Destri, S.; Moreau, J.; Pasini, M.; Porzio, W.; Vercelli, B.; Bolognesi, A., All-Conjugated Diblock Copolymer Approach To Improve Single Layer Green Electroluminescent Devices. *Chem. Mater.* **2011,** *23*, 810-816.

65. Murphy, T. W., Maximum Spectral Luminous Efficacy of White Light. *J. Appl. Phys.* **2012,** *111*, 104909.

66. Lai, C. F.; Li, J. S.; Shen, C. W., High-Efficiency Robust Free-Standing Composited Phosphor Films with 2D and 3D Nanostructures for High-Power Remote White LEDs. *ACS Appl. Mater. Interfaces* **2017,** *9*, 4851-4859.

67. Zabiliute, A.; Vaicekauskas, R.; Vitta, P.; Zukauskas, A., Phosphor-Converted LEDs with Low Circadian Action for Outdoor Lighting. *Opt. Lett.* **2014,** *39*, 563-566.

68. Giovanella, U.; Pasini, M.; Freund, C.; Botta, C.; Porzio, W.; Destri, S., Highly Efficient Color-Tunable OLED Based on Poly(9,9-dioctylfluorene) Doped with a Novel Europium Complex. *J. Phys. Chem. C* **2009,** *113*, 2290-2295.

69. Das, D.; Gopikrishna, P.; Narasimhan, R.; Singh, A.; Dey, A.; Iyer, P. K., White Polymer Light Emitting Diodes Based on PVK: The Effect of the Electron Injection Barrier

on Transport Properties, Electroluminescence and Controlling the Electroplex Formation. *Phys. Chem. Chem. Phys.* **2016,** *18*, 33077-33084.

70. (a) Hayashi, K.; Nakanotani, H.; Inoue, M.; Yoshida, K.; Mikhnenko, O.; Nguyen, T.-Q.; Adachi, C., Suppression of Roll-Off Characteristics of Organic Light-Emitting Diodes by Narrowing Current Injection/Transport Area to 50 nm. *Appl. Phys. Lett.* **2015,** *106*, 093301; (b) Giebink, N. C.; Forrest, S. R., Quantum Efficiency Roll-Off at High Brightness in Fluorescent and Phosphorescent Organic Light Emitting Diodes. *Phys. Rev. B* **2008,** *77*, 235215.

71. Gong, X.; Robinson, M. R.; Ostrowski, J. C.; Moses, D.; Bazan, G. C.; Heeger, A. J., High-Efficiency Polymer-Based Electrophosphorescent Devices. *Adv. Mater.* **2002,** *14*, 581-585.

Appendix.

Published articles

Inorganic Chemistry

Article

pubs.acs.org/IC

Exploring the Transphobia Effect on Heteroleptic NHC Cycloplatinated Complexes

Sara Fuertes,[†] Andrés J. Chueca,[†] and Violeta Sicilia*[,‡]

[†]Departamento de Química Inorgánica, Facultad de Ciencias, Instituto de Síntesis Química y Catálisis Homogénea (ISQCH), CSIC-Universidad de Zaragoza, Pedro Cerbuna 12, 50009 Zaragoza, Spain

[‡]Departamento de Química Inorgánica, Escuela de Ingeniería y Arquitectura de Zaragoza, Instituto de Síntesis Química y Catálisis Homogénea (ISQCH), CSIC-Universidad de Zaragoza, Campus Río Ebro, Edificio Torres Quevedo, 50018 Zaragoza, Spain

Supporting Information

ABSTRACT: The synthesis of 1-(4-cyanophenyl)-1*H*-imidazol (**1**) has been carried out by an improved method. Then its corresponding imidazolium iodide salt, **2**, has been used to prepare the N-heterocyclic carbene (NHC) cycloplatinated compound $[\{Pt(\mu\text{-}Cl)(C\text{^}C^*)\}_2]$ (**4**) (HC^C*-κC* = 1-(4-cyanophenyl)-3-methyl-1*H*-imidazol-2-ylidene) following a step-by-step protocol. The intermediate complex $[PtCl(\eta^3\text{-}2\text{-}Me\text{-}C_3H_4)(HC\text{^}C^*\text{-}\kappa C^*)]$ (**3**) has also been isolated and characterized. Using **4** as precursor, several heteroleptic complexes of stoicheometry [PtCl(C^C*)L] (L = PPh_3 (**5**), pyridine (py, **6**), 2,6-dimethylphenyl isocyanide (CNXyl, **7**), and 2-mercapto-1-methylimidazole (MMI, **8**)) and $[Pt(C\text{^}C^*)LL']PF_6$ (L = PPh_3, L′ = py (**9**), CNXyl (**10**), and MMI (**11**)) have been synthesized. Complexes **6**−**8** were obtained as a mixture of *cis*- and *trans*-(C*,L) isomers, while *trans*-(C*,L) isomer was the only one observed for complexes **5** and **9**−**11**. Their geometries have been discussed in terms of the degree of transphobia (T) of pairs of trans ligands and supported by theoretical calculations. The trans influence of the two σ Pt−C bonds present in these molecules, $Pt\text{−}C_{Ar}$ and $Pt\text{−}C^*_{(NHC)}$, has been compared from the J_{Pt-P} values observed in the new complex $[Pt(C\text{^}C^*)(dppe)]PF_6$ (dppe = 1, 2-bis(diphenylphosphino)-ethane, **12**).

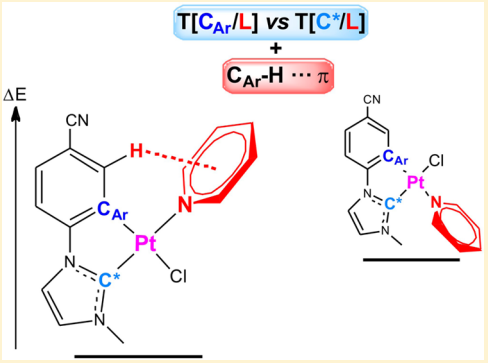

INTRODUCTION

The chemistry of platinum(II) complexes has attracted much interest in the past decade due to their phosphorescence properties and potential use as dopants in LEDS,[1] chemical sensors,[2] or biolabeling agents,[2b,3] with particular consideration given to C^N-cyclometalated derivatives.[1b,4] The C^C*-cyclometalated N-heterocyclic carbenes (NHC) may surpass the high ligand field splitting capacity of the conventional C^N-cyclometalated ligands, since they present two C−σ bonds. This implies an even greater heightening of the d−d energy levels on the metal center, enlarging the energy gap with the emissive excited states, avoiding the thermal quenching and improving the quantum yields.[5] Furthermore, as a consequence of the strong metal−ligand binding, metal complexes of C^C*-cyclometalated NHCs are very robust and stable which may provide long-term functional materials.

NHCs have been widely used in organometallic chemistry and particularly in the targeted fields of transition-metal catalysis,[6] liquid crystals,[7] biomedicine,[8] and luminescent materials.[5,8d,9] In particular, platinum(II) compounds containing C^C*-cyclometalated NHCs ligands have received much attention in the past decade.[9k,10] Most of them are photoluminescent β-diketonates or β-ketoiminates derivatives prepared straightforward in one-pot reactions. Variations regarding substituents in the NHC or the β-diketonate groups and also regarding the size of the π system have been studied to tune their photophysical properties.[10a−l] However, these preparative methods are slightly limited in terms of reactivity and ligand exchange reactions. Normally, ancillary ligands account for secondary roles within the molecular complex, but they could be determinant when modulating their emissive properties[11] or tuning their catalytic activity and selectivity.[10m,n,12]

In this context, as part of our previous work, we prepared and studied the photophysical properties of many heteroleptic complexes of Pt(II) with the 7,8-benzoquinolinate and different monodentate auxiliary ligands.[11] Now, we have conducted our ongoing research to new platinum(II) complexes with C^C*-cyclometalated NHCs. Generic compounds, such as $[\{Pt(\mu\text{-}Cl)(C\text{^}C^*)\}_2]$, are expected to be useful starting materials for complexes containing the "Pt(C^C*)" moiety, because different kinds of ancillary ligands can be coordinated in the vacant sites resulting from chlorine-bridge cleavage or chlorine-atoms elimination. We recently reported the synthesis of $[\{Pt(\mu\text{-}Cl)(C\text{^}C^*)\}_2]$ (HC^C* = 3-methyl-1-(naphthalen-2-yl)-1*H*-imidazol-2-ylidene).[13] Thus, the first goal of this work, the synthesis of the generic precursor $[\{Pt(\mu\text{-}Cl)(C\text{^}C^*)\}_2]$ (**4**) (HC^C*-κC* = 1-(4-cyanophenyl)-3-methyl-1*H*-imidazol-2-

Received: July 23, 2015
Published: October 8, 2015

DOI: 10.1021/acs.inorgchem.5b01655
Inorg. Chem. 2015, 54, 9885−9895

ylidene) following the same strategy, was achieved. Therefore, the use of [{Pt(μ-Cl)(η^3-2-Me-C_3H_4)}$_2$] to accomplish the cyclometalation of the NHCs through the intermediate carbene complex [PtCl(η^3-2-Me-C_3H_4) (HC^C*-κC*)] (**3**) endorses the generality and viability of this step-by-step synthetic protocol for [{Pt(μ-Cl)(C^C*)}$_2$]

Then we explored the use of **4** as a precursor for the preparation of new heteroleptic complexes such as [PtCl-(C^C*)L] (L = PPh_3 (**5**), py (**6**), CNXyl (**7**), and 2-mercapto-1-methylimidazole (MMI, **8**)) and [Pt(C^C*)LL′]$^+$ (L = PPh_3; L′ = py (**9**), CNXyl (**10**), and MMI (**11**)). Some of them were obtained as a mixture of two isomers, *cis*- and *trans*-(C*,L), while others were obtained selectively as the *trans*-(C*,L) one. The geometries observed for them have been discussed in terms of the degree of transphobia (T) of pairs of trans ligands,[14] which has been related with the trans influence of the two σ Pt−C bonds present in the molecule, Pt−C_{Ar} and Pt−$C^*_{(NHC)}$. The trans influence of σ C_{Ar} and σ C* has been evaluated from the $J_{Pt,P}$ values observed in the new complex [Pt(C^C*) (dppe)]$^+$ (**12**).

EXPERIMENTAL SECTION

General Comments. Information describing materials, instrumental methods used for characterization and spectroscopic studies, DFT computational details, and X-ray structures together with the characterization data of **1**−**12** are contained in the Supporting Information. All chemicals were used as supplied, and [{Pt(μ-Cl)(η^3-2-Me-C_3H_4)}$_2$][15] was prepared following the literature procedure.

*1-(4-Cyanophenyl)-1H-imidazole (**1**).* Slight modifications of previous synthetic methods were employed.[16] To a solution of 4-bromobenzonitrile (800.0 mg, 4.35 mmol) in degassed dimethyl sulfoxide (12 mL), imidazole (592.5 mg, 8.70 mmol), K_2CO_3 (1202.9 mg, 8.70 mmol), and CuI (165.8 mg, 8.70 mmol) were added in the presence of 4 Å molecular sieves (500.0 mg). After 70 h at 110 °C under an argon atmosphere the crude was cooled down to rt, washed with 100 mL of ethyl acetate, and then filtered through Celite. The solution was treated with H_2O (2 × 20 mL) and brine (2 × 20 mL). The organic layer was dried using anhydrous $MgSO_4$. Evaporation under reduced pressure yielded a white solid which was washed with hexane to give **1** as a white-off powder. Yield: 609.5 mg, 83%. ^{1}H NMR (400 MHz, DMSO-d_6): δ = 8.46 (dd, $^3J_{H,H}$ = 1.3, $^3J_{H,H}$ = 0.9, 1H, H_1), 8.09 (d, $^3J_{H6,H7}$ = 8.8, 2H, H_7), 7.99 (d, $^3J_{H6,H7}$ = 8.8, 2H, H_6), 7.98 (m, 1H, Im), 7.16 (dd, $^3J_{H,H}$ = 1.3, $^3J_{H,H}$ = 0.9, 1H, Im). ^{13}C{^{1}H} NMR (101 MHz, DMSO-d_6): δ = 140.1 (s, C_5), 135.7 (s, C_1), 134.1 (s, 2C, C_7), 130.5 (s, 1C, Im), 120.4 (s, 2C, C_6), 118.3 (s, CN), 117.6 (s, 1C, Im), 109.0 (s, C_8). IR (ATR, cm^{-1}): ν = 2224 (m, CN).

*1-(4-Cyanophenyl)-3-methyl-1H-imidazolium Iodide (**2**).* Methyl iodide (0.3 mL, 4.83 mmol) was added to a solution of **1** (544.5 mg, 3.22 mmol) in dried THF (10 mL) under Ar atmosphere. The mixture was refluxed for 48 h, and after cooling, the white precipitate was filtered and washed with THF (5 mL) and diethyl ether (5 mL) and dried under vacuum to give **2** as a pure solid. Yield: 967.9 mg, 97%. Anal. Calcd for $C_{11}H_{10}IN_3$: C, 42.46; H, 3.24; N, 13.51. Found: C, 42.03; H, 3.33; N, 13.48. ^{1}H NMR (400 MHz, DMSO-d_6): δ = 9.91 (s, br, 1H, H_1), 8.39 (dd, $^3J_{H2,H3}$ = 1.9, $^3J_{H2,H1}$ = 1.8, 1H, H_2), 8.21 (d, $^3J_{H6,H7}$ = 8.8, 2H, H_7), 8.02 (d, 2H, H_6), 8.00 (m, 1H, H_3), 3.96 (s, 3H, H_4). ^{13}C{^{1}H} NMR plus HMBC and HSQC (101 MHz, DMSO-d_6): δ = 137.9 (s, C_5), 136.5 (s, C_1), 134.4 (s, 2C, C_7), 124.6 (s, C_3), 122.5 (s, 2C, C_6), 120.7 (s, C_2), 117.7 (s, CN), 112.2 (s, C_8), 36.3 (s, C_4). IR (ATR, cm^{-1}): ν = 2235 (m, CN). MS (MALDI+): *m*/*z* 184.1 (HC∧C*H)$^+$.

[PtCl(η^3-2-Me-C_3H_4)(HC^C-κC*)] (**3**) (HC^C* = 1-(4-Cyanophenyl)-3-methyl-1H-imidazol-2-ylidene).* To a suspension of **2** (893.7 mg, 2.87 mmol) in anhydrous dichloromethane (30 mL), Ag_2O (332.8 mg, 1.44 mmol) was added in the absence of light under an argon atmosphere. After 3 h of stirring at rt, [{Pt(η^3-2-Me-C_3H_4)(μ-Cl)}$_2$] (779.1 mg, 1.36 mmol) was added and the mixture was allowed to react for 3 h to give a yellow precipitate (AgI), which was separated by filtration through Celite under Ar. The resulting solution was evaporated to dryness and treated with *n*-hexane (3 × 15 mL) to afford **3** as a pale-yellow solid. Yield: 1.1222 g, 83%. Anal. Calcd for $C_{15}H_{16}ClN_3Pt$: C, 38.42; H, 3.43; N, 8.96. Found: C, 38.23; H, 3.35; N, 8.52. ^{1}H NMR (400 MHz, methylene chloride-d_2): δ = 7.95 (d, $^3J_{H,H}$ = 8.8, 2H, H_7), 7.74 (d, $^3J_{H,H}$ = 8.8, 2H, H_6), 7.26 (d, $^3J_{H2,H3}$ = 2.1, $^4J_{H,Pt}$ = 13.4, 1H, H_2), 7.15 (d, $^4J_{H,Pt}$ = 10.6, 1H, H_3), 3.91 (s, 3H, Me (NHC)), 3.64 (m, $1H_{syn}$, η^3-2-Me-C_3H_4), 2.63 (m, $^2J_{H,Pt}$ = 28.3, $1H_{syn}$, η^3-2-Me-C_3H_4), 2.37 (m, $^2J_{H,Pt}$ = 34.1, $1H_{anti}$, η^3-2-Me-C_3H_4), 1.74 (s, $^3J_{H,Pt}$ = 64.7, 3H, Me, η^3-2-Me-C_3H_4), 1.44 (m, $1H_{anti}$, η^3-2-Me-C_3H_4). ^{13}C{^{1}H} NMR plus HMBC and HSQC (101 MHz, methylene chloride-d_2): δ = 177.4 (s, C_1), 144.1 (s, C_5), 133.2 (s, 2C, C_6), 126.2 (s, 2C, C_7), 123.6 (s, $^3J_{C,Pt}$ = 41.3, C_3), 120.7 (s, $^3J_{C,Pt}$ = 42.4, C_2), 118.6 (s, CN), 118.4 (s, $C^{2\prime}$, η^3-2-Me-C_3H_4), 112.1 (s, C_8), 58.1 (s, $^1J_{C,Pt}$ = 77.6, $C^{1\prime}$, η^3-2-Me-C_3H_4), 38.3 (s, C_4 (Me), NHC)), 37.1 (s, $C^{3\prime}$, η^3-2-Me-C_3H_4), 23.4 (s, $^2J_{C,Pt}$ = 40.1, $C^{4\prime}$ (Me), η^3-2-Me-C_3H_4). ^{195}Pt{^{1}H} NMR (85.6 MHz, methylene chloride-d_2): δ = −4460. IR (ATR, cm^{-1}): ν = 285 (s, Pt−Cl), 2228 (w, CN).

[{Pt(μ-Cl)(C^C)}$_2$] (**4**).* Compound **3** (500.0 mg, 1.07 mmol) was refluxed in 2-methoxyethanol (15 mL) for 3 h, and then it was cooled down to rt. The resulting solid was filtered and washed with dichloromethane (10 mL) and diethyl ether (15 mL). Then it was treated with activated carbon in hot acetonitrile (3 × 40 mL), and the suspension was filtered through Celite. The resulting solution was evaporated to dryness, and the residue was washed with hexane to give a yellow solid, **4**. Yield: 357.6 mg, 81%. Anal. Calcd for $C_{22}H_{16}Cl_2N_6Pt_2$: C, 32.01; H, 1.95; N, 10.18. Found: C, 31.63; H, 2.33; N, 10.16. ^{1}H NMR (400 MHz, DMSO-d_6): δ = 8.72 (s, br, $^3J_{H7,Pt}$ = 60, 1H, H_7), 8.14 (d, $^3J_{H2,H3}$ = 1.7, 1H, H_2), 7.63 (dd, $^3J_{H9,H10}$ = 8.0, $^4J_{H9,H7}$ = 1.5, 1H, H_9), 7.57 (d, 1H, H_{10}), 7.53 (d, 1H, H_3), 4.14 (s, 3H, H_4). ^{13}C{^{1}H} NMR plus HMBC and HSQC (101 MHz, DMSO-d_6): δ = 156.0 (s, C_1), 149.8 (s, C_5), 137.0 (s, C_7), 129.3 (s, C_9), 127.9 (s, C_6), 125.5 (s, C_3), 119.6 (s, CN), 115.7 (s, C_2), 112.3 (s, C_{10}), 106.9 (s, C_8), 37.6 (s, C_4). IR (ATR, cm^{-1}): ν = 266 (s, Pt−Cl), 2250 (w, CN), 2215 (w, CN).

trans-(C,P)[Pt(Cl)(C^C*)(PPh_3)] (**5**).* PPh_3 (128.1 mg, 0.48 mmol) was added to a suspension of **4** (177.8 mg, 0.22 mmol) in dichloromethane (30 mL) at −8 °C (ice/brine bath). After 1 h of reaction, the solvent was removed under reduced pressure. The residue was treated with MeOH (5 mL), filtered, and washed with MeOH (3 mL) to give **5** as a pale yellow solid. Yield: 193.5 mg, 67%. Anal. Calcd for $C_{29}H_{23}ClN_3PPt$: C, 51.60; H, 3.43; N, 6.22. Found: C, 51.26; H, 3.49; N, 6.18. ^{1}H NMR (400 MHz, methylene chloride-d_2): δ = 7.72 (m, 6H, H*o* (PPh_3)), 7.52−7.35 (m, 10H, H*m*, H*p* (PPh_3) and H_2), 7.24 (dd, $^3J_{H9,H10}$ = 8.0, $^4J_{H9,H7}$ = 1.6, 1H, H_9), 7.05 (d, $^4J_{H10,Pt}$ = 14.2, 1H, H_{10}), 6.99 (m, 1H, H_3), 6.88 (m, $^3J_{H7,Pt}$ = 64.0, 1H, H_7), 4.29 (s, 3H, H_4). ^{13}C{^{1}H} NMR plus HMBC and HSQC (101 MHz, methylene chloride-d_2): δ = 170.1 (s, C_1), 150.5 (s, C_5), 141.0 (d, $^3J_{C7,P}$ = 8.7, $^2J_{C7,Pt}$ = 57.0, C_7), 135.5 (d, $^2J_{C,P}$ = 11.3, $^3J_{C,Pt}$ = 20.7, 6C, C_o (PPh_3)), 130.7 (s, 3C, C_p (PPh_3)), 130.1 (d, $^1J_{C,P}$ = 53.6, 3C, C_i (PPh_3)), 128.5 (s, C_6), 128.1 (d, $^3J_{C,P}$ = 10.6, 6C, C_m (PPh_3)), 127.8 (s, C_9), 124.3 (d, $^4J_{C,P}$ = 6.1, $^4J_{C3,Pt}$ = 26.0, C_3), 118.8 (s, CN), 113.9 (s, $^4J_{C2,Pt}$ = 40.1, C_2), 111.0 (s, $^3J_{C10,Pt}$ = 32.5, C_{10}), 108.0 (s, C_8), 38.6 (s, C_4). ^{31}P{^{1}H} NMR (162 MHz, methylene chloride-d_2): δ = 28.6 (s, $^1J_{P,Pt}$ = 2868.0). ^{195}Pt{^{1}H} NMR (85.6 MHz, methylene chloride-d_2): δ = −4227.0 (d). IR (ATR, cm^{-1}): ν = 279 (m, Pt−Cl), 2218 (w, CN). MS (MALDI+): *m*/*z* 639.1 [Pt(C^C*) (PPh_3)]$^+$.

cis/trans-(C,N) [Pt(Cl)(C^C*)(py)] (**6**).* Pyridine (Py) (24.8 μL, 0.30 mmol) was added to a suspension of **4** (115.2 mg, 0.14 mmol) in dichloromethane (30 mL) at −8 °C (ice/brine bath). After 2 h of stirring, the solvent was removed under reduced pressure. The residue was treated with MeOH (5 mL), filtered, and washed with MeOH (3 mL) to give **6-*t*** (92%)/**6-*c*** (8%) as a yellow solid. Yield: 99.9 mg, 73%. Anal. Calcd for $C_{16}H_{13}ClN_4Pt$: C, 39.07; H, 2.66; N, 11.39. Found: C, 38.67; H, 2.73; N, 11.22. ^{1}H NMR data for **6-*t*** (400 MHz, methylene chloride-d_2): δ = 8.81 (dd, $^3J_{H,H}$ = 6.4, $^4J_{H,H}$ = 1.6, $^3J_{H,Pt}$ = 28.0, 2H, H*o* (py)), 7.97 (tt, $^3J_{H,H}$ = 7.7, $^4J_{H,H}$ = 1.6, 1H, H*p* (py)), 7.56 (m, 2H, H*m* (py)), 7.38 (dd, $^3J_{H9,H10}$ = 8.0, $^4J_{H9,H7}$ = 1.7, 1H, H_9), 7.33 (d, $^3J_{H2,H3}$ =

DOI: 10.1021/acs.inorgchem.5b01655
Inorg. Chem. 2015, 54, 9885−9895

2.1, 1H, H_2), 7.06 (d, $^4J_{H10,Pt}$ = 16.8, 1H, H_{10}), 6.94 (d, $^4J_{H3,Pt}$ = 9.1, 1H, H_3), 6.69 (d, $^3J_{H7,Pt}$ = 61.8, 1H, H_7), 4.24 (s, 3H, H_4). ^{1}H NMR data for **6-*c***: δ = 8.91 (dd, $^3J_{H,H}$ = 6.3, $^4J_{H,H}$ = 1.6, $^3J_{H,Pt}$ = 20.7, 2H, H*o* (py)), 8.41 (d, $^3J_{H7,H9}$ = 1.6, $^3J_{H7,Pt}$ = 55.1, 1H, H_7), 7.91 (tt, $^3J_{H,H}$ = 7.8, $^4J_{H,H}$ = 1.6, 1H, H*p* (py)), 3.06 (s, 3H, H_4). ^{13}C{^{1}H} NMR plus HMBC and HSQC for **6-*t*** (101 MHz, methylene chloride-d_2): δ = 152.7 (s, C_1), 152.0 (s, $^2J_{C,Pt}$ = 12.2, 2C, C_o (py)), 150.3 (s, C_5), 138.5 (s, C_p (py)), 135.2 (s, $^2J_{C7,Pt}$ = 37.8, C_7), 131.3 (s, C_6), 128.3 (s, C_9), 126.1 (s, $^3J_{C,Pt}$ = 31.2, 2C, C_m (py)), 123.1 (s, $^3J_{C3,Pt}$ = 38.4, C_3), 119.4 (s, CN), 114.4 (s, $^3J_{C2,Pt}$ = 47.2, C_2), 110.7 (s, $^3J_{C10,Pt}$ = 36.1, C_{10}), 108.1 (s, C_8), 37.6 (s, C_4). ^{195}Pt{^{1}H} NMR (85.6 MHz, methylene chloride-d_2): δ = −3731.9 (s, br, **6-*t***); − 3775.4 (s, **6-*c***). IR (ATR, cm^{-1}): ν = 271 (m, Pt−Cl), 2220 (w, CN). MS (MALDI+): *m*/*z* 456.0 [Pt(C^C*) (py)]$^+$.

cis/trans-(C,C) [Pt(Cl)(C^C*)(CNXyl)]* (**7**). 2,6-Dimethylphenyl isocyanide (CNXyl) (35.7 mg, 0.27 mmol) was added to a suspension of **4** (100.0 mg, 0.12 mmol) in dichloromethane (30 mL) at −8 °C (ice/brine bath). After 2.5 h of stirring, the solvent was removed under reduced pressure. The residue was treated with MeOH (0 °C, 5 mL), filtered, and washed with MeOH (3 mL) to give **7-*t*** (86%)/**7-*c*** (14%) as a yellow solid. Yield: 61.8 mg, 47%. Anal. Calcd for $C_{20}H_{17}ClN_4Pt$: C, 44.16; H, 3.15; N, 10.30. Found: C, 44.09; H, 3.02; N, 9.92. ^{1}H NMR data for **7-*t*** (400 MHz, methylene chloride-d_2): δ = 7.97 (d, $^4J_{H9,H7}$ = 1.7, $^3J_{H7,Pt}$ = 77.3, 1H, H_7), 7.47 (dd, $^3J_{H9,H10}$ = 8.0, 1H, H_9), 7.36 (d, $^3J_{H2,H3}$ = 2.0, $^4J_{H2,Pt}$ = 5.3, 1H, H_2), 7.33 (t, $^3J_{Hp,Hm}$ = 7.7, 1H, H_p (Xyl)), 7.21 (d, 2H, H_m (Xyl)), 7.14 (d, $^4J_{H10,Pt}$ = 15.4, 1H, H_{10}), 6.97 (d, $^4J_{H3,Pt}$ = 7.9, 1H, H_3), 4.28 (s, 3H, H_4), 2.51 (s, 6H, Me (Xyl)). ^{1}H NMR data for **7-*c***: δ = 8.45 (d, $^4J_{H7,H10}$ = 1.7, $^3J_{H,Pt}$ = 47.2, 1H, H_7), 7.43 (dd, $^3J_{H9,H10}$ = 8.0, 1H, H_9), 7.09 (d, 1H, H_{10}), 7.00 (d, $^4J_{H3,Pt}$ = 12.3, 1H, H_3), 3.92 (s, 3H, H_4), 2.45 (s, 6H, Me (Xyl)). ^{13}C{^{1}H} NMR plus HMBC and HSQC for **7-*t*** (101 MHz, methylene chloride-d_2): δ = 167.7 (s, C_1), 149.5 (s, C_5), 140.8 (s, $^2J_{C7,Pt}$ = 72.4, C_7), 135.8 (s, 2C, C_o (Xyl)), 129.7 (s, C_p (Xyl)), 128.7 (s, C_9), 128.1 (s, 2C, C_m (Xyl)), 123.9 (s, $^3J_{C3,Pt}$ = 30.9, C_3), 119.0 (s, CN), 114.8 (s, C_2), 111.6 (s, $^3J_{C10,Pt}$ = 32.9, C_{10}), 109.5 (s, C_8), 37.3 (s, C_4), 18.7 (s, 2C, Me (Xyl)). ^{195}Pt{^{1}H} NMR (85.6 MHz, methylene chloride-d_2): δ = −4042.7 (t, $^2J_{Pt,N}$ = 89.7 Hz, **7-*t***); − 4160.2 (m, **7-*c***). IR (ATR, cm^{-1}): ν = 285 (m, Pt−Cl), 2161 (s, CN, CNXyl), 2217 (w, CN, NHC). MS (MALDI+): *m*/*z* 508.1 [Pt(C^C*) (CNXyl)]$^+$.

cis/trans-(C,S) [Pt(Cl)(C^C*)(MMI)]* (**8**). 2-Mercapto-1-methylimidazole (MMI) (37 mg, 0.32 mmol) was added to a suspension of **4** (120.0 mg, 0.15 mmol) in acetone (30 mL) at −8 °C (ice/brine bath). After 1 h of stirring, the mixture was filtered through Celite, and the filtrated was evaporated to dryness. The residue was treated with diethyl ether (5 mL), filtered, and washed with diethyl ether (3 mL). The resulting orange solid was recrystallized from CH_2Cl_2/Et_2O to give **8-*t*** (86%)/**8-*c*** (14%). Yield: 78.6 mg, 51%. Anal. Calcd for $C_{15}H_{14}ClN_5PtS$: C, 34.19; H, 2.68; N, 13.29; S, 6.09. Found: C, 34.57; H, 2.97; N, 13.13; S, 6.75. ^{1}H NMR data for **8-*t*** (400 MHz, methylene chloride-d_2): δ = 12.72 (s, 1H, NH, MMI), 8.27 (s, $^3J_{H7,Pt}$ = 65.9, 1H, H_7), 7.41 (d, $^3J_{H9,H10}$ = 7.6, 1H, H_9), 7.30 (d, $^3J_{H2,H3}$ = 2.1, 1H, H_2), 7.04 (d, $^4J_{H10,Pt}$ = 14.3, 1H, H_{10}), 6.92 (d, $^4J_{H3,Pt}$ = 8.9, 1H, H_3), 6.87 (m, 1H, $H_{4'}$, MMI), 6.84 (m, 1H, $H_{5'}$, MMI), 4.19 (s, 3H, H_4), 3.75 (s, 3H, NMe, MMI). ^{1}H NMR data for **8-*c***: δ = 8.47 (d, $^4J_{H7,H9}$ = 1.1, $^3J_{H7,Pt}$ = 57.5, 1H, H_7), 4.04 (s, 3H, H_4), 3.68 (s, 3H, NMe, MMI). ^{13}C{^{1}H} NMR plus HMBC and HSQC (101 MHz, methylene chloride-d_2) for **8-*t***: δ = 159.3 (s, C_1), 156.1 (s, C═S, MMI), 149.9 (s, C_5), 135.4 (s, $^2J_{C7,Pt}$ = 37.1, C_7), 126.7 (s, C_6), 128.4 (s, C_9), 123.6 (s, $^3J_{C3,Pt}$ = 37.3, C_3), 120.4 (s, $C_{5'}$, MMI), 119.8 (s, CN), 115.1 (s, $C_{4'}$, MMI), 113.6 (s, $^3J_{C2,Pt}$ = 45.2, C_2), 110.7 (s, $^3J_{C10,Pt}$ = 35.8, C_{10}), 107.5 (s, C_8), 37.9 (s, C_4), 34.5 (s, NMe, MMI). ^{195}Pt{^{1}H} NMR (85.6 MHz, methylene chloride-d_2): δ = −3856.5 (s, **8-*t***); −3884.2 (s, **8-*c***). IR (ATR, cm^{-1}): ν = 268 (m, Pt−Cl), 2216 (w, CN), 3100 (w, NH). MS (MALDI+): *m*/*z* 491.0 [Pt(C^C*) (MMI)]$^+$.

trans-(C,P) [Pt(C^C*)(py)(PPh$_3$)]PF$_6$* (**9**). Pyridine (15.8 μL, 0.20 mmol) and KPF_6 (36.9 mg, 0.20 mmol) were added to a pale yellow suspension of **5** (132.6 mg, 0.20 mmol) in acetone (30 mL). After 1 h of stirring at room temperature, the solvent was evaporated to dryness and the residue treated with dichloromethane (35 mL) and filtered through Celite. Then the solvent was removed under reduced pressure, and the residue was treated with diethyl ether (10 mL), filtered, and washed with diethyl ether (5 mL). The solid was recrystallized from acetone (0 °C)/Et_2O to give **9** as a pale yellow solid. Yield: 88.3 mg, 49%. Anal. Calcd for $C_{34}H_{28}F_6N_4P_2Pt$: C, 47.28; H, 3.27; N, 6.49. Found: C, 46.86; H, 3.05; N, 6.47. ^{1}H NMR (400 MHz, methylene chloride-d_2): δ = 8.40 (dd, $^3J_{H,H}$ = 6.2, $^4J_{H,H}$ = 1.1, $^3J_{H,Pt}$ = 23.0, 2H, H*o* (py)), 7.69 (tt, $^3J_{H,H}$ = 7.7, $^4J_{H,H}$ = 1.4, 1H, H*p* (py)), 7.59 (m, 6H, H*o* (PPh_3)), 7.53−7.45 (m, 4H, H_2, H*p* (PPh_3)), 7.36 (m, 6H, H*m* (PPh_3)), 7.31 (dd, $^3J_{H9,H10}$ = 8.1, $^4J_{H9,H7}$ = 1.7, 1H, H_9), 7.19 (m, 3H, H_{10}, H*m* (py)), 7.03 (m, 1H, H_3), 6.85 (m, $^3J_{H7,Pt}$ = 58.8, 1H, H_7), 2.87 (s, 3H, H_4). ^{13}C{^{1}H} NMR plus HMBC and HSQC (101 MHz, methylene chloride-d_2): δ = 171.2 (d, $^2J_{C,P}$ = 136.2, C_1), 151.9 (s, $^2J_{C,Pt}$ = 10.0, 2C, C_o (py)), 150.8 (s, C_5), 142.9 (d, $^3J_{C7,P}$ = 9.6, $^2J_{C7,Pt}$ = 55.4, C_7), 139.3 (s, C_p (py)), 134.7 (d, $^2J_{C,P}$ = 11.7, 6C, C_o (PPh_3)), 131.7 (s, 3C, C_p (PPh_3)), 129.9 (s, C_9), 129.0 (d, $^3J_{C,P}$ = 10.0, 6C, C_m (PPh_3)), 127.5 (s, 2C, C_p (py)), 124.6 (d, $^4J_{C3,P}$ = 4.8, $^3J_{C3,Pt}$ = 31.3, C_3), 118.4 (s, CN), 115.1 (s, br, $^3J_{C2,Pt}$ = 40.2, C_2), 111.7 (s, $^3J_{C10,Pt}$ = 29.2, C_{10}), 108.3 (s, C_8), 35.3 (s, C_4). ^{31}P{^{1}H} NMR (162 MHz, methylene chloride-d_2): δ = 28.2 (s, $^1J_{P,Pt}$ = 2881.6). ^{195}Pt{^{1}H} NMR (85.6 MHz, methylene chloride-d_2): δ = −4274.6 (d). Λ_M (5 × 10^{-4} M acetone solution) = 76.87 Ω^{-1} cm^2 mol^{-1}. IR (ATR, cm^{-1}): ν = 2226 (w, CN). MS (MALDI+): *m*/*z* 639.1 [Pt(C^C*)(PPh$_3$)]$^+$.

trans-(C,P) [Pt(C^C*)(CNXyl)(PPh$_3$)]PF$_6$ (**10**). Method a.* 2,6-Dimethylphenyl isocyanide (CNXyl) (20.6 mg, 0.15 mmol) and KPF_6 (28.9 mg, 0.15 mmol) were added to a pale yellow suspension of **5** (103.8 mg, 0.15 mmol) in acetone (30 mL). After 1 h of stirring at room temperature, the solvent was evaporated to dryness and the residue treated with dichloromethane (20 mL) and filtered through Celite. Then the solvent was removed under reduced pressure, and the residue was treated with diethyl ether (5 mL), filtered, and washed with diethyl ether (3 mL) to give **10** as a pale yellow solid. Yield: 124.9 mg, 89%.

Method b. PPh_3 (34 mg, 0.129 mmol) and KPF_6 (23 mg, 0.125 mmol) were added to a yellow suspension of **7-*c***/**7-*t*** (14/86%) (70 mg, 0.128 mmol) in acetone (10 mL). After 1 h of stirring at room temperature, the solvent was evaporated to dryness and the residue treated with dichloromethane (20 mL) and filtered through Celite. Then the solvent was removed under reduced pressure, treated with diethyl ether (5 mL), filtered, and washed with diethyl ether (3 mL) to give **10** as a pale yellow solid. Yield: 91.1 mg, 77%. Anal. Calcd for $C_{38}H_{32}F_6N_4P_2Pt$: C, 49.84; H, 3.52; N, 6.12. Found: C, 49.59; H, 3.34; N, 6.05. ^{1}H NMR (400 MHz, methylene chloride-d_2): δ = 7.67 (m, 6H, H*o* (PPh_3)), 7.56 (d, $^3J_{H2,H3}$ = 2.1, 1H, H_2), 7.46−7.35 (m, 10H, H*m*, H*p* (PPh_3)) and H_9), 7.30 (d, $^3J_{H10,H9}$ = 8.8, 1H, H_{10}), 7.28 (d, $^3J_{H2,H3}$ = 2.1, 1H, H_3), 7.26 (t, $^3J_{H,H}$ = 7.7, 1H, H*p* (Xyl)), 7.08 (d, $^3J_{H,H}$ = 7.7, 2H, H*m* (Xyl)), 7.02 (s, br, $^3J_{H7,Pt}$ = 50.7, 1H, H_7), 3.91 (s, 3H, H_4), 2.12 (s, 6H, Me (Xyl)). ^{13}C{^{1}H} NMR plus HMBC and HSQC (101 MHz, methylene chloride-d_2): δ = 169.3 (d, $^2J_{C,P}$ = 127.7, C_1), 151.6 (s, C_5), 143.5 (d, $^3J_{C7,P}$ = 9.2, $^2J_{C7,Pt}$ = 51.0, C_7), 138.6 (s, C_6), 134.8 (s, 2C, C_o (Xyl)), 134.5 (d, $^2J_{C,P}$ = 11.7, 6C, C_o (PPh_3)), 132.4 (s, 3C, C_p (PPh_3)), 131.4 (s, C_9), 130.8 (s, C_p (Xyl)), 129.5 (d, $^3J_{C,P}$ = 11.0, 6C, C_m (PPh_3)), 128.7 (d, $^1J_{C,P}$ = 57.2, 3C, C_i (PPh_3)), 128.6 (s, 2C, C_m (Xyl)), 125.3 (s, br, C_3), 118.7 (s, CN), 116.1 (s, C_2), 112.4 (s, $^3J_{C10,Pt}$ = 25.8, C_{10}), 109.7 (s, C_8), 39.2 (s, C_4), 18.2 (s, Me (Xyl)). ^{31}P{^{1}H} NMR (162 MHz, methylene chloride-d_2): δ = 19.3 (s, $^1J_{P,Pt}$ = 2585.2). ^{195}Pt{^{1}H} NMR (85.6 MHz, methylene chloride-d_2): δ = −4697 (dt, $^2J_{Pt,N}$ = 61.7 Hz,). Λ_M (5 × 10^{-4} M acetone solution) = 70.63 Ω^{-1} cm^2 mol^{-1}. IR (ATR, cm^{-1}): ν = 2231 (m, CN), 2187 (s, C≡NXyl). MS (MALDI+): *m*/*z* 770.1 [Pt(C^C*) (CNXyl) (PPh$_3$)]$^+$.

trans-(C,P) [Pt(C^C*)(PPh$_3$)(MMI)]PF$_6$* (**11**). 2-Mercapto-1-methylimidazole (MMI) (22.0 mg, 0.19 mmol) and KPF_6 (34.8 mg, 0.19 mmol) were added to a pale yellow suspension of **5** (125.0 mg, 0.19 mmol) in acetone (30 mL). After 1.5 h of stirring at room temperature, the solvent was evaporated to dryness and the residue was treated with dichloromethane (7 × 10 mL) and filtered through Celite. Then the solvent was removed under reduced pressure, and the residue was treated with diethyl ether (10 mL), filtered, and washed

DOI: 10.1021/acs.inorgchem.5b01655
Inorg. Chem. 2015, 54, 9885−9895

Scheme 1. Synthesis of Compounds 1−4[a]

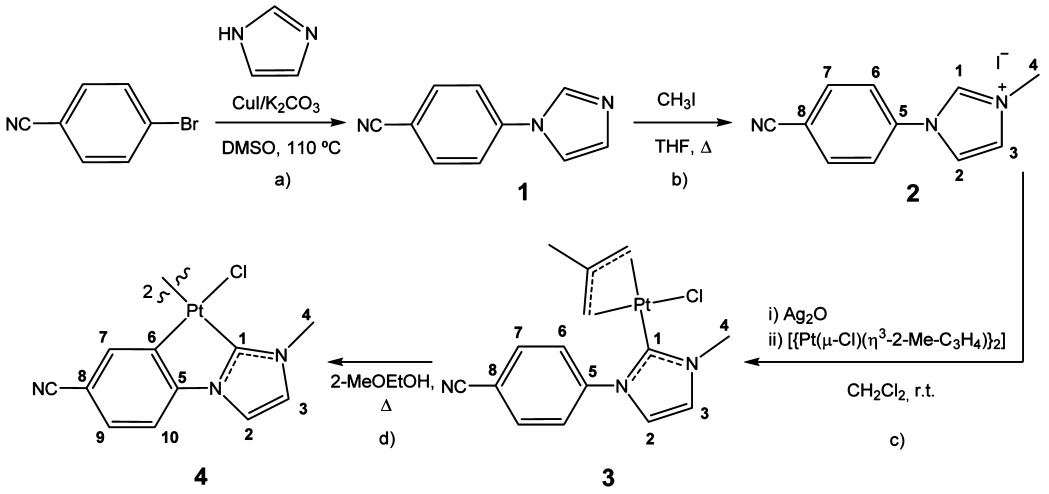

[a]Numerical scheme for NMR purporses.

with 5 mL more. The orange solid was washed with dichloromethane (3 × 4 mL) to give **11** as a pale yellow solid. Yield: 59.2 mg, 36%. Anal. Calcd for $C_{33}H_{29}F_6N_5P_2PtS$: C, 44.10; H, 3.25; N, 7.79; S, 3.57. Found: C, 43.72; H, 3.27; N, 7.69; S, 3.85. ^{1}H NMR (400 MHz, acetone-d_6) δ = 11.70 (s, 1H, NH (MMI)), 8.06 (d, $^3J_{H2,H3}$ = 1.7, 1H, H_2), 7.77 (m, 6H, H*o* (PPh_3)), 7.61−7.54 (m, 4H, H_{10} and H*p* (PPh_3)), 7.49 (m, 7H, H_3 and H*m* (PPh_3)), 7.43 (dd, $^3J_{H9,H10}$ = 8.2, $^4J_{H9,H7}$ = 1.6, 1H, H_9), 7.18 (m, 1H, $H_{5'}$, MMI), 7.05 (m, 1H, $H_{4'}$, MMI), 6.97 (m, $^3J_{H7,Pt}$ = 59.4, 1H, H_7), 4.08 (s, 3H, H_4), 3.32 (s, 3H, NMe, MMI). ^{13}C NMR (101 MHz, acetone-d_6) δ 170.7 (d, $^2J_{C1,P}$ = 144.4, C_1), 153.7 (s, C═S (MMI)), 151.8 (s, C_5), 142.6 (d, $^3J_{C7,Pt}$ = 56.1, $^3J_{C7,P}$ = 8.9, C_7), 136.1 (d, $^2J_{C,P}$ = 11.2, 6C, C_o (PPh_3)), 132.3 (d, $^4J_{C,P}$ = 11.2, 3C, C_p (PPh_3)), 130.5 (d, $^1J_{C,P}$ = 54.38, 3C, C_i (PPh_3)), 130.4 (s, C_9) 129.2 (d, $^3J_{C,P}$ = 10.7, 6C, C_m (PPh_3)), 126.7 (d, $^4J_{C,P}$= 5.1, C_3), 123.2 (s, $C_{5'}$, MMI), 119.2 (s, CN), 116.7 (s, $C_{4'}$, MMI), 116.5 (s, br, C_2), 113.1 (s, $^3J_{C10,Pt}$ = 29.2, C_{10}), 109.2 (s, C_8), 38.3 (s, C_4), 34.7 (s, NMe, MMI). ^{31}P{^{1}H} NMR (162 MHz, acetone-d_6): δ = 26.1 (s, $^1J_{P,Pt}$ = 2786.3). ^{195}Pt{^{1}H} NMR (85.6 MHz, acetone-d_6): δ = −4533.7 (d). Λ_M (5 × 10^{-4} M acetone solution) = 84.26 Ω^{-1} cm^2 mol^{-1}. IR (ATR, cm^{-1}): ν = 2224 (m, CN). MS (MALDI+): *m*/*z* 753.2 [Pt(C^C*)(MMI) (PPh_3)]$^+$, 639.1 [Pt(C^C*)(PPh_3)]$^+$.

[Pt(C^C)(dppe)]PF_6 (12).* 1,2-Bis(diphenylphosphino)ethane (dppe) (118.3 mg, 0.30 mmol) and KPF_6 (55.8 mg, 0.30 mmol) were added to a suspension of **4** (122.6 mg, 0.15 mmol) in acetone (30 mL). After 2.5 h of stirring at rt the solvent was removed in vacuo. Dichloromethane (50 mL) was then added, and the resulting suspension was filtered through Celite. The solvent was removed under reduced pressure, and Et_2O (20 mL) was added to the residue to obtain **12** as a white solid. Yield: 245.3 mg, 90%. Anal. Calcd for $C_{37}H_{32}F_6N_3P_3Pt$: C, 48.27; H, 3.50; N, 4.56. Found: C, 47.93; H, 3.35; N, 4.49. ^{1}H NMR (400 MHz, methylene chloride-d_2): δ = [7.96−7.80] (m, 8H, H_o (dppe)), [7.69−7.54] (m, 13H, H_2 and H_m, H_p (dppe)), 7.43 (dd, $^3J_{H9,10}$ = 8.4, $^4J_{H9,7}$ = 1.7, 1H, H_9), 7.34 (m, $^3J_{H7,Pt}$ = 50.6, 1H, H_7), 7.31 (dd, $^3J_{H10,9}$ = 8.4, $^5J_{H10,P}$ = 2.3, 1H, H_{10}), 7.05 (m, $^4J_{H3,Pt}$ = 9.1, 1H, H_3), 3.04 (s, 3H, H_4), 2.37 (m, 4H, CH_2 (dppe)). ^{13}C{^{1}H} NMR plus HMBC and HSQC (101 MHz, methylene chloride-d_2): δ = 172.7 (dd, $^2J_{C1,Ptrans}$ = 126.9; $^2J_{C1,Pcis}$ = 8.8, C_1), 151.0 (s, C_5), 143.9 (dd, $^2J_{C6,Ptrans}$ = 103.5, $^2J_{C1,Pcis}$ = 6.0, C_6), 142.5 (dd, $^3J_{C7,Ptrans}$ = 9.9; $^3J_{C7,Pcis}$ = 2.8, $^2J_{C7,Pt}$ = 54, C_7), 134.1 (d, $^2J_{C,P}$ = 12.1, 4C, C_o (dppe)), 133.6 (d, $^2J_{C,P}$ = 12.3, 4C, C_o (dppe)), 132.8 (s, 4C, C_p (dppe)), 131.1 (s, C_9), 130.0 (d, $^3J_{C,P}$ = 11.0, 4C, C_m (dppe)), 129.7 (d, $^3J_{C,P}$ = 11.0, 4C, C_m (dppe)), 124.9 (d, $^4J_{C3,P}$ = 4.0, $^3J_{C3,Pt}$ = 29.0, C_3), 118.5 (s, CN), 116.4 (d, $^4J_{C2,P}$ = 2.0, $^3J_{C3,Pt}$ = 33.0, C_2), 112.04 (s, $^3J_{C10,Pt}$ = 21.7, C_{10}), 110.7 (m, C_8), 38.9 (s, C_4), 31.7 (dd, $^1J_{C,P}$ = 37.6, $^2J_{C,P}$ = 10.0, CH_2 (dppe)), 30.6 (dd, $^1J_{C,P}$ = 39.8, $^2J_{C,P}$ = 12.4, CH_2 (dppe)). ^{31}P{^{1}H} NMR (162 MHz, methylene chloride-d_2): δ = 50.2 (d, $^2J_{P,P}$ = 7.0, $^1J_{P,Pt}$ = 2673.8, trans C*), 43.1 (d, $^1J_{P,Pt}$ = 2014.6, trans C_{ph}). ^{195}Pt{^{1}H} NMR (85.6 MHz, methylene chloride-d_2): δ = −4996 (dd). Λ_M (5 × 10^{-4} M acetone solution) = 69.01 Ω^{-1} cm^2 mol^{-1}. IR (ATR, cm^{-1}): ν = 2223 (m, CN). MS (MALDI+): *m*/*z* 775.2 [Pt(C^C*)(dppe)]$^+$

RESULTS

Improved Method of Preparation of a NHC Ligand and Its Use in the Stepwise Synthesis of [{Pt(μ-Cl)(C^C*)}$_2$] (HC^C*-κC*= 1-(4-Cyanophenyl)-3-methyl-1*H*-imidazol-2-ylidene). The synthesis of the N-heterocyclic carbene (NHC) 1-(4-cyanophenyl)-1*H*-imidazol (**1**) has been previously reported.[16a,b] However, we prepared it by a slightly modified method (Scheme 1, path a, Experimental Section) to avoid the use of coligands (pyrrolidinylmethylimidazole) and the purification step by column chromatography. 4-Bromobenzonitrile was coupled with imidazole in DMSO at 110 °C using copper(I) iodide and potassium carbonate in the presence of 4 Å molecular sieves. After workup, **1** was obtained by precipitation with *n*-hexane in good yield (83%). Then the addition of methyl iodide to a refluxing THF solution of **1** rendered the corresponding imidazolium salt: 1-(4-cyanophenyl)-3-methyl-1*H*-imidazolium iodide (**2**) (Scheme 1, path b, and Experimental Section).

Compound **2** was reacted with silver(I) oxide for 3 h and subsequently with [{Pt(μ-Cl)(η^3-2-Me-C_3H_4)}$_2$] (η^3-2-Me-C_3H_4 = η^3-2-methylallyl) to yield the neutral complex [PtCl(η^3-2-Me-C_3H_4) (HC^C*-κC*)] (**3**), which was isolated as a pale yellow and air-stable solid in very good yield (83%, see Experimental Section and Scheme 1, path c). Spectroscopic IR and NMR data support the proposed structure for complex **3**. Its IR spectrum shows an absorption band at 285 cm^{-1}, which is consistent with the presence of a terminal Pt−Cl bond in trans disposition to a ligand with a large trans influence such as η^3-2-Me-C_3H_4[13,14c] and another one at 2228 cm^{-1} due to the cyano group of the HC^C* ligand.

The disappearance of the signal attributed to H1 in the free ligand **2** (9.91 ppm) and the presence of Pt satellites in the signals corresponding to the H2 and H3 protons of the imidazolyl moiety (see Figure S1 in the SI) indicate that the imidazolium salt has been successfully anchored to the Pt center through the C1 of the N-heterocyclic carbene (HC^C*-

DOI: 10.1021/acs.inorgchem.5b01655
Inorg. Chem. 2015, 54, 9885−9895

κC*). This statement was confirmed by the similarities of the ^{195}Pt{^{1}H} resonance (δ = −4460 ppm) and the ^{1}H and ^{13}C{^{1}H} ones corresponding to the imidazolyl moiety and the methyl allyl group (η^3-2-Me-C_3H_4) with those of [PtCl(η^3-C_4H_7)(HC^C*-κC*)] (HC^C* = 3-methyl-1-(naphthalen-2-yl)-1*H*-imidazol-2-ylidene).[13]

A refluxing suspension of **3** in 2-methoxyethanol yielded the precipitation of a dark-colored solid which was recrystallized in hot acetonitrile solution (see Scheme 1, path d, and Experimental Section) to render **4** as a pure yellow solid in very good yield (81%). Compound **4** was not soluble in the common organic solvents, only in DMSO. The NMR data of **4** in DMSO-d_6 show the absence of the allyl group and the metalation of the 1-(4-cyanophenyl)-3-methyl-1*H*-imidazol-2-ylidene) (HC^C*-κC*) through the C6 (see Experimental Section and Figure S2 in the SI). This is evident by the lack of the H6 resonance and by the presence of a broad singlet corresponding to H7 at 8.72 ppm with a Pt−H coupling constant of ca. 60 Hz. The observed C1 resonance (δ = 156.0 ppm) is in good agreement with the literature values[10a−c,e,h,13,17] for related cyclometalated platinum(II) compounds.

These results embrace the feasibility of this stepwise synthetic pathway for [{Pt(μ-Cl)(C^C*)}$_2$] systems; since in this work, we have been able to reproduce the same strategy described by ourselves to prepare C^N[14b,c] and more recently C^C*[13]-cyclometalated complexes of platinum(II).

Reactivity of 4. Synthesis and Characterization of [PtCl(C^C*)L] (L = PPh_3 (5), py (6-*t*/6-*c*), CNXyl (7-*t*/7-*c*), MMI (8-*t*/8-*c*)). The dinuclear complex [{Pt(μ-Cl)(C^C*)}$_2$] (**4**) reacts with several neutral P, N, C, and S donor ligands, such as PPh_3, py, CNXyl, and MMI in a 1:2 molar ratio at low temperature (−8 °C) (Scheme 2 and Experimental Section) to

Scheme 2. Synthetic Pathway to Compounds 5−8

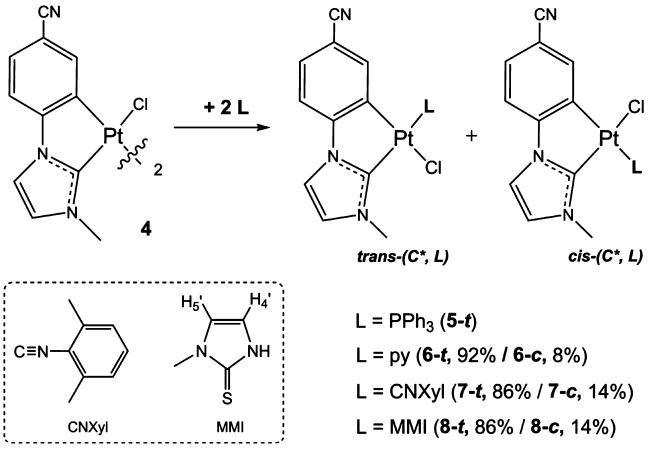

give the mononuclear complexes [PtCl(C^C*)L] (L = PPh_3 (**5**); py (**6**-*t*/**6**-*c*), CNXyl (**7**-*t*/**7**-*c*), MMI (**8**-*t*/**8**-*c*)). X-ray and spectroscopic data discussed below indicate that compound **5** was obtained as a solid with *trans*-(C*,L) being the only isomer observed, while in all other cases (**6**−**8**), cleavage of the bridging system rendered both isomers *cis*- and *trans*-(C*,L) with the trans isomer being the main one, especially when L is py (**6**).

For compound **7**, several reaction conditions were tested at room temperature and also in refluxing chloroform. End results were cis/trans mixtures with the same ratios. Analytical and spectroscopic data of compounds **5**−**8** are consistent with the proposed stoichiometry for them (see Experimental Section in the SI). Relevant structural information was provided by multinuclear NMR spectra (see Experimental Section in the SI and Table 1). It deserves to be noted that the ^{1}H NMR resonances corresponding to both cyanophenyl and imidazole fragments of C^C* are clearly altered by the coordination of the ancillary ligands (L). Especially sensitive to both the nature of L and the geometric disposition of the ligands around the Pt center are the H7 and H4 resonances. In all cases, as depicted in Figure 1, the H7 resonances of the *trans*-(C*,L) isomers appear more shielded than those of the cis derivatives.

Within the trans isomer complexes, in particular, when L = PPh_3 (**5**) and py (**6**-*t*), the H7 resonance undergoes an important upfield shift comparing with that in complexes with L = CNXyl (**7**-*t*) and MMI (**8**-*t*) (Table 1). This effect has been associated with the anisotropic shielding effect caused by the proximity in space of the aromatic ring current of the phenyl (**5**) and pyridine (**6**-*t*) groups to the H7.[14b,c,18] This C−H7···π interaction was also observed in the X-ray structure of **5**, as discussed below. Likewise, in the *cis*-(C*,L) isomers of complexes **6**−**8**, the H4 resonance is the one that suffers from the anisotropic effect since it moves upfield in relation to the trans isomers, the effect being more intense when L is pyridine (3.06 **6**-*c*; 4.24 **6**-*t*). In both geometric isomers, the H7 signal appears accompanied by platinum satellites. The Pt−H7 coupling constants of the trans isomers are larger than those of the cis derivatives, which is in agreement with the higher trans influence of the L ligands comparing to the Cl.[11c,14a,19]

It is worth noting that the cis/trans isomer ratios of **6**−**8** from the worked up solids match with those from the crude reaction mixtures, as proven by NMR experiments. We also confirmed that these ratios do not change over the time.

As expected, the ^{195}Pt{^{1}H} spectrum of **5** exhibits only a doublet at −4227 ppm with a ^{195}Pt−^{31}P coupling constant of 2868 Hz, while two ^{195}Pt resonances were observed for each one of the complexes **6**−**8**, due to the existence of both isomers (Figure 2). The main one, which corresponds to the trans isomer, appears less shielded than the cis one in all three cases.

In agreement with its formulation, the ^{31}P{^{1}H} NMR spectrum of **5** shows only one sharp signal at 28.6 ppm flanked by platinum satellites. The ^{195}Pt−^{31}P coupling constant value is typical of a P−Pt−C trans arrangement,[19,20] making evident the strong trans influence of the carbene atom (C*).

The molecular structure of **5** (see Figure 3), obtained by X-ray diffraction analysis of a single crystal of it, confirmed the complex to be the isomer *trans*-(C*,P)[PtCl(C^C*)(PPh_3)]. Data analysis is discussed below.

Synthesis and Characterization of the new Cationic "Pt(C^C*)" Complexes: *trans*-(C*,P)-[Pt(C^C*)(PPh_3)L′]PF_6 (L′ = py (9), CNXyl (10), MMI (11)) and [Pt(C^C*)(dppe)]PF_6 (12). With the aim of preparing new heteroleptic compounds with the N-heterocyclic carbene {Pt(C^C*)LL′}, various strategies were followed (see Scheme 3). Using different starting materials **4**, **5**, or **7**, we have been able to prepare the first cationic complexes with the "Pt(C^C*)" moiety. Hence, the addition of equimolecular amounts of KPF_6 and L′ to a solution of **5** in acetone rendered compounds **9**−**11** as pure solids (Scheme 3, path a). The formulation and geometry proposed are in agreement with the spectroscopic and crystallographic data discussed below. As inferred from these data, the PPh_3 remains coordinated trans to the C*. Interestingly, compound **10** can also be prepared by adding

DOI: 10.1021/acs.inorgchem.5b01655
Inorg. Chem. 2015, 54, 9885−9895

Table 1. Significant NMR Data for Compound Characterization[a]

	δH ($J_{Pt,H}$)		δC ($J_{Pt,C}$)				
compd	H7	H4	C1	C7	C3	δP ($J_{Pt,P}$)	δPt
5[b]	6.88 (64.0)	4.29	170.1	141.0 (57.0)	124.3 (26.0)	28.6 (2868.0)	−4227.0
6-*t*	6.69 (61.8)	4.24	152.7	135.2 (37.8)	123.1 (38.4)		−3731.9
6-*c*	8.41 (55.1)	3.06					−3775.4
7-*t*	7.97 (77.3)	4.28	167.7	140.8 (72.4)	123.9 (30.9)		−4042.7
7-*c*	8.45 (47.2)	3.92					−4160.2
8-*t*	8.27 (65.9)	4.19	159.3	135.4 (37.1)	123.6 (37.3)		−3856.5
8-*c*	8.47 (57.5)	4.04					−3884.2
9[b]	6.85 (58.8)	2.87	171.2	142.9 (55.4)	124.6 (31.3)	28.2 (2881.6)	−4274.6
10[b]	7.02 (50.7)	3.91	169.3	143.5 (51.0)	125.3	19.3 (2585.2)	−4697.0
11[b]	6.97 (59,4)	4.08	170.7	142.6 (56.1)	126.7	26.1 (2786.3)	−4533.7
12	7.34 (50.6)	3.04	172.7	142.5 (54.0)	124.9 (29.0)	(*t*-C*): 50.2 (2673.8) (*c*-C*): 43.1 (2014.6)	−4996.0

[a] δ (ppm), *J* (Hz). [b] *trans*-(C*,P) isomer is the only one observed.

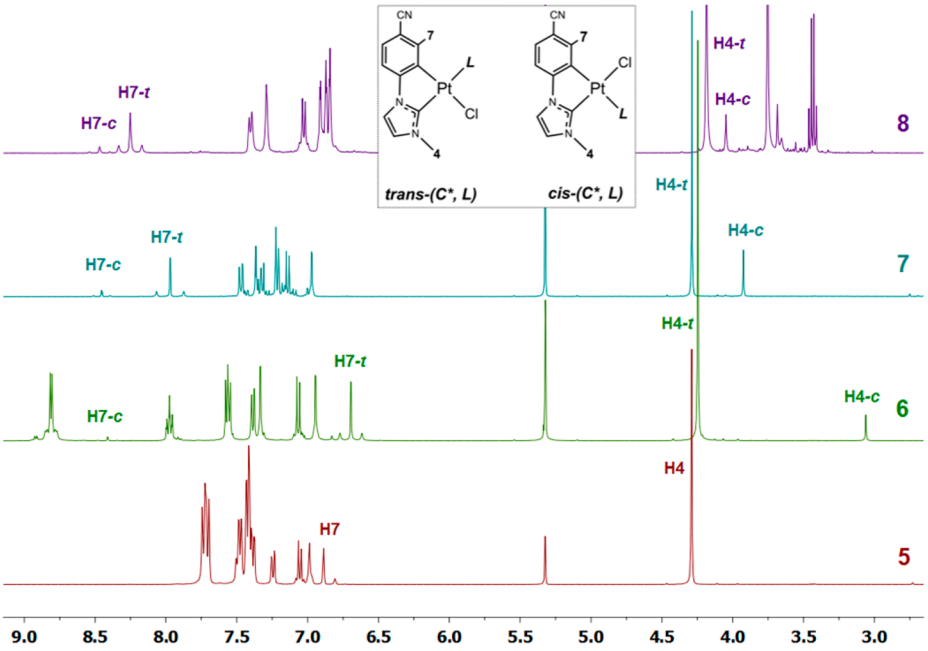

Figure 1. ^{1}H NMR spectra of **5**−**8** in CD_2Cl_2.

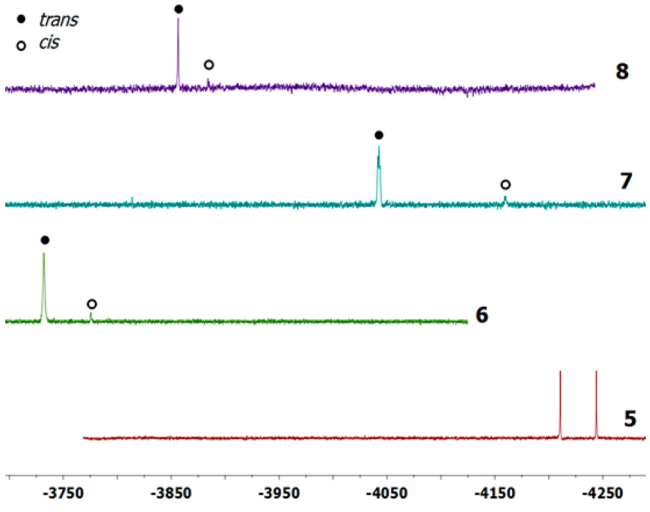

Figure 2. $^{195}Pt\{^{1}H\}$ spectra of **5**−**8** in CD_2Cl_2.

KPF_6 and PPh_3 to the mixture of cis/trans isomers of complex **7** (see Scheme 3, path b). Therefore, in this case, the main fraction of this reaction does not proceed with stereoretention, since the CNXyl ligand, which is located trans to C* in **7-*t***, migrates to the cis position by the coordination of the PPh_3. When a suspension of **4** in acetone was treated with KPF_6 and dppe (1:2 molar ratio) compound **12** was formed, a mononuclear species with the dppe acting as a chelate ligand.

Relevant structural information arises from the multinuclear NMR spectra (see Experimental Section, Table 1, and Figures S4 in the SI). The $^{31}P\{^{1}H\}$ NMR spectra of **9**−**11** show a singlet flanked by platinum satellites. The δP and $^{195}Pt-^{31}P$ coupling constants are quite similar to those found in complex **5**, indicating a *trans*-(C*,PPh_3) arrangement in these complexes. In the ^{31}P NMR spectrum of **12**, the two different P atoms appear as two doublet signals accompanied by Pt satellites. The chemical shifts and the observed P−P coupling of 7 Hz confirm the chelating arrangement of the dppe around the platinum center.[21]

DOI: 10.1021/acs.inorgchem.5b01655
Inorg. Chem. 2015, 54, 9885−9895

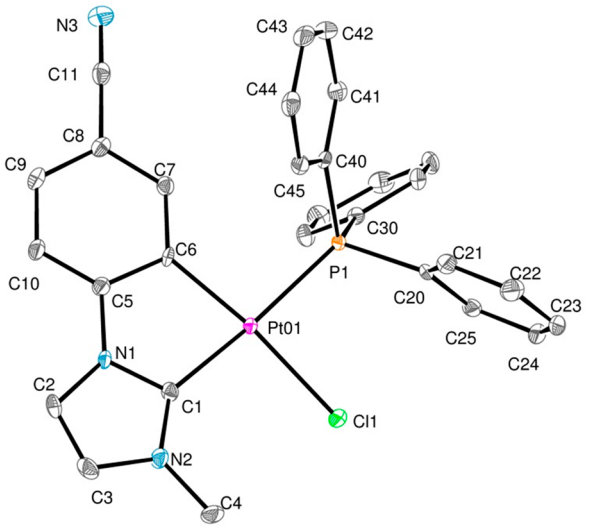

Figure 3. Molecular structure of complex **5·MeOH**. Thermal ellipsoids are drawn at the 50% probability level. Solvent molecules and hydrogen atoms have been omitted for clarity.

Scheme 3. Synthethic Pathway to Cationic Complexes 9−12

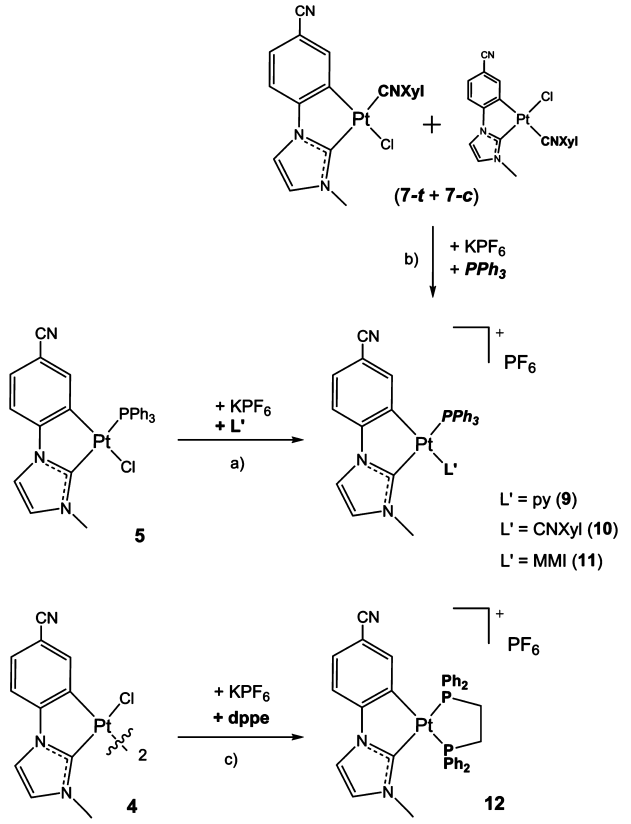

According to the geometry proposed (see Scheme 3), H7 resonances appear in the range of 6.80−7.30 ppm due to the anisotropic shielding effect caused by the proximity in space of the phenyl groups of the PPh_3. When L′ is pyridine and dppe, the H4 resonance also suffers from the anisotropic shielding effect, since it moves upfield (2.87 **9**, 3.04 **12**) comparing with that in complexes **10** and **11** (3.91 **10**, 4.08 **11**).

Significant are also the $^{195}Pt\{^1H\}$ spectra (see Figure 4 and Table 1) which confirm the presence of a single isomer in each case. They exhibit doublets for compounds **9**−**11** and a doublet

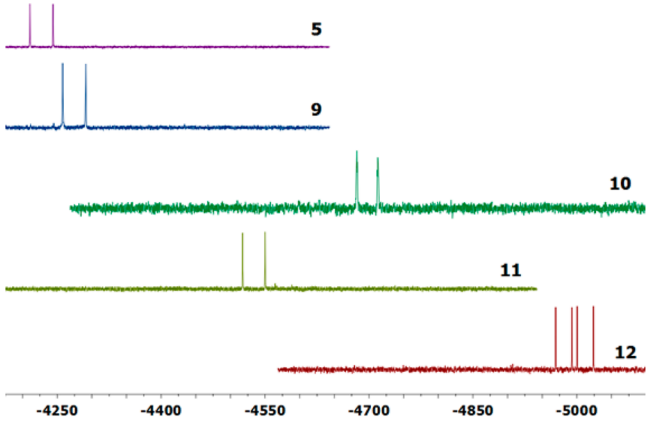

Figure 4. $^{195}Pt\{^1H\}$ spectra of **5** and **9**−**12** in CD_2Cl_2.

of doublets for **12** due to the coupling with the ^{31}P nuclei; these chemical shifts are ranging from −4274 to −4996 ppm.

The structural information obtained from the NMR spectra was confirmed by X-ray diffraction studies on compounds **9**−**12**, as can be seen in Figures 5 and 6 (for complexes **10** and **12**) and Figures S6 and S8 for complexes **9** and **11**).

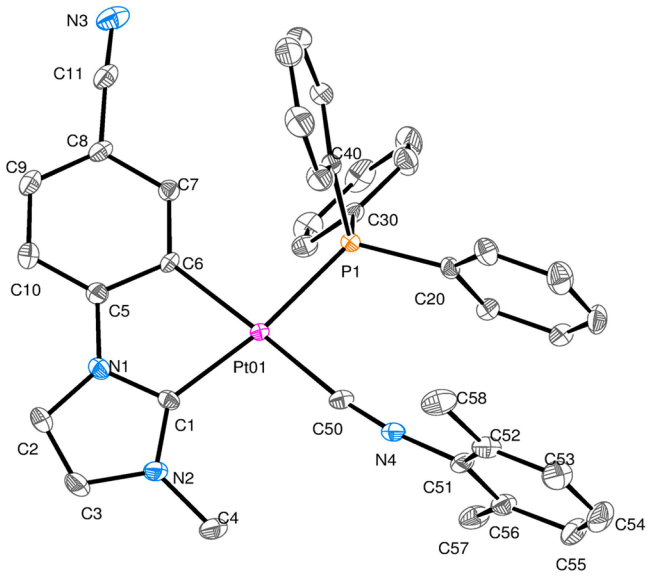

Figure 5. Molecular structure of the complex **10·0.5 OEt_2**. Thermal ellipsoids are drawn at the 50% probability level. Hydrogen atoms, PF_6, and solvent molecules have been omitted for clarity.

Crystal Structure Determination. Single-crystal X-ray diffraction studies were performed on compounds **5** and **9**−**12** to confirm their molecular structures. Crystallographic data are given in Table S1, and a selection of bond lengths and angles is shown in Table 2. As shown in Figures 3, 5, 6, and S5−S9 (in the SI), the Pt center lies in a distorted square planar coordination environment as a consequence of the small bite angle of the NHC-cyclometalated (C^C*) ligand [79.83(11)−78.54(13)°]. This angle together with the Pt−C6 and Pt−C1(C*) distances are similar to those found in other five-membered metalacycles of Pt(II) with N-heterocyclic carbenes.[10a−h,13] PPh_3 and L (L = Cl **5**, py **9**, CNXyl **10** and MMI **11**) complete the coordination sphere of platinum(II), whereas in **12**, a chelate dppe ligand does.

DOI: 10.1021/acs.inorgchem.5b01655
Inorg. Chem. 2015, 54, 9885−9895

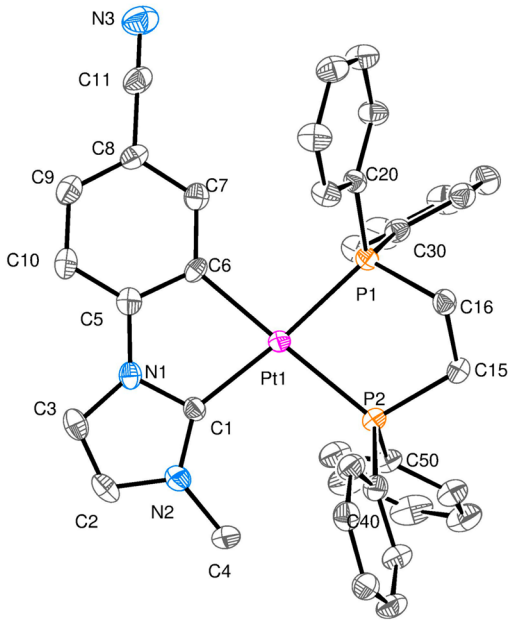

Figure 6. Molecular structure of complex **12**·CH_2Cl_2. Thermal ellipsoids are drawn at the 50% probability level. Hydrogen atoms, PF_6, and solvent molecules have been omitted for clarity.

The Pt−Cl,[14b,c,22] Pt−N,[23] Pt−C,[11c,f] Pt−S,[24] and Pt−P[19,25] distances are within the typical range for platinum(II) compounds with these trans to σ-bonded carbon atoms. The Pt−C6 bond lengths are clearly altered by the ancillary ligand coordinated at the trans position [from 2.015(3) (Cl, **5**) to 2.080(4) Å (P, **12**)], while the Pt−C1 ones are practically the same regardless of the neutral (**5**) or cationic (**9**−**12**) nature of the complexes. These are the first examples of [Pt(C^C*)-L′L]$^{0,+}$ heteroleptic complexes studied by X-ray diffraction. Thus far, all crystal structures of NHC-cycloplatinated compounds have been reported with diketonate derivatives.[10a−h]

The chelating dppe ligand adopts the gauche conformation with a P−CH_2−CH_2−P torsion angle of 46.7°. The Pt−P2 bond length is slightly longer than the Pt−P1 one, due to the higher trans influence of the C_{Ar}. Nevertheless, both distances and the small bite angle (83.15°) are similar to those of related compounds.[21c,26]

The cyclometalated NHC carbene ligand itself is not completely planar; it exhibits a small interplanar angle between the cyanophenyl and the imidazole fragments of 2.45(10)° (**5**), 6.42(9)° (**9**), 12.35(13)° (**10**), 5.79(8)° (**11**), and 5.81(14)° (**12**). As well as the molecular complexes that show dihedral angles between the platinum coordination plane (Pt01, C1, C6, P1, X) and the NHC ligand (N1−N3, C1−C11) of 10.7(2)° (**5**), 10.9(8)° (**9**), 8.83(8)° (**10**), 10.39(3)° (**11**), and 10.27(5) (**12**).[27] The rings of the ancillary ligands are almost perpendicular to the platinum coordination plane with dihedral angles of 78.94(9)° (N4, C12−C16, **9**), 82.48(12)° (N4, C50−C56, **10**), and 89.18(4)° (N4, N5, C50−C53, **11**).

Further inspection of the molecule packing within the crystal structures revealed the presence of weak intra- and intermolecular interactions (see the SI); however, no Pt···Pt contacts were observed. In all crystal structures (Figures 3, 5, 6, and S5−S9) we find an edge-to-face, also known as T-shaped, C−H···π interaction: the H7 hydrogen atom is pointing to the phenyl ring of the PPh_3 ligand, showing moderately short distances (C−H···π; C7···C_{ph} (PPh_3) = 3.22 (**5**), 3.28 (**9**), 3.35 (**10**), 3.15 (**11**) and 3.23 Å (**12**)). Only in **9** and **12**, there is a C−H···π interaction between the Me group (C4) and the pyridine or phenyl rings (C4···C_{py} = 3.42 Å (**9**), C4···C_{ph} = 3.23 Å (**12**)). Also in **9**−**11**, the phenyl group of the PPh_3 displays short intramolecular π···π interactions (3.11−3.58 Å) with the rings of the ancillary ligands (py, CNXyl, MMI), which are placed almost parallel to each other [15.30(11)° (**9**), 5.42(16)° (**10**), 9.47(9)° (**11**)]. Additionally, compound **9** crystallizes with one water molecule, which is holding a hydrogen bond with the CN group of the cyclometalated NHC fragment (see Figure S6). Finally, in **9** and **12**, the molecules arrange themselves in pairs in a head-to-tail fashion supported by π···π intermolecular contacts between the NHC fragments (3.70 (**9**) and 3.32 Å (**12**)), see Figures S6 and S9).

DISCUSSION

As shown above, cleavage of the chlorine-bridge system in [{Pt(μ-Cl)(C^C*)}$_2$] (**4**) by different ancillary ligands (L) led to the clean formation of *trans*-(C*,L)-[PtCl (C^C*)L] when L is PPh_3 (**5**). If L is py, CNXy, and MMI, the bridge-splitting reaction gave mixtures of cis/trans isomers (**6**−**8**).

In an attempt to explain this behavior we used the term transphobia degree (T) of pairs of trans ligands, which has been accepted by many authors to explain the geometries of stable square-planar complexes of d^8 transition metals. The degree of T has been assumed to be related to the trans influence in such a way that the greater the trans influence of two ligands the greater the transphobia and the cis disposition of them will be the favored geometry. In this sense the heteroleptic complexes [PtCl(C^N)L] (HC^N = 3,8-dinitro-6-phenylphenanthridine, 2-(4-bromophenyl)imidazol [1,2-*a*]pyridine; L= PPh_3, tht, C≡NR (R = ^{t}Bu, 2,6-dimethylphenyl)), and [Pt(C^P)(C≡CPh)L] (C^P = $CH_2C_6H_4P(o\text{-tolyl})_2$-$\kappa$C,P; L = CO, py, tht) exist as the *trans*-(C,Cl) isomer as expected on the basis of the transphobia degree (T) of pairs of trans ligands.[14a,b] However, the steric requirements of the ligands involved can also play an important role in determining the geometries of these

Table 2. Selected Bond Lengths (Angstroms) and Angles (degrees) for 5 and 9−12

	5·**MeOH** (X = Cl(1))	**9**·H_2O (X = N(4))	**10**·0.5 Et_2O (X = C(50))	**11** (X = S(1))	**12**·CH_2Cl_2 (X = P(2))
Pt(1)−C(1)	2.030(3)	2.033(3)	2.035(4)	2.037(3)	2.055(4)
Pt(1)−C(6)	2.015(3)	2.035(3)	2.065(4)	2.047(3)	2.080(4)
Pt(1)−P(1)	2.3024(7)	2.3075(9)	2.3171(11)	2.3046(8)	2.2787(13)
Pt(1)−X	2.3860(7)	2.099(3)	1.974(4)	2.3781(13)	2.3218(13)
C(1)−Pt(1)−C(6)	79.83(11)	78.54(13)	78.58(17)	79.54(10)	79.05(17)
C(6)−Pt(1)−P(1)	96.60(8)	95.90(10)	93.35(12)	94.67(7)	96.00(12)
C(1)−Pt(1)−X	95.85(8)	94.94(12)	98.74(17)	97.45(8)	101.91(13)
P(1)−Pt(1)−X	88.92(2)	89.45(8)	89.39(13)	89.28(3)	83.15(5)

DOI: 10.1021/acs.inorgchem.5b01655
Inorg. Chem. 2015, 54, 9885−9895

complexes. In this sense, complex [Pt(C^P)(C≡CPh)PPh_3], exhibits the *trans*-(C,C≡CPh) geometry instead of the expected one considering electronic preferences (*trans*-C,PPh_3), which was attributed to the crowding associated with the cis disposition of the P(*o*-tolyl)$_2$ and PPh_3 groups.[14a]

Therefore, we tried to explain the preferred geometry for complexes [PtCl(C^C*)L] (**5**–**8**) and [Pt(C^C*) (PPh_3)L]$^+$ (**9**–**11**) on the basis of the transphobia effect (T). With this purpose we studied the relative trans influences of the two σ Pt–C bonds present in the Pt(C^C*) unit, both expected to have a great trans influence, and those of the auxiliary ligands (Cl, PPh_3, py, CNXyl, MMI), comparing the $^1J_{Pt,P}$, $^2J_{Pt,C}$, and $^3J_{Pt,H}$ values affected by the ligands located at their trans positions.

The $^1J_{Pt,P}$ values observed for complexes *trans*-(C*,P) [PtCl(C^C*) (PPh_3)] (**5**) and [Pt(C^C*) (PPh_3)L′]PF_6 (L′ = py (**9**), CNXyl (**10**), MMI (**11**)) range from 2585.2 to 2881.6 Hz, which are typical of a P–Pt–C trans arrangement.[19,20] These values are also very similar to those observed in Q[Pt(CH_2–C_6H_4–P(*o*-tolyl)$_2$)(C≡CPh)$_2$] (Q = Li^+ (2746 Hz), NBu_4^+ (2603 Hz)) with the Pt–P bond trans to a Pt–C acetylide one.[14a] In addition, the $J_{Pt,P}$ corresponding to the P trans to C* (2673.8 Hz) in [Pt(C^C*) (dppe)]PF_6 (**12**) was found to be similar to that observed in complexes with phosphine ligands located in the trans position, such as [Pt(C^P)(dppe)]$^+$ [C^P = {(*R*)-1-[1-diphenylphosphino]-ethyl}naphthyl-C,P; $J_{Pt,P(transP)}$ = 2770 Hz,[21c] or [Pt(dppe)(PAn-H)]$^+$ [PAn = 9-diphenylphosphinoanthracene; $J_{Pt,P(transP)}$ = 2796],[26d] indicating that the C* displays a great trans influence, similar to alkynyl or phosphine ligands.

Then we focused again on complex [Pt(C^C*) (dppe)]PF_6 (**12**), and we observed the $^1J_{Pt,P}$ values for the P trans to C_{Ar} and C* are 2014.6 and 2673.8 Hz, respectively. These values indicate that the trans influence of C_{Ar} is slightly greater than that of C*. The same assessment was inferred from the $^3J_{Pt,Ho(py)}$ in complex **6** which exhibits different values when pyridine is facing C_{Ar} (**6-*c***, 20.7 Hz) or C* (**6-*t***, 28.0 Hz). Moreover, an evaluation of the electronic effects of the different L ligands can be undertaken by comparison of the spectroscopic and crystallographic data of complexes with the same stoichiometry and configuration, such as *trans*-(C*,P)-[Pt(C^C*) (PPh_3)L]$^{0,+}$ (L = Cl (**5**), py (**9**), CNXyl (**10**), MMI (**11**)) or *cis*-(C*,L)-[PtCl(C^C*)L] (L = py (**6-*c***), CNXyl (**7-*c***), MMI (**8-*c***)) (Table 1). On the basis of the observed $^3J_{Pt,H7}$ (64.0 (**5**), 58.8 (**9**), 50.7 (**10**), and 59.4 Hz (**11**)) and $^2J_{Pt,C7}$ (57.0 (**5**), 55.4 (**9**), 51.0 (**10**), and 56.1 Hz (**11**)) in the *trans*-(C*,P) named complexes, the trans influence order seems to be CNXyl > py ≈ MMI > Cl. An additional comparison of the values of δC1 (170.1 ppm (**5**), 152.7 (**6-*t***), 167.7 (**7-*t***), 159.3 (**8-*t***)) and $^3J_{Pt,C3}$ (26.0 Hz (**5**), 38.4 (**6-*t***), 30.9 (**7-*t***), 37.3 (**8-*t***)) in complexes *trans*-(C*,L)-[PtCl(C^C*)L] (L = PPh_3 (**5**), py (**6-*t***), CNXyl (**7-*t***), MMI (**8-*t***)) indicates that the trans influence of PPh_3 is even greater than that of CNXyl. Finally, X-ray data analysis of **5** and **9**–**12** (Table 2) indicates that the longest Pt–C6 distances correspond to those of **12** and **10**, with the dppe and CNXyl located at the trans position. Therefore, the trans influence of all the used ancillary ligands seems to follow the order PPh_3/dppe > CNXyl > py ≈ MMI > Cl.

Taking into account all these assumptions T[C_{Ar}/L)] > T[C*/L] and T[C_{Ar}/PPh_3)] > T[C_{Ar}/CNXyl)] > T[C_{Ar}/py)] ≈ T[C_{Ar}/MMI)] > T[C_{Ar}/Cl)]. Therefore, the T[C_{Ar}/PPh_3)] should be the greatest one, and the experimental results seem to indicate that the difference between T[C_{Ar}/PPh_3)] and T[C*/PPh_3] is big enough to direct clean formation of *trans*-(C*,PPh_3) complexes **5** and **9**–**11**.

However, the difference between T[C_{Ar}/L)] and T[C*/L] (L = py, CNXyl, MMI, Cl) is, in each case, not big enough to avoid the formation of mixtures of isomers. On the basis of the order of T[C_{Ar}/L] named above, the cleavage of the chlorine-bridge system in [{Pt(μ-Cl)(C^C*)}$_2$] (**4**) by py to give complex **6** was expected to be no more stereoselective than that with CNXyl or MMI, but it is. Other factors to promote the greater stability of **6-*t***, such as the steric hindrance between py and the imidazol fragment of C^C* in the cis isomer, can be excluded. Given that the H7 and H4 resonances in **6-*t*** and **6-*c*** suffer a great anisotropic shielding effect, which was discussed in the NMR section, we considered the C–H···π (py) interactions to be involved in it. C–H···π interactions have been known to play a key role in the stereoselectivity of coordination compounds among other fields in chemistry.[28] It has been widely reported that intramolecular C–H···π hydrogen bonds can induce the formation of single linkage isomers.[29] In both isomers of **6**, a C–H···π interaction could be possible: Csp^3–H4 (Me)···π (py) in **6-*c*** and a T-shaped Csp^2–H7 (Ar)···π (py) in **6-*t***. As reported before, the interaction energy involving a T-shaped aromatic C–H is somewhat stronger than that of the aliphatic ones.[28a,30] Thus, we would expect **6-*t*** to be more stable than **6-*c***. DFT calculations for models of **6-*c*/-*t*** in a solution of CH_2Cl_2 were carried out (see Figure 7). In effect, isomer **6-*t*** with the C–H7 pointing at the pyridine ring is 1.01 kcal mol^{-1} more stable than **6-*c***. This subtle difference in energy added to the bigger T[C_{Ar}/py)] vs T[C*/py] results to be reasonably determining for the high stereoselectivity of isomers in **6**.

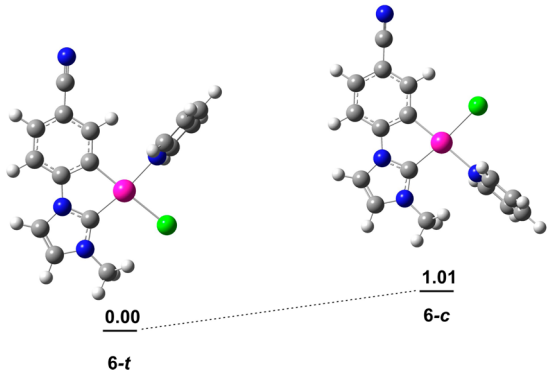

Figure 7. DFT-computed energies for the **6-*c*/-*t*** isomers (ΔE, kcal mol^{-1}).

In complexes **5** and **9**–**11**, their X-ray structures and NMR data also show the presence of Csp^2–H7(Ar)···π interactions, which will contribute together with the difference of T[C_{Ar}/L)] vs T[C*/L] to the selective formation of the *trans*-(C*,PPh_3) isomer, as experimentally observed.

CONCLUSIONS

The synthetic method for **1** has been greatly improved, and the corresponding imidazolium salt, **2**, has been successfully anchored and subsequently cyclometalated to the Pt center, which endorse the generality and viability of this step-by-step synthetic pathway for cyclometalated NHCs complexes, [{Pt(μ-Cl)(C^C*)}$_2$]. The chlorine-bridge complex **4** has

DOI: 10.1021/acs.inorgchem.5b01655
Inorg. Chem. 2015, 54, 9885–9895

been revealed as a useful starting material for neutral and cationic heteroleptic complexes containing the "Pt(C^C*)" moiety, **5**−**12**.

The transphobia degree (T) of pairs of trans ligands, as inferred from spectroscopic data, resulted was $T[C_{Ar}/L)] > T[C^*/L]$ and $T[C_{Ar}/PPh_3)] > T[C_{Ar}/CNXyl)] > T[C_{Ar}/py)] \approx T[C_{Ar}/MMI)] > T[C_{Ar}/Cl)]$. The difference between $T[C_{Ar}/L)]$ and $T[C^*/L]$ (L = py, CNXyl, MMI) is not enough to avoid the formation of mixtures of cis/trans isomers during the splitting of the chlorine bridge in **4** by L, but in all cases, the *trans*-(C*,L)-[PtCl(C^C*)L] isomer is the major species, especially when L is py. In this case, the intramolecular T-shaped C_{Ar}−H···π (py) interaction seems to contribute to the stabilization of this isomer, as proven by DFT calculations. Otherwise, the greatest $T[C_{Ar}/PPh_3)]$ together with the intramolecular T-shaped C_{Ar}−H···π (Ph) interactions present in the *trans*-(C*,PPh_3)-[Pt(C^C*)(PPh_3)L] complexes (L = Cl (**5**), py (**9**), CNXyl (**10**), MMI (**11**)) would account for the stereoselective formation of this isomer in each case, as experimentally observed.

■ ASSOCIATED CONTENT

Ⓢ Supporting Information

The Supporting Information is available free of charge on the ACS Publications website at DOI: 10.1021/acs.inorgchem.5b01655.

General procedures and materials, computational, and crystallographic details; full NMR spectra of **3** and **4**; full NMR spectra of **6** and **10** (selected as examples of the neutral and cationic derivatives; X-ray structures; tables of atomic coordinates of compounds (PDF)
Crystallographic data (CIF)

■ AUTHOR INFORMATION

Corresponding Author

*E-mail: sicilia@unizar.es.

Notes

The authors declare no competing financial interest.

■ ACKNOWLEDGMENTS

This work was supported by the Spanish Ministerio de Economía y Competitividad (MINECO)/FEDER (Project CTQ2012-35251 led by Dr. Babil Menjón) and the Departamento de Industria e Innovación del Gobierno de Aragón and Fondo Social Europeo (Grupo Consolidado E21: Química Inorgánica y de los Compuestos Organometálicos led by Dr. José M. Casas). The authors thank the Centro de Supercomputación de Galicia (CESGA) for generous allocation of computational resources and Dr. Antonio Martín for his valuable help with some of the X-ray structure determinations.

■ REFERENCES

(1) (a) Murphy, L.; Williams, J. A. G. *Top. Organomet. Chem.* **2010**, *28*, 75−111. (b) Williams, J. A. G. *Top. Curr. Chem.* **2007**, *281*, 205−268. (c) Zhou, G.; Wang, Q.; Wang, X.; Ho, C.-L.; Wong, W.-Y.; Ma, D.; Wang, L.; Lin, Z. *J. Mater. Chem.* **2010**, *20*, 7472−7484.

(2) (a) Zhao, Q.; Li, F.; Huang, C. *Chem. Soc. Rev.* **2010**, *39*, 3007−3030. (b) Wong, K. M.-C.; Chan, M. M.-Y.; Yam, V. W.-W. *Adv. Mater.* **2014**, *26*, 5558−5568. (c) Taylor, S. D.; Howard, W.; Kaval, N.; Hart, R.; Krause, J. A.; Connick, W. B. *Chem. Commun.* **2010**, *46*, 1070−1072.

(3) (a) Wang, P.; Leung, C. H.; Ma, D. L.; Sun, R. W. Y.; Yan, S. C.; Chen, Q. S.; Che, C. M. *Angew. Chem., Int. Ed.* **2011**, *50*, 2554−2558. (b) Wang, P.; Leung, C. H.; Ma, D. L.; Lu, W.; Che, C. M. *Chem. - Asian J.* **2010**, *5*, 2271−2280. (c) Koo, C. K.; Wong, K. L.; Man, C. W. Y.; Lam, Y. W.; So, K. Y.; Tam, H. L.; Tsao, S. W.; Cheah, K. W.; Lau, K. C.; Yang, Y. Y.; Chen, J. C.; Lam, M. H. W. *Inorg. Chem.* **2009**, *48*, 872−878.

(4) (a) Williams, J. A. G.; Develay, S.; Rochester, D. L.; Murphy, L. *Coord. Chem. Rev.* **2008**, *252*, 2596−2611. (b) Williams, J. A. G. In *Topics in Organometallic Chemistry*; Bozec, H., Guerchais, V., Eds.; Springer: New York, 2009; Vol. *28*.

(5) Sajoto, T.; Djurovich, P. I.; Tamayo, A.; Yousufuddin, M.; Bau, R.; Thompson, M. E.; Holmes, R. J.; Forrest, S. R. *Inorg. Chem.* **2005**, *44*, 7992−8003.

(6) (a) Bugaut, X.; Glorius, F. *Chem. Soc. Rev.* **2012**, *41*, 3511−3522. (b) Fortman, G. C.; Nolan, S. P. *Chem. Soc. Rev.* **2011**, *40*, 5151−5169. (c) Liddle, S. T.; Edworthy, I. S.; Arnold, P. L. *Chem. Soc. Rev.* **2007**, *36*, 1732−1744. (d) Herrmann, W. A. *Angew. Chem., Int. Ed.* **2002**, *41*, 1290−1309. (e) Kühl, O. *Chem. Soc. Rev.* **2007**, *36*, 592−607. (f) Wang, F. J.; Liu, L. J.; Wang, W. F.; Li, S. K.; Shi, M. *Coord. Chem. Rev.* **2012**, *256*, 804−853. (g) Nelson, D. J. *Eur. J. Inorg. Chem.* **2015**, *2015*, 2012−2027. (h) Levin, E.; Ivry, E.; Diesendruck, C. E.; Lemcoff, N. G. *Chem. Rev.* **2015**, *115*, 4607−4692. (i) Diez-Gonzalez, S.; Marion, N.; Nolan, S. P. *Chem. Rev.* **2009**, *109*, 3612−3676.

(7) (a) Lin, I. J. B.; Vasam, C. S. *J. Organomet. Chem.* **2005**, *690*, 3498−3512. (b) Huang, R. T. W.; Wang, W. C.; Yang, R. Y.; Lu, J. T.; Lin, I. J. B. *Dalton Trans.* **2009**, 7121−7131. (c) Lee, C. K.; Vasam, C. S.; Huang, T. W.; Wang, H. M. J.; Yang, R. Y.; Lee, C. S.; Lin, I. J. B. *Organometallics* **2006**, *25*, 3768−3775.

(8) (a) Melaiye, A.; Sun, Z. H.; Hindi, K.; Milsted, A.; Ely, D.; Reneker, D. H.; Tessier, C. A.; Youngs, W. J. *J. Am. Chem. Soc.* **2005**, *127*, 2285−2291. (b) Hindi, K. M.; Panzner, M. J.; Tessier, C. A.; Cannon, C. L.; Youngs, W. J. *Chem. Rev.* **2009**, *109*, 3859−3884. (c) Raubenheimer, H. G.; Cronje, S. *Chem. Soc. Rev.* **2008**, *37*, 1998−2011. (d) Mercs, L.; Albrecht, M. *Chem. Soc. Rev.* **2010**, *39*, 1903−1912.

(9) (a) Yam, V. W. W.; Cheng, E. C. C. In *Photochemistry and Photophysics of Coordination Compounds II*; Balzani, V., Campagna, S., Eds.; Springer-Verlag: Berlin, 2007; Vol. *281*, pp 269−309. (b) Hock, S. J.; Schaper, L.-A.; Herrmann, W. A.; Kuhn, F. E. *Chem. Soc. Rev.* **2013**, *42*, 5073−5089. (c) Son, S. U.; Park, K. H.; Lee, Y. S.; Kim, B. Y.; Choi, C. H.; Lah, M. S.; Jang, Y. H.; Jang, D. J.; Chung, Y. K. *Inorg. Chem.* **2004**, *43*, 6896−6898. (d) Unger, Y.; Zeller, A.; Ahrens, S.; Strassner, T. *Chem. Commun.* **2008**, 3263−3265. (e) Holmes, R. J.; Forrest, S. R.; Sajoto, T.; Tamayo, A.; Djurovich, P. I.; Thompson, M. E.; Brooks, J.; Tung, Y. J.; D'Andrade, B. W.; Weaver, M. S.; Kwong, R. C.; Brown, J. J. *Appl. Phys. Lett.* **2005**, *87*, 243507. (f) Chang, C. F.; Cheng, Y. M.; Chi, Y.; Chiu, Y. C.; Lin, C. C.; Lee, G. H.; Chou, P. T.; Chen, C. C.; Chang, C. H.; Wu, C. C. *Angew. Chem., Int. Ed.* **2008**, *47*, 4542−4545. (g) Hsieh, C. H.; Wu, F. I.; Fan, C. H.; Huang, M. J.; Lu, K. Y.; Chou, P. Y.; Yang, Y. H. O.; Wu, S. H.; Chen, I. C.; Chou, S. H.; Wong, K. T.; Cheng, C. H. *Chem. - Eur. J.* **2011**, *17*, 9180−9187. (h) Sasabe, H.; Takamatsu, J.; Motoyama, T.; Watanabe, S.; Wagenblast, G.; Langer, N.; Molt, O.; Fuchs, E.; Lennartz, C.; Kido, J. *Adv. Mater.* **2010**, *22*, 5003. (i) Lu, K. Y.; Chou, H. H.; Hsieh, C. H.; Yang, Y. H. O.; Tsai, H. R.; Tsai, H. Y.; Hsu, L. C.; Chen, C. Y.; Chen, I. C.; Cheng, C. H. *Adv. Mater.* **2011**, *23*, 4933−4937. (j) Visbal, R.; Ospino, I.; Lopez-de-Luzuriaga, J. M.; Laguna, A.; Gimeno, M. C. *J. Am. Chem. Soc.* **2013**, *135*, 4712−4715. (k) Haneder, S.; Da Como, E.; Feldmann, J.; Lupton, J. M.; Lennartz, C.; Erk, P.; Fuchs, E.; Molt, O.; Munster, I.; Schildknecht, C.; Wagenblast, G. *Adv. Mater.* **2008**, *20*, 3325−3330.

(10) (a) Tronnier, A.; Nischan, N.; Metz, S.; Wagenblast, G.; Münster, I.; Strassner, T. *Eur. J. Inorg. Chem.* **2014**, *2014*, 256−264. (b) Tronnier, A.; Pöthig, A.; Herdtweck, E.; Strassner, T. *Organometallics* **2014**, *33*, 898−908. (c) Tronnier, A.; Metz, S.; Wagenblast, G.; Münster, I.; Strassner, T. *Dalton Trans.* **2014**, *43*, 3297−3305. (d) Tronnier, A.; Nischan, N.; Strassner, T. *J. Organomet. Chem.* **2013**, *730*, 37−43. (e) Tronnier, A.; Risler, A.; Langer, N.; Wagenblast, G.; Münster, I.; Strassner, T. *Organometallics* **2012**, *31*, 7447−7452. (f) Hudson, Z. M.; Sun, C.; Helander, M. G.; Chang, Y. L.; Lu, Z. H.;

DOI: 10.1021/acs.inorgchem.5b01655
Inorg. Chem. 2015, 54, 9885−9895

Wang, S. N. *J. Am. Chem. Soc.* **2012**, *134*, 13930−13933. (g) Hudson, Z. M.; Blight, B. A.; Wang, S. N. *Org. Lett.* **2012**, *14*, 1700−1703. (h) Unger, Y.; Meyer, D.; Molt, O.; Schildknecht, C.; Münster, I.; Wagenblast, G.; Strassner, T. *Angew. Chem., Int. Ed.* **2010**, *49*, 10214−10216. (i) Tronnier, A.; Schleicher, D.; Strassner, T. *J. Organomet. Chem.* **2015**, *775*, 155−163. (j) Tronnier, A.; Pöthig, A.; Metz, S.; Wagenblast, G.; Münster, I.; Strassner, T. *Inorg. Chem.* **2014**, *53*, 6346−6356. (k) Tronnier, A.; Heinemeyer, U.; Metz, S.; Wagenblast, G.; Muenster, I.; Strassner, T. *J. Mater. Chem. C* **2015**, *3*, 1680−1693. (l) Ko, S.-B.; Park, H.-J.; Gong, S.; Wang, X. N.; Lu, Z.-H.; Wang, S. N. *Dalton Trans.* **2015**, *44*, 8433−8443. (m) Zhang, Y. X.; Jullien, H.; Brissy, D.; Retailleau, P.; Voituriez, A.; Marinetti, A. *ChemCatChem* **2013**, *5*, 2051−2057. (n) Jullien, H.; Brissy, D.; Sylvain, R.; Retailleau, P.; Naubron, J.-V.; Gladiali, S.; Marinetti, A. *Adv. Synth. Catal.* **2011**, *353*, 1109−1124. (o) Brissy, D.; Skander, M.; Jullien, H.; Retailleau, P.; Marinetti, A. *Org. Lett.* **2009**, *11*, 2137−2139.

(11) (a) Fernández, S.; Forniés, J.; Gil, B.; Gómez, J.; Lalinde, E. *Dalton Trans.* **2003**, 822−830. (b) Fornies, J.; Fuertes, S.; Lopez, J. A.; Martin, A.; Sicilia, V. *Inorg. Chem.* **2008**, *47*, 7166−7176. (c) Diez, A.; Fornies, J.; Fuertes, S.; Lalinde, E.; Larraz, C.; Lopez, J. A.; Martin, A.; Moreno, M. T.; Sicilia, V. *Organometallics* **2009**, *28*, 1705−1718. (d) Forniés, J.; Fuertes, S.; Martin, A.; Sicilia, V.; Gil, B.; Lalinde, E. *Dalton Trans.* **2009**, 2224−2234. (e) Díez, A.; Fornies, J.; Larraz, C.; Lalinde, E.; López, J. A.; Martin, A.; Moreno, M. T.; Sicilia, V. *Inorg. Chem.* **2010**, *49*, 3239−3259. (f) Fornies, J.; Sicilia, V.; Borja, P.; Casas, J. M.; Diez, A.; Lalinde, E.; Larraz, C.; Martin, A.; Moreno, M. T. *Chem. - Asian J.* **2012**, *7*, 2813−2823.

(12) Palacios, L.; Di Giuseppe, A.; Castarlenas, R.; Lahoz, F. J.; Perez-Torrente, J. J.; Oro, L. A. *Dalton Trans.* **2015**, *44*, 5777−5789 and references therein..

(13) Fuertes, S.; Garcia, H.; Peralvarez, M.; Hertog, W.; Carreras, J.; Sicilia, V. *Chem. - Eur. J.* **2015**, *21*, 1620−1631.

(14) (a) Casas, J. M.; Fornies, J.; Fuertes, S.; Martin, A.; Sicilia, V. *Organometallics* **2007**, *26*, 1674−1685. (b) Sicilia, V.; Fuertes, S.; Martin, A.; Palacios, A. *Organometallics* **2013**, *32*, 4092−4102. (c) Fornies, J.; Sicilia, V.; Larraz, C.; Camerano, J. A.; Martin, A.; Casas, J. M.; Tsipis, A. C. *Organometallics* **2010**, *29*, 1396−1405. (d) Slater, J. W.; Lydon, D. P.; Alcock, N. W.; Rourke, J. P. *Organometallics* **2001**, *20*, 4418−4423. (e) Vicente, J.; Abad, J. A.; Martinez-Viviente, E.; Jones, P. G. *Organometallics* **2002**, *21*, 4454−4467.

(15) Mabbott, D. J.; Mann, B. E.; Maitlis, P. M. *J. Chem. Soc., Dalton Trans.* **1977**, 294−299.

(16) (a) Huang, Y. Z.; Miao, H.; Zhang, Q. H.; Chen, C.; Xu, J. *Catal. Lett.* **2008**, *122*, 344−348. (b) Zhu, L. B.; Cheng, L.; Zhang, Y. X.; Xie, R. G.; You, J. S. *J. Org. Chem.* **2007**, *72*, 2737−2743. (c) Wang, H. F.; Li, Y. M.; Sun, F. F.; Feng, Y.; Jin, K.; Wang, X. N. *J. Org. Chem.* **2008**, *73*, 8639−8642.

(17) Bernhammer, J. C.; Huynh, H. V. *Organometallics* **2014**, *33*, 172−180.

(18) (a) Edwards, G. L.; Black, D. S. C.; Deacon, G. B.; Wakelin, L. P. G. *Can. J. Chem.* **2005**, *83*, 980−989. (b) Newman, C. P.; Casey-Green, K.; Clarkson, G. J.; Cave, G. W. V.; Errington, W.; Rourke, J. P. *Dalton Trans.* **2007**, 3170−3182. (c) Perez, S.; Lopez, C.; Caubet, A.; Solans, X.; Font-Bardia, M. *J. Organomet. Chem.* **2004**, *689*, 3184−3196.

(19) Zucca, A.; Maidich, L.; Carta, V.; Petretto, G. L.; Stoccoro, S.; Agostina Cinellu, M.; Pilo, M. I.; Clarkson, G. J. *Eur. J. Inorg. Chem.* **2014**, *2014*, 2278−2287.

(20) (a) Maidich, L.; Zuri, G.; Stoccoro, S.; Cinellu, M. A.; Zucca, A. *Dalton Trans.* **2014**, *43*, 14806−14815. (b) Minghetti, G.; Zucca, A.; Stoccoro, S.; Cinellu, M. A.; Manassero, M.; Sansoni, M. *J. Organomet. Chem.* **1994**, *481*, 195−204.

(21) (a) Haghighi, M. G.; Rashidi, M.; Nabavizadeh, S. M.; Jamali, S.; Puddephatt, R. J. *Dalton Trans.* **2010**, *39*, 11396−11402. (b) Garrou, P. E. *Chem. Rev.* **1981**, *81*, 229−266. (c) Jia, Y.-X.; Li, B.-B.; Li, Y.; Pullarkat, S. A.; Xu, K.; Hirao, H.; Leung, P.-H. *Organometallics* **2014**, *33*, 6053−6058.

(22) (a) Meijer, M. D.; Kleij, A. W.; Williams, B. S.; Ellis, D.; Lutz, M.; Spek, A. L.; van Klink, G. P. M.; van Koten, G. *Organometallics* **2002**, *21*, 264−271. (b) Zucca, A.; Cinellu, M. A.; Minghetti, G.; Stoccoro, S.; Manassero, M. *Eur. J. Inorg. Chem.* **2004**, *2004*, 4484−4490. (c) Zucca, A.; Petretto, G. L.; Stoccoro, S.; Cinellu, M. A.; Manassero, M.; Manassero, C.; Minghetti, G. *Organometallics* **2009**, *28*, 2150−2159. (d) Martin, R.; Crespo, M.; Font-Bardia, M.; Calvet, T. *Organometallics* **2009**, *28*, 587−597.

(23) (a) Rao, Y.-L.; Wang, S. N. *Inorg. Chem.* **2009**, *48*, 7698−7713. (b) Harris, C. F.; Vezzu, D. A. K.; Bartolotti, L.; Boyle, P. D.; Huo, S. Q. *Inorg. Chem.* **2013**, *52*, 11711−11722. (c) Karakostas, N.; Mavridis, I. M.; Seintis, K.; Fakis, M.; Koini, E. N.; Petsalakis, I. D.; Pistolis, G. *Chem. Commun.* **2014**, *50*, 1362−1365. (d) Jude, H.; Krause Bauer, J. A.; Connick, W. B. *Inorg. Chem.* **2004**, *43*, 725−733.

(24) (a) Fornies, J.; Sicilia, V.; Casas, J. M.; Martin, A.; Lopez, J. A.; Larraz, C.; Borja, P.; Ovejero, C. *Dalton Trans.* **2011**, *40*, 2898−2912. (b) Jacquot-Rousseau, S.; Khatyr, A.; Schmitt, G.; Knorr, M.; Kubicki, M. M.; Blacque, O. *Inorg. Chem. Commun.* **2005**, *8*, 610−613. (c) Hudson, Z. M.; Zhao, S.-B.; Wang, R.-Y.; Wang, S. N. *Chem. - Eur. J.* **2009**, *15*, 6131−6137. (d) Chuchuryukin, A. V.; Chase, P. A.; Mills, A. M.; Lutz, M.; Spek, A. L.; van Klink, G. P. M.; van Koten, G. *Inorg. Chem.* **2006**, *45*, 2045−2054.

(25) (a) Crespo, M.; Anderson, C. M.; Kfoury, N.; Font-Bardia, M.; Calvet, T. *Organometallics* **2012**, *31*, 4401−4404. (b) Alcarazo, M.; Radkowski, K.; Goddard, R.; Furstner, A. *Chem. Commun.* **2011**, *47*, 776−778. (c) Anderson, C.; Crespo, M.; Rochon, F. D. *J. Organomet. Chem.* **2001**, *631*, 164−174. (d) Rodríguez, J.; Zafrilla, J.; Albert, J.; Crespo, M.; Granell, J.; Calvet, T.; Font-Bardia, M. *J. Organomet. Chem.* **2009**, *694*, 2467−2475.

(26) (a) DePriest, J.; Zheng, G. Y.; Woods, C.; Rillema, D. P.; Mikirova, N. A.; Zandler, M. E. *Inorg. Chim. Acta* **1997**, *264*, 287−296. (b) Haghighi, M. G.; Nabavizadeh, S. M.; Rashidi, M.; Kubicki, M. *Dalton Trans.* **2013**, *42*, 13369−13380. (c) Saha, R.; Abdul Qaium, M.; Debnath, D.; Younus, M.; Chawdhury, N.; Sultana, N.; Kociok-Köhn, G.; Ooi, L.; Raithby, P. R.; Kijima, M. *Dalton Trans.* **2005**, 2760−2765. (d) Hu, J.; Lin, R.; Yip, J. H. K.; Wong, K.-Y.; Ma, D.-L.; Vittal, J. J. *Organometallics* **2007**, *26*, 6533−6543.

(27) Nardelli, M. *J. Appl. Crystallogr.* **1995**, *28*, 659−659.

(28) (a) Nishio, M.; Umezawa, Y.; Honda, K.; Tsuboyama, S.; Suezawa, H. *CrystEngComm* **2009**, *11*, 1757−1788. (b) Saigo, K.; Kobayashi, Y. *Chem. Rec.* **2007**, *7*, 47−56. (c) Nishio, M.; Umezawa, Y. *Topics in Stereochemistry* **2006**, *25*, 255−302.

(29) (a) Yamanari, K.; Nozaki, T.; Fuyuhiro, A.; Kushi, Y.; Kaizaki, S. *J. Chem. Soc., Dalton Trans.* **1996**, 2851−2856. (b) Yamanari, K.; Nozaki, T.; Fuyuhiro, A.; Kaizaki, S. *Chem. Lett.* **1996**, 35−36. (c) Nakamura, M.; Okawa, H.; Kida, S. *Bull. Chem. Soc. Jpn.* **1985**, *58*, 3377−3378. (d) Onaka, S.; Furuta, H.; Takagi, S. *Angew. Chem., Int. Ed. Engl.* **1993**, *32*, 87−88. (e) Chowdhury, S. K.; Joshi, V. S.; Samuel, A. G.; Puranik, V. G.; Tavale, S. S.; Sarkar, A. *Organometallics* **1994**, *13*, 4092−4096.

(30) Tsuzuki, S.; Honda, K.; Uchimaru, T.; Mikami, M.; Tanabe, K. *J. Am. Chem. Soc.* **2002**, *124*, 104−112.

■ NOTE ADDED AFTER ASAP PUBLICATION

This paper was published on the Web on October 8, 2015, with errors in Table 1. The corrected version was reposted on October 8, 2015.

DOI: 10.1021/acs.inorgchem.5b01655
Inorg. Chem. 2015, 54, 9885−9895

Inorganic Chemistry

Article

pubs.acs.org/IC

Heteroleptic Cycloplatinated N-Heterocyclic Carbene Complexes: A New Approach to Highly Efficient Blue-Light Emitters

Sara Fuertes,[†] Andrés J. Chueca,[†] Lorenzo Arnal,[†] Antonio Martín,[†] Umberto Giovanella,[‡] Chiara Botta,[‡] and Violeta Sicilia*[,§]

[†]Departamento de Química Inorgánica, Facultad de Ciencias, Instituto de Síntesis Química y Catálisis Homogénea, CSIC, Universidad de Zaragoza, Pedro Cerbuna 12, 50009 Zaragoza, Spain

[‡]Istituto per lo Studio delle Macromolecole, Consiglio Nazionale delle Ricerche (CNR), Via Corti 12, 20133 Milano, Italy

[§]Departamento de Química Inorgánica, Escuela de Ingeniería y Arquitectura de Zaragoza, Instituto de Síntesis Química y Catálisis Homogénea, CSIC, Universidad de Zaragoza, Campus Río Ebro, Edificio Torres Quevedo, 50018 Zaragoza, Spain

Supporting Information

ABSTRACT: New heteroleptic compounds of platinum(II)-containing cyclometalated N-heterocyclic carbenes, [PtCl(R-C^C*)(PPh_3)] [R-CH^C*-κC* = 3-methyl-1-(naphthalen-2-yl)-1*H*-imidazol-2-ylidene (R-C = Naph; **1A**), 1-[4-(ethoxycarbonyl)phenyl]-3-methyl-1*H*-imidazol-2-ylidene (R = CO_2Et; **1B**), and [Pt(R-C^C*)(py)(PPh_3)]PF_6 (py = pyridine; R-C = Naph, **2A**; R = CO_2Et, **2B**], have been prepared and fully characterized. All of them were obtained as the *trans*-(C*,PPh_3) isomer in high yields. The selectivity of their synthesis has been explained in terms of the degree of transphobia (T) of pairs of ligands in trans positions. X-ray diffraction studies on both **2A** and **2B** revealed that only in **2A**, containing a C^C* with a more extended π system, do the molecules assemble themselves into head-to-tail pairs through intermolecular $\pi\cdots\pi$ contacts. The photophysical properties of **2A** and **2B** and those of the related compounds [Pt(NC-C^C*)(PPh_3)L]PF_6 [NC-CH^C*-κC* = 1-(4-cyanophenyl)-3-methyl-1*H*-imidazol-2-ylidene; L = pyridine (py; **2C**), 2,6-dimethylphenylisocyanide (CNXyl; **3C**), and 2-mercapto-1-methylimidazole (MMI; **4C**)] have been examined to analyze the influence of the R substituent on R-C^C* (R-C = Naph; R = CO_2Et, CN) and that of the ancillary ligands (L) on them. Experimental data and time-dependent density functional theory calculations showed the similarity of the electronic features associated with R-C^C* (R = CN, CO_2Et) and their difference with respect to R-C^C* (R-C = Naph). All of the compounds are very efficient blue emitters in poly(methyl methacrylate) films under an argon atmosphere, with QY values ranging from 68% (**2B**) to 93% (**2C**). In the solid state, the color of the emission changes to yellowish-orange for compounds **2A** (λ_{max} = 600 nm) and **3C** (λ_{max} = 590 nm) because of the formation of aggregates through intermolecular $\pi\cdots\pi$ interactions. **2C** and **3C** were chosen to fabricate fully solution-processed electroluminescent devices with blue-light (**2C**), yellow-orange-light (**3C**), and white-light (mixtures of **2C** and **3C**) emission from neat films of the compounds as emitting layers.

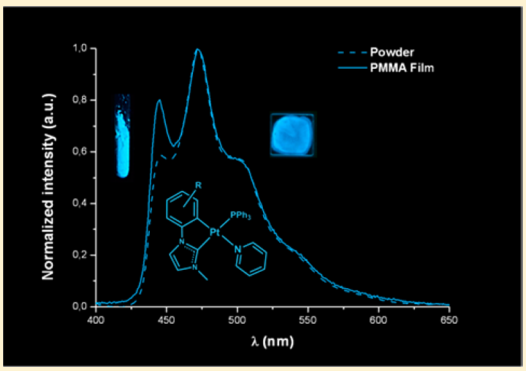

INTRODUCTION

Extensive investigations on phosphorescent transition-metal complexes have been carried out in the past decade, driven especially by their applicability in organic light-emitting devices (OLEDs), particularly those of ruthenium(II), iridium(III), and platinum(II).[1−5] The efficiency in the emission of visible light is attributed to the strong spin−orbit coupling induced by the heavy-metal atom that facilitates both fast intersystem crossing and formally spin-forbidden triplet radiative decay, which lead to conversion rates of up to 100%.[6−8]

Currently, most blue-emitting materials with high quantum yield (QY) are based on iridium(III) as the metal ion, but the number of platinum(II) compounds is increasingly growing.[3,9−16] Population of a high-energy excited state required for an efficient blue emission upon excitation competes with the photo or thermal population of high-lying metal dd* states, with the latter leading to severe geometrical distortions of the molecules, which result in nonradiative deactivation and degradation via bond-breaking processes.[17] In the chemistry of platinum(II), a common approach for the design of efficient and stable blue-phosphorescent systems is the incorporation of strong field ligands into the metal coordination sphere, such as C-deprotonated imines able to act as bidentate,[18,19] tridentate[11,17,20] and even tetradentate[21−24] ligands. The use of bidentate ligands has the advantage of the allowed electronic tunability of the platinum(II) complexes by varying the ancillary ligands. In this context, cyclometalated N-heterocyclic

Received: November 22, 2016
Published: April 7, 2017

DOI: 10.1021/acs.inorgchem.6b02826
Inorg. Chem. 2017, 56, 4829−4839

carbenes (NHCs; C^C*) may surpass the high ligand-field-splitting capacity of the C^N ligands because they present two C−σ bonds. Another consequence of the presence of strong carbon−metal bonds is the robustness and/or stability of the carbene complexes, which may provide long-term functional materials.[10−16,25,26] Up to now, most platinum(II) compounds containing C^C* cyclometalated ligands contain β-diketonate ligands[16,25−34] or two equal monodentate ligands[35] to complete the coordination sphere of the platinum center, but it is a constraining factor in the design of a variety of complexes. In a previous work, we reported that, based on the NMR data, the trans influence of the carbene (C*) is very high and not much different from that of the metalated carbon atom, in such a way that attempts to synthesize heteroleptic platinum(II) complexes containing bidentate C^C* cyclometalated ligands, [Pt(C^C*)-LL′], render mixtures of the *trans*- and *cis*-(C*,L) isomers.[36] However, we concluded that if L = PPh_3 the degree of transphobia T[CAr/PPh_3)] of this pair of ligands in trans positions is larger than T[C*/PPh_3] and directs the selective formation of the *trans*-(C*,PPh_3) isomer in such a way that the heteroleptic complexes [PtCl(NC-C^C*)(PPh_3)] (**1C**) and [Pt(NC-C^C*)(PPh_3)L]PF_6 [L = pyridine (py; **2C**), 2,6-dimethylphenylisocyanide (CNXyl; **3C**), 2-mercapto-1-methylimidazole (MMI; **4C**)] could be selectively obtained as the *trans*-(C*,PPh_3) isomer, and they are the only heteroleptic C^C* cyclometalated compounds of platinum(II) reported so far.[36]

Aiming to explore the generality of this assessment, we have expanded research to the synthesis of new related compounds by varying the cyclometalated NHC ligands: [Pt(R-C^C*)Cl(PPh_3)] (R-C = Naph, **1A**; R = CO_2Et, **1B**) and [Pt(R-C^C*)(py)(PPh_3)]PF_6 (R-C = Naph, **2A**; R = CO_2Et, **2B**). We have also studied the photophysical properties of the ionic compounds **2A**−**2C**, **3C**, and **4C**, both experimentally and theoretically, through time-dependent density functional theory (TD-DFT) calculations, trying to compare the effect of varying either C^C* or the L ligand on it (L = py, CNXyl, MMI). Moreover, compounds **2C** and **3C** were chosen to fabricate OLEDs with blue-light (**2C**), yellow-orange-light (**3C**), and white-light (mixtures of **2C** and **3C**) emission. OLEDs were fabricated by a fully solution-processed technology with a nondoped emitting layer (EML) thanks to the good processability of the compounds. Most of the work on platinum-based OLEDs deals with devices fabricated with vacuum evaporation techniques[37−39] because of the low solubility and/or poor ability of these compounds to form thin homogeneous films when deposited from solution. To the best of our knowledge, the solution-processed devices so far reported have been obtained with an EML composed of host−guest systems where the platinum emitter is blended in either polymeric or molecular hosts in order to reduce aggregation quenching processes and to increase the film homogeneity, for both molecular[40−44] and dendrimeric emitters.[45,46] For these reasons, all of the devices reported so far with a nondoped EML have been obtained by using vacuum-processed technologies.[47,48] On the other hand, nondoped devices offer many advantages, such as higher color stability and simpler device structure. Moreover, for blue-emitting devices, the use of blends imposes strict requirements on the host triplet-energy levels, whose energy must be high enough to prevent back-transfer processes. To the best of our knowledge, the results reported in this paper represent the first example of solution-processed platinum-based devices obtained with a nondoped EML. With this very simple approach, by mixing two compounds at different ratios, we are able to tune the OLED emission from blue to yellow-orange, passing through white.

EXPERIMENTAL SECTION

General Comments. Instrumental methods used for characterization and spectroscopic studies, DFT computational details, X-ray structures, and details of the preparation of poly(methyl methacrylate) (PMMA) films and the fabrication of electroluminescent devices are contained in the Supporting Information. All chemicals were used as supplied, and [{Pt(μ-Cl)(η^3-2-Me-C_3H_4)}$_2$],[49] [{Pt(μ-Cl)-(Naph^C*)}$_2$] (**A**),[33] [{Pt(μ-Cl)(CO_2Et-C^C*)}$_2$] (**B**),[35] [{Pt(μ-Cl)(NC-C^C*)}$_2$] (**C**), and **1C**−**4C**[36] were prepared following literature procedures.

Synthesis of [PtCl(Naph^C*)(PPh_3)] (1A). PPh_3 (158.6 mg, 0.59 mmol) was added to a suspension of **A** (233.4 mg, 0.27 mmol) in dichloromethane (30 mL) at room temperature. After 1 h of reaction, the solution was filtered through Celite and the solvent was removed under reduced pressure. The residue was treated with methanol (MeOH; 5 mL), filtered, and washed with MeOH (2 mL) to give **1A** as a pale-yellow solid. Yield: 282.2 mg, 76%. Anal. Calcd for $C_{32}H_{26}ClN_2PPt·CH_2Cl_2$: C, 50.49; H, 3.60; N, 3.57. Found: C, 50.82; H, 3.39; N, 3.50. ^{1}H NMR (400 MHz, methylene chloride-d_2): δ 7.75−7.83 (m, 6H, H_o(PPh_3)), 7.62 (d, $^3J_{12,11}$ = 8.1 Hz, 1H, H_{12}), 7.53 (m, 1H, H_2), 7.34−7.46 (m, 10H, H_m(PPh_3), H_p(PPh_3), and H_{14}), 7.24 (ddd, $^3J_{11,12}$ = 8.1 Hz, $^3J_{11,10}$ = 7.0 Hz, $^4J_{11,9}$ = 1.3 Hz, 1H, H_{11}), 7.08 (m, $^3J_{H,Pt}$ = 68.6 Hz, 1H, H_7), 7.06 (ddd, $^3J_{10,9}$ = 8.1 Hz, $^3J_{10,11}$ = 7.0 Hz, $^4J_{10,12}$ = 1.2 Hz, 1H, H_{10}), 7.00 (m, 1H, H_3), 6.62 (d, $^3J_{9,10}$ = 8.1 Hz, 1H, H_9), 4.31 (s, 3H, H_4). ^{13}C{^{1}H} NMR plus HMBC and HSQC (101 MHz, methylene chloride-d_2): δ 171.9 (s, C1), 146.1 (s, C5), 138.5 (d, $^3J_{C7,P}$ = 8.2 Hz, C7), 135.9 (d, $^2J_{C,P}$ = 10.9 Hz, $^3J_{C,Pt}$ = 19.7 Hz, 6C, C_o(PPh_3)), 130.7 (s, 3C, C_p(PPh_3)), 128.3 (d, $^2J_{C,P}$ = 10.1 Hz, 6C, C_m(PPh_3)), 127.1, 127.0 (s, 2C, C9 and C12), 125.1, 125.0 (s, 2C, C11 and C10), 124.7 (d, $^4J_{C,P}$ = 5.8 Hz, C3), 114.7 (s, C2), 107.5 (s, C14), 38.5 (s, C4). ^{31}P{^{1}H} NMR (162 MHz, methylene chloride-d_2): δ 30.1 (s, $^1J_{P,Pt}$= 2913.5 Hz). ^{195}Pt{^{1}H} NMR (85.6 MHz, methylene chloride-d_2): δ −4210.5 (d). IR (ATR, cm^{-1}): ν 303 (m, Pt−Cl). MS (MALDI$^+$): m/z 664.3 ([Pt(Naph^C*)-(PPh_3)]$^+$), 700.3 (**1A**$^+$).

Synthesis of [PtCl(CO_2Et-C^C*)(PPh_3)] (1B). It was prepared following the method described for **1A**. PPh_3 (84.5 mg, 0.31 mmol) and **B** (130.6 mg, 0.14 mmol). Yield: 157.5 mg, 77%. Anal. Calcd for $C_{31}H_{28}ClN_2O_2PPt$: C, 51.56; H, 3.90; N, 3.88. Found: C, 51.95; H, 3.85; N, 3.89. ^{1}H NMR (400 MHz, methylene chloride-d_2): δ 7.68−7.78 (m, 6H, H_o(PPh_3)), 7.61 (dd, $^3J_{9,10}$ = 8.1 Hz, $^4J_{9,7}$ = 1.7 Hz, 1H, H_9), 7.55 (m, $^3J_{H,Pt}$ = 66.5 Hz, 1H, H_7), 7.33−7.46 (m, 10H, H_m(PPh_3), H_p(PPh_3), and H_2), 7.04 (d, $^3J_{10,9}$ = 8.1 Hz, $^4J_{H,Pt}$ = 22.1 Hz, 1H, H_{10}), 6.97 (m, 1H, H_3), 4.30 (s, 3H, H_4), 3.94 (q, $^3J_{H,H}$ = 7.2 Hz, 2H, CH_2(OEt)), 1.00 (t, $^3J_{H,H}$ = 7.2 Hz, 3H, CH_3(OEt)). ^{13}C{^{1}H} NMR plus HMBC and HSQC (101 MHz, methylene chloride-d_2): δ 172.0 (s, C1), 166.3 (s, CO_2Et), 151.1 (s, C5), 140.9 (d, $^3J_{C7,P}$ = 9.5 Hz, C7), 135.8 (d, $^2J_{C,P}$ = 11.2 Hz, $^3J_{C,Pt}$ = 22.0 Hz, 6C, C_o(PPh_3)), 131.4 (s, C6), 130.9 (d, $^4J_{C,P}$ = 2.3 Hz, 3C, C_p(PPh_3)), 128.4 (d, $^2J_{C,P}$ = 10.5 Hz, 6C, C_m(PPh_3)), 125.9 (s, C9), 124.5 (d, $^4J_{C,P}$ = 6.1 Hz, C3), 114.5 (d, $^4J_{C,P}$ = 2.6 Hz, C2), 111.0 (s, C10), 60.6 (s, CH_2(OEt)), 38.5 (s, C4), 14.4 (s, CH_3(OEt)). ^{31}P{^{1}H} NMR (162 MHz, methylene chloride-d_2): δ 29.9 (s, $^1J_{P,Pt}$ = 2910.9 Hz). ^{195}Pt{^{1}H} NMR (85.6 MHz, methylene chloride-d_2): δ −4247.0 (d). IR (ATR, cm^{-1}): ν 286 (m, Pt−Cl), 1704 (m, C═O). MS (MALDI$^+$): m/z 686.1 ([Pt(CO_2Et-C^C*)(PPh_3)]$^+$).

Synthesis of [Pt(Naph^C*)(py)(PPh_3)]PF_6 (2A). Pyridine (16.0 μL, 0.20 mmol) and KPF_6 (37.5 mg, 0.20 mmol) were added to a pale-yellow suspension of **1A** (139.6 mg, 0.20 mmol) in acetone (30 mL). After 1 h of stirring at room temperature, the solvent was evaporated to dryness and the residue treated with dichloromethane (35 mL) and filtered through Celite. Then, the solvent was removed under reduced pressure, and the residue was treated with diethyl ether (10 mL), filtered, and washed with diethyl ether (5 mL) to give **2A** as a pale-yellow solid. Yield: 144.6 mg, 82%. Anal. Calcd for $C_{37}H_{31}F_6N_3P_2Pt$:

DOI: 10.1021/acs.inorgchem.6b02826
Inorg. Chem. 2017, 56, 4829−4839

C, 50.01; H, 3.52; N, 4.73. Found: C, 49.76; H, 3.28; N, 4.46. ^{1}H NMR (400 MHz, methylene chloride-d_2): δ 8.44 (d, $^{3}J_{H,H}$ = 6.6 Hz, $^{3}J_{H,Pt}$ = 21.7 Hz, 2H, H_o(py)), 7.60−7.72 (m, 9H, H_o(PPh_3), H_p(py), H_2, and H_{12}), 7.51 (s, $^{4}J_{H,Pt}$ = 10.0 Hz, 1H, H_{14}), 7.45 (m, 3H, H_p(PPh_3), 7.30−7.37 (m, 6H, H_m(PPh_3)), 7.29 (ddd, $^{3}J_{11,12}$ = 8.1 Hz, $^{3}J_{11,10}$ = 7.0 Hz, $^{4}J_{11,9}$ = 1.2 Hz, 1H, H_{11}), 7.19 (m, 2H, H_m(py)), 7.12 (ddd, $^{3}J_{10,9}$ = 8.1 Hz, $^{3}J_{10,11}$ = 7.0 Hz, $^{4}J_{10,12}$ = 1.2 Hz, 1H, H_{10}), 7.08 (d, $^{3}J_{7,P}$ = 2.4 Hz, $^{3}J_{H,Pt}$ = 61.2 Hz, 1H, H_7), 7.03 (m, 1H, H_3), 6.82 (d, $^{3}J_{9,10}$ = 8.1 Hz, 1H, H_9), 2.87 (s, 3H, H_4). ^{13}C{^{1}H} NMR plus HMBC and HSQC (101 MHz, methylene chloride-d_2): δ 171.9 (d, $^{2}J_{C1,P}$ = 137.5 Hz, C1), 152.4 (s, C_o(py)), 146.1 (s, C5), 141.1 (d, $^{3}J_{C7,P}$ = 9.6 Hz, C7), 139.5 (s, C_p(py)), 135.2 (d, $^{2}J_{C,P}$ = 11.6 Hz, $^{3}J_{C,Pt}$ = 20.3 Hz, 6C, C_o(PPh_3)), 131.7 (s, 3C, C_p(PPh_3)), 129.1 (d, $^{2}J_{C,P}$ = 10.5 Hz, 6C, C_m(PPh_3)), 127.7 (s, C_m(py)), 127.3, 127.1 (s, 2C, C9 and C12), 126.1 (s, C11), 125.5 (s, C10), 124.8 (d, $^{4}J_{C,P}$ = 5.0 Hz, C3), 121.4 (s, C6), 115.0 (s, C2), 108.5 (s, $^{4}J_{C14,Pt}$ = 26.5 Hz, C14), 35.6 (s, C4). ^{31}P{^{1}H} NMR (162 MHz, methylene chloride-d_2): δ 29.8 (s, $^{1}J_{P,Pt}$ = 2926.2 Hz). ^{195}Pt{^{1}H} NMR (85.6 MHz, methylene chloride-d_2): δ −4253.5 (d). IR (ATR, cm^{-1}): ν 829 (s, PF_6), 556 (s, PF_6). MS (MALDI$^+$): m/z 664.3 ([Pt(Naph^C*)(PPh_3)]$^+$). Λ_M (5 × 10^{-4} M acetone solution): 73.35 cm^2 Ω^{-1} mol^{-1}.

Synthesis of [Pt(CO_2Et-C^C*)(py)(PPh_3)]PF_6 (2B). It was prepared following the method described for **2A** with pyridine (24.7 μL, 0.31 mmol), KPF_6 (28.7 mg, 0.15 mmol), and **1B** (110.5 mg, 0.15 mmol). Yield: 115.2 mg, 83%. Anal. Calcd for $C_{36}H_{33}F_6N_3O_2P_2Pt$: C, 47.48; H, 3.65; N, 4.61. Found: C, 47.47; H, 3.65; N, 4.72. ^{1}H NMR (400 MHz, methylene chloride-d_2): δ 8.45 (d, $^{3}J_{H,H}$ = 5.0 Hz, $^{3}J_{H,Pt}$ = 21.7 Hz, 2H, H_o(py)), 7.64−7.72 (m, 2H, H_p(py) and H_9), 7.56−7.64 (m, 6H, H_o(PPh_3)), 7.41−7.52 (m, 5H, H_2, H_7, and H_p(PPh_3)), 7.33 (m, 6H, H_m(PPh_3)), 7.21 (m, 2H, H_m(py)), 7.14 (d, $^{3}J_{10,9}$ = 8.2 Hz, $^{4}J_{H,Pt}$ = 11.0 Hz, 1H, H_{10}), 7.07 (m, 1H, H_3), 3.92 (q, $^{3}J_{H,H}$ = 7.1 Hz, 2H, CH_2(OEt)), 2.90 (s, 3H, H_4), 0.95 (t, $^{3}J_{H,H}$ = 7.1 Hz, 3H, CH_3(OEt)). ^{13}C{^{1}H} NMR plus HMBC and HSQC (101 MHz, methylene chloride-d_2): δ 172.8 (d, $^{2}J_{C1,P}$ = 136.2 Hz, C1), 165.9 (s, CO_2Et), 152.4 (s, C_o(py)), 151.3 (s, C5), 142.4 (d, $^{3}J_{C7,P}$ = 9.7 Hz, C7), 139.8 (s, C_p(py)), 135.2 (d, $^{2}J_{C,P}$ = 11.5 Hz, $^{3}J_{C,Pt}$ = 21.1 Hz, 6C, C_o(PPh_3)), 132.0 (d, $^{4}J_{C,P}$ = 2.0 Hz, 3C, C_p(PPh_3)), 129.3 (d, $^{3}J_{C,P}$ = 10.8 Hz, 6C, C_m(PPh_3)), 128.0 (s, C_m(py)), 127.8 (s, C9), 124.9 (d, $^{4}J_{C,P}$ = 4.8 Hz, C3), 122.9 (d, $^{2}J_{C,P}$ = 6.2 Hz, C6), 115.5 (d, $^{4}J_{C,P}$ = 2.3 Hz, C2), 111.6 (s, $^{3}J_{C,Pt}$ = 29.2 Hz, C10), 60.7 (s, CH_2(OEt)), 35.9 (s, C4), 14.3 (s, CH_3(OEt)). ^{31}P{^{1}H} NMR (162 MHz, methylene chloride-d_2): δ 29.2 (s, $^{1}J_{P,Pt}$ = 2930.0 Hz). ^{195}Pt{^{1}H} NMR (85.6 MHz, methylene chloride-d_2): δ −4288.0 (d). IR (ATR, cm^{-1}): ν 832 (s, PF_6), 556 (s, PF_6), 1707 (m, C═O). MS (MALDI$^+$): m/z 686.1 ([Pt(CO_2Et-C^C*)(PPh_3)]$^+$). Λ_M (5 × 10^{-4} M acetone solution): 71.84 cm^2 Ω^{-1} mol^{-1}

RESULTS AND DISCUSSION

Synthesis and characterization of [PtCl(R-C^C*)(PPh_3)] and [Pt(R-C^C*)(py)(PPh_3)]PF_6. The dinuclear complexes [{Pt(μ-Cl)(R-C^C*)}$_2$] (R-C = Naph, **A**; R = CO_2Et, **B**) react with PPh_3 in a 1:2 molar ratio in dichloromethane at room temperature (Scheme 1, path a, and the Experimental Section) to give the mononuclear complexes *trans*-(C*,P)[PtCl(R-C^C*)(PPh_3)] (R-C = Naph, **1A**; R = CO_2Et, **1B**). Then, compounds [Pt(R-C^C*)(py)(PPh_3)]PF_6 (R-C = Naph, **2A**; R = CO_2Et, **2B**) were synthesized by treating **1A** and **1B** with 1 equiv of KPF_6 and an excess of pyridine in acetone at room temperature (see Scheme 1, path b, and the Experimental Section); they were isolated from their solutions as pure solids in high yield (ca. 83%).

All of the spectroscopic and crystallographic data discussed below support the formulation proposed for all of these new compounds and their *trans*-(C*,PPh_3) geometry, like in the previously reported compounds **1C**−**4C**.[36]

Scheme 1. Syntheses of Compounds[a]

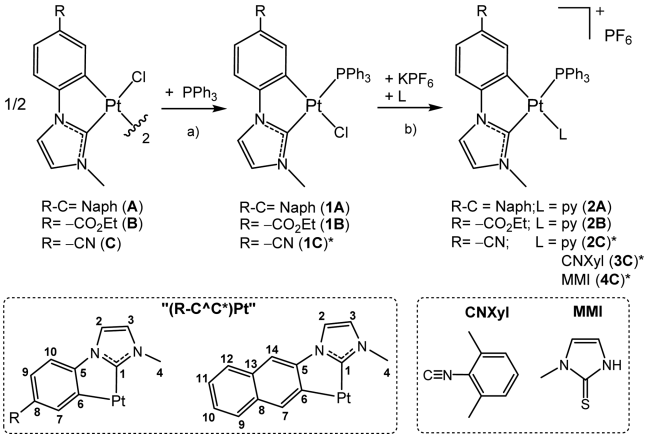

[a]Asterisks indicate that these compounds were already synthesized and characterized; see the Experimental Section.

Very relevant structural information was provided by multinuclear NMR spectra. The ^{1}H NMR spectra of **1A**, **1B**, **2A**, and **2B** show the expected signals for the C^C* group and auxiliary ligands with intensity ratios corresponding to the proposed stoichiometries (see the Experimental Section and Figures S1−S4). It is worth noting that resonances corresponding to H7, H9, and H10 protons in compounds **1A** and **2A** appear to be more shielded than the H14, H12, and H11 ones because of the anisotropic effect caused by the proximity in space of the aromatic ring current of the phenyl group of PPh_3. This same phenomenon is also observed in the H4 resonance of complexes **2A** and **2B** (δ ∼ 2.90 ppm), which undergo an important upfield shift compared to those of the corresponding chloride counterparts, **1A** and **1B** (δ ∼ 4.30 ppm). In this case, the anisotropic shielding effect is associated with the pyridine ring coordinated in a cis position to the carbenic fragment.[36] In agreement with their formulation, the ^{31}P{^{1}H} NMR spectra of **1A**−**2B** show only one sharp signal at ca. 30 ppm flanked by platinum satellites, and their ^{195}Pt{^{1}H} NMR spectra exhibit the expected doublets ranging from −4210.5 to −4288.0 ppm (see the Experimental Section and Figure S5). The δP, δPt and ^{195}Pt−^{31}P coupling constants are very similar to those found in the related complexes **1C** and **2C**,[36] with a *trans*-(C*,PPh_3) geometry, and are in the range of complexes with a P−Pt−C trans arrangement,[50−52] making evident the strong trans influence of the carbene atom (C*) of the two R-C^C* groups (R-C = Naph; R = CO_2Et) as well. As inferred from the ^{195}Pt NMR spectral data, the naphthyl derivatives (**1A** and **2A**) appear downfield-shifted (17−37 ppm) with respect to those of the ethoxycarbonyl (**1B** and **2B**) and the cyano (**1C** and **2C**) ones, indicating that the larger π system induces an important withdrawal of electron density from the platinum center. These spectral and electronic features were also observed in related compounds [Pt(R-C^C*)(CNR')$_2$]PF_6.[35] In addition, the ^{13}C{^{1}H} NMR spectra of **2A** and **2B** revealed the presence of a doublet at ∼172 ppm with a ^{31}P−^{13}C coupling constant value of ca. 136 Hz, corresponding to the quaternary carbenic carbon (C1). However, those of **1A** and **1B** could only be detected by 2D ^{1}H−^{13}C HMBC correlation experiments (see Figures S1 and S2).

As inferred from these NMR data, cleavage of the bridging system rendered compounds *trans*-(C*,PPh_3)[PtCl(R-C^C*)(PPh_3)] (R-C = Naph, **1A**; R = CO_2Et, **1B**) as unique isomers

DOI: 10.1021/acs.inorgchem.6b02826
Inorg. Chem. 2017, 56, 4829−4839

and the subsequent replacement of Cl by py in the coordination environment of platinum proceeds with stereoretention, giving compounds *trans*-(C*,PPh_3)[Pt(R-C^C*)(py)(PPh_3)]PF_6 (R-C= Naph, **2A**; R = CO_2Et, **2B**). These results were expected considering the degree of transphobia (T) of pairs of ligands in trans positions.[53−57] In our previous work, we concluded that T[C_{Ar}/L] > T[C*/L] and T[C_{Ar}/PPh_3] > T[C_{Ar}/py] > T[C_{Ar}/Cl], in such a way that T[C_{Ar}/PPh_3] should be the greatest one. The current experimental results indicated that, as was observed in the case of compounds **1C−4C**, the difference between T[C_{Ar}/PPh_3] and T[C*/PPh_3] is big enough to direct the selective formation of *trans*-(C*,PPh_3) complexes **1A**, **1B**, **2A**, and **2B** as pure compounds. This conclusion was confirmed by the single-crystal X-ray diffraction analysis of **2A** and **2B** shown in the following.

Crystal Structure Determination of [Pt(R-C^C*)(py)(PPh_3)]PF_6. The crystal structures of **2A** and **2B** were determined by X-ray diffraction studies (see Figures 1 and S6−S8 and Table S1). The asymmetric unit of **2A** contains two molecules (Pt1 and Pt2) with similar structural details (see Figure S6). The platinum(II) center exhibits a distorted square-planar environment due to the small bite angle of the cyclometalated NHC ligands R-C^C* [79.48(13)−80.09(13)°]. This C−Pt−C bite angle and both Pt−C bond lengths are similar to those observed for other five-membered metalacycles of platinum(II) with NHCs.[26−30,33,35,36,58−60] PPh_3 and pyridine complete the coordination sphere of the platinum center. The Pt−N[36,61−64] and Pt−P[36,50,65−68] bond distances are within the typical range for platinum(II) compounds, with these trans to σ-bonded carbon atoms. The pyridine rings are placed almost perpendicular to the platinum coordination planes (Pt, C, C, P, and N) with dihedral angles of 85.44° (Pt1, **2A**), 80.20° (Pt2, **2A**), and 74.89° (**2B**). In their crystal structure packings, intramolecular and very weak intermolecular interactions were observed (see Figures S7 and S8). As observed in the ^{1}H NMR spectra, there are C−H···π intramolecular interactions between the methyl groups (C4/C41) and the pyridine rings in **2A** [d(C4···C_g) = 3.267 Å and d(C41···C_{g2}) = 3.381 Å], whereas in **2B**, those contacts are significantly longer [d(C4···C_g) = 3.788 Å, where C_g are the centroids of the pyridine rings]. Also, there are π···π intramolecular interactions (3.11−3.59 Å) between one of the phenyl groups of the PPh_3 and pyridine rings.

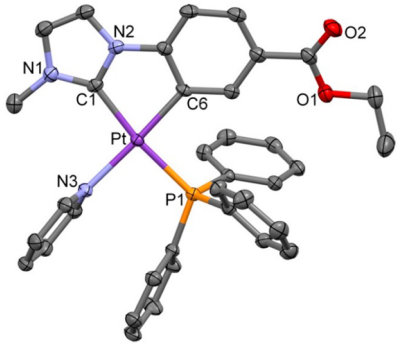

Figure 1. Molecular structure of the complex cation of **2B**. Selected bond lengths (Å) and angles (deg): Pt−C1 2.031(3), Pt−C6 2.035(3), Pt−P1 2.3031(8), Pt−N3 2.116(3); C1−Pt−C6 79.48(13), C6−Pt−P1 93.08(9), C1−Pt−N3 96.81(12), P1−Pt−N3 90.94(8). Solvent molecules, PF_6^-, and hydrogen atoms have been omitted for clarity. Thermal ellipsoids are drawn at the 50% probability level.

In **2A**, the molecules arrange themselves in head-to-tail pairs, showing a clear offset stacking with rather long intermolecular π···π contacts (~3.50 Å; see Figure S7), whereas in **2B**, the molecules are located far apart with no π···π interactions between each other.

Additionally, in both crystal structures (**2A** and **2B**), there are some weak C−H···F contacts [d(C−F) = 3.03 Å; d(H−F) = 2.30 Å; see Figure S8][69−71] between the cationic complexes and the PF_6^- anion, which is in agreement with the low conductivity measurements.

Photophysical Properties of Compounds [Pt(R-C^C*)(py)(PPh_3)]PF_6 [R-C = Naph (2A); R = CO_2Et (2B), CN (2C)] and [Pt(NC-C^C*)(PPh_3)L]PF_6 [L = CNXyl (3C), MMI (4C)]. In this section, we compare the absorption and emission properties of two sets of compounds, **2A−2C** and **2C−4C**, aiming to study how the photophysical properties of these ionic compounds are affected by variation of the NHC group or ancillary ligands, respectively. UV−vis spectral data of **2A−4C** are listed in Table S2. As shown in Figure 2, in a diluted

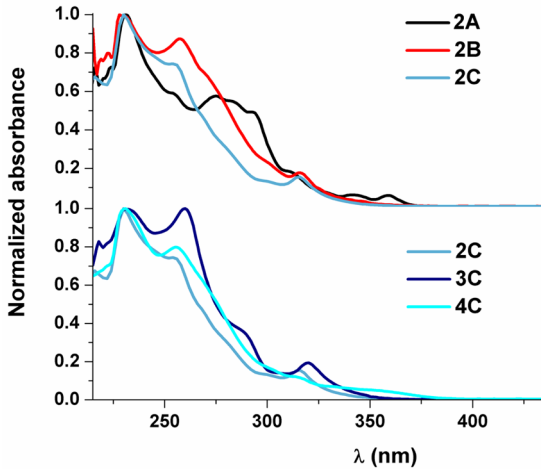

Figure 2. Normalized absorption spectra in CH_2Cl_2 (5×10^{-5} M) at room temperature.

CH_2Cl_2 solution, they all display strong absorption bands at $\lambda \leq 300$ nm ($\varepsilon > 10^4$ M^{-1} cm^{-1}), which are normally attributed to the singlet intraligand (^{1}IL) transitions of the NHC ligand.

Complexes **2B** and **2C** show almost identical UV−vis spectra with the lowest-energy absorption at around 315 nm ($\varepsilon \sim 10^3$ M^{-1} cm^{-1}), suggesting that the electronic features of the R-C^C* (R = CO_2Et, CN) ligands are comparable and quite different from those of the naphthyl counterpart, **2A**.

The latter exhibits an additional low-energy (LE) band at $\lambda \sim$ 350 nm ($\varepsilon \sim 10^3$ M^{-1} cm^{-1}), which is very similar to that observed in complexes with the same cyclometalated NHC ligand (Naph^C*).[33,35] It appears to be slightly shifted to higher energies compared to the isocyanide derivatives [(Naph^C*)Pt(CNR′)$_2$]PF_6 (R′ = *t*-Bu, Xyl),[35] which indicates participation of the ancillary ligands in it. The involvement of the auxiliary ligands in the lowest-energy absorptions can also be noticed for complexes **2C−4C**. The one corresponding to the isocyanide derivative, **3C** (λ = 320 nm), is shown to be clearly red-shifted with respect to the pyridine one, **2C** (λ = 316 nm), while that of **4C** becomes a less intense shoulder (λ = 314 nm) accompanied by an additional

DOI: 10.1021/acs.inorgchem.6b02826
Inorg. Chem. 2017, 56, 4829−4839

Table 1. Population Analysis (%) of FOs in the Ground State for 2A−2C and 4C in a Solution of CH_2Cl_2

					population analysis (%)															
	eV				platinum				R-C^C*				PPh_3				L			
MO	2A	2B	2C	4C	2A	2B	2C	4C	2A	2B	2C	4C	2A	2B	2C	4C	2A	2B	2C	4C
L+1	−1.57	−1.66	−1.72	−1.37	26	5	5	23	34	7	4	25	14	1	1	46	26	87	90	6
L	−1.72	−1.89	−1.99	−2.00	11	20	20	23	15	64	69	67	4	8	7	7	70	8	4	3
H	−6.28	−6.72	−6.88	−6.46	9	25	24	9	90	74	75	3	1	1	1	3	0	0	0	85
H−1	−6.60	−7.16	−7.24	−6.85	18	61	56	24	80	8	4	74	1	30	39	1	1	1	1	1

band at λ = 352 nm. This lowest-energy absorption of **4C** (352 nm) obeys Beer's law, suggesting that it is due to transitions in the molecular species and that no significant aggregation occurs within the concentration range from 10^{-3} to 10^{-6} M (see Figure S9). UV−vis spectra of all complexes were recorded in different solvents (Table S2), showing no significant solvatochromism, except for compound **2A** (see Figure S10). It presents a slightly negative solvatochromism in the lower-energy spectral region (λ > 340 nm), which indicates the existence of charge-transfer (CT) transitions.[72]

Solid-state diffuse-reflectance spectra are depicted in Figure S11. They show no particular differences compared to those observed in a solution of CH_2Cl_2. Therefore, the weak intermolecular $\pi-\pi$ and C−H···F interactions observed in their X-ray structures (at ca. 100 K) seem to have no important effects in the absorption at room temperature.

DFT and TD-DFT calculations in a solution of CH_2Cl_2 for **2A−2C** and **4C** have been carried out to provide correct assignments for the UV−vis absorptions and also to evaluate the effect of both cyclometalated R−C^C* and ancillary ligands (L) on the photophysical properties.

The optimized geometries of the ground state, S_0, and T_1 (Tables S3−S10) were carried out at the M06/SDD(Pt)/6-31G* (ligand atoms) level. The geometric parameters of the optimized structures (S_0) agree reasonably well with the experimental values (Tables S11 and S12). Diagrams of the frontier molecular orbitals (FOs) in the ground state are depicted in Figure S12, and the relative compositions of the different energy levels are reported in Table 1. Excitation energies at the ground-state geometry were calculated by TD-DFT in a CH_2Cl_2 solution, and selected low-lying transitions are listed in Table S13. The composition of the FOs of **2B** and **2C** are practically identical, which confirms the similarities of the electronic features of the R-C^C* (R = CN, CO_2Et) cyclometalated groups. In these cases, the highest occupied molecular orbitals (HOMOs) are mainly constructed from π orbitals of the C^C* ligand (ca. 75%) and dπ orbitals of the platinum center (25%) and the lowest unoccupied molecular orbitals (LUMOs) are similar to the HOMOs but with some contribution of the ancillary ligands: 20% platinum, ca. 65% C^C*, 8% PPh_3, and 7% py. However, in the case of **2A**, the HOMO is almost entirely localized on the Naph^C* fragment (90%), while the LUMO is mostly centered on the pyridine (70%) with small contributions of Naph^C* (ca. 15%) and platinum (ca. 10%) orbitals. By a comparison of **2C** and **4C**, it can be observed that in **4C** the presence of MMI instead of py in the coordinating sphere of platinum leads to a HOMO mainly based on the auxiliary ligand (MMI, 85%) with only a low contribution of platinum and R-C^C* orbitals, while no significant changes are induced in the LUMO composition with respect to that in **2C**, which is mostly centered on the R-C^C* orbitals. Thus, by modification of both ligands, either R-C (C^C*) or L, the nature and composition of the FOs, and therefore the nature of the lowest-energy singlet transition, change considerably. The calculated S_1 in CH_2Cl_2 arises from HOMO to LUMO transitions for **2B**, **2C**, and **4C**, while for **2A**, it arises mainly from H → L (39%) and H → L+1 (36%) transitions.

Considering that the calculated allowed absorptions are in good qualitative agreement with the experimental UV−vis spectra (Figures 3 and S13−S15), the lowest-energy absorption

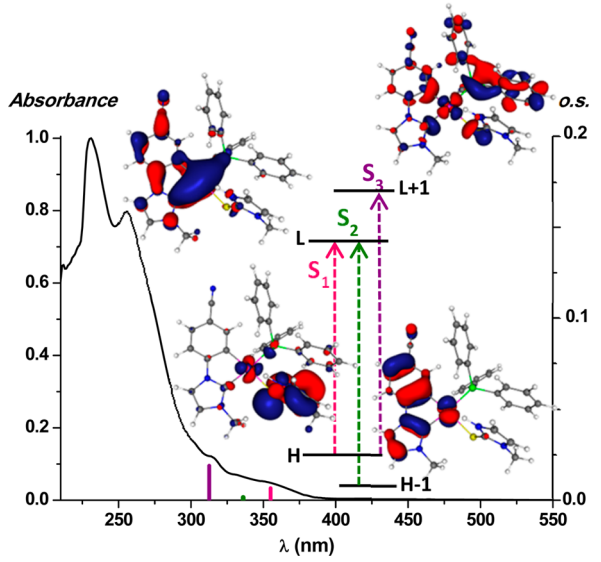

Figure 3. Normalized UV−vis absorption spectrum of **4C** in CH_2Cl_2 and calculated transitions in CH_2Cl_2 (colored bars) with the diagrams of the FOs.

bands can be attributed to mixed transitions: ILCT [π(NHC) → π*(NHC)]/LL′CT [π(NHC) → π*(L′)] for **2B** and **2C** and LL′CT [π(NHC) → π*(py)]/ILCT [π(NHC) → π*(NHC)]/LMCT [π(NHC) → 5d(Pt)] for **2A** and L′LCT [π*(MMI) → π*(NHC)]/L′MCT [π*(MMI) → 5d(Pt)] for **4C**. Complex **4C** shows also a very weak calculated absorption at 336 nm (S_2; see Figure 3) that implicates the H−1 → L (95%) transition. Its energy and electronic nature are very similar to the calculated S_1 transition in complexes **2B** and **2C**.

Emission data are summarized in Table 2. The phosphorescence of all complexes in CH_2Cl_2 (10^{-5} M, 298 K) is quenched, even under an argon atmosphere, which may be due to thermal nonradiative processes.[34] Nonetheless, in a rigid matrix (CH_2Cl_2 solution at 77 K), these molecules show bright and long-lived luminescence. All compounds show well-resolved vibronic emissions, and their excitation profiles mimic the corresponding UV−vis absorptions. In the case of **2A**, containing a Naph^C* cyclometalated group, the phosphorescence appears at λ_{max} ~ 474 nm with a substantially long monoexponential decay (~480 μs). The analogous

DOI: 10.1021/acs.inorgchem.6b02826
Inorg. Chem. 2017, 56, 4829−4839

Table 2. Photophysical Data for Complexes 2A−2C, 3C, and 4C

compd	media (T/K)	λ_{ex} (nm)	λ_{em} (nm)	τ (μs)[d]	ϕ[e]
2A	CH_2Cl_2[a] (77)	355	474_{max}, 511, 551, 598	481	
	CH_2Cl_2[b] (77)	357	474_{max}, 511, 551, 598	478	
	PMMA film	340	476_{max}, 511, 600_{sh}		0.87
	solid (298)	368	557, 600_{max}, 650	35	0.06
	solid (77)	361	541_{sh}, 552, 581_{sh}, 597_{max}, 648_{sh}	65	
2B	CH_2Cl_2[a] (77)	315	444_{max}, 475, 506, 545_{sh}	23	
	CH_2Cl_2[b] (77)	360	447_{max}, 477, 509, 545_{sh}	24	
	PMMA film	330	448, 476_{max}, 503, 543_{sh}		0.68
	solid (298)	360	455, 474_{max}, 501	2.6	0.19
	Solid (77)	364	455, 474_{max}, 505	15	
2C	CH_2Cl_2[a] (77)	314	444_{max}, 474, 505, 538_{sh}	23	
	CH_2Cl_2[b] (77)	355	447_{max}, 477, 509, 538_{sh}	22	
	PMMA film	320	446, 472_{max}, 500, 540_{sh}		0.93
	solid (298)	350	446, 472_{max}, 500, 540_{sh}	17	0.35
	solid (77)	355	447, 469_{max}, 500, 540_{sh}	25	
3C	CH_2Cl_2[a] (77)	320	449_{max}, 480, 513, 543	26.9	
	CH_2Cl_2[b] (77)	350	450, 483_{max}, 515, 545, 615	24	
		400	545_{max}, 615_{sh}	1.6	
		450	545_{sh}, 615_{max}	2.0	
	PMMA film	340	453, 480_{max}, 511, 550_{sh}		0.87
	solid (298)	465	590	1.2	0.11
	solid (77)	350	465, 488_{max}, 524	20	
		390	465, 488, 545_{max}	1.8	
		460	545_{sh}, 615_{max}	2.2	
4C[c]	CH_2Cl_2[a] (77)	314, 355	444_{max}, 474, 506, 543_{sh}	19	
	CH_2Cl_2[b] (77)	320, 375	449_{max}, 479, 512, 548_{sh}	14	
		450	558	4	
	solid (298)	370	449, 474_{max}, 505, 538_{sh}	2.6	0.11
	solid (77)	370	444, 474_{max}, 506, 538_{sh}	12.7	

[a] 10^{-5} M. [b] 10^{-3} M. [c] Not soluble to prepare PMMA films in 10^{-2} M CH_2Cl_2. [d] Measurements at λ_{max}. [e] PMMA films in an argon atmosphere.

complexes **2B** and **2C**, as well as **3C** and **4C**, all of them containing R-C^C* (R = CN, CO_2Et) cyclometalated groups, exhibit a phosphorescent emission (λ_{max} ∼ 450 nm) blue-shifted with respect to **2A** (see Figure 4) and shorter decays (about 20 μs). Among those complexes containing the NC-C^C* cyclometalated group, **2C**−**4C**, the Xyl derivative (**3C**) produces an emission slightly shifted to lower energies with respect to those of **2C** and **4C**. The emissive behavior (emission energy and lifetime) of **2A** in a CH_2Cl_2 rigid matrix is very similar to that observed in other compounds containing the same "(Naph^C*)Pt" fragment.[33,35] Thus, taking into account all of these data and the TD-DFT calculations, the phosphorescent emission of **2A** can be mainly assigned to ^{3}ILCT [π(NHC) → π*(NHC)] transitions mixed with some, if any, ^{3}LL′CT [π(NHC) → π*(L)]/^{3}LMCT [π(NHC) → 5d(Pt)] character. The emission bands of **2B** and **2C**−**4C** are tentatively ascribed to transitions of monomeric species derived from ^{3}ILCT [π(NHC) → π*(NHC)]/^{3}LL′CT [π(NHC) → π*(L′)] excited states. It is worth noting that the LE absorption (S_1) of **4C** was attributed in the UV−vis section to mixed transitions L′LCT [π*(MMI) → π*(NHC)]/L′MCT [π*(MMI) → 5d(Pt)]. However, the emission features are identical with those observed for **2B**, **2C**, and **3C**, which correspond to the assignment of the S_2-calculated absorption.

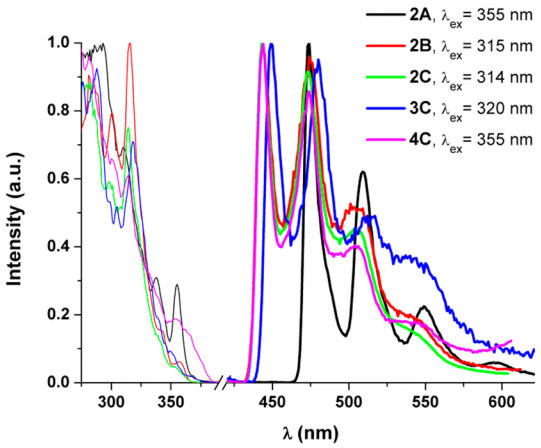

Figure 4. Normalized excitation (—) and emission (thick —) spectra in a rigid matrix of CH_2Cl_2 (10^{-5} M) at 77 K.

In fact, if assuming the lowest-energy absorption (S_1) as the emissive state, the geometry of the first excited state (T_1) should show a decrease of the Pt−S bond distance with respect to that of the ground state (S_0; see Table S11) because an electron would be promoted from a dπ*[Pt/S(MMI)] antibonding orbital in the excitation process (see the HOMO in Figure 3 or S12).

However, this is not observed, and the Pt−S distance remains invariable (Δ = 0.01). Nonetheless, there is a shortening of the Pt−C6 and Pt−C1 distances in the T_1 structure compared to those of the S_0 one, which may be attributed to promoting an electron from a dπ*(Pt/NHC) antibonding orbital (see the HOMO−1 in Figure 3 or S12) in the excitation process. This same shortening is also detected in the T_1 structures of **2B** and **2C**. Thus, the emissive behavior of

DOI: 10.1021/acs.inorgchem.6b02826
Inorg. Chem. 2017, 56, 4829−4839

2B, **2C**, and **4C** is practically identical and seems to arise from the S_1 (**2B** and **2C**) and S_2 (**4C**) low-lying absorptions. At higher concentration (10^{-3} M), the pyridine complexes **2A**–**2C** display the same emission profiles and lifetimes as those obtained in diluted solution (10^{-5} M), whereas for **3C** and **4C**, the emission profile depends on the excitation wavelength. In complex **3C**, upon monitoring of the spectra at λ_{ex} = 400 nm, an unstructured LE band at 545 nm becomes the predominant one, while emission at 615 nm can be selectively tuned by exciting at λ_{ex} = 450 nm. In complex **4C**, a LE emission band at 558 nm is observed upon excitation at 450 nm (see Figure S16). The excitation maxima of these LE bands appearing in the LE spectral region (~400 and 450 nm) and their lifetime decays (on the order of 2–4 μs) are shorter than those of the monomer emissions. As a result of taking all of this into consideration, we tentatively ascribe these LE bands to $^3\pi\pi^*$ transitions from aggregates formed by intermolecular interactions. This wavelength-dependent behavior was formerly observed in some of the isocyanide derivatives [Pt(C^C*)-$(CNR)_2$]PF_6.[35]

The spectra of the PMMA films of all of these complexes perfectly match with those in a rigid matrix of CH_2Cl_2 (see Figure 5 and Table 2). Thus, the origin of the emissions for all

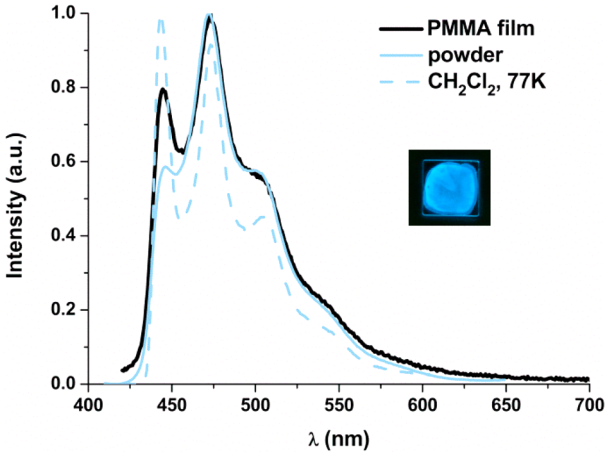

Figure 5. Normalized emission spectra of **2C**. Picture taken under UV light (λ_{ex} = 365 nm).

complexes in PMMA seems to be the same as those in a rigid matrix. QY measurements revealed that all complexes are very good blue emitters at room temperature. To the best of our knowledge, the QY values (68–93%) are among the highest ones for blue emitters of platinum(II).[25,26,28−30,32,34,58,73]

Experiments with pure powders showed that, at 298 and 77 K, complexes **2B**, **2C**, and **4C** exhibit a phosphorescent blue emission (see Figure 6) with patterns and lifetimes very similar to those in a rigid matrix of CH_2Cl_2.

Hence, their emissions most likely originate from the same excited states. However, the naphthyl derivative, **2A**, shows an orange emission with a maximum at ca. 600 nm either at 298 K or at 77 K (see Figures 6 and S17) instead of the blue one displayed in PMMA and a rigid matrix of CH_2Cl_2. Its apparent vibronic spacings (1286 cm^{-1}), which match the skeletal vibrational frequency of the NHC ligand, and the lifetime values allow it to be ascribed to $^3\pi\pi^*$ transitions from aggregates formed by intermolecular $\pi\cdots\pi$ interactions among the "Naph^C*" moieties.[25,33,35]

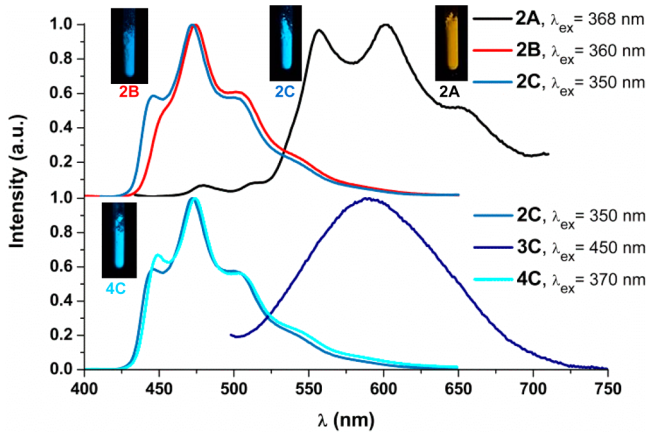

Figure 6. Normalized emission spectra in the solid state at 298 K. Pictures under UV light (λ_{ex} = 365 nm).

Complex **3C** shows at 298 K an unstructured broad band with a maximum at 590 nm that fits a short monoexponential decay (τ = 1.2 μs). Upon cooling to 77 K, the emissive behavior resembles the wavelength-dependent one registered in a rigid matrix of CH_2Cl_2 (10^{-3} M; see Figure S18). QY measurements carried out on neat solid powders (6–35%) revealed that the emissions are generally quenched because of the presence of dioxygen in the measuring chamber. The QY value is particularly low for complex **2A**, which could be attributed to the low efficiency of the emissive $^3\pi\pi^*$ excited states.

Thermogravimetric analysis of these blue emitters indicated that under argon at 1 atm they are stable at temperatures over 200 °C [247.31 °C, **2A**; 244.47 °C, **2B**; 206.82 °C, **2C**; 269.64 °C, **3C**; 239.12 °C, **4C**].

Electroluminescence (EL). **2C** and **3C** were chosen to fabricate OLEDs with blue and yellow-orange emissions, respectively, while devices containing mixtures of the two have been considered in order to obtain intermediate colors (i.e., white-light emission). Despite the conventional approach used for solution-processable organometallic platinum complex, i.e., dispersion in a conjugated host matrix with proper additives to achieve good charge-carrier balancing, we explore here a simpler bilayer structure consisting of a hole injection layer covered with a neat compound as the EML, thanks to its good film-forming ability. As the hole injection layer, a film of poly(vinylcarbazole) (PVK) is deposited onto the ITO/PEDOT:PSS-coated glass by following the procedure reported elsewhere.[74] Afterward, a neat film of **2C** or **3C** is deposited by spin coating from a $CHCl_3$ solution. This simple and unconventional, for organometallic phosphors, device architecture exhibited an unexpectedly good electrooptical performance.

In Figure 7, the EL spectra of **2C** and **3C** and of four mixtures of them at different weight ratios are reported. The EL spectrum of **2C** well corresponds to its photoluminescence (PL) spectrum with structured blue emission at 452 and 478 nm (see Figure S19). The EL spectrum of **3C** displays the broad band at 550 nm associated with its excimer emission (see Figure S20). The EL spectra of the **2C**/**3C** mixtures with a **3C** content of 50% or higher display mainly the emission of **3C**, while a balanced emission from the two compounds is obtained for the device with a **3C** content of 10–20%, giving nearly white-light emission (see Figures 7 and S21). The situation is quite different in the corresponding PL spectra, whose dominant emission comes from the **2C** compound (see Figure

DOI: 10.1021/acs.inorgchem.6b02826
Inorg. Chem. 2017, 56, 4829–4839

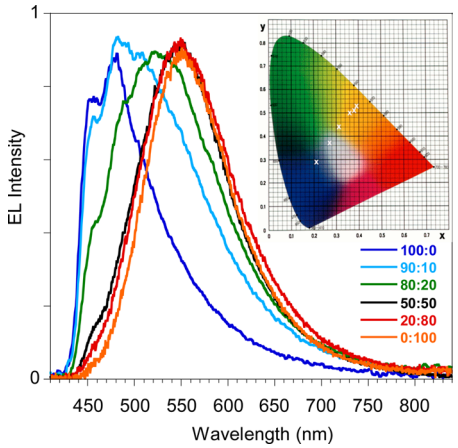

Figure 7. EL spectra of ITO/PEDOT:PSS/PVK/EML/Ba/Al devices with an EML of spin-coated **2C**, **3C**, and **2C**/**3C** at different weight ratios, driven at 5 V. The CIE 1931 chromaticity diagram is reported with the (*x*, *y*) positions of the OLED emission.

S22). The different behaviors of the PL and EL spectra of the **2C**/**3C** mixtures are mainly related to the higher efficiency of the **3C**-based device compared to the **2C** one (see Table 3).

Table 3. OLED Performances

weight ratio				
2C	**3C**	EQE (%)	L_{MAX} (cd m^{-2})	CIE 1931 (*x*, *y*)
0	100	0.3	50	(0.39, 0.53)
20	80	0.2	101	(0.38, 0.51)
50	50	0.1	9	(0.36, 0.50)
80	20	0.02	5	(0.31, 0.44)
90	10	0.007	6	(0.27, 0.37)
100	0	0.01	4	(0.21, 0.29)

These observations suggest a more favorable energy barrier for carrier injection in **3C**, in agreement with the positions of their HOMO−LUMO energy levels (see Figure S23). Despite the fact that the devices are not optimized in terms of the platinum complex layer thickness and charge-carrier regulation, they display encouraging good performance (see Table 3 and Figure S24) and stability, considering the simple and unusual bilayer device architecture unexplored for organometallic complexes processed by solution methods.

CONCLUSIONS

In this work, we report the selective synthesis of new heteroleptic cycloplatinated NHC compounds [PtCl(R-C^C*)(PPh$_3$)] (R-C = Naph, **1A**; R = CO_2Et, **1B**) and [Pt(R-C^C*)(py)(PPh$_3$)]PF$_6$ (R-C = Naph, **2A**; R = CO_2Et, **2B**) as a sole isomer, the *trans*-(C*,PPh$_3$) one. As previously observed in the synthesis of compounds [PtCl(NC-C^C*)(PPh$_3$)] (**1C**) and [Pt(NC-C^C*)(PPh$_3$)L]PF$_6$ (L = py, **2C**; CNXyl, **3C**; MMI, **4C**), the difference between T[CAr/PPh$_3$] and T[C*/PPh$_3$] was large enough to direct the clean formation of the *trans*-(C*,PPh$_3$) isomer, in such a way that this feature seems to be of general application.

Compounds **2A**−**2C**, **3C**, and **4C** prove to be among the most efficient platinum(II) blue or greenish-blue emitters in PMMA films with QY values, measured under an argon atmosphere, ranging from 68% **2B** to 93% **2C**. The emission properties of all of them match those in a rigid matrix of CH_2Cl_2. In these conditions, no significant changes in the emission properties of compounds **2C**−**4C**, differing only in the nature of one ancillary ligand, were observed. A comparison of the emission properties of compounds **2A**−**2C** differing only in the R-C^C* group shows that in **2A** the larger π system induces an important withdrawal of the electron density from the platinum center, resulting in a bathochromic shift of its emission (ca. 30 nm) with respect to those of the analogous **2B** and **2C** and in a much slower emissive decay because of the predominant ILCT character of its emission. Both the experimental data and TD-DFT calculations bring to light the practically identical electronic features of the R-C^C* moiety (R = CN, CO_2Et). In the solid state, as much **2A** as **3C** shows a weak yellowish-orange emission attributable to $\pi-\pi^*$ excited states of aggregates formed by intermolecular $\pi\cdots\pi$ interactions. Compounds **2C** and **3C** were chosen to fabricate OLEDs. Thanks to the good processability of the compounds, this is the first example of platinum-based devices fabricated by a fully solution-processed technology with a nondoped EML. This very simple approach allowed us to tune the OLED emission from blue (**2C**) to yellow-orange (**3C**), passing through white (mixtures of **2C** and **3C**).

ASSOCIATED CONTENT

Supporting Information

The Supporting Information is available free of charge on the ACS Publications website at DOI: 10.1021/acs.inorgchem.6b02826.

General procedures and instrumentation, crystallographic and computational details, ^{1}H, ^{13}C{^{1}H}, and ^{195}Pt{^{1}H} NMR spectra of **1A**, **1B**, **2A**, and **2B**, X-ray crystallographic data and structures, UV−vis data and figures, DFT and TD-DFT calculations, emission spectra, cyclic voltammograms, and EL spectra (PDF)

Crystallographic data in CIF format for compounds **2A** and **2B** (CIF)

AUTHOR INFORMATION

Corresponding Author

*E-mail: sicilia@unizar.es.

ORCID

Antonio Martín: 0000-0002-4808-574X

Chiara Botta: 0000-0001-8722-0417

Violeta Sicilia: 0000-0002-0257-0483

Notes

The authors declare no competing financial interest.

ACKNOWLEDGMENTS

This work was supported by the Spanish Ministerio de Economía y Competitividad (MINECO)/FEDER (Project CTQ2015-67461-P led by Dr. Babil Menjón) and the Departamento de Industria e Innovación del Gobierno de Aragón and Fondo Social Europeo (Grupo Consolidado E21: Química Inorgánica y de los Compuestos Organometálicos led by Dr. José M. Casas). The authors thank the Centro de Supercomputación de Galicia for generous allocation of computational resources. A.J.C. acknowledges support of a FPI grant from the Spanish government. U.G. and C.B. acknowledge support of Project I-Zeb, III Accordo Quadro CNR, Regione Lombardia.

DOI: 10.1021/acs.inorgchem.6b02826
Inorg. Chem. 2017, 56, 4829−4839

DEDICATION

Dedicated to Professor Elena Lalinde on the occasion of her 60th birthday.

REFERENCES

(1) Xu, H.; Chen, R.; Sun, Q.; Lai, W.; Su, Q.; Huang, W.; Liu, X. Recent Progress in Metal−Organic Complexes for Optoelectronic Applications. *Chem. Soc. Rev.* **2014**, *43*, 3259−3302.

(2) Xiao, L.; Chen, Z.; Qu, B.; Luo, J.; Kong, S.; Gong, Q.; Kido, J. Recent Progresses on Materials for Electrophosphorescent Organic Light-Emitting Devices. *Adv. Mater.* **2011**, *23*, 926−952.

(3) Chi, Y.; Chou, P. T. Transition-Metal Phosphors with Cyclometalating Ligands: Fundamentals and Applications. *Chem. Soc. Rev.* **2010**, *39*, 638−655.

(4) Tang, M.-C.; Chan, A. K.-W.; Chan, M.-Y.; Yam, V. W.-W. Platinum and Gold Complexes for OLEDs. *Top. Curr. Chem.* **2016**, *374*, 46.

(5) Yu, T.; Tsang, D. P.-K.; Au, V. K.-M.; Lam, W. H.; Chan, M.-Y.; Yam, V. W.-W. Deep Red to Near-Infrared Emitting Rhenium(I) Complexes: Synthesis, Characterization, Electrochemistry, Photophysics, and Electroluminescence Studies. *Chem. - Eur. J.* **2013**, *19*, 13418−13427.

(6) Yersin, H. Triplet Emitters for OLED Applications. Mechanisms of Exciton Trapping and Control of Emission Properties. *Top. Curr. Chem.* **2004**, *241*, 1−26.

(7) Yersin, H.; Rausch, A. F.; Czerwieniec, R.; Hofbeck, T.; Fischer, T. The Triplet State of Organo-Transition Metal Compounds. Triplet Harvesting and Singlet Harvesting for Efficient OLEDs. *Coord. Chem. Rev.* **2011**, *255*, 2622−2652.

(8) Williams, J. A. G. *Photochemistry and Photophysics of Coordination Compounds II*; Springer: Berlin, 2007.

(9) Li, K.; Tong, G. S. M.; Wan, Q.; Cheng, G.; Tong, W.-Y.; Ang, W.-H.; Kwong, W.-L.; Che, C.-M. Highly Phosphorescent Platinum(II) Emitters: Photophysics, Materials and Biological Applications. *Chem. Sci.* **2016**, *7*, 1653−1873.

(10) Li, K.; Guan, X.; Ma, C.-W.; Lu, W.; Chen, Y.; Che, C.-M. Blue Electrophosphorescent Organoplatinum(II) Complexes with Dianionic Tetradentate Bis(carbene) Ligands. *Chem. Commun.* **2011**, *47*, 9075−9077.

(11) Li, K.; Chen, Y.; Lu, W.; Zhu, N.; Che, C.-M. A Cyclometalated Platinum(II) Complex with a Pendent Pyridyl Motif as Solid-State Luminescent Sensor for Acidic Vapors. *Chem. - Eur. J.* **2011**, *17*, 4109−4112.

(12) Li, K.; Cheng, G.; Ma, C.; Guan, X.; Kwok, W.-M.; Chen, Y.; Lu, W.; Che, C.-M. Light-Emitting Platinum(II) Complexes Supported by Tetradentate Dianionic bis(N-Heterocyclic Carbene) Ligands: towards Robust Blue Electrophosphors. *Chem. Sci.* **2013**, *4*, 2630−2644.

(13) Zhang, Y.; Garg, J. A.; Michelin, C.; Fox, T.; Blacque, O.; Venkatesan, K. Synthesis and Luminescent Properties of cis Bis-N-Heterocyclic Carbene Platinum(II) Bis-Arylacetylide Complexes. *Inorg. Chem.* **2011**, *50*, 1220−1228.

(14) Zhang, Y.; Clavadetscher, J.; Bachmann, M.; Blacque, O.; Venkatesan, K. Tuning the Luminescent Properties of Pt(II) Acetylide Complexes through Varying the Electronic Properties of N-Heterocyclic Carbene Ligands. *Inorg. Chem.* **2014**, *53*, 756−771.

(15) Bachmann, M.; Suter, D.; Blacque, O.; Venkatesan, K. Tunable and Efficient White Light Phosphorescent Emission Based on Single Component N-Heterocyclic Carbene Platinum(II) Complexes. *Inorg. Chem.* **2016**, *55*, 4733−4745.

(16) Leopold, H.; Heinemeyer, U.; Wagenblast, G.; Münster, I.; Strassner, T. Changing the Emission Properties of Phosphorescent C^C*-Cyclometalated Thiazol-2-ylidene Platinum(II) Complexes by Variation of the β-Diketonate Ligands. *Chem. - Eur. J.* **2017**, *23*, 1118−1128 and references cited therein.

(17) Rausch, A. F.; Murphy, L.; Williams, J. A. G.; Yersin, H. Improving the Performance of Pt(II) Complexes for Blue Light Emission by Enhancing the Molecular Rigidity. *Inorg. Chem.* **2012**, *51*, 312−319.

(18) Brooks, J.; Babayan, Y.; Lamansky, S.; Djurovich, P. I.; Tsyba, I.; Bau, R. T.; Thompson, M. E. Synthesis and Characterization of Phosphorescent Cyclometalated Platinum Complexes. *Inorg. Chem.* **2002**, *41*, 3055−3066.

(19) Huo, S.; Carroll, J.; Vezzu, D. A. K. Design, Synthesis, and Applications of Highly Phosphorescent Cyclometalated Platinum Complexes. *Asian J. Org. Chem.* **2015**, *4*, 1210−1245.

(20) Williams, J. A. G.; Beeby, A.; Davies, E. S.; Weinstein, J. A.; Wilson, C. An Alternative Route to Highly Luminescent Platinum(II) Complexes: Cyclometalation with N^C^N-Coordinating Dipyridylbenzene Ligands. *Inorg. Chem.* **2003**, *42*, 8609−8611.

(21) Feng, K.; Zuniga, C.; Zhang, Y.-D.; Kim, D.; Barlow, S.; Marder, S. R.; Brédas, J. L.; Weck, M. Norbornene-Based Copolymers Containing Platinum Complexes and Bis(carbazolyl)benzene Groups in Their Side-Chains. *Macromolecules* **2009**, *42*, 6855−6864.

(22) Kui, S. C. F.; Chow, P. K.; Tong, G. S. M.; Lai, S.-L.; Cheng, G.; Kwok, C.-C.; Low, K.-H.; Ko, M. Y.; Che, C.-M. Robust Phosphorescent Platinum(II) Complexes Containing Tetradentate O^N^C^N Ligands: Excimeric Excited State and Application in Organic White-Light-Emitting Diodes. *Chem. - Eur. J.* **2013**, *19*, 69−73.

(23) Hang, X.-C.; Fleetham, T.; Turner, E.; Brooks, J.; Li, J. Highly Efficient Blue-Emitting Cyclometalated Platinum(II) Complexes by Judicious Molecular Design. *Angew. Chem., Int. Ed.* **2013**, *52*, 6753−6756.

(24) Turner, E.; Bakken, N.; Li, J. Cyclometalated Platinum Complexes with Luminescent Quantum Yields Approaching 100%. *Inorg. Chem.* **2013**, *52*, 7344−7351.

(25) Tronnier, A.; Wagenblast, G.; Münster, I.; Strassner, T. Phosphorescent Platinum(II) Complexes with C^C* Cyclometalated NHC Dibenzofuranyl Ligands: Impact of Different Binding Modes on the Decay Time of the Excited State. *Chem. - Eur. J.* **2015**, *21*, 12881−12884 and references cited therein.

(26) Hudson, Z. M.; Sun, C.; Helander, M. G.; Chang, Y. L.; Lu, Z. H.; Wang, S. N. Highly Efficient Blue Phosphorescence from Triarylboron-Functionalized Platinum(II) Complexes of N-Heterocyclic Carbenes. *J. Am. Chem. Soc.* **2012**, *134*, 13930−13933.

(27) Tronnier, A.; Nischan, N.; Metz, S.; Wagenblast, G.; Münster, I.; Strassner, T. Phosphorescent C^C* Cyclometalated Pt^{II} Dibenzofuranyl-NHC Complexes − An Auxiliary Ligand Study. *Eur. J. Inorg. Chem.* **2014**, *2014*, 256−264.

(28) Tronnier, A.; Metz, S.; Wagenblast, G.; Münster, I.; Strassner, T. Blue phosphorescent nitrile containing C^C* cyclometalated NHC platinum(II) complexes. *Dalton Trans.* **2014**, *43*, 3297−3305.

(29) Tronnier, A.; Risler, A.; Langer, N.; Wagenblast, G.; Münster, I.; Strassner, T. A Phosphorescent C^C* Cyclometalated Platinum(II)-Dibenzothiophene NHC Complex. *Organometallics* **2012**, *31*, 7447−7452.

(30) Unger, Y.; Meyer, D.; Molt, O.; Schildknecht, C.; Münster, I.; Wagenblast, G.; Strassner, T. Green−Blue Emitters: NHC-Based Cyclometalated [Pt(C^C*)(acac)] Complexes. *Angew. Chem., Int. Ed.* **2010**, *49*, 10214−10216.

(31) Tronnier, A.; Pöthig, A.; Metz, S.; Wagenblast, G.; Münster, I.; Strassner, T. Enlarging the π System of Phosphorescent (C^C*) Cyclometalated Platinum(II) NHC Complexes. *Inorg. Chem.* **2014**, *53*, 6346−6356.

(32) Tenne, M.; Metz, S.; Wagenblast, G.; Münster, I.; Strassner, T. C^C* Cyclometalated Platinum(II) N-Heterocyclic Carbene Complexes with a Sterically Demanding β-Diketonato Ligand − Synthesis, Characterization and Photophysical Properties. *Dalton Trans.* **2015**, *44*, 8444−8455.

(33) Fuertes, S.; Garcia, H.; Peralvarez, M.; Hertog, W.; Carreras, J.; Sicilia, V. Stepwise Strategy to Cyclometallated Pt^{II} Complexes with N-Heterocyclic Carbene Ligands: A Luminescence Study on New β-Diketonate Complexes. *Chem. - Eur. J.* **2015**, *21*, 1620−1631.

(34) Ko, S.-B.; Park, H.-J.; Gong, S.; Wang, X. N.; Lu, Z.-H.; Wang, S. N. Blue Phosphorescent N-Heterocyclic Carbene Chelated Pt(II) Complexes with an α-Duryl-β-Diketonato Ancillary Ligand. *Dalton Trans.* **2015**, *44*, 8433−8443.

DOI: 10.1021/acs.inorgchem.6b02826
Inorg. Chem. 2017, 56, 4829−4839

(35) Fuertes, S.; Chueca, A. J.; Perálvarez, M.; Borja, P.; Torrell, M.; Carreras, J.; Sicilia, V. White Light Emission from Planar Remote Phosphor Based on NHC Cycloplatinated Complexes. *ACS Appl. Mater. Interfaces* **2016**, *8*, 16160−16169.
(36) Fuertes, S.; Chueca, A. J.; Sicilia, V. Exploring the Transphobia Effect on Heteroleptic NHC Cycloplatinated Complexes. *Inorg. Chem.* **2015**, *54*, 9885−9895.
(37) Lu, W.; Mi, B.-X.; Chan, M. C. W.; Hui, Z.; Che, C.-M.; Zhu, N.; Lee, S.-T. Light-Emitting Tridentate Cyclometalated Platinum(II) Complexes Containing σ-Alkynyl Auxiliaries: Tuning of Photo- and Electrophosphorescence. *J. Am. Chem. Soc.* **2004**, *126*, 4958−4971.
(38) Kavitha, J.; Chang, S.-Y.; Chi, Y.; Yu, J.-K.; Hu, Y.-H.; Chou, P.-T.; Peng, S.-M.; Lee, G.-H.; Tao, Y.-T.; Chien, C.-H.; Carty, A. J. In Search of High-Performance Platinum(II) Phosphorescent Materials for the Fabrication of Red Electroluminescent Devices. *Adv. Funct. Mater.* **2005**, *15*, 223−229.
(39) Mydlak, M.; Mauro, M.; Polo, F.; Felicetti, M.; Leonhardt, J.; Diener, G.; De Cola, L.; Strassert, C. A. Controlling Aggregation in Highly Emissive Pt(II) Complexes Bearing Tridentate Dianionic N^N^N Ligands. Synthesis, Photophysics, and Electroluminescence. *Chem. Mater.* **2011**, *23*, 3659−3667.
(40) Cebrián, C.; Mauro, M.; Kourkoulos, D.; Mercandelli, P.; Hertel, D.; Meerholz, K.; Strassert, C. A.; De Cola, L. Luminescent Neutral Platinum Complexes Bearing an Asymmetric N^N^N Ligand for High-Performance Solution-Processed OLEDs. *Adv. Mater.* **2013**, *25*, 437−442.
(41) Cheng, G.; Chow, P.-K.; Kui, S. C. F.; Kwok, C.-C.; Che, C.-M. Light-Emitting Devices: High-Efficiency Polymer Light-Emitting Devices with Robust Phosphorescent Platinum(II) Emitters Containing Tetradentate Dianionic O^N^C^N Ligands. *Adv. Mater.* **2013**, *25*, 6765−6770.
(42) Li, H.; Li, J.; Ding, J.; Yuan, W.; Zhang, Z.; Zou, L.; Wang, X.; Zhan, H.; Xie, Z.; Cheng, Y.; Wang, L. Design, Synthesis, and Optoelectronic Properties of Dendrimeric Pt(II) Complexes and Their Ability to Inhibit Intermolecular Interaction. *Inorg. Chem.* **2014**, *53*, 810−821.
(43) Mróz, W.; Botta, C.; Giovanella, U.; Rossi, E.; Colombo, A.; Dragonetti, C.; Roberto, D.; Ugo, R.; Valore, A.; Williams, J. A. G. Cyclometallated Platinum(II) Complexes of 1,3-di(2-pyridyl)benzenes for Solution-Processable WOLEDs Exploiting Monomer and Excimer Phosphorescence. *J. Mater. Chem.* **2011**, *21*, 8653−8661.
(44) Li, H.; Ding, J.; Xie, Z.; Cheng, Y.; Wang, L. Synthesis, Characterization and Electrophosphorescent Properties of Mononuclear Platinum(II) Complexes Based on 2-Phenylbenzoimidazole Derivatives. *J. Organomet. Chem.* **2009**, *694*, 2777−2785.
(45) Kong, F. K.-W.; Tang, M.-C.; Wong, Y.-C.; Chan, M.-Y.; Yam, V. W.-W. Design Strategy for High-Performance Dendritic Carbazole-Containing Alkynylplatinum(II) Complexes and Their Application in Solution-Processable Organic Light-Emitting Devices. *J. Am. Chem. Soc.* **2016**, *138*, 6281−6291.
(46) Li, H.; Yuan, W.; Wang, X.; Zhan, H.; Xie, Z.; Cheng, Y. Enhancement of Luminescence Performance from the Alteration of Stacking Patterns of Pt(II) Dendrimers. *J. Mater. Chem. C* **2015**, *3*, 2744−2750.
(47) Hsu, C.-W.; Ly, K. T.; Lee, W.-K.; Wu, C.-C.; Wu, L.-C.; Lee, J.-J.; Lin, T.-C.; Liu, S.-H.; Chou, P.-T.; Lee, G.-H.; Chi, Y. Triboluminescence and Metal Phosphor for Organic Light-Emitting Diodes: Functional Pt(II) Complexes with Both 2-Pyridylimidazol-2-ylidene and Bipyrazolate Chelates. *ACS Appl. Mater. Interfaces* **2016**, *8*, 33888−33898.
(48) Tseng, C.-H.; Fox, M. A.; Liao, J.-L.; Ku, C.-H.; Sie, Z.-T.; Chang, C.-H.; Wang, J.-Y.; Chen, Z.-N.; Lee, G.-H.; Chi, Y. Luminescent Pt(II) Complexes Featuring Imidazolylidene−Pyridylidene and Dianionic Bipyrazolate: from Fundamentals to OLED Fabrications. *J. Mater. Chem. C* **2017**, *5*, 1420−1435.
(49) Mabbott, D. J.; Mann, B. E.; Maitlis, P. M. Cationic (η^3-allylic)(η^4-diene)-Palladium and -Platinum Complexes. *J. Chem. Soc., Dalton Trans.* **1977**, 294−299.
(50) Zucca, A.; Maidich, L.; Carta, V.; Petretto, G. L.; Stoccoro, S.; Agostina Cinellu, M.; Pilo, M. I.; Clarkson, G. J. Cyclometalated Complexes of Platinum(II) with 2-Vinylpyridine. *Eur. J. Inorg. Chem.* **2014**, *2014*, 2278−2287.
(51) Maidich, L.; Zuri, G.; Stoccoro, S.; Cinellu, M. A.; Zucca, A. Assembly of Symmetrical and Unsymmetrical Platinum(II) Rollover Complexes with Bidentate Phosphine Ligands. *Dalton Trans.* **2014**, *43*, 14806−14815.
(52) Minghetti, G.; Zucca, A.; Stoccoro, S.; Cinellu, M. A.; Manassero, M.; Sansoni, M. Six-Membered Cyclometallated Derivatives of Platinum(II) Derived from 2-Benzylpyridines. Crystal and Molecular Structure of [Pt(L)(Ph_3P)Cl] (HL = 2-(1-methylbenzyl)-pyridine). *J. Organomet. Chem.* **1994**, *481*, 195−204.
(53) Vicente, J.; Abad, J. A.; Martinez-Viviente, E.; Jones, P. G. Study of the Reactivity of 2-Acetyl-, 2-Cyano-, 2-Formyl-, and 2-Vinylphenyl Palladium(II) Complexes. Mono- and Triinsertion of an Isocyanide into the Pd−C Bond. A 2-Cyanophenyl Palladium Complex as a Ligand. *Organometallics* **2002**, *21*, 4454−4467.
(54) Vicente, J.; Abad, J. A.; Hernández-Mata, F. S.; Jones, P. G. An Unusual Palladium Complex Involved in an Unusual Rearrangement of Ortho-palladated Aryldithioacetals. *J. Am. Chem. Soc.* **2002**, *124*, 3848−3849.
(55) Vicente, J.; Arcas, A.; Gálvez-López, M. D.; Jones, P. G. Bis(2,6-initroaryl)platinum(II) Complexes. Cis/Trans Isomerization. *Organometallics* **2006**, *25*, 4247−4259.
(56) Casas, J. M.; Fornies, J.; Fuertes, S.; Martin, A.; Sicilia, V. New Mono- and Polynuclear Alkynyl Complexes Containing Phenylacetylide as Terminal or Bridging Ligand. X-ray Structures of the Compounds NBu_4[Pt($CH_2C_6H_4P$(o-tolyl)$_2$-κC,P)(C≡CPh)$_2$], [Pt($CH_2C_6H_4P$(o-tolyl)$_2$-κC,P)(C≡CPh)(CO)], [{Pt($CH_2C_6H_4P$(o-tolyl)$_2$-κC,P)(μ-C≡CPh)}$_2$], and [{Pt($CH_2C_6H_4P$(o-tolyl)$_2$-κC,P)(C≡CPh)$_2$Cu}$_2$]. *Organometallics* **2007**, *26*, 1674−1685.
(57) Sicilia, V.; Fuertes, S.; Martin, A.; Palacios, A. N-Assisted CPh−H Activation in 3,8-Dinitro-6-phenylphenanthridine. New C,N-Cyclometalated Compounds of Platinum(II): Synthesis, Structure, and Luminescence Studies. *Organometallics* **2013**, *32*, 4092−4102.
(58) Tronnier, A.; Pöthig, A.; Herdtweck, E.; Strassner, T. C^C* Cyclometalated Platinum(II) NHC Complexes with β-Ketoimine Ligands. *Organometallics* **2014**, *33*, 898−908.
(59) Tronnier, A.; Nischan, N.; Strassner, T. C^C*-Cyclometalated Platinum(II) Complexes with Trifluoromethyl-Acetylacetonate Ligands − Synthesis and Electronic Effects. *J. Organomet. Chem.* **2013**, *730*, 37−43.
(60) Hudson, Z. M.; Blight, B. A.; Wang, S. N. Efficient and High Yield One-Pot Synthesis of Cyclometalated Platinum(II) beta-Diketonates at Ambient Temperature. *Org. Lett.* **2012**, *14*, 1700−1703.
(61) Rao, Y.-L.; Wang, S. N. Impact of Constitutional Isomers of ($BMes_2$)phenylpyridine on Structure, Stability, Phosphorescence, and Lewis Acidity of Mononuclear and Dinuclear Pt(II) Complexes. *Inorg. Chem.* **2009**, *48*, 7698−7713.
(62) Harris, C. F.; Vezzu, D. A. K.; Bartolotti, L.; Boyle, P. D.; Huo, S. Q. Synthesis, Structure, Photophysics, and a DFT Study of Phosphorescent C*N^N- and C^N^N-Coordinated Platinum Complexes. *Inorg. Chem.* **2013**, *52*, 11711−11722.
(63) Karakostas, N.; Mavridis, I. M.; Seintis, K.; Fakis, M.; Koini, E. N.; Petsalakis, I. D.; Pistolis, G. Highly Efficient and Unidirectional Energy Transfer within a Tightly Self-Assembled Host-Guest Multichromophoric Array. *Chem. Commun.* **2014**, *50*, 1362−1365.
(64) Jude, H.; Krause Bauer, J. A.; Connick, W. B. Tuning the Electronic Structures of Platinum(II) Complexes with a Cyclometalating Aryldiamine Ligand. *Inorg. Chem.* **2004**, *43*, 725−733.
(65) Crespo, M.; Anderson, C. M.; Kfoury, N.; Font-Bardia, M.; Calvet, T. Reductive Elimination from Cyclometalated Platinum(IV) Complexes To Form Csp2−Csp3 Bonds and Subsequent Competition between Csp2−H and Csp3−H Bond Activation. *Organometallics* **2012**, *31*, 4401−4404.
(66) Alcarazo, M.; Radkowski, K.; Goddard, R.; Furstner, A. Metal Complexes with Carbene Ligands Stabilized by Lateral Enamines. *Chem. Commun.* **2011**, *47*, 776−778.

DOI: 10.1021/acs.inorgchem.6b02826
Inorg. Chem. 2017, 56, 4829−4839

(67) Anderson, C.; Crespo, M.; Rochon, F. D. Stereoselective Oxidative Addition of Methyl Iodide to Chiral Cyclometallated Platinum(II) Compounds Derived from (R)-(+)-1-(1-naphthylethylamine). Crystal Structure of [PtMe{3-(*R*)-($C_{10}H_7$)-CHMeNCHC$_4$H$_2$S}PPh$_3$]. *J. Organomet. Chem.* **2001**, *631*, 164−174.
(68) Rodríguez, J.; Zafrilla, J.; Albert, J.; Crespo, M.; Granell, J.; Calvet, T.; Font-Bardia, M. Cyclometallated Platinum(II) Compounds with Imine Ligands Derived from Amino Acids: Synthesis and Oxidative Addition Reactions. *J. Organomet. Chem.* **2009**, *694*, 2467−2475.
(69) Diez, A.; Fornies, J.; Fuertes, S.; Lalinde, E.; Larraz, C.; Lopez, J. A.; Martin, A.; Moreno, M. T.; Sicilia, V. Synthesis and Luminescence of Cyclometalated Compounds with Nitrile and Isocyanide Ligands. *Organometallics* **2009**, *28*, 1705−1718.
(70) Graber, S.; Doyle, K.; Neuburger, M.; Housecroft, C. E.; Constable, E. C.; Costa, R. D.; Orti, E.; Repetto, D.; Bolink, H. J. A Supramolecularly-Caged Ionic Iridium(III) Complex Yielding Bright and Very Stable Solid-State Light-Emitting Electrochemical Cells. *J. Am. Chem. Soc.* **2008**, *130*, 14944−14945.
(71) Jude, H.; Rein, F. N.; White, P. S.; Dattelbaum, D. M.; Rocha, R. C. Synthesis, Structure, and Electronic Properties of a Dimer of Ru(bpy)(2) Doubly Bridged by Methoxide and Pyrazolate. *Inorg. Chem.* **2008**, *47*, 7695−7702.
(72) Williams, J. A. G. Photochemistry and Photophysics of Coordination Compounds: Platinum. *Top. Curr. Chem.* **2007**, *281*, 205−268.
(73) Soellner, J.; Tenne, M.; Wagenblast, G.; Strassner, T. Phosphorescent Platinum(II) Complexes with Mesoionic 1*H*-1,2,3-Triazolylidene Ligands. *Chem. - Eur. J.* **2016**, *22*, 9914−9918.
(74) Giovanella, U.; Betti, P.; Botta, C.; Destri, S.; Moreau, J.; Pasini, M.; Porzio, W.; Vercelli, B.; Bolognesi, A. All-Conjugated Diblock Copolymer Approach to Improve Single Layer Green Electroluminescent Devices. *Chem. Mater.* **2011**, *23*, 810−816.

DOI: 10.1021/acs.inorgchem.6b02826
Inorg. Chem. 2017, 56, 4829−4839

ACS APPLIED MATERIALS & INTERFACES

Research Article

www.acsami.org

White Light Emission from Planar Remote Phosphor Based on NHC Cycloplatinated Complexes

Sara Fuertes,[†] Andrés J. Chueca,[†] Mariano Perálvarez,[‡] Pilar Borja,[†] Marc Torrell,[‡] Josep Carreras,[‡] and Violeta Sicilia*[,§]

[†]Departamento de Química Inorgánica, Facultad de Ciencias, Instituto de Síntesis Química y Catálisis Homogénea (ISQCH), CSIC−Universidad de Zaragoza, Pedro Cerbuna 12, 50009, Zaragoza, Spain

[‡]IREC, Catalonia Institute for Energy Research, Jardins de les Dones de Negre 1, PL2, 08930 Sant Adrià de Besòs, Barcelona Spain

[§]Departamento de Química Inorgánica, Escuela de Ingeniería y Arquitectura de Zaragoza, Instituto de Síntesis Química y Catálisis Homogénea (ISQCH), CSIC−Universidad de Zaragoza, Campus Río Ebro, Edificio Torres Quevedo, 50018, Zaragoza, Spain

Supporting Information

ABSTRACT: We report on the generation of bright white luminescence through solid-state illumination of remote phosphors based on novel cycloplatinated N-heterocyclic carbene (NHC) compounds. Following a stepwise protocol we got the new NHC compound [{Pt(μ-Cl)(C^C*)}$_2$] (**4**) (HC^C*-κC* = 1-(4-(ethoxycarbonyl)phenyl)-3-methyl-1*H*-imidazol-2-ylidene), which was used together with the related ones **4a** (HC^C*-κC*= 1-(4-cyanophenyl)-3-methyl-1*H*-imidazol-2-ylidene) and **4b** (HC^C*-κC*= 3-methyl-1-(naphthalen-2-yl)-1*H*-imidazol-2-ylidene) as starting materials for the synthesis of the new ionic derivatives [Pt(R-C^C*) (CNR′)$_2$]PF$_6$ (R = −COOEt, R′ = *t*-Bu (**5**), Xyl (**6**); R = −CN, R′ = *t*-Bu (**7**), Xyl (**8**); R^C = Naph, R′ = *t*-Bu (**9**), Xyl (**10**)). The X-ray structures of **6** and **8**−**10** have been determined. The photophysical properties of these cationic compounds have been studied and supported by the time-dependent-density functional theory (TD-DFT) calculations. The compounds **5**, **8**, and **9** have been revealed as the most efficient emitters in the solid state with quantum yields of 41%, 21%, and 40%, respectively. White-light remote-phosphors have been prepared just by stacking different combinations of these compounds and [Pt(bzq) (CN) (CN^{t}Bu)] (**R1**) as blue (**5**, **8**), yellow (**9**), and red (**R1**) components onto the same substrate. The CCT (correlated color temperature) and the CRI (color rendering index) of the emitted white-light have been tuned by accurately controlling the individual contributions.

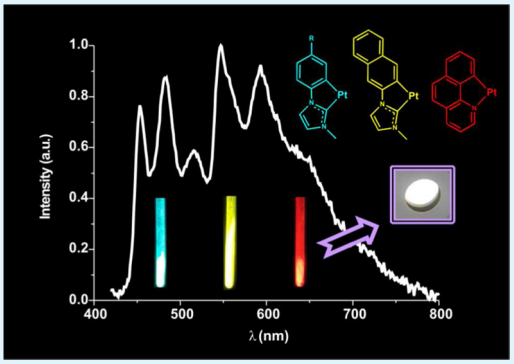

KEYWORDS: *N-heterocyclic carbenes, metalacycles, platinum, remote-phosphors, white light*

INTRODUCTION

General lighting accounts for around 15% of the world's electricity consumption, and it is expected that demand will rise 50% by 2030. In light of this, it is widely accepted that corrective measures to minimize energy consumption have to be taken. One of these measures is the massive deployment of solid-state lighting (SSL) technology in the general lighting arena.[1] LEDs, with outstanding energy-conversion efficiency (up to 50%) together with their significant durability (around 25 000 h) and sustainability, have the potential for inducing important energy savings. Given the inherently narrow emission from conventional *p*−*n* junctions, the achieving white light emission requires the implementation of additional strategies. At present, the technology provides two options: The first approach is implementing a RGB (red, green, and blue) multichip in which the three emitters are closely packaged forming a chromaticity-tunable light source. The second approach is based on the use of phosphor materials. Such compounds are used to transmit and down-convert the UV or blue light delivered from a LED pumping source into longer wavelengths, which are combined to create white light. Of course, under this approach, chromaticity is no longer dynamically tunable but can be established by monitoring fabrication parameters. Today, most general lighting applications are based on this option because of the uneven efficiency observed across the visible range in direct-emission LEDs. In addition, the emission properties of LEDs based on phosphor conversion are far less sensitive to temperature than direct-emission LEDs, allowing simpler (and less expensive) control strategies to maintain chromaticity than in the case RGB multichip option. Regarding the structure of these phosphor-based white LEDs, the majority is based on integrating the active powder on the LED chip, that is, into the package (PC-LEDs, phosphor-converted LEDs). In this configuration, the phosphor is subjected to the heat generated at the *p*−*n* junction. Relatively high temperatures can affect the phosphor performance and an efficiency drop can be

Received: March 17, 2016
Accepted: June 7, 2016
Published: June 7, 2016

DOI: 10.1021/acsami.6b03288
ACS Appl. Mater. Interfaces 2016, 8, 16160−16169

observed. A second strategy to get white light is the remote configuration. This concept, existing for more than ten years, is current drawing renewed attention due to the sizable gains with respect to systems based on PC-LEDs.[2] The phosphor is now applied as a separate 2D or 3D component optically pumped by an UV or blue LED rather than being included as a part of the package. Under this scheme, the phosphor blocks the line-of-sight to the LEDs, reducing the glare and improving user visual comfort. Moreover, placing the emitting centers far from the LED-dye pump-source its operating temperature is lower and more stable thus providing improved lifetime (lower thermal degradation) and color stability. Apart from this, the remote phosphor, placed far away from the LED dye and incorporated into a highly efficient reflector system, reduces the chances of chip reabsorption as well as harvests a notably percentage of the light emitted backward, increasing the total output power, especially if compared to white PC-LEDs.

Concerning the chemical composition of these phosphors, those used in the SSL industry are generally based on rare-earth-doped inorganic compounds. Materials like aluminates, silicates, garnets or nitrides incorporate rare-earth elements, typically Ce^{3+} and Eu^{2+}, as activator ions. However, despite the extraordinary quantum efficiency of these compounds, some logistic problems are foreseen on the horizon. One of them is the dependency on China policies, responsible of about 85% of the global production. The other is the relative scarcity of rare earth elements that unavoidable leads to a long-term price rise.[3] In this framework, it becomes clear that new approaches are needed in order to minimize the dependence of the lighting market on rare-earth availability. The work presented here represents our approach to face this issue. The strategy basically consists in using, organometallic compounds as phosphor converters, in particular in a remote configuration, taking advantage of the aforementioned benefits associated with these systems. The idea arose from the very appealing properties exhibited by this kind of compounds when incorporated as phosphorescent dyes for PHOLEDs (phosphorescent-OLEDs) and WOLEDs (white-OLEDs).[4−9] In our first work in this application field,[10] we showed, by the first time, the potential of NHC cycloplatinated complexes to provide white light when combined with blue LED pump. In that case, the phosphor was introduced within the LED package by mixing it with a conventional transparent encapsulant. Unfortunately, fast decrease of the emission was observed, probably related to both heat degradation, due to the proximity to the LED junction, and photon-induced degradation linked to the intense pump flux. The remote phosphor configuration presented here eliminates the former.

From the point of view of chemical science, the use of NHCs as cyclometalated ligands with two C-σ bonds implicates an even greater heightening of the d-d energy levels on the metal center, enlarging the energy gap with the emissive excited states, avoiding the thermal quenching and improving the quantum yields.[11] Examples of phosphorescent compounds of platinum(II) containing C^C*-cyclometalated NHCs ligands are still fairly limited.[12−24]

Heteroleptic square planar platinum(II) complexes with different kinds of ancillary ligands show significant scope for tuning their emissive properties over the entire visible spectra by modification of the cyclometalated and/or the ancillary ligands.[25−32]

Keeping on with our stepwise protocol to prepare C^N-[31,32] and C^C*-[10,33] cyclometalated platinum(II) complexes, we report here the synthesis of the new NHC compound [{Pt(μ-Cl)-(C^C*)}$_2$] (**4**) (HC^C*-κC* = 1-(4-(ethoxycarbonyl)phenyl)-3-methyl-1*H*-imidazol-2-ylidene), which was used together with the related ones **4a** (HC^C*-κC*= 1-(4-cyanophenyl)-3-methyl-1*H*-imidazol-2-ylidene) and **4b** (HC^C*-κC*= 3-methyl-1-(naphthalen-2-yl)-1*H*-imidazol-2-ylidene) as starting materials for the synthesis of a series of ionic derivatives [Pt(R-C^C*) (CNR′)$_2$]PF$_6$ (R = −COOEt, R′ = *t*-Bu (**5**), Xyl (**6**); R = −CN, R′ = *t*-Bu (**7**), Xyl (**8**); R^C = Naph, R′ = *t*-Bu (**9**), Xyl (**10**)). The effects of the R and R′ substituents on the photophysical properties have been studied. Moreover, we have prepared the first optical devices using C^C*- and C^N-cyclometalated platinum(II) complexes as blue (**5**, **8**), yellow (**9**) and red ([Pt(bzq) (CN) (CN^{t}Bu)], bzq = benzo[*h*]-quinoline; **R1**) emitters in the implementation of remote-phosphors for white light illumination.

EXPERIMENTAL SECTION

General Comments. Instrumental methods used for characterization and spectroscopic studies, DFT computational details and X-ray structures together with the synthetic procedures and characterization data are contained in the Supporting Information. All chemicals were used as supplied and [{Pt(μ-Cl)(η^3-2-Me-C$_3$H$_4$)}$_2$],[34] [{Pt(μ-Cl) (NC-C^C*)}$_2$] (**4a**),[33] [{Pt(μ-Cl) (Naph-C^C*)}$_2$] (**4b**)[10] and [Pt(bzq) (CN) (CN^{t}Bu)] (**R1**)[30] were prepared following the literature procedures. Slight modifications of previous synthetic methods were employed to prepare **1**.[35−38]

Remote-phosphor fabrication. The deposition of the phosphors was carried out via screen printing using suspensions of complexes **5**, **8**, **9** and [Pt(bzq) (CN) (CN^{t}Bu)] (**R1**) as blue (**5**, **8**), yellow (**9**) and red (**R1**) components on a commercial transparent terpineol based ink vehicle (fuel cell materials 311006), on top of a glass disc of 1.6 mm thick and 27 mm diameter. Each layer deposited contained a total weight of 1.5 mg. Complexes with different ancillary ligands such as **8** and **9** are not compatible because ligand exchange processes have been observed to occur and they should be deposited in different layers and with ink vehicle layers in between to avoid the contact. However, complexes **5** and **9** containing the same ancillary ligand, ^{t}BuNC, could be mixed together in the same suspension. Besides, complex **R1** was suspended together with the ink vehicle and deposited as red layer. To control the final chromatic properties of the device, the amount of each phosphor was determined by their individual spectra and their respective quantum efficiency. In practice, this was correlated to the number of sublayers of each suspension deposited and the proportion of the platinum complexes in the suspensions. In general, all the compounds are deposited by successive steps (multiple sublayers), except the red one (**R1**) that is obtained by a single deposition. The order of the compounds on the glass substrate has been established according to energy of their respective emissions, aiming at avoiding (or minimizing) the reabsorption of the light emitted by previous phosphors. Therefore, the first layer to be deposited will be that with the shorter emission wavelength.

Device 1 (DEV1). A suspension of 40% (**5** + **9**) w/w was prepared by mixing **9** (30.0 mg, 0.042 mmol) and **5** (68.0 mg, 0.092 mmol) with 147 mg of ink vehicle. Compound **R1** was mixed with the ink vehicle to give a 10% w/w suspension. The final composition was set as 15 sublayers of (**5** + **9**), 3 sublayers of ink vehicle and 1 layer of **R1**.

Device 2 (DEV2). A suspension of 40% (**5** + **9**) w/w was prepared by mixing **9** (12.2 mg, 0.017 mmol) and **5** (56.5 mg, 0.077 mmol) with 103 mg of ink vehicle. Compound **R1** was mixed with the ink vehicle to give a 10% w/w suspension. The final composition was set as 26 sublayers of (**5** + **9**), 3 sublayers of ink vehicle and 1 layer of **R1**.

Device 3 (DEV3). Suspensions of **8** (40% w/w) (50.0 mg, 0.064 mmol), **9** (40% w/w) (46.5 mg, 0.065 mmol), and **R1** (10% w/w) were prepared and supported on the glass disc separately. The final composition was set as 3 sublayers of **8**, 3 sublayers of ink vehicle, 4 sublayers of **9**, 3 sublayers of ink vehicle, and 1 layer of **R1**.

DOI: 10.1021/acsami.6b03288
ACS Appl. Mater. Interfaces 2016, 8, 16160−16169

RESULTS AND DISCUSSION

Stepwise Synthesis of the C^C*-Cyclometalated N-Heterocyclic Carbene Complex [{Pt(μ-Cl)(C^C*)}$_2$] (4) (HC^C*-κC*= 1-(4-(Ethoxycarbonyl)phenyl)-3-methyl)-1*H*-imidazol-2-ylidene). The N-heterocyclic carbene precursor **1**, the corresponding imidazolium salt, 1-(4-ethoxycarbonylphenyl)-3-methyl-1*H*-imidazolium iodide **2**, the carbene complex [PtCl(η^3-2-Me-C_3H_4) (HC^C*-κC*)] (**3**) (HC^C*-κC*= 1-(4-ethoxycarbonylphenyl)-3-methyl)-1*H*-imidazol-2-ylidene) and the C^C*-cyclometalated N-heterocyclic carbene complex [{Pt(μ-Cl)(C^C*)}$_2$] **4** were achieved following our previously reported stepwise protocol for C^C*-cyclometalated complexes of platinum(II),[10,33] see Scheme S1. NMR and IR spectroscopic data (see SI) are consistent with the proposed structures for species **1**−**4** and similar to the observed ones for analogous compounds with different C^C*groups.[10,33] The new complex, **4**, and the related [{Pt(μ-Cl)(R-C^C*)}$_2$] (R = CN (**4a**); R−C = Naph (**4b**)) were used as starting materials for the synthesis of new phosphorescent Pt(II) derivatives to compare their emitting properties.

Synthesis and Characterization of [Pt(R−C^C*)(CNR′)$_2$]PF$_6$ (R′ = *t*-Bu, Xyl). Compounds **5**−**10** were prepared by treatment of a suspension of the corresponding dinuclear chloride compound [{Pt(μ-Cl)(R-C^C*)}$_2$] (R = COOEt (**4**), CN (**4a**); R−C = Naph (**4b**)) with 2 equiv of KPF_6 and 4 equiv of CNR′ (R′ = *tert*-butyl (^{t}Bu), 2,6-dimethylphenyl (Xyl)) in acetone. After removing the KCl, all compounds **5**−**10** were obtained from their corresponding solutions as pure solids in good yields (77−88%) (see Scheme 1 and Experimental Section).

Scheme 1. Reactions and Numerical Scheme for NMR Purposes

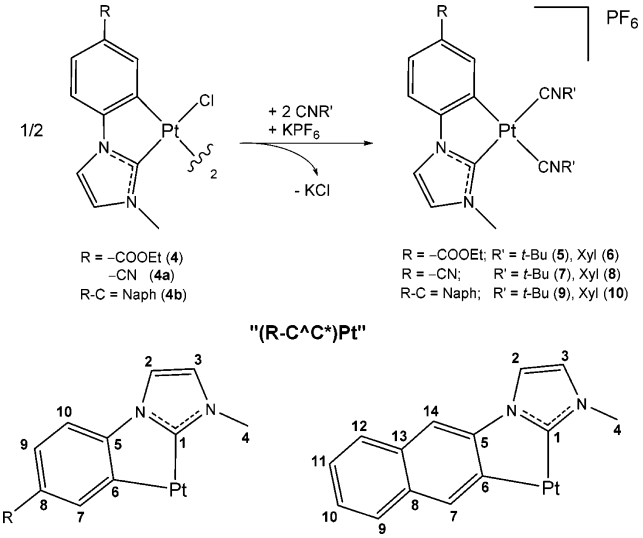

Their IR spectra show two absorptions at ∼2200 cm^{-1} due to ν(C≡N) assignable to terminal isocyanide ligands.[29,31,32,39,40] The MALDI(+) mass spectra show the corresponding [Pt(R−C^C*) (CNR′)$_2$]$^+$ peaks and the conductivity measurements confirm their behavior as 1:1 electrolytes. The ^{1}H NMR spectra of **5**−**10** show the expected signals for the R−C^C* and the CNR′ ligands with intensity ratios corresponding to the proposed stoichiometry (NMR spectra of **5** and **6** are shown as examples in Figures S3 and S4). As depicted in Figure 1, the

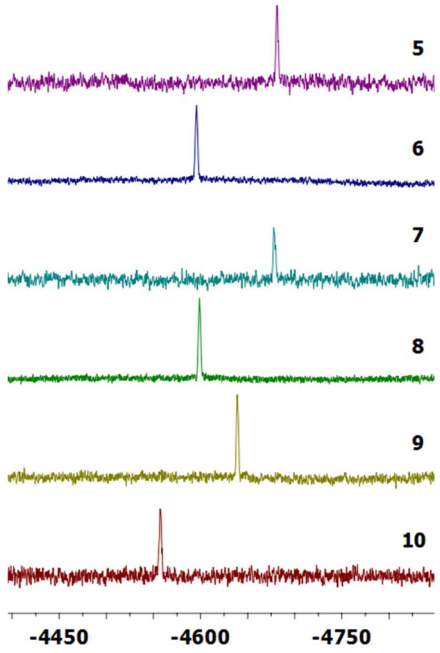

Figure 1. ^{195}Pt{^{1}H} NMR spectra of **5**−**10** in CD_2Cl_2.

^{195}Pt NMR spectra of **5**−**10** exhibit the corresponding singlets at about −4600 ppm with those of the Xyl derivatives (**6**, **8**, and **10**) being less shielded (∼80 ppm) than those of the ^{t}Bu ones (**5**, **7**, and **9**).

This may be related to the presence of the electron-withdrawing Xyl ring.[27] Also, as inferred from the ^{195}Pt chemical shifts of **5**, **7**, **9** (or **6**, **8**, **10**) the CN and COOEt groups present electronic features rather similar, while the larger π system due to the extra aromatic ring in the naphthyl derivatives withdraw more electron density from the platinum center causing the downfield shift (∼40 ppm) of the ^{195}Pt NMR signals for **9** and **10** when compared to those of **5**−**8**.

Single crystals of **6** and **8**−**10** were studied by X-ray crystallography (Figures 2 and S5−S8 and Tables S1 and S2). In all these complexes the platinum(II) center exhibits a distorted square-planar environment because of the the small bite angle of the cyclometalated ligand (R−C^C*) [78.8(12)−79.9(6)°].

This angle and the Pt−C1 and Pt−C6 bond lengths are similar to those observed for other platinum compounds with cyclometalated NHCs.[10,12−20,33,21−24] Two isocyanide ligands complete the coordination sphere of platinum(II). The Pt−C(CNR′) and C≡N bond lengths are comparable to those observed in other Pt(II) isocyanide complexes.[27,31,32,39−42] The distances Pt−C20 and Pt−C30 are almost identical, in agreement with the rather similar trans influence of both carbon atoms (C1, C6).[33]

The CNR′ ligands show the expected linear arrangement. In complexes **6**, **8**, and **10**, one of the Xyl rings (C31−C36) is not coplanar with the Pt coordination plane (Pt1, C1, C6, C20, C30), forming dihedral angles of 52.3(11)° **6**, 67.09(3)° **8**, 68.13(18)°, and 70.53(19) **10**.[43]

The cation complexes in **6** arrange themselves in head-to-tail pairs supported by π···π, C−H···π, and C−H···O intermolecular contacts. Figure S5 illustrates how the Xyl ring of the coplanar group overlaps with the NHC ligand (3.30 Å) while the other one is pointing to the ester group, assisted by the C−H···O contacts (C37−O2 = 3.43 Å). Also, neighbor

DOI: 10.1021/acsami.6b03288
ACS Appl. Mater. Interfaces 2016, 8, 16160−16169

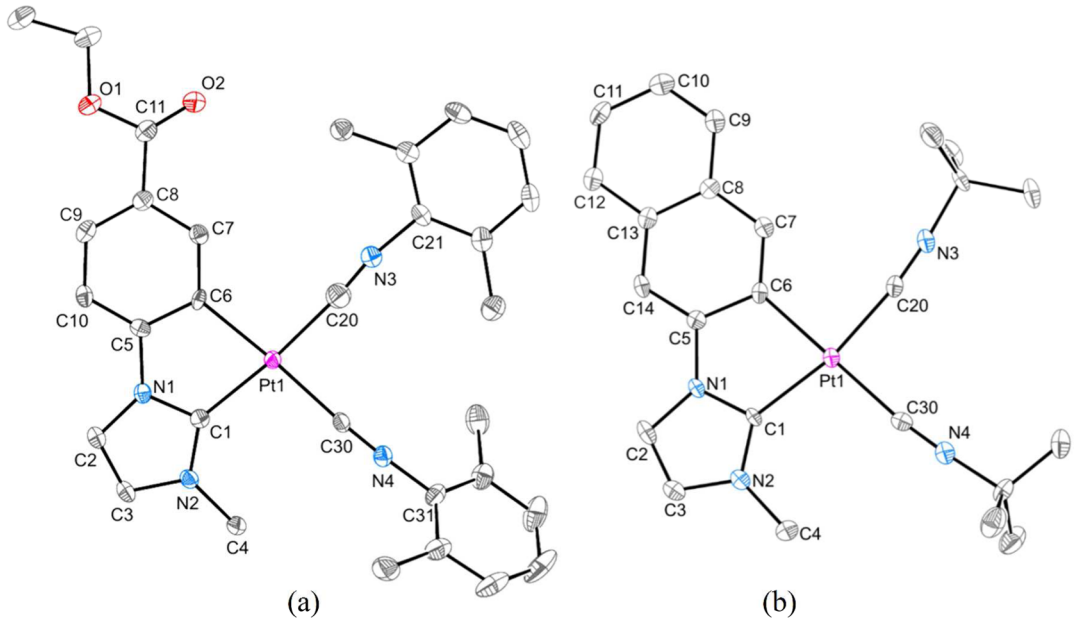

Figure 2. Molecular structures of the cations of **6** (a) and **9·Me$_2$CO** (b). Thermal ellipsoids are drawn at the 50% probability level. Hydrogen atoms and solvent molecules have been omitted for clarity.

molecular pairs are packed in a head-to-tail fashion through offset $\pi-\pi$ interactions between the NHC fragments 3.29 Å (see Figure S5b). There are no Pt···Pt interactions within the pairs (5.28 Å) or between adjacent pairs (7.64 Å). A similar arrangement is observed for complexes **8** and **10** (Figures S6b and S8b). While in complex **9**, the molecules arrange in a head-to-tail fashion and assemble themselves into 1D chains via $\pi\cdots\pi$ interactions between the NHC fragments (~3.5 Å) and C−H···π contacts between the Me (NHC) and NHC groups (C4−C10 = 3.62 Å) (see Figure S7). No metallophilic contacts are observed (Pt···Pt 5.60 Å).

Absorption Spectra and DFT Calculations. UV−vis spectra data of compounds **5**−**10** are summarized in Table S3. As shown in Figure 3, they all display strong absorption bands

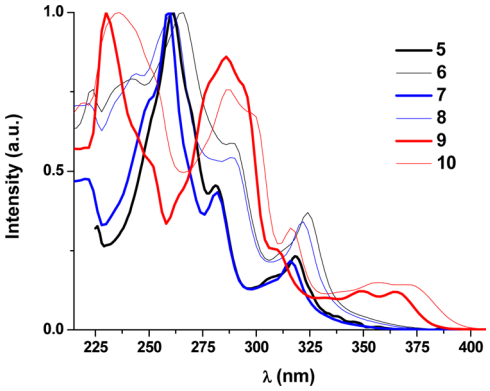

Figure 3. Normalized absorption spectra of **5**−**10** in CH_2Cl_2 (5×10^{-5} M).

at ~260 (**5**−**8**) and 290 nm (**9** and **10**) ($\varepsilon > 10^4$ $M^{-1}cm^{-1}$) which are normally attributed to the ^{1}IL or metal-perturbed IL transitions of the NHC ligand. Complexes **5**−**8** also show less intense ($\varepsilon \approx 10^3$ $M^{-1}cm^{-1}$) lowest energy absorption bands at λ around 320 nm. The similitude of the UV−vis spectra of compounds **5** and **6** with those of **7** and **8**, indicates that the electronic features of the R-groups (CN and COOEt) of the C^C* ligands are rather similar.

For complexes **9** and **10**, the lowest energy absorption band appears at λ > 360 nm, which may be due to the presence of a more extended conjugation in the R−C^C* ligand. The low-energy absorptions (λ > 300 nm) appear slightly shifted to the red when R′ is Xyl with respect to those when R′ = ^{t}Bu, thus suggesting a certain contribution of the ancillary ligands to the frontier orbitals (FOs). UV−vis spectra of **5**−**10** present a moderate negative solvatochromism (see Figure S9) in the lower energy spectral region (λ > 350 nm), which is characteristic of charge transfer (CT) transitions.[44] The solid-sate diffuse reflectance UV−vis spectra (Figure S10) show no particular differences with respect to those observed in dichloromethane solution.

For a correct assignment of the absorption bands and to better analyze the effect of the R and R′-substituents on the photophysical properties, we have carried out DFT and TD-DFT calculations in CH_2Cl_2 solution for **6** and **8**−**10** (Tables S4−S9 and Figures 4 and S11−S13). The highest occupied molecular orbitals HOMOs are mainly constructed from π-orbitals of the C^C* ligand (85−96%) with a small contribution of the platinum (dπ) (3−12%) and the isocyanide ligands (1−4%). In particular, in **9** and **10**, the HOMO is almost entirely localized on the naphthyl fragment (>90%). By contrast, the lowest unoccupied molecular orbitals LUMOs are distributed over the platinum center (23−30%), the C^C* (37−49%) and CNR′ (26−35%) ligands. The calculated allowed transitions are in good agreement with the experimentally observed absorption maxima (Figures 4, S12, and S13). The major contribution (>94%) to the lowest energy calculated absorptions (S_1) for **6** and **8**−**10** is the HOMO → LUMO transition. Therefore, they can be attributed to mixed LL′CT [π(NHC) → π^*(CNR′)]/LMCT [π(NHC) → 5d(Pt)] transitions, with an important ILCT [(NHC)] character for complexes **9** and **10**. The major contribution (>91%) to the S_2 excited state for **6** and **8**−**10** is the H-1 → LUMO transition which has a mixed L′MCT [π(CNR′) → 5d(Pt)]/L′LCT [π(CNR′) → π^* (NHC)]

DOI: 10.1021/acsami.6b03288
ACS Appl. Mater. Interfaces 2016, 8, 16160−16169

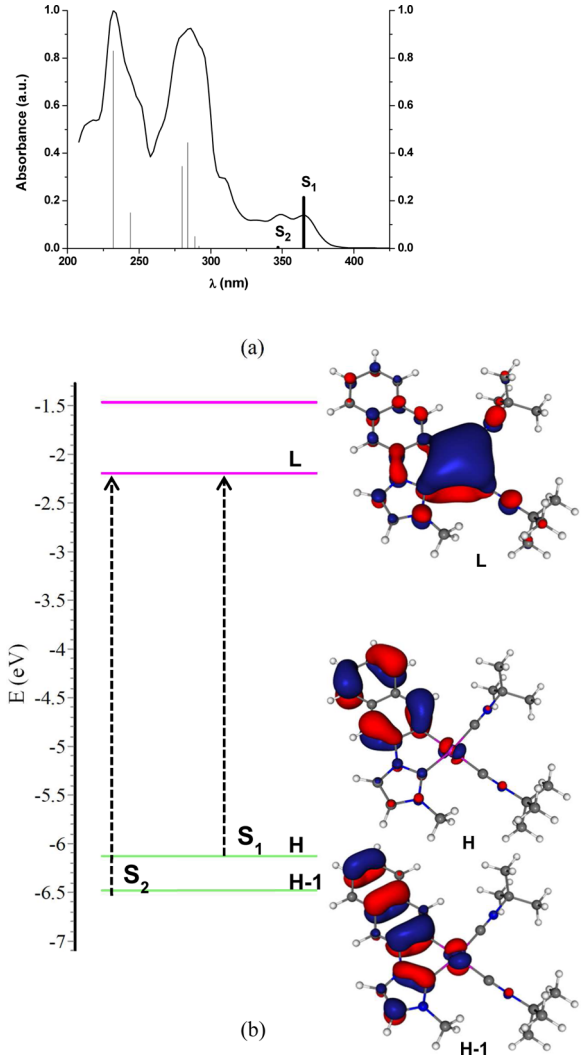

Figure 4. (a) Normalized UV−vis absorption spectrum of **9** in CH_2Cl_2, calculated transitions in CH_2Cl_2 (bars); (b) Calculated molecular orbitals for **9**.

character for **6** and **8** while LMCT [π(NHC) → 5d(Pt)]/LL′CT [π(NHC) → π^*(CNR′)] for **9** and **10**. From these data it is also evident that the electronic features of the R-groups (CN and COOEt) of the C^C* ligands are rather similar and quite different from the Naph-C^C* one, in which the presence of a more extended conjugation in the R-C^C* ligand increases the contribution of R-C fragment to the HOMO and H-1 at the expense of the imidazole fragment and the isocyanide ligands. Because of that, the HOMO−LUMO and H-1−LUMO energy gaps result smaller for complexes **9** and **10** with respect to those of **6** and **8**.

Additionally, calculations for complexes **9** and **10** also show the red shift of the lowest-lying absorption when R′ is Xyl with respect to that when R′ = ^{t}Bu in line with the experimental UV−vis data.

Emission Spectra. Emission data for **5**−**10** are summarized in Table S10. All complexes do not display phosphorescence in solution of CH_2Cl_2 (10^{-5} M) under Ar atmosphere at rt, which may be due to the thermal quenching by solvent molecules.[22] However, in a rigid matrix (CH_2Cl_2 solution at 77 K), these molecules show bright and long live luminescence. Compounds **5**−**8** show highly structured emissions with maxima at $\lambda \sim 460$ nm (see Figure 5) and apparent vibronic

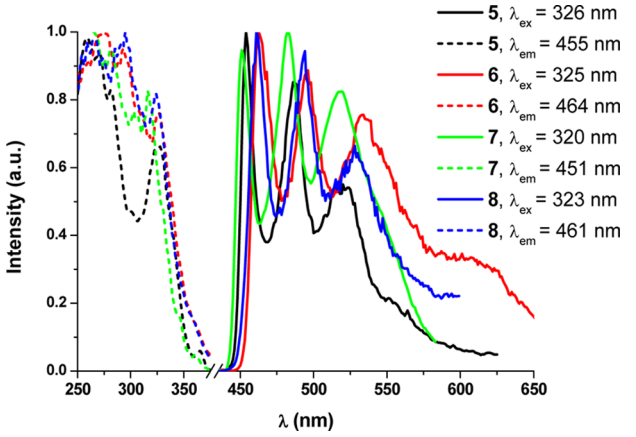

Figure 5. Normalized excitation and emission spectra of **5**−**8** at 77 K in rigid matrix of CH_2Cl_2 (10^{-5} M).

spacings [1345−1401 cm^{-1}] corresponding to the C═C/C═N stretches of the cyclometalated NHC ligand. The excitation spectra exhibit identical profiles to the corresponding UV−vis absorption spectra. Lifetime measurements fit to one component (14−26 μs). Therefore, from these data and considering the TD-DFT calculations, these phosphorescent emissions can be assigned to mixed ^{3}LL′CT [π(NHC) → π^*(CNR′)]/^{3}LMCT [π(NHC) → 5d(Pt)] transitions of monomeric species. As stated in the UV−vis and TD-DFT sections, the emission bands of the Xyl derivatives (**6**, **8**) are red-shifted with respect to those of the ^{t}Bu ones (**5**, **7**).

At higher concentration (10^{-3} M) complexes **5**, **6**, and **8**, show an additional unstructured low energy (LE) band when exciting at longer wavelengths λex >450 nm (see Figure S14), although it is rather weak for complex **5**. The excitation maxima of this LE band appear red-shifted, and their lifetime decays (in the order of 2−4 μs) are shorter than those of the monomer emissions. Thus, taking into account all this and their crystal packing, we tentatively ascribe this LE band to $^3\pi\pi^*$ transitions from aggregates formed by intermolecular interactions.

Neat solid samples of **5**−**8** display bright blue emissions (see Figure 6) with band profiles and lifetimes that resemble those

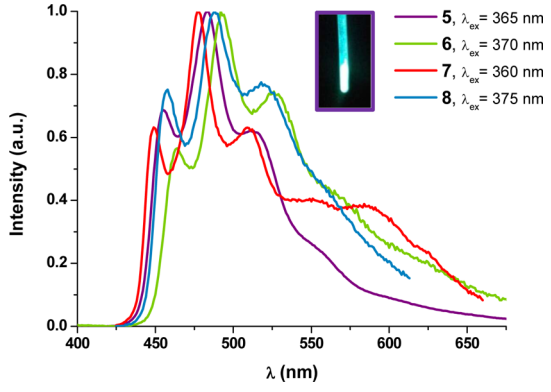

Figure 6. Normalized emission spectra of **5**−**8** in solid state at 298 K. Picture of **5** under UV light (λ_{ex} = 365 nm).

obtained in rigid matrix of CH_2Cl_2, which can be assigned to the same excited states. For complexes **5**−**7**, the LE band (λ_{max} = 643 nm **5**, 620 nm **6**, 590 nm **7**) attributable to $^3\pi\pi^*$ transitions can be selectively obtained upon excitation at λex >450 nm (see Figure S15). Complexes **9** and **10** exhibit a rather

DOI: 10.1021/acsami.6b03288
ACS Appl. Mater. Interfaces 2016, 8, 16160−16169

different emissive behavior to that observed for complexes **5**−**8**. In the solid state, compound **9** displays a yellow emission band with maximum at 540 nm (see Figure 7) either at 298 or at 77 K. However, in rigid matrix of CH_2Cl_2 (10^{-3} and 10^{-5} M, 77 K), a highly structured band is observed at 481 nm. The intricate emission profile is not dependent on the excitation wavelength.

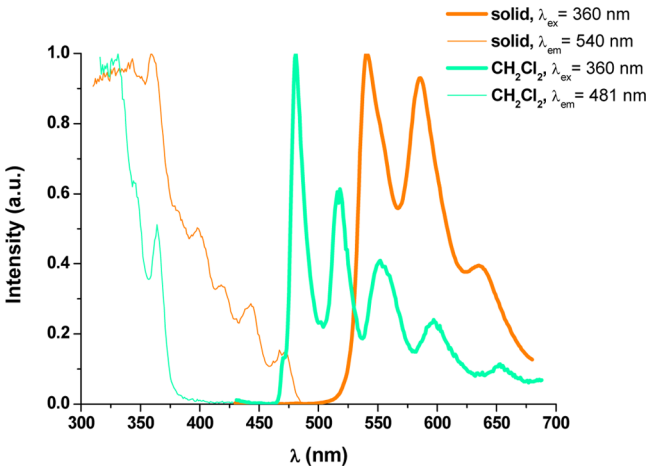

Figure 7. Normalized excitation and emission spectra of **9** in solid state and in rigid matrix of CH_2Cl_2 (10^{-5} M, 77 K). Picture of **9** under UV light (λ_{ex} = 365 nm).

The decay lifetimes suggest the contribution of two different bands: HE band (481 and 518 nm) and LE band (553 and 597 nm). As shown in Figures S16 and S17, this emissive pattern was also observed in **10**. In this case, the emission spectrum can be tuned by using different excitation wavelengths. In rigid matrix of CH_2Cl_2 (10^{-3} M, 77K), the HE band completely disappears when exciting upon 450 nm. In the light of its long lifetime and DFT calculations, the HE band can be assigned to ^{3}ILCT [(NHC)] transitions with some, if any, ^{3}LL′CT [π(NHC) → π^*(CNR′)]/^{3}LMCT [π(NHC) → 5d(Pt)] character. Besides, the HE band of the Xyl derivative (**10**) is not red-shifted with respect to that of the ^{t}Bu one (**9**), which is in agreement with the IL character of the excited state. In the other hand, the structured LE band which exhibits shorter decay lifetime and red-shifted excitation profile compared to those of the HE band can be tentatively assigned to a mixed LL′CT [π(NHC) → π^*(CNR′)]/LMCT [π(NHC) → 5d(Pt)] transition with some $^3\pi\pi^*$ character. In this case, the emission band of **10** does appear 11 nm (352 cm^{-1}) shifted to the red when compared to that of **9**, suggesting the participation of the ancillary ligand (CNR′) in the excited state. Quantum yield (Φ) measurements were carried out on neat solid samples of **5**−**10**. Complexes **5**, **8**, and **9** are

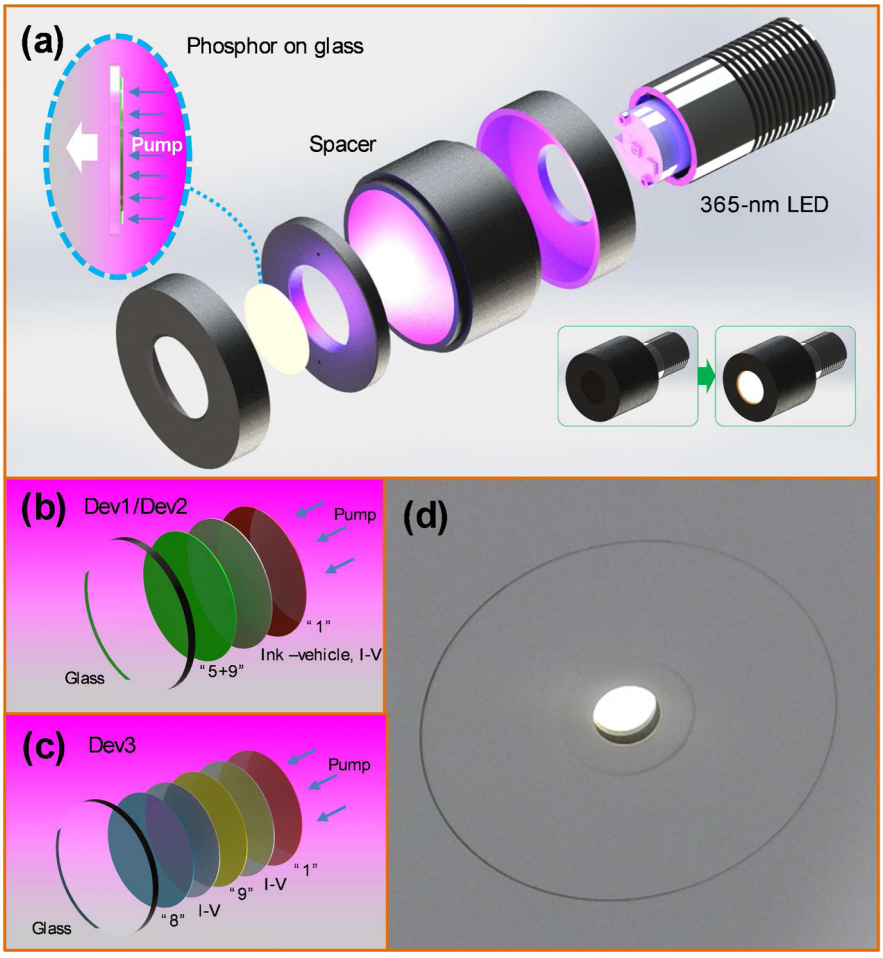

Figure 8. (a) Exploded view of the sample holder used to pump the phosphors and coupling the resulting emission into the integrating sphere. (b) Schematic drawing of the phosphor stacks of **DEV1** and **DEV2**. The difference between them is the number of layers of the mix "**5** + **9**" (15 and 26, respectively). (c) Structure of **DEV3**. (d) Real image of the resulting white emission from **DEV2**.

DOI: 10.1021/acsami.6b03288
ACS Appl. Mater. Interfaces 2016, 8, 16160−16169

very good emitters at r.t. with values of 41%, 21% and 40%, respectively (see Table S10).

To obtain intense and high CRI white light at reasonable CCT values, complexes **5**, **8**, **9** and [Pt(bzq) (CN) (CN^{t}Bu)] (**R1**) have been selected as blue (**5**, **8**), yellow (**9**), and red (**R1**) basic components. Several devices for remote operation were prepared by depositing the active materials on common glass disks. It is important to underline that the interest of the remote phosphor scheme lies in the fact that, far from the LED−dye, the emitters gain in stability and reliability. Concerning our particular case, we have observed that placing the phosphors far from the pumping source (i.e., LED−dye), in a remote configuration and avoiding direct contact between them, the degradation of the emission is notably reduced by compared to the conformal option. In normal operation, the junction of the LED can reach temperatures in the range of 70−100 °C (depending on the operation current and dissipation strategies). In the conformal option, phosphor is subjected to the heat generated by the junction that affects to both emission efficiency and phosphor stability. Furthermore, if the phosphor's efficiency is not very high, sizable part of the pump energy absorbed is transformed into heat, increasing even further the temperature of the LED-junction and the phosphor. This translates into faster degradation of the system (see Figure S18). To combine the luminescence from the different components and tailor the overall spectral shape, different slurries have been sequentially deposited. Keeping in mind the objective of high CRI luminescence, the thickness and concentration of each individual layer have been calculated accordingly to their respective quantum efficiencies.

After a meticulous optimization of the samples, devices **DEV1−DEV3** were selected because of their suitability for general lighting applications (CRI, CCT, etc.). Once a phosphor disk has been prepared, it is ready to be studied under UV illumination. To do that, the disk has been introduced in the holder structure shown in Figure 8a. The phosphor plate has been mounted with the coating facing the pump source. Since commercial disks used are not UV grade, sizable absorption of the UV pump is expected. In this configuration, we ensure that the visible light coming from the phosphor stack is efficiently transmitted to the analysis stage. On the other hand, it is worth noticing that phosphor stacks have been constructed by placing the phosphor with the higher energy close to the glass, so the reabsorption of light emitted by previous phosphors within the stacks with lower energy emission is avoided (see Figure 8b and 8c). Luminescence spectra of the different devices are represented in Figure 9. At glance, it is observed how the variations of the relative compositions aforementioned have direct influence on the luminescence spectral shape.

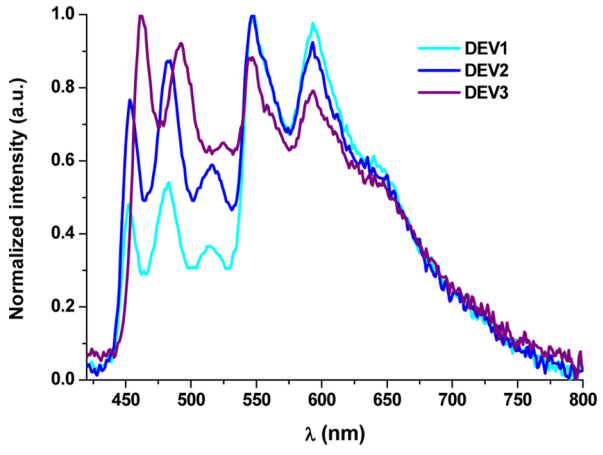

Figure 9. Normalized emission spectra of devices **DEV1−DEV3**.

The spectra represented in Figure 9 have been exploited to extract different photometric and chromatic parameters. The results of this analysis are summarized in Table 1. This chart shows that the luminous fluxes and efficiencies of the different samples are, in general, relatively low, especially if compared to conventional devices. However, in spite of this, the values of luminous efficacy of the radiation are very promising, kept in all cases within the optimum range for general lighting.[45]

CRI, CCT, and CIE (see Figure 10) parameters are also very appealing. CRI values are relatively high, around 80, whereas

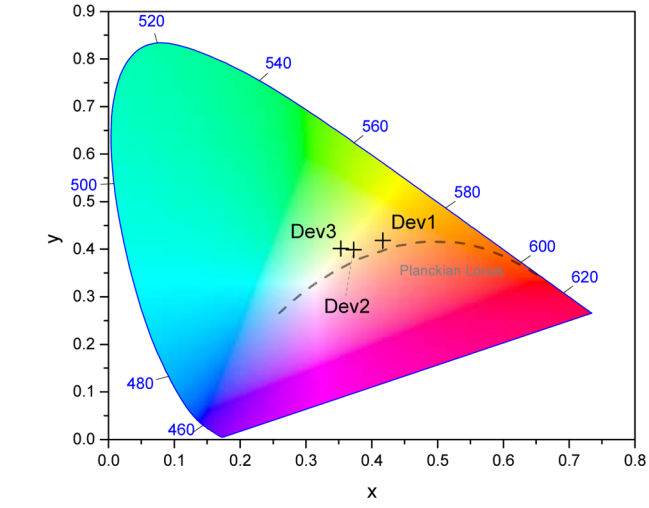

Figure 10. CIE coordinates of devices **DEV1−DEV3**.

the correlated color temperatures fall within the suitable range for lighting.[46,47]

For more details, **DEV1** exhibits an emission with a CCT (3477 K) in the warm/neutral range. The CRI is the lowest among the three samples (77.0). As previously stated, the delivered light output is low (1.49 lm) but in consonance with the rest of the samples. In spite of this, the spectral power distribution is compensated (LER 317.2 lm/W) turning this

Table 1. Key Performance Data of Devices

device	LF (lm)[a]	wall-plug efficiency (%)[b]	LE (lm/W)[c]	LER (lm/W)[d]	CRI[e]	CCT[f]	CIE [x,y][g]
DEV1	1.49	0.85	0.27	317.2	77.0	3477	0.4168, 0.4183
DEV2	1.68	1.00	0.30	304.6	82.6	4356	0.3724, 0.3988
DEV3	1.26	0.76	0.23	300.9	81.3	4897	0.3532, 0.4018

[a]Luminous flux. [b]Wall-plug efficiency. [c]Luminous efficacy. [d]Luminous efficacy of the radiation. [e]Color rendering index. [f]Correlated color temperature. [g]CIE coordinates.

DOI: 10.1021/acsami.6b03288
ACS Appl. Mater. Interfaces 2016, 8, 16160−16169

sample into suitable for general lighting. The results of **DEV2** reveal that, by addition of complex **5**, with emission in the blue/green range, the white luminescence becomes "colder" (blue-shifted) than the one observed in **DEV1** (4356 K). The CRI and total light output are the best among all the devices (82.6 and 1.68 lm, respectively). In agreement to the LER (304.6 lm/W), also in this case the light is suitable for general lighting applications. Concerning **DEV3**, the use of compound **8** instead of **5** makes the emission more bluish (4897K) but always within the suitable ranges. The luminous flux is the poorest among the three structures analyzed (1.26 lm) but, in compensation, the CRI is reasonable good (81.3). Finally, also in this case, the LER vale is very promising and adequate for its implementation in lighting systems.

In light of the results, it becomes clear that the method reported here has proven to be effective in controlling the spectral power distribution of the emitting devices and, subsequently, their colorimetric properties. Nevertheless, a common feature has been observed in all the samples under test. Under a CW incident flux of about 92 mW at 365 nm, which is equivalent to a CW irradiance of 187.4 W/m^2, the emission of all the structures rapidly decreases. Figure 11 shows, as an example,

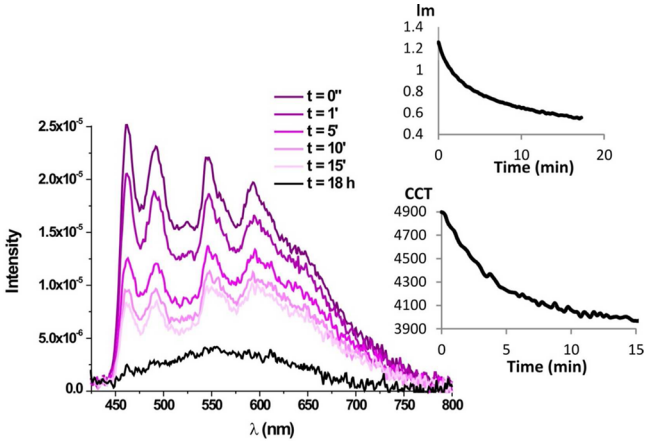

Figure 11. Emission spectra of the degradation studies of **DEV3**. Inset: Evolution of the luminous flux (up) and evolution of the CCT (down) with time upon irradiation at 365 nm.

the reduction of the luminescence intensity of **DEV3** with time. As observed, the total flux drops down to 50% in approximately 8 min. In this particular case, the fastest degeneration corresponds to compound **8** (blue/green range), as supported by the red−shift of the emission shown in the lower insert.

It is expected that the low light power delivered and fast degradation of the emission in these devices could be improved by following two particular strategies: (a) implementing a high-reflectance mixing chamber (painted in barium sulfate, for example) to harvest part of the light emitted backward by the excited phosphor (approximately 50% of the total) and (b) the use of pulsed excitation as opposed to CW operation. With an adequate modulation of the pump light, fast enough to not be perceived by the human eye and slow enough to respect phosphor emission fall- and rise-times, a 50% duty-cycle square wave would be able to roughly induce 50% degradation reduction.

CONCLUSIONS

The C^C*-cyclometalated N-heterocyclic carbene complex [{Pt(μ-Cl)(R-C^C*)}$_2$] (R = COOEt (**4**)) was available by following the same stepwise protocol than that for the related compounds **4a** (R= CN) and **4b** (R−C= Naph) and all of them were used to prepare the ionic derivatives [Pt(R-C^C*)(CNR′)$_2$]PF$_6$ (R = −COOEt, CN; R^C= Naph; R′ = *t*-Bu, Xyl (**5**−**10**)). As concluded from the spectroscopic and theoretical data, the CN and COOEt substituents in the C^C* group display similar electronic features and compounds **5**−**8** exhibit all of them blue luminescence in the solid state. However, in the naphthyl complexes the larger π system due to the extra aromatic ring lead to the lowering of the HOMO−LUMO gap and to a more extended assembly of the complexes through $\pi\cdots\pi$ contacts in compound **9** in such a way that it displays a bright yellow luminescence in the solid state. Also, the electron-withdrawing Xyl ring produces red shifts in the absorption and emission bands as well as downfield shifts of the ^{195}Pt NMR signals when compared to those of the of the ^{t}Bu ones. Complexes **5**, **8**, **9**, and **R1** have been tested as blue (**5**, **8**), yellow (**9**), and red (**R1**) components of remote-phosphors for white light illumination. White light with CCT, CRI, and LER values within acceptable margins for general light applications has been achieved through the compositional optimization of three different devices, demonstrating the suitability of the method reported here for controlling colorimetric features.

ASSOCIATED CONTENT

Supporting Information

The Supporting Information is available free of charge on the ACS Publications website at DOI: 10.1021/acsami.6b03288.

Crystallographic data for compounds **6** and **8**−**10** (CIF)
General procedures, computational and crystallographic details, synthetic procedures and characterization data, full NMR spectra of **3** and **4**, NMR spectra of **5** and **6** (selected as examples), X-ray structures, UV−vis data, TD-DFT calculations, tables of data and pictures of the representative frontier orbitals, UV−vis spectra and calculated transitions in CH_2Cl_2, and emission spectra (PDF)

AUTHOR INFORMATION

Corresponding Author

*E-mail: sicilia@unizar.es.

Notes

The authors declare no competing financial interest.

ACKNOWLEDGMENTS

This work was supported by the Spanish MINECO (Project CTQ2015-67461-P led by Dr. Babil Menjón and Project TEC2012-38901-C02-01, led by Dr. Mariano Perálvarez), the Departamento de Industria e Innovación del Gobierno de Aragón and Fondo Social Europeo (Grupo Consolidado E21: Química Inorgánica y de los Compuestos Organometálicos led by Dr. José M. Casas) and Project HI-LED funded by the European Union Seventh Framework Programme (FP7/2007-2013 under grant agreement no. 619912). A. C. acknowledges the support of a FPI grant from the Spanish government. The authors thank Bibiana Colldeforns (IREC) for her help in screen printing depositions They also thank the Centro de Supercomputación de Galicia (CESGA).

REFERENCES

(1) Lighting Research and Development. *Multi-Year Program Plan 2013*, DOE/EERE-0961; U. S. Department of Energy, 2013

DOI: 10.1021/acsami.6b03288
ACS Appl. Mater. Interfaces 2016, 8, 16160−16169

(2) Narendran, N.; Gu, Y.; Freyssinier-Nova, J. P.; Zhu, Y. Extracting Phosphor-Scattered Photons to Improve White LED Efficiency. *Phys. Status Solidi A* **2005**, *202* (6), R60−R62.
(3) U. S. Department of Energy. *Critical Materials Strategy 2011*, DOE/PI-0009; U. S. Department of Energy, 2012.
(4) Fukagawa, H.; Shimizu, T.; Hanashima, H.; Osada, Y.; Suzuki, M.; Fujikake, H. Highly Efficient and Stable Red Phosphorescent Organic Light-Emitting Diodes Using Platinum Complexes. *Adv. Mater.* **2012**, *24*, 5099−5103 and references therein.
(5) Cebrián, C.; Mauro, M.; Kourkoulos, D.; Mercandelli, P.; Hertel, D.; Meerholz, K.; Strassert, C. A.; De Cola, L. Luminescent Neutral Platinum Complexes Bearing an Asymmetric N^N^N Ligand for High-Performance Solution-Processed OLEDs. *Adv. Mater.* **2013**, *25*, 437−442.
(6) Choy, W. C. H.; Chan, W. K.; Yuan, Y. Recent Advances in Transition Metal Complexes and Light-Management Engineering in Organic Optoelectronic Devices. *Adv. Mater.* **2014**, *26*, 5368−5399.
(7) Fleetham, T.; Ecton, J.; Wang, Z.; Bakken, N.; Li, J. H. Single-Doped White Organic Light-Emitting Device with an External Quantum Efficiency Over 20%. *Adv. Mater.* **2013**, *25*, 2573−2576 and references therein.
(8) Cheng, G.; Chow, P.-K.; Kui, S. C. F.; Kwok, C.-C.; Che, C.-M. High-Efficiency Polymer Light-Emitting Devices with Robust Phosphorescent Platinum(II) Emitters Containing Tetradentate Dianionic O^N^C^N Ligands. *Adv. Mater.* **2013**, *25*, 6765−6770.
(9) Li, G.; Fleetham, T.; Li, J. Efficient and Stable White Organic Light-Emitting Diodes Employing a Single Emitter. *Adv. Mater.* **2014**, *26*, 2931−2936.
(10) Fuertes, S.; Garcia, H.; Peralvarez, M.; Hertog, W.; Carreras, J.; Sicilia, V. Stepwise Strategy to Cyclometallated Pt-II Complexes with N-Heterocyclic Carbene Ligands: A Luminescence Study on New β-Diketonate Complexes. *Chem. - Eur. J.* **2015**, *21*, 1620−1631.
(11) Sajoto, T.; Djurovich, P. I.; Tamayo, A.; Yousufuddin, M.; Bau, R.; Thompson, M. E.; Holmes, R. J.; Forrest, S. R. Blue and Near-UV Phosphorescence from Iridium Complexes with Cyclometalated Pyrazolyl or N-Heterocyclic Carbene Ligands. *Inorg. Chem.* **2005**, *44*, 7992−8003.
(12) Tronnier, A.; Nischan, N.; Metz, S.; Wagenblast, G.; Münster, I.; Strassner, T. Phosphorescent C−C* Cyclometalated Pt II Dibenzofuranyl-NHC Complexes - An Auxiliary Ligand Study. *Eur. J. Inorg. Chem.* **2014**, *2014*, 256−264.
(13) Tronnier, A.; Pöthig, A.; Herdtweck, E.; Strassner, T. C−C* Cyclometalated Platinum(II) NHC Complexes with β-Ketoimine Ligands. *Organometallics* **2014**, *33*, 898−908.
(14) Tronnier, A.; Metz, S.; Wagenblast, G.; Münster, I.; Strassner, T. Blue Phosphorescent Nitrile Containing C−C* Cyclometalated NHC Platinum(II) Complexes. *Dalton Trans.* **2014**, *43*, 3297−3305.
(15) Tronnier, A.; Nischan, N.; Strassner, T. C^C*-Cyclometalated Platinum(II) Complexes with Trifluoromethyl-acetylacetonate Ligands − Synthesis and Electronic Effects. *J. Organomet. Chem.* **2013**, *730*, 37−43.
(16) Tronnier, A.; Risler, A.; Langer, N.; Wagenblast, G.; Münster, I.; Strassner, T. A Phosphorescent C^C* Cyclometalated Platinum(II) Dibenzothiophene NHC Complex. *Organometallics* **2012**, *31*, 7447−7452.
(17) Hudson, Z. M.; Sun, C.; Helander, M. G.; Chang, Y. L.; Lu, Z. H.; Wang, S. N. Highly Efficient Blue Phosphorescence from Triarylboron-Functionalized Platinum(II) Complexes of N-Heterocyclic Carbenes. *J. Am. Chem. Soc.* **2012**, *134*, 13930−13933.
(18) Hudson, Z. M.; Blight, B. A.; Wang, S. N. Efficient and High Yield One-Pot Synthesis of Cyclometalated Platinum(II) β-Diketonates at Ambient Temperature. *Org. Lett.* **2012**, *14*, 1700−1703.
(19) Unger, Y.; Meyer, D.; Molt, O.; Schildknecht, C.; Münster, I.; Wagenblast, G.; Strassner, T. Green−Blue Emitters: NHC-Based Cyclometalated [Pt(C^C*) (acac)] Complexes. *Angew. Chem., Int. Ed.* **2010**, *49*, 10214−10216.
(20) Tronnier, A.; Schleicher, D.; Strassner, T. (C^C*)-Cyclometalated Platinum(II) Imidazo[1,5-a]pyridine NHC Complexes − Synthesis and Characterization. *J. Organomet. Chem.* **2015**, *775*, 155−163.
(21) Tronnier, A.; Heinemeyer, U.; Metz, S.; Wagenblast, G.; Muenster, I.; Strassner, T. Heteroleptic Platinum(II) NHC Complexes with a C^C* Cyclometalated Ligand - Synthesis, Structure and Photophysics. *J. Mater. Chem. C* **2015**, *3*, 1680−1693.
(22) Ko, S.-B.; Park, H.-J.; Gong, S.; Wang, X. N.; Lu, Z.-H.; Wang, S. N. Blue Phosphorescent N-Heterocyclic Carbene Chelated Pt(II) Complexes with an α-duryl-β-diketonato Ancillary Ligand. *Dalton Trans.* **2015**, *44*, 8433−8443.
(23) Tronnier, A.; Pöthig, A.; Metz, S.; Wagenblast, G.; Münster, I.; Strassner, T. Enlarging the π System of Phosphorescent (C^C*) Cyclometalated Platinum(II) NHC Complexes. *Inorg. Chem.* **2014**, *53*, 6346−6356.
(24) Haneder, S.; Da Como, E.; Feldmann, J.; Lupton, J. M.; Lennartz, C.; Erk, P.; Fuchs, E.; Molt, O.; Munster, I.; Schildknecht, C.; Wagenblast, G. Controlling the Radiative Rate of Deep-Blue Electrophosphorescent Organometallic Complexes by Singlet-Triplet Gap Engineering. *Adv. Mater.* **2008**, *20*, 3325−3330.
(25) Fernández, S.; Forniés, J.; Gil, B.; Gómez, J.; Lalinde, E. Synthesis, Structural Characterisation and Photophysics of Anionic Cyclometalated Bis(alkynyl) (benzo[h]quinolinate) Platinate(II) Species. *Dalton Trans.* **2003**, 822−830.
(26) Fornies, J.; Fuertes, S.; Lopez, J. A.; Martin, A.; Sicilia, V. New Water Soluble and Luminescent Platinum(II) Compounds, Vapochromic Behavior of K(H_2O) [Pt(bzq) ($CN)_2$], New Examples of the Influence of the Counterion on the Photophysical Properties of d(8) Square-Planar Complexes. *Inorg. Chem.* **2008**, *47*, 7166−7176.
(27) Diez, A.; Fornies, J.; Fuertes, S.; Lalinde, E.; Larraz, C.; Lopez, J. A.; Martin, A.; Moreno, M. T.; Sicilia, V. Synthesis and Luminescence of Cyclometalated Compounds with Nitrile and Isocyanide Ligands. *Organometallics* **2009**, *28*, 1705−1718.
(28) Forniés, J.; Fuertes, S.; Martin, A.; Sicilia, V.; Gil, B.; Lalinde, E. Extended Structures Containing Pt(II)−Tl(I) Bonds. Effect of these Interactions on the Luminescence of Cyclometalated Pt(II) Compounds. *Dalton Trans.* **2009**, 2224−2234.
(29) Díez, A.; Fornies, J.; Larraz, C.; Lalinde, E.; López, J. A.; Martin, A.; Moreno, M. T.; Sicilia, V. Structural and Luminescence Studies on $\pi\cdots\pi$ and Pt···Pt Interactions in Mixed Chloro-Isocyanide Cyclometalated Platinum(II) Complexes. *Inorg. Chem.* **2010**, *49*, 3239−3259.
(30) Fornies, J.; Sicilia, V.; Borja, P.; Casas, J. M.; Diez, A.; Lalinde, E.; Larraz, C.; Martin, A.; Moreno, M. T. Luminescent Benzoquinolate-Isocyanide Platinum(II) Complexes: Effect of Pt···Pt and $\pi\cdots\pi$ Interactions on their Photophysical Properties. *Chem. - Asian J.* **2012**, *7*, 2813−2823.
(31) Fornies, J.; Sicilia, V.; Larraz, C.; Camerano, J. A.; Martin, A.; Casas, J. M.; Tsipis, A. C. One-Pot and Step-by-Step N-Assisted C-Ph-H Activation in 2-(4-Bromophenyl)imidazol[1,2-a]pyridine: Synthesis of a New C,N-Cyclometalated Compound [{Pt(C^N)(μ-Cl)}$_2$] as Precursor of Luminescent Platinum(II) Compounds. *Organometallics* **2010**, *29*, 1396−1405.
(32) Sicilia, V.; Fuertes, S.; Martin, A.; Palacios, A. N-Assisted C-Ph-H Activation in 3,8-Dinitro-6-phenylphenanthridine. New C,N-Cyclometalated Compounds of Platinum(II): Synthesis, Structure, and Luminescence Studies. *Organometallics* **2013**, *32*, 4092−4102.
(33) Fuertes, S.; Chueca, A. J.; Sicilia, V. Exploring the Transphobia Effect on Heteroleptic NHC Cycloplatinated Complexes. *Inorg. Chem.* **2015**, *54*, 9885−9895.
(34) Mabbott, D. J.; Mann, B. E.; Maitlis, P. M. Cationic (η^3-Allylic) (η^4-diene)-Palladium and Platinum Complexes. *J. Chem. Soc., Dalton Trans.* **1977**, 294−299.
(35) Huang, Y. Z.; Miao, H.; Zhang, Q. H.; Chen, C.; Xu, J. Cu_2O: a Simple and Efficient Reusable Catalyst for N-Arylation of Nitrogen-Containing Heterocycles with Aryl Halides. *Catal. Lett.* **2008**, *122*, 344−348.
(36) Ghorbani-Vaghei, R.; Hemmati, S.; Veisi, H. An in situ Generated CuI/metformin Complex as a Novel and Efficient Catalyst for C−N and C−O Cross-Coupling Reactions. *Tetrahedron Lett.* **2013**, *54*, 7095−7099.

DOI: 10.1021/acsami.6b03288
ACS Appl. Mater. Interfaces 2016, 8, 16160−16169

(37) Zhu, L. B.; Cheng, L.; Zhang, Y. X.; Xie, R. G.; You, J. S. Highly Efficient Copper-Catalyzed N-Arylation of Nitrogen-Containing Heterocycles with Aryl and Heteroaryl Halides. *J. Org. Chem.* **2007**, *72*, 2737−2743.
(38) Wang, H. F.; Li, Y. M.; Sun, F. F.; Feng, Y.; Jin, K.; Wang, X. N. 1,2,3,4-Tetrahydro-8-hydroxyquinoline-Promoted Copper-Catalyzed Coupling of Nitrogen Nucleophiles and Aryl Bromides. *J. Org. Chem.* **2008**, *73*, 8639−8642.
(39) Lai, S. W.; Lam, H. W.; Lu, W.; Cheung, K. K.; Che, C. M. Observation of Low-Energy Metal-Metal-to-Ligand Charge Transfer Absorption and Emission: Electronic Spectroscopy of Cyclometalated Platinum(II) Complexes with Isocyanide Ligands. *Organometallics* **2002**, *21*, 226−234.
(40) Vicente, J.; Arcas, A.; Fernández-Hernández, J. M.; Aullón, G.; Bautista, D. Acetonyl Platinum(II) Complexes. *Organometallics* **2007**, *26*, 6155−6169.
(41) Sun, Y.; Ye, K.; Zhang, H.; Zhang, J.; Zhao, L.; Li, B.; Yang, G.; Yang, B.; Wang, Y.; Lai, S. W.; Che, C. M. Luminescent One-Dimensional Nanoscale Materials with Pt-II-Pt-II Interactions. *Angew. Chem., Int. Ed.* **2006**, *45*, 5610−5613.
(42) Dylla, A. G.; Janzen, D. E.; Pomije, M. K.; Mann, K. R. A Comparison of Isomers: trans- and cis-Dicyanobis(para-ethylisocyanobenzene)Platinum. *Organometallics* **2007**, *26*, 6243−6247.
(43) Nardelli, M. PARST95 − An Update to PARST: A System of Fortran Routines for Calculating Molecular Structure Parameters from the Results of Crystal Structure Analyses. *J. Appl. Crystallogr.* **1995**, *28*, 659−659.
(44) Williams, J. A. G. Photochemistry and Photophysics of Coordination Compounds: Platinum. *Top. Curr. Chem.* **2007**, *281*, 205−268.
(45) Erdem, T.; Demir, H. V. Color Science of Nanocrystal Quantum Dots for Lighting and Displays. *Nanophotonics* **2013**, *2*, 57−81.
(46) D'Andrade, B. W.; Forrest, S. R. White Organic Light-Emitting Devices for Solid-State Lighting. *Adv. Mater.* **2004**, *16*, 1585−1595.
(47) Gather, M. C.; Köhnen, A.; Meerholz, K. White Organic Light-Emitting Diodes. *Adv. Mater.* **2011**, *23*, 233−248.

DOI: 10.1021/acsami.6b03288
ACS Appl. Mater. Interfaces 2016, 8, 16160−16169

CRYSTAL GROWTH & DESIGN

Article

pubs.acs.org/crystal

Pt_2Tl Building Blocks for Two-Dimensional Extended Solids: Synthesis, Crystal Structures, and Luminescence

Sara Fuertes,[†] Andrés J. Chueca,[†] Antonio Martín,[†] and Violeta Sicilia*[,‡]

[†]Departamento de Química Inorgánica, Facultad de Ciencias, Instituto de Síntesis Química y Catálisis Homogénea (ISQCH), CSIC - Universidad de Zaragoza, Pedro Cerbuna 12, 50009, Zaragoza, Spain

[‡]Departamento de Química Inorgánica, Escuela de Ingeniería y Arquitectura de Zaragoza, Instituto de Síntesis Química y Catálisis Homogénea (ISQCH), CSIC - Universidad de Zaragoza, Campus Río Ebro, Edificio Torres Quevedo, 50018, Zaragoza, Spain

Supporting Information

ABSTRACT: The β-diketonate compounds of Pt(II), [Pt(R-C^C*)(acac)] (acacH = acetylacetone, R-CH^C* = 1-(4-cyanophenyl)-3-methyl-1*H*-imidazol-2-ylidene (NC−CH^C*) **1A**, 1-(4-(ethoxycarbonyl)phenyl)-3-methyl-1*H*-imidazol-2-ylidene (CO_2Et-CH^C*) **1B**, 1-(3,5-dichlorophenyl)-3-methyl-1*H*-imidazol-2-ylidene (Cl-CH^C*) **1C**) containing cyclometalated N-heterocyclic carbenes were synthesized from compounds [{Pt(μ-Cl)(R-C^C*)}$_2$] (R = CN **A**, CO_2Et **B**, Cl **C**). Compound **C** was prepared for the first time following a step-by-step protocol used to synthesize **A** and **B**. The X-ray structures of complexes **1B** and **1C** show that only in **1B** the molecules stack in pairs through intermolecular Pt···Pt (3.370 Å) and $\pi-\pi$ (~3.43 Å) interactions between the NHC ligand and the acac. The reaction of compounds **1A−1C** with $TlPF_6$ (2:1 molar ratio) leads to the clusters [{Pt(R-C^C*)(acac)}$_2$Tl]$^+$ (R = CN **2A**, CO_2Et **2B**, Cl **2C**), which exhibit a "Pt_2Tl" sandwich structure, where two slightly distorted square planar "Pt(R-C^C*)(acac)" subunits are bonded to a Tl(I) center through donor−acceptor Pt−Tl bonds. Compounds **2A** and **2B** show an extended two-dimensional lattice in the solid state through intermolecular Pt··Pt and Tl−E (E = N, O) interactions; meanwhile **2C** forms discrete molecules without any kind of intermolecular interaction among them. The effects of the R substituent and the Pt−Tl interactions on the crystal structures and the photophysical properties have been investigated.

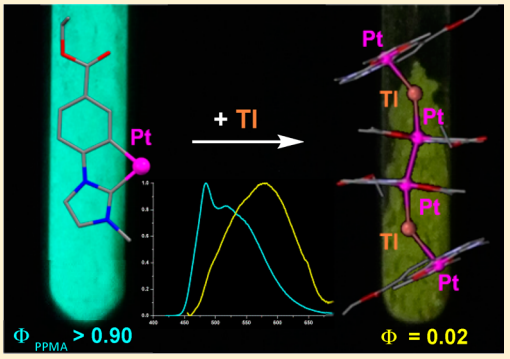

INTRODUCTION

The Lewis basic properties of transition metals play an important role for catalytic cycles[1−3] and also lead to metal clusters through the formation of metal−metal dative bonds.[4−9] The high electron density of Pt(II) in square-planar complexes has been demonstrated many times by their role as the Lewis base unit in unsupported metal-only Lewis pair (MOLP) compounds. Among Pt(II) → M (M = Cu^I, Ag^I, Au^I, Cd^{II}, Hg^{II}, Tl^I, Sn^{II}, Pb^{II}) MOLP complexes,[5,9] the silver-containing ones are still the most numerous,[5] but examples of Pt(II) (d^8) → Tl(I) ($d^{10}s^2$) clusters[10,11] are increasing since A. L. Balch published [Tl_2Pt(CN)$_4$], the first blue-luminescent columnar compound containing Pt−Tl bonds.[12] In this field luminescent Pt^{II}−Tl^I MOLP clusters have been reported showing diverse structural configurations, including dinuclear (PtTl),[13−15] trinuclear (Pt_2Tl,[10,16] $PtTl_2$[12,17−19]), tetranuclear (Pt_3Tl, (PtTl)$_2$),[13,19,20] hexanuclear clusters (Pt_2Tl_4, Pt_3Tl_3),[20−22] or infinite networks,[10,11,16,21,23] many of them containing C,N-cycloplatinated compounds as the Lewis base unit.[10,13,15,20] In many cases their luminescent properties have been demonstrated to depend on the Pt−Tl interactions.[10,12−21] Moreover, the formation of the metal−metal bond affects the crystal packing allowing or hindering the molecular assembly through $\pi-\pi$ interactions, with the subsequent effect on the emitting properties.[11,13]

The use of N-heterocyclic carbenes (NHCs) as cyclometalated ligands has been revealed as a key to get stable and very efficient Pt(II) phosphorescent emitters.[24−27] Compared to C,N-cycloplatinated compounds, the even greater heightening of the d-d energy levels on the metal center, enlarging the energy gap with the emissive excited states, avoids the thermal quenching and improves the emission quantum yields. Examples of phosphorescent compounds of platinum(II) containing C^C*-cyclometalated NHCs ligands are still fairly limited, and the effect of metallophilic interactions on the emission properties have been barely investigated.[28] Because of that, our task in this work was to prepare unsupported Pt^{II}−Tl^I MOLP structures, containing cyclometalated N-heterocyclic carbene complexes of Pt(II) as Lewis base units to gauge for the first time the ability of this kind of Pt(II) complex to act as Lewis bases for these kinds of interactions, the stability of these interactions, and the effect of them in the photophysical properties of the mononuclear Pt(II) complexes.

With this purpose we prepared the β-diketonate compounds [Pt(R-C^C*)(acac)] (acacH = acetylacetone, R-CH^C* = 1-(4-

Received: May 10, 2017
Revised: June 27, 2017
Published: July 5, 2017

DOI: 10.1021/acs.cgd.7b00662
Cryst. Growth Des. 2017, 17, 4336−4346

Scheme 1. Synthesis of Compounds and Numerical Scheme for NMR Purposes

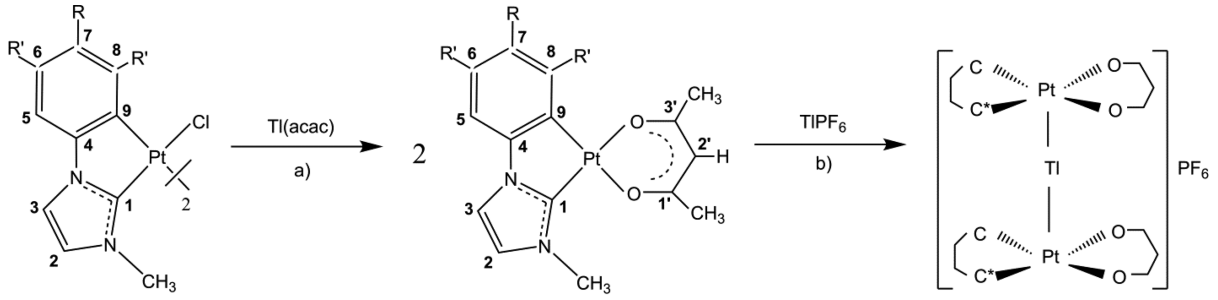

cyanophenyl)-3-methyl-1*H*-imidazol-2-ylidene (CN−CH^C*) **1A**, 1-(4-(ethoxycarbonyl)phenyl)-3-methyl-1*H*-imidazol-2-ylidene (CO_2Et-CH^C*) **1B**, 1-(3,5-dichlorophenyl)-3-methyl-1*H*-imidazol-2-ylidene (Cl-CH^C*) **1C**) and the Pt_2Tl clusters derived from them. In this way we have been able to compare first the effect of the R-C^C group on the luminescent properties of the mononuclear Pt(II) complexes and in their ability to form Pt_2Tl clusters. The luminescence of these mononuclear compounds has been explained considering the time-dependent density functional theory (TD-DFT) calculations and X-ray diffraction studies.

The synthesis of **1A**−**1C** was carried out using compounds $[\{Pt(\mu\text{-Cl})(C\text{^}C^*)\}_2]$ (CN-C^C* **A**, CO_2Et-C^C* **B**, Cl−C^C* **C**) as starting materials, like in a previous work.[26] Compound **C** was prepared for the first time following our stepwise protocol for this kind of complex and has been fully described in the Supporting Information.

EXPERIMENTAL SECTION

General Comments. Instrumental methods used for characterization and spectroscopic studies, density functional theory (DFT) computational details, X-ray structures, stepwise synthesis of compound $[\{Pt(\mu\text{-Cl})(Cl-C\text{^}C^*)\}_2]$ (**C**), and spectroscopic data for **1A**−**1C** and **2A**−**2C** are contained in the Supporting Information. All chemicals were used as supplied and $[\{Pt(\mu\text{-Cl})(NC\text{-}C\text{^}C^*)\}_2]$ (**A**)[29] and $[\{Pt(\mu\text{-Cl})(EtO_2C\text{-}C\text{^}C^*)\}_2]$ (**B**)[25] were prepared following the literature procedures.

Synthesis and Characterization. *[Pt(NC-C^C*)(acac)] (**1A**).* Tlacac (146.2 mg, 0.48 mmol) was added to a yellow suspension of **A** (207.2 mg, 0.25 mmol) in dichloromethane (40 mL) at r.t. After being stirred for 4 h, the resulting mixture was filtered through Celite, washed with dichloromethane (120 mL), and evaporated to dryness. Addition of methanol (3 × 5 mL) to the residue rendered a solid which was recrystallized by redissolving in 15 mL of dichloromethane/diethyl ether (3:1), filtering through Celite and evaporating to dryness. Addition of methanol (3 × 5 mL) to the residue rendered **1A** as a pure white solid. Yield: 178.2 mg, 78%. Elemental analysis calcd (%) for $C_{16}H_{15}N_3O_2Pt$: C 40.34, H 3.17, N 8.82; found: C 40.20, H 3.43, N 8.78. MS MALDI (+): *m*/*z*: 476.1 $[M]^+$.

[Pt(EtO_2C−C^C)(acac)] (**1B**).* It was prepared following the method described for **1A**. Tlacac (63.4 mg, 0.21 mmol) and **B** (100.1 mg, 0.11 mmol). **1B**: white solid, yield: 80.4 mg, 71%. Elemental analysis calcd (%) for $C_{18}H_{20}N_2O_4Pt$: C 41.30, H 3.85, N 5.35; found: C 41.04, H 3.90, N 5.32. MS MALDI (+): *m*/*z*: 523.2 $[M]^+$.

[Pt(Cl−C^C)(acac)] (**1C**).* It was prepared following the method described for **1A**. Tlacac (98.2 mg, 0.32 mmol) and **C** (153.9 mg, 0.17 mmol). **1C**: white solid, yield: 120.2 mg, 72%. Elemental analysis calcd (%) for $C_{15}H_{14}N_2Cl_2O_2Pt$: C 34.63, H 2.71, N 5.39; found: C 34.29, H 2.70, N 5.36. MS MALDI (+): *m*/*z*: 520.1 $[M]^+$.

[{Pt(NC-C^C)(acac)}$_2$Tl]PF_6 (**2A**).* $TlPF_6$ (26.6 mg, 0.074 mmol) was added to a solution of **1A** (70.3 mg, 0.15 mmol) in a mixture of dichloromethane and acetone (20 mL/5 mL). After 2.5 h stirring in the dark, the solvent was removed under reduced pressure, and the residue was treated with diethyl ether (20 mL) and filtered, to give **2A** as a yellow solid. Yield: 73.4 mg, 76%. Elemental analysis calcd (%) for $C_{32}H_{30}F_6N_6O_4PPt_2Tl$: C 29.52, H 2.32, N 6.45; found: C 29.63, H 2.43, N 6.60. MS MALDI (+): *m*/*z*: 680.2 $[Pt(NC\text{-}C\text{^}C^*)(acac)Tl]^+$.

[{Pt(EtO_2C−C^C)(acac)}$_2$Tl]PF_6 (**2B**).* It was prepared following the method described for **2A**. $TlPF_6$ (27.7 mg, 0.077 mmol) and **1B** (80.4 mg, 0.15 mmol). **2B**: bright yellow solid, yield: 84.1 mg, 78%. Elemental analysis calcd (%) for $C_{36}H_{40}F_6N_4O_8PPt_2Tl$: C 30.97, H 2.89, N 4.01; found: C 30.64, H 2.71, N 4.21MS MALDI (+): *m*/*z*: 1251.6 $[M]^+$; 727.2 $[Pt(EtO_2C\text{−}C\text{^}C^*)(acac)Tl]^+$.

[{Pt(Cl−C^C)(acac)}$_2$Tl]PF_6 (**2C**).* It was prepared following the method described for **2A**. $TlPF_6$ (29.7 mg, 0.083 mmol) and **1C** (86.0 mg, 0.17 mmol). **2C**: pale yellow solid, yield: 85.8 mg, 75%. Elemental analysis Calcd (%) for $C_{30}H_{28}Cl_4F_6N_4O_4PPt_2Tl$: C 25.92, H 2.03, N 4.03; found: C 25.66, H 1.82, N 4.21. MS MALDI (+): *m*/*z*: 1245.2 $[M]^+$, 725.0 $[Pt(Cl\text{−}C\text{^}C^*)(acac)Tl]^+$.

RESULTS AND DISCUSSION

Stepwise Synthesis of Compounds [Pt(R-C^C*)(acac)] (R = CN 1A, CO_2Et 1B, Cl 1C). The *β*-diketonate compounds $[Pt(R\text{-}C\text{^}C^*)(acac)]$ (**1A**−**1C**) were synthesized by reaction of the corresponding chlorine bridged compounds $[\{Pt(\mu\text{-Cl})(R\text{-}C\text{^}C^*)\}_2]$ (R = CN **A**, CO_2Et **B**, Cl **C**) with Tl(acac) in a 1:2 molar ratio (see Experimental Section and Scheme 1, path a), which led to the precipitation of TlCl and formation of the neutral complexes **1A**−**1C**. This procedure was reported by us for the synthesis of the analogous compound derived from 3-methyl-1-(naphthalen-2-yl)-1*H*-imidazol-2-ylidene,[26] although compound **1A** was already reported and prepared by Egen et al. following a different procedure.[30]

The synthetic procedure of **1A**−**1C** requires the availability of the dichloro bridged complexes **A**−**C**. Then, the new compound **C** was prepared following the step-by-step method used previously for **A** and **B**[25,29] (see Supporting Information: description, Scheme S1 and Figures S1−S4). The IR spectra of compounds **1A**−**1C** show two *ν*(C═O) stretching vibrations at significantly lower energies than those found for the free ligand (ca. 1720 cm^{-1}) which are indicative of the diketonate chelation to the metal center.[26]

Their ^1H and ^{13}C NMR spectra show the expected signals for the cyclometalated NHC group and evidence the non-equivalence of the two halves of the *β*-diketonate ligand, as correspondence for a chelate coordination (see NMR data and Figure S5 in the Supporting Information). The ^{195}Pt NMR spectra exhibit the corresponding singlets at about −3400 ppm

DOI: 10.1021/acs.cgd.7b00662
Cryst. Growth Des. 2017, 17, 4336−4346

for **1A** and **1B** and at −3167 ppm for **1C**. As shown in Figure S6, the platinum signal is less shielded in **1C** (downfield shift of ∼300 ppm) when compared with the others, probably due to the more electron-withdrawing character of the Cl−C^C* ligand.

The molecular structures of **1B** and **1C** were determined by single-crystal X-ray diffraction (Figures 1 and S7). In both the

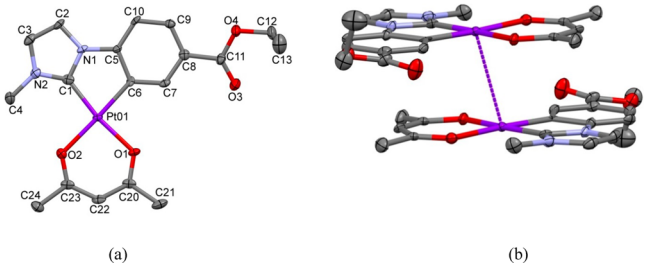

(a) (b)

Figure 1. (a) Molecular structure of **1B**. Selected bond lengths (Å) and angles (deg): Pt01−C(1) 1.945(6); Pt01−C(6) 1.976(5); Pt01−O(1) 2.046(4); Pt01−O(2) 2.075(4); C(1)−Pt01−C(6) 80.4(2); O(1)−Pt01−O(2) 91.39(16); C(1)−Pt01−O(2) 97.1(2); C(6)−Pt01−O(1) 90.98(19). (b) Dimer-like stacking view of **1B** (d Pt−Pt = 3.370 Å). Thermal ellipsoids are drawn at the 50% probability level. Hydrogen atoms have been omitted for clarity.

two complexes, the platinum(II) center exhibits a distorted square-planar environment due to the small bite angle of the NHC cyclometalated ligand (C^C*) [ca. 80.0°]. A chelate diketonate ligand, with the O−Pt−O angle close to 90°, completes the coordination sphere of Pt(II). The Pt−C* bond length [1.945(6) **1B**, 1.946(3) Å **1C**] is shorter than the Pt−C_{Ph} one [1.976(5) Å **1B**, 2.015(3) Å **1C**], as usual in compounds with cyclometalated NHCs groups.[25,26,29,31−35] Also, the Pt−O distances are similar to those found in related complexes.[26,27] In the solid state, complex **1B** arranges together in pairs, in a head-to-tail fashion through intermolecular Pt···Pt (3.370 Å) and $\pi-\pi$ (∼3.43 Å) interactions between the NHC ligand and the acac (see Figure 1b).[26] However, in **1C**, neither Pt···Pt nor $\pi\cdots\pi$ intermolecular interactions were observed in the crystal, but C−H···Cl short contacts, as can be seen in Supporting Information (Figure S8).

Synthesis and Characterization of the Clusters [{Pt(R-C^C*)acac}$_2$Tl](PF$_6$) (R = CN 2A, CO$_2$Et 2B, Cl 2C). Treatment of the β-diketonate compounds [Pt(R-C^C*)(acac)] (R = CN **1A**, CO_2Et **1B**, Cl **1C**) with $TlPF_6$ (2:1 molar ratio) in CH_2Cl_2/acetone led to the clusters [{Pt(R-C^C*)(acac)}$_2$Tl]-PF_6 (R = CN **2A**, CO_2Et **2B**, Cl **2C**), which were obtained as analytical pure solids in good yield and characterized by ^{1}H NMR, IR, mass spectrometry (see Experimental Section, Scheme 1 (path b) and Supporting Information) and X-ray crystallography. Their MALDI(+) spectra show the molecular peaks associated with [{Pt(R-C^C*)(acac)}$_2$Tl]$^+$ and [Pt(R-C^C*)-(acac)Tl]$^+$, which might suggest the integrity of the trimetallic species. However, in solution at room and low (−80 °C) temperatures, the ^{1}H and ^{195}Pt{^{1}H} NMR spectra of **2A**−**2C** fit those of their corresponding starting materials (see ^{195}Pt{^{1}H} NMR spectra of **2A** in Figure S9), indicating the breakdown of the Pt−Tl bonds. The photophysical data (see below) of all of these compounds were investigated and are in agreement with the rupture of the Pt−Tl bonds in solution.

The X-ray crystal structures of **2A**, **2B**, and **2C** were performed on single crystals obtained from solutions of them in acetone (**2A**, **2B**) or CH_2Cl_2 (**2C**) (Table 1 and Figures 2−4). As can be seen, compounds **2A**−**2C** show a "Pt_2Tl" sandwich structure,

Table 1. Selected Bond Lengths (Å) and Angles (deg) for Complexes 2A−2C

	2A	2B	2C
Pt(1A)−C(1A)	1.947(5)	1.953(9)	1.958(5)
Pt(1A)−C(6A)	1.979(5)	1.994(8)	2.023(4)
Pt(1A)−O(1A)	2.050(3)	2.059(5)	2.042(3)
Pt(1A)−O(2A)	2.069(4)	2.073(6)	2.051(4)
Pt(1B)−C(1B)	1.939(5)	1.956(8)	1.951(4)
Pt(1B)−C(6B)	1.988(5)	1.993(8)	2.010(4)
Pt(1B)−O(1B)	2.058(3)	2.069(6)	2.052(3)
Pt(1B)−O(2B)	2.075(3)	2.063(6)	2.054(3)
Pt(1A)−Tl	3.2164(3)	3.0758(4)	3.0230(2)
Pt(1B)−Tl	3.0499(3)	2.9431(4)	2.9962(2)
Tl−E	2.8970(51) (E = N3A)	2.7715(67) (E = O3A)	3.3237(1) (E = Cl1A)
Tl−E′	2.9942(48) (E′ = N3B)	2.8419(77) (E′ = O3B)	3.5717(4) (E′ = Cl1B)
Tl−E″	2.7692(42) (E″ = O3)		3.0633(4) (E″ = F4)
Tl−E‴			3.497(4) (E‴ = Cl4)
Pt(1A)···Pt(1A′)	3.340(1)	3.401(1)	
Pt(1B)···Pt(1B′)	3.310(1)	3.240(1)	
Pt(1A)−Tl-Pt(1B)	169.813(9)	144.512(18)	119.475(8)
C(1A)−Pt(1A)−C(6A)	80.0(2)	80.2(3)	80.04(19)
O(1A)−Pt(2A)−O(2A)	90.20(14)	90.5(2)	89.34(15)
C(1B)−Pt(1B)−C(6B)	79.8(2)	80.6(3)	80.07(18)
O(1B)−Pt(2B)−O(2B)	91.04(13)	91.2(2)	89.09(13)

where two slightly distorted square planar "Pt(R-C^C*)(acac)" subunits are bonded to a Tl(I) center through Pt−Tl bonds. In each complex, the two Pt → Tl bonds exhibit intermetallic distances slightly different from one to another (3.0499(3) Å, 3.2164(3) Å **2A**; 2.9431(4) Å, 3.0758(3) Å **2B**; 2.9962(2) Å, 3.0230(2) Å **2C**), but all of them are in the range of those observed in complexes containing Pt(II)−Tl(I) donor−acceptor bonds with no bridging ligands between the metal centers.[10]

In the case of **2A** and **2B**, the Pt−Tl vectors are almost perpendicular to the Pt coordination planes (angles with the normal: 18.9(1)° Pt1A, 5.7(1)° Pt1B, **2A**; 11.4(2)° Pt1A, 10.8(1)° Pt1B, **2B**), which reveal an almost square pyramidal environment around the platinum center with the thallium atom being located on the apical position shared by both the two pyramids with a Pt−Tl−Pt angle of 169.813(9)° **2A** and 144.512(18)° **2B**.

In these compounds the platinum coordination planes are almost parallel (interplanar angle: 14.8(1)° **2A**, 34.8(2)° **2B**) but lie somewhat staggered [torsion angle O1A−Pt1A−Pt1B−O1B: 40.6° **2A**, 90.7° **2B**]. In the case of **2A** an additional acetone molecule interacts with the Tl(I) center through a weak Tl−O bond (2.7692(42) Å). The Tl−O separation is comparable to those in other complexes[10,15,19,36] but significantly longer than the sum of the covalent radii (2.21 Å).[23]

The trinuclear "Pt_2Tl" units rearrange in the crystal generating two-dimensional (2D) networks through additional stabilizing contacts. On one hand, the "Pt_2Tl" units stack through intermolecular Pt···Pt (3.340 Å, 3.310 Å **2A**; 3.401 Å, 3.240 Å **2B**) interactions[37−43] and weak $\pi-\pi$ contacts between the NHC and the acac ligands[26] (the shortest atomic separation between two neighboring units is 3.467 Å **2A**; 3.429 Å **2B**, see Figures 2b and 3b), giving rise to almost linear PtB−Tl−PtA··PtA−Tl−PtB···PtB wires in **2A** [angles: PtB−Tl−PtA: 169.813°, Tl−PtA··PtA: 158.77°, Tl−PtB···PtB: 165.32°] and zigzag chains in **2B**

DOI: 10.1021/acs.cgd.7b00662
Cryst. Growth Des. 2017, 17, 4336−4346

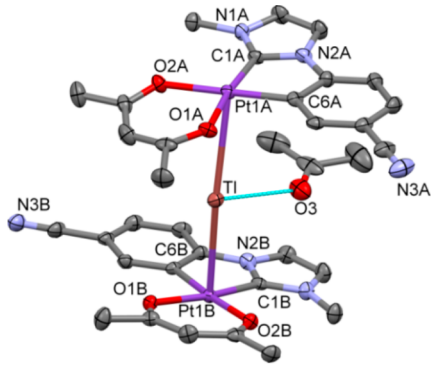

(a)

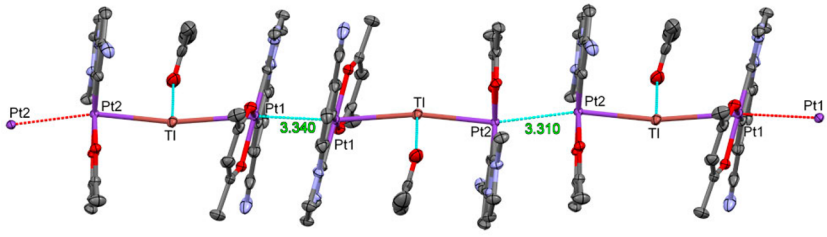

(b)

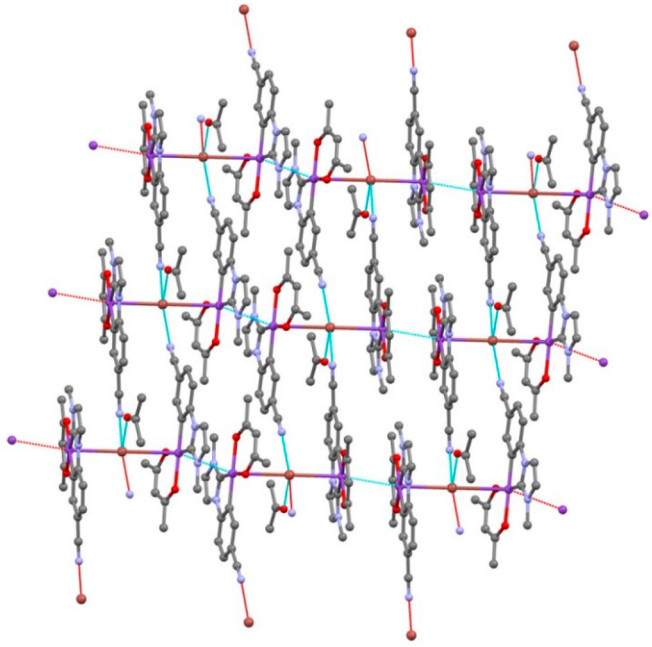

(c)

Figure 2. (a) Molecular structure of **2A**. Thermal ellipsoids are drawn at the 50% probability level. Hydrogen atoms and PF_6 have been omitted for clarity. (b, c) Supramolecular structure views.

[angles: PtB−Tl−PtA: 145.512°, Tl−PtA··PtA: 177.80°, Tl−PtB···PtB: 160.07°]. These chains appear linked together through two additional Tl−E (E′) (E, E′ = N **2A**, O **2B**) bonds with the R substituents of the R−C^C* groups (R= CN **2A**, CO_2Et **2B**) belonging to the two adjacent chains (see Figures 2c and 3c). The Tl−N (NC-C^C*) and Tl−O (CO_2Et-C^C*) distances are longer than expected for covalent bonds but shorter than the sum of the covalent radii of Tl^I (1.55 Å) and the van der Waals radii of N (1.55 Å) and O (1.52 Å).[44] The Tl···N separations are comparable to those found in derivatives

DOI: 10.1021/acs.cgd.7b00662
Cryst. Growth Des. 2017, 17, 4336−4346

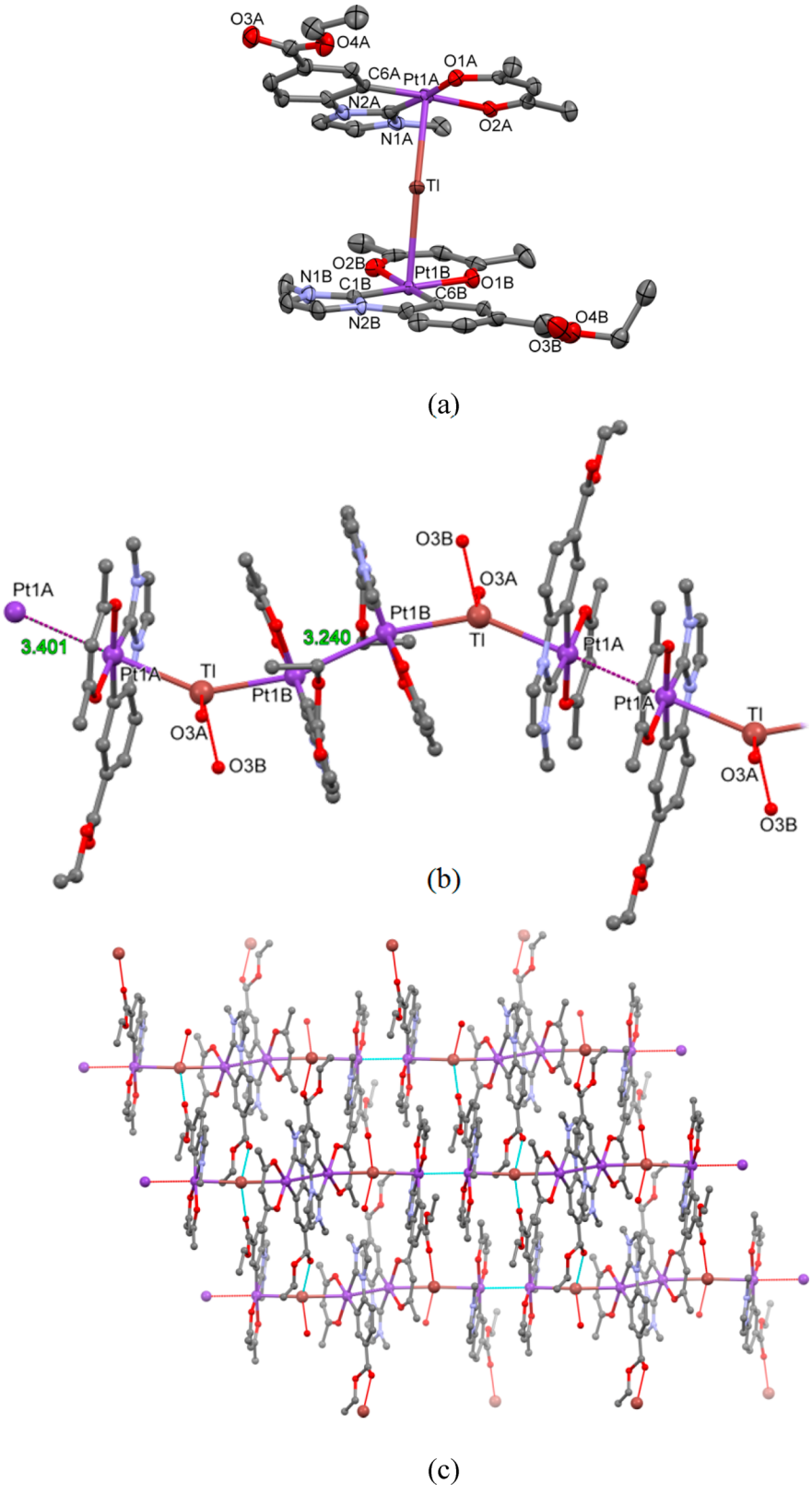

Figure 3. (a) Molecular structure of **2B**. Thermal ellipsoids are drawn at the 50% probability level. Hydrogen atoms and PF_6 have been omitted for clarity. (b and c) Supramolecular structure views.

containing Tl···N interactions, such as $[PtTl(C^N)(CN)_2]$-(C^N = 7,8-benzoquinolinate (bzq), 2-phenylpyridinate (ppy)) or $[\{PtTl(bzq)(CC\text{-}C_5H_4N\text{-}2)_2\}_2]$[13] and [*trans*,*trans*,*trans*-$Tl_2\{Pt(C_6F_5)_2(CN)_2\}$ $(CH_3COCH_3)_2]_n$.[19] Then, the five-coordinated Tl(I) center in **2A** is located in the middle of the base of a square-pyramid with bond angles around the Tl(I) center close to 90° [angles: Pt1A−Tl−N3B: 92.0°, Pt1B−Tl−N3B: 95.0°, Pt1A−Tl−N3A: 81.2°, Pt1B−Tl−N3A: 93.3°, O3−

DOI: 10.1021/acs.cgd.7b00662
Cryst. Growth Des. 2017, 17, 4336−4346

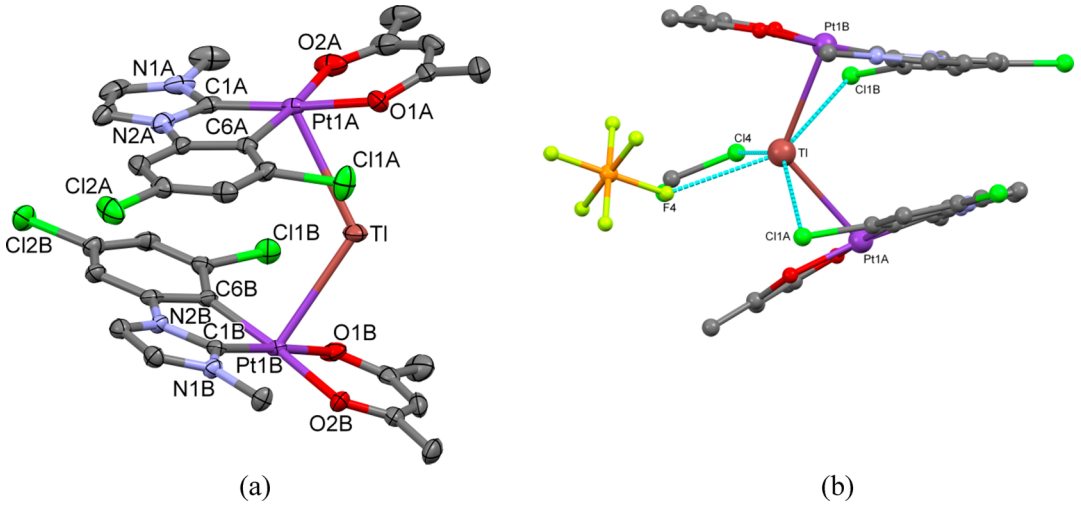

Figure 4. (a) Molecular structure of **2C**. Thermal ellipsoids are drawn at the 50% probability level. Hydrogen atoms have been omitted for clarity. (b) Structure view of the Tl···E interactions.

Tl−N3B: 89.5°, O3−Tl−N3A: 101.6°, Pt1A−Tl−O3: 86.2°, Pt1B−Tl−O3:86.5°]. Single crystals of **2B** were also obtained from an acetone solution; however in this case the Tl(I) center does not coordinate any acetone molecule and exhibits a distorted tetrahedral coordination environment [angles: Pt1A−Tl−O3A: 108.5.0°, Pt1A−Tl−O3B: 110.8°, Pt1B−Tl−O3A: 93.1°, Pt1B−Tl−O3B: 87.8°, O3A−Tl−O3B: 107.6°].

Compound **2C**, unlike **2A** and **2B**, is a discrete molecule and not a 2D lattice, because of the absence of intermolecular or packing interactions (see Figure S10). In compound **2C**, the Tl(I) in addition to the two Pt−Tl bonds (*d* Pt−Tl: 3.0230(2) Å, 2.9962(2) Å; Pt−Tl−Pt: 119.475(8)°) establishes two intramolecular Tl···Cl contacts (*d* Tl···Cl = 3.3237(1) and 3.5717(4) Å), one with each of the "Pt(Cl−C^C*)(acac)" fragments, a Tl···F contact (*d* Tl···F = 3.063 Å) with the anion and a Tl···Cl contact (*d* Tl··Cl = 3.497 Å) with a CH_2Cl_2 molecule, to complete a distorted octahedral coordination environment (Figure 4b). All the Tl−E (E = Cl, F) distances are rather long, but lower than the sum of the van der Waals radii of Tl(I) (1.96 Å), and F (1.47 Å) or Cl (1.75 Å).[44] In this molecule, the Pt−Tl vectors are further away from the perpendicular to the Pt coordination planes (angles: 25.2(1)° Pt1A, 19.6(1)° Pt1B) than in compounds **2A** and **2B**, and the angle Pt−Tl−Pt (119.475(8)°) is far away from the ones observed in **2A** and **2B**, probably forced by the existence of the two intramolecular Tl···Cl contacts.

It should be noted that in **1B**, the molecules arrange themselves in dimers through Pt···Pt interactions, not giving rise to 1D wires, as observed in **2B** and **2A**. Presumably, the Pt−Tl donor−acceptor bond decreases the electron density on the platinum, playing a similar role to that of π-acceptor ligands, thereby reducing electronic repulsions between the Pt centers and favoring the 1D chain formation through Pt···Pt interactions.[45−47]

Photophysical Properties of Compounds [Pt(R-C^C*)(acac)] (R = CN 1A, CO_2Et 1B, Cl 1C) and the Corresponding Clusters [{Pt(R-C^C*)(acac)}$_2$Tl]PF_6 (2A−2C). The photophysical properties of **1A** were previously described by Da Como et al.,[48] but we have included them in this discussion with comparative purposes.

Absorption Spectra. UV−vis spectroscopic data of compounds **1A−1C** and **2A−2C** have been listed in Table S1. The spectra of **1A−1C** in solution of CH_2Cl_2 (see Figure S11) display low intensity absorptions ($\varepsilon > 10^3$ M^{-1} cm^{-1}) at low energies ($\lambda > 290$ nm). In the case of **1C**, they appear clearly shifted to higher energies with respect to those of **1A** and **1B**, indicating the participation and the effect of the R-C^C* (R = CN, CO_2Et, Cl) group in these absorptions. In the case of **1A**, these absorptions are very similar to those of **1B** in energy and profile, in agreement with the similar electronic features observed previously for the R-C^C* (R = CN, CO_2Et) groups.[24]

The solid-sate diffuse reflectance UV−vis spectra (Figure S12) show additional broad bands at low energy when compared with those observed in dichloromethane solution, which can be tentatively attributed to the existence of intermolecular Pt−Pt interactions, on the light of the X-ray structure of **1B** and those of other related complexes.[26]

DFT and TD-DFT calculations in solution of CH_2Cl_2 for **1B** and **1C** have been carried out to provide correct assignments for the UV−vis absorptions and also to evaluate the effect of the cyclometalated R-C^C* group (see full data and discussion in Supporting Information). Considering the composition of the frontier molecular orbitals (FOs), the calculated allowed absorptions, which are in good agreement with the experimental UV−vis spectra (Figure S14), and the origin of calculated S_1, which arises mainly from a HOMO to LUMO transition (79% **1B**, 62% **1C**), the lowest energy absorption band can be attributed basically to L′LCT [π(acac) → π^*(NHC)] transitions for **1C**, and mixed L′LCT [π(acac) → π^*(NHC)]/MLCT [5d(Pt) → π^*(NHC)] transitions for **1B**. Although S_2 arises mainly from an H-1 to LUMO transition, it is very similar in nature to S_1. Taking into account the similarities in the electronic features of the R-C^C* (R = CN, CO_2Et) groups observed in the absorption spectra of **1A** and **1B** as well as in those of other compounds reported previously,[24] the nature of the lowest energy absorptions of **1A** is expected to be quite similar in nature to those of **1B**.

The absorption spectra of complexes **2A−2C** in 2-MeTHF solutions (10^{-4} M) are all identical to those of their respective precursors, **1A−1C** (see Figure S15), which match with the rupture of the Pt−Tl bonds in solution, as deduced from their NMR spectra. Similar behavior was previously observed in related extended structures with M−Tl bonds [M(C^N)(CN)$_2$Tl] (M = Pt,[13] Pd,[26] C^N = 7,8-benzoquinolinate, 2-

DOI: 10.1021/acs.cgd.7b00662
Cryst. Growth Des. 2017, 17, 4336−4346

phenylpyridinate). The absorption spectra of powdery solid samples of **2A**–**2C** basically fit with those of the starting materials (Figure S16). In the low-energy region just **2B** displays an additional absorption with respect to its precursor, with λ_{max} at 400 nm (see Figure 5). Keeping in mind the shorter Pt–Tl and

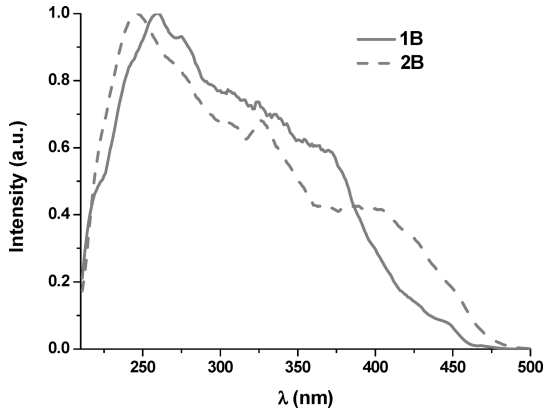

Figure 5. Normalized diffuse reflectance spectra of powdery solid samples of **1B** and **2B** at r.t.

Pt···Pt distances in the network of **2B** compared to those of **2A**, this absorption could be attributed to metal–metal-to-ligand charge transfer (^{1}MMLCT) [dσ*(Pt–Pt) → π*(NHC)] transitions likely to have been affected by the Pt–Tl bonds.

Emission Spectra. Emission data are summarized in Table 2. In diluted glassy solutions of 2-MeTHF (10^{-5} M, 77 K), compounds **1A**–**1C** show blue well resolved vibronic emissions (see Figure S17) that do not change at higher concentration (10^{-3} M, Figure S18). Their vibrational spacings [1367–1406 cm^{-1}] correspond to the C=C/C=N stretches of the cyclometalated NHC ligand (C^C*), suggesting their involvement in the excited state. The emissions of **1A** and **1B** ($\lambda_{max} \approx$ 440 nm) are red-shifted with respect to that of **1C** (λ_{max} = 417 nm), probably due to the participation of the R-substituent in the stabilization of the LUMO, as revealed by the DFT studies. Emissions and lifetime decays of **1A** and **1B** are identical to those observed in $[Pt(R\text{-}C\hat{}C^*)(py)(PPh_3)]PF_6$[24] and very similar $[Pt(R\text{-}C\hat{}C^*)(CNR')_2]PF_6$[25] which contain the same "(R-C^C*)Pt" fragments. Thus, taking into account all this and the TD-DFT calculations, the phosphorescent emissions of **1A**–**1C** can be mainly ascribed to transitions of monomeric species derived from ^{3}ILCT [(NHC)] transitions mixed with some, if any, ^{3}L′LCT [π(acac) → π*(NHC)]/^{3}MLCT [5d(Pt) → π*(NHC)] in the case of **1A** and **1B** and with ^{3}L′LCT [π(acac) → π*(NHC)] for **1C**.

Emission spectra for the 5 wt % films of complexes **1A**–**1C** in poly(methyl methacrylate) (PMMA) are wavelength dependent, as can be shown in Figure 6. Upon excitation at λ = 330 nm, all the three compounds show a phosphorescent emission in the blue to green region of the visible spectrum, like in glassy 2-MeTHF, with quantum yields up to 0.93 (**1B**), very similar to that of **1A** (0.98), while just 0.04 for **1C** (Table 2). However, upon excitation at λ > 390 nm, there is a dramatic change in the emission profiles whereby a low-energy (LE) structureless band with maxima at ca. 540 nm becomes predominant, while the HE is still observed but as a low intensity shoulder.

Intrigued by this behavior, we carried out further experiments only focused on **1A** and **1B** since **1C** is barely emissive. Therefore, their emission spectra were registered in PMMA

Table 2. Emission Data for Complexes 1A–2C

C.	medium (T/K) [wt %]	λ_{ex}/nm	λ_{em}/nm	τ/μs [λ_{max}][a]	ϕ
1A	PMMA film [5 wt %][b]	330	441, 470$_{max}$, 503, 536$_{sh}$		0.98
		390	443, 474, 535$_{max}$		0.72
	PMMA film [40 wt %][b]	330	443, 474, 535$_{max}$		0.46
	solid (298 K)	400	462$_{sh}$, 479$_{max}$, 513, 555	0.28 (77%), 0.65 (23%)	0.04
	solid (77 K)	400	451, 477, 512$_{max}$	0.78 (70%), 3.1 (30%) [451], 0.35 (55%), 1.2 (45%) [512]	
	2-Me-THF (77 K)[c]	332	439$_{max}$, 468, 500, 523$_{sh}$	17.1	
1B	PMMA film [5 wt %][b]	330	446, 474$_{max}$, 502, 536$_{sh}$		0.93
		390	452, 484$_{sh}$, 532$_{max}$		0.59
	PMMA film [40 wt %][b]	330	452, 484$_{sh}$, 532$_{max}$		0.82
	solid (298 K)	400	485$_{max}$, 519, 550	2.1 (60%), 1.0 (40%) [485], 1.5 (83%), 2.8 (17%) [519]	0.48
	solid (77 K)	400	461, 495, 554$_{max}$	2.6 [461], 3.8 [554]	
	2-Me-THF (77 K)[c]	332	442$_{max}$, 472, 502, 536$_{sh}$	16.9	
1C	PMMA film [5 wt %][b]	330	425, 450$_{max}$, 475		0.04
		400	540		0.09
	solid (298 K)	380	433, 452$_{max}$, 476, 516	3	0.07
	solid (77 K)	380	432, 456$_{max}$, 482, 515$_{sh}$	11.6	
	2-Me-THF (77 K)[c]	320	417$_{max}$, 443, 472, 500$_{sh}$	15.6	
2A	solid (298 K)	380	450, 478$_{max}$, 506	0.64 [450] 0.43(80%), 1.44 (20%) [478] 0.44 (77%), 1.8 (23%) [506]	0.17
	solid (77 K)	380	500	1.7	
	2-Me-THF (77 K)[c]	330	439$_{max}$, 469, 500, 524$_{sh}$	16.5	
2B	solid (298 K)	474	580	0.31 (67%), 1.15 (33%)	0.02
	solid (77 K)	474	561	0.95	
	2-Me-THF (77 K)[c]	332	443$_{max}$, 473, 505, 534$_{sh}$	16.7	
2C	solid (298 K)	351	425, 450$_{max}$, 480, 514	1.3 (54%), 2.4 (46%) [450] 1.8 [480], 1.9 [514]	0.10
	solid (77 K)	343	421$_{sh}$, 448$_{sh}$, 494$_{max}$	3.3 (44%), 8.6 (56%) [494]	
	2-Me-THF (77 K)[c]	320	417$_{max}$, 444, 472, 501$_{sh}$	13.2	

[a]Lifetime measured at the λ_{max}. [b]298 K. [c]10^{-5} M; at 10^{-3} M, the same emission and τ were obtained.

coated films at different weight concentrations ranging from 0.5 wt % to 40 wt %. As can be seen in Figure 7 (**1B**) and Figure S19 (**1A**), pure highly structured emissions were found at a concentration of 0.5 wt %. When increasing the weight percentage of the complex in the PMMA film, the intensity of

DOI: 10.1021/acs.cgd.7b00662
Cryst. Growth Des. 2017, 17, 4336–4346

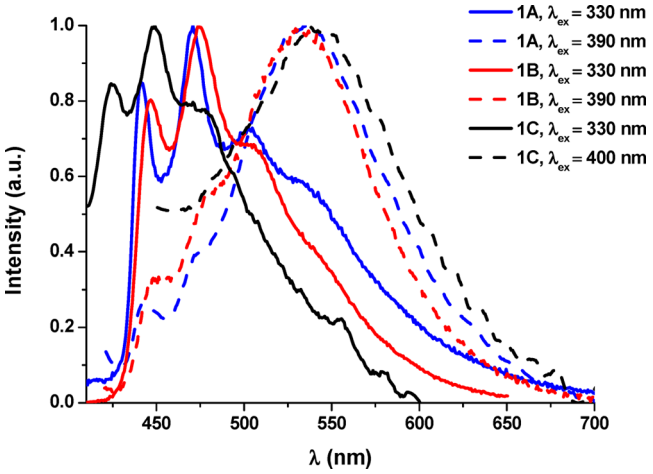

Figure 6. Normalized emission spectra of **1A**−**1C** in 5 wt % PMMA film.

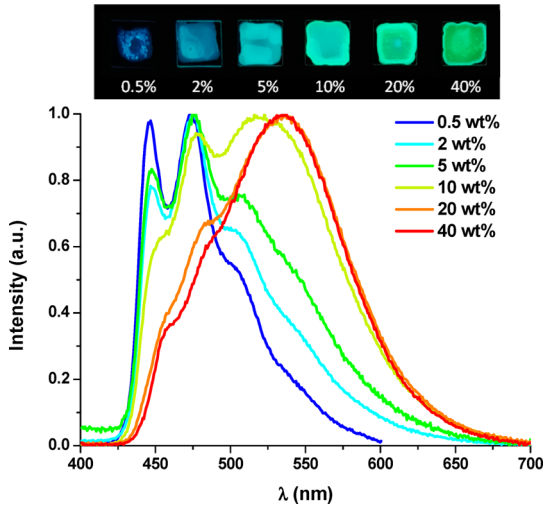

Figure 7. Normalized emission spectra of **1B** at λ_{ex} = 360 nm. Pictures under UV light (λ_{ex} = 365 nm).

the LE increases and that of the HE band decreases, resulting in a green emission as much for 20 wt % as for 40 wt % films. At 40 wt %, the green emission shows no dependence with the λ_{ex} (see Figure S20).

At 40 wt % concentration the QY values of the green emission kept fairly high for **1B** (0.82), while the emission of **1A** (QY = 0.46) became slightly self-quenched. In all likelihood, the LE bands can be attributed to metal−metal-to ligand charge transfer (^{3}MMLCT) [dσ*(Pt−Pt) → π*(NHC)] transitions, generated by the existence of aggregates in the ground state through Pt−Pt interactions, as observed in the X-ray structure of **1B**. The excimeric nature of this LE emission is discarded since the excitation spectrum of **1B** in PMMA film at 40 wt % is very similar to that obtained for the solid state one (see Figure S21). Therefore, the dual emission observed in PMMA films of **1A**−**1C** is likely due to a relatively slow internal conversion between the two emissive states ^{3}ILCT(NHC)/^{3}MMLCT at 298 K.[11]

In the solid state, powdery samples of **1A**−**1C** display bright blue and greenish blue emissions ($\lambda_{max} \approx$ 480 nm for **1A** and **1B**; λ_{max}= 452 nm for **1C**) with the emission of compound **1C** located further into the blue region of the spectrum than the others (Figure S22). Upon cooling to 77 K, the emission of **1C** appears a bit more structured and with a longer lifetime, being quite similar to the one obtained in 2-MeTHF solution (Figure 8).

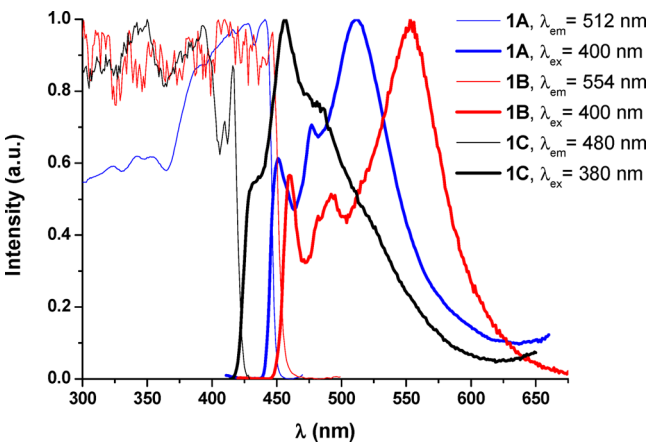

Figure 8. Normalized excitation (−) and emission (—) spectra of **1A**−**1C** in solid state at 77 K.

However, both **1A** and **1B** (see Figure 8), regardless the excitation wavelength (350 to 450 nm), display broad bands with λ_{max} = 512 and 554 nm, respectively, accompanied by high energy (HE) structured emissions at 451 (**1A**) and 461 (**1B**) nm. These HE bands resemble to those obtained in PMMA films with a low doping concentration (<5 wt %) and in solution of 2-MeTHF. Likewise, the LE bands of **1A** (512 nm) and **1B** (554 nm) are closely related to those obtained in PMMA films (>10 wt % and λ_{ex} >360 nm). Therefore, these dual emissions (HE and LE bands) may come from the excited states discussed above (^{3}ILCT [(NHC)] and ^{3}MMLCT, respectively).

The emissive behavior of the Pt_2Tl clusters, **2A**−**2C**, was investigated to compare it with that of **1A**−**1C**. As expected, in glassy solutions of 2-MeTHF compounds **2A**−**2C** give the same emission bands and lifetime decays than **1A**−**1C** either at diluted (10^{-5} M) or concentrated solutions (10^{-3} M), which once again, evidence the rupture of the M−Tl bonds in solution even at 77 K (Figure S23). Emission spectra of **2A**−**2C** in 5 wt % PMMA films closely resemble those of their corresponding precursors, **1A**−**1C** (see Figure S24), which pointed us to consider that in PMMA films the Pt−Tl bonds, if present, are negligible.

In solid state at room temperature, the Pt_2Tl complexes display vibronic bands like their corresponding starting materials except **2B**, which shows a structureless broad band considerably shifted to lower energies (Figures 9 and 10), in line with the features observed in the absorption spectra of powdery samples of them (Figures 5 and S16). At 77 K the emission of **2B** becomes a narrow unstructured band at 561 nm (Figure 9).

Considering that the excitation spectra match the absorption one, the short lifetime decay and the X-ray structure, the emission of **2B** could be mainly attributed to ^{3}MMLCT [dσ*(Pt−Pt) → π*(NHC)] transitions somewhat disturbed by the Pt−Tl bonds.

Upon cooling to 77 K the emission profile of **2A** retains a minor contribution of the HE band but displays a predominant unstructured LE emission band at ca. 500 nm (Figure 10). This LE band appears just slightly blue-shifted with respect to the LE band of **1A**, but it shows similar lifetime and excitation spectra, so the same ^{3}MMLCT nature can be presumed for it. It should be stressed that even though the crystal structures obtained for **2A** and **2B** show similar 2D networks, in **2A**, the presence of an

DOI: 10.1021/acs.cgd.7b00662
Cryst. Growth Des. 2017, 17, 4336−4346

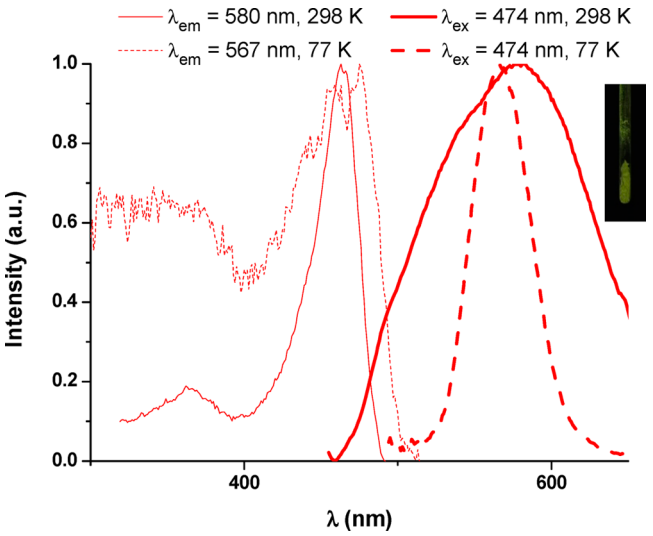

Figure 9. Normalized excitation (−) and emission (—) spectra of **2B** in the solid state. Picture under UV light (λ_{ex} = 365 nm) at 298 K.

extended metallic [Pt−Pt−Tl−Pt−Pt−] chain is not reflected in its absorption or emissive properties at room temperature (see Figure S25). However, at 77 K the emission of **2A** also depends on the intermolecular Pt···Pt interactions.

For **2C**, consisting of Pt_2Tl discrete molecules, the emission profile and its biexponential decay differ from those of the starting complex as much at 298 K as at 77 K, indicating that it is affected by the Pt−Tl bonds. At 77 K the mayor LE band appears slightly red-shifted in relation to those of other trinuclear derivatives $(NBu_4)_3[\{Pt(C_6F_5)_4\}_2Tl]$ (450 nm, 298 K; 445 nm, 77 K),[16] $[Tl_2Pt(CN)_4]$ (448 nm),[12] which were attributed to a metal-centered phosphorescence process [Pt(5dz^2) → Tl(6pz)] (^{3}MM′CT) within the trinuclear entity. The observed shift in **2C** might be attributed to the contribution of the planar and low-lying C^C* and acac ligands to the frontier orbitals, which likely reduces the gap of the transition, more than to the existence of stronger Pt−Tl bonds, as deduced by comparing intermetallic distances (2.9962(2), 3.0230(2) Å, **2C** − vs 2.9777(4), 3.0434(4) Å $[\{Pt(C_6F_5)_4\}_2Tl]_3$,]). Therefore, the emission can be tentatively ascribed to charge transfer from the platinum fragments to the thallium [^{3}(L+L′)MM′CT],[10] with some contribution of ^{3}MM′LCT/^{3}IL [d/sσ*(Pt−Tl) → π*(C^C*)] excited states. For powdery samples of **2C** at 77 K the existence of close excited states generated by small differences in the molecular arrangement cannot be excluded, which could explain the huge width of the emission band.

CONCLUSIONS

The new cyclometalated NHC compound $[\{Pt(\mu\text{-}Cl)(R\text{-}C^C^*)\}_2]$ (R = Cl, **C**) was successfully prepared following our stepwise protocol. From **C** and the related ones **A** (R = CN) and **B** (R = CO_2Et) the mononuclear complexes [Pt(R-C^C*)-(acac)] (R = CN **1A**, CO_2Et **1B**, Cl **1C**) were obtained. They reacted with $TlPF_6$ in a 2:1 molar ratio to give the corresponding hetero-trinuclear cluster $[\{Pt(R\text{-}C^C^*)(acac)\}_2Tl]^+$ (**2A**, **2B**, **2C**) which are held together by donor−acceptor Pt−Tl bonds, confirming the ability of this kind of Pt(II) complex to act as a Lewis base for this kind of interaction. These metal−metal bonds present in the solid state break down in solution even at low temperatures (−80 °C).

The crystallographic, spectroscopic, and photophysical study of **1A**−**1C** and their corresponding Pt_2Tl clusters discovered that electron withdrawing substituents, such as CN and CO_2Et, in the 4-position of the cyclometalated ring confer very high PLQY to the mononuclear complexes and enable the Pt_2Tl clusters to self-assemble in a 2D extended lattice through intermolecular Pt−Pt, π−π, Tl−N, or Tl−O interactions. By contrast, the presence of two Cl substituents in positions 3 and 5 of the cyclometalated ring severely reduces the emission efficiency of the mononuclear **1C** compared to those of **1A** and **1B** and also leads to a discrete Pt_2Tl cluster (**2C**) because it allows the Tl center to satisfy its electronic demand through intramolecular Tl−Cl contacts.

Complexes **1A** and **1B** show in 5 wt % films in PMMA dual emissions, blue (HE) and green-yellow (LE) bands, attributed to ^{3}ILCT and ^{3}MMLCT excited states, respectively. By controlling the excitation wavelength and the concentration of the complex

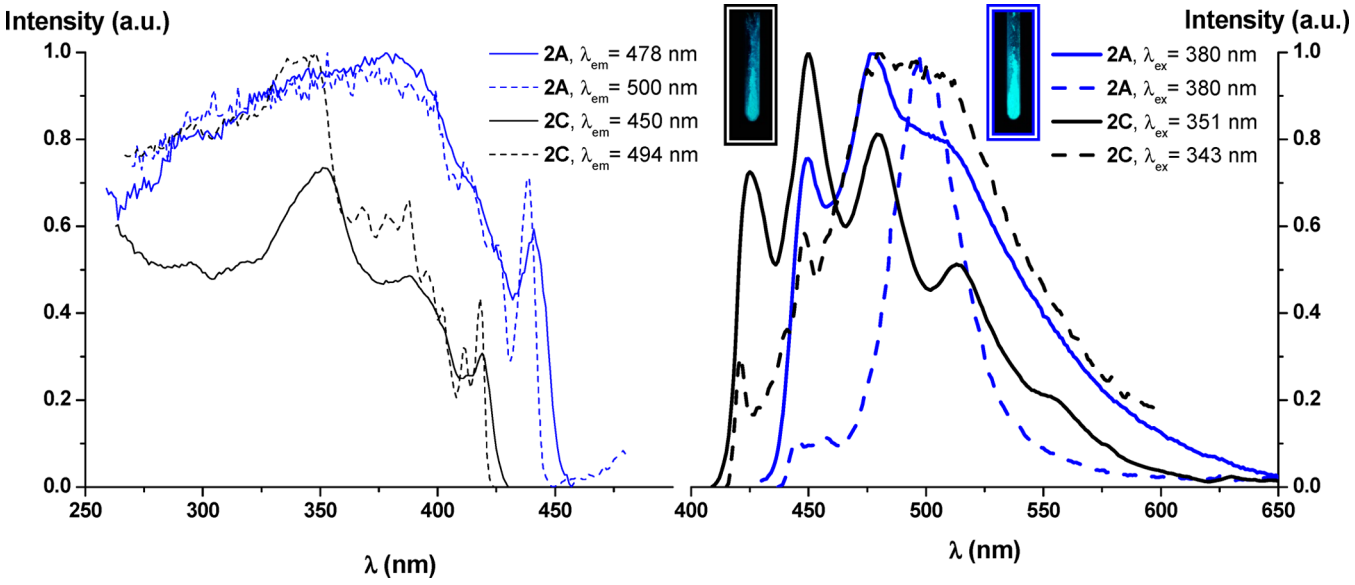

Figure 10. Normalized excitation (right) and emission (left) spectra of **2A** and **2C** in the solid state at 298 K (−) and 77 K (---). Pictures under UV light (λ_{ex} = 365 nm) at 298 K.

DOI: 10.1021/acs.cgd.7b00662
Cryst. Growth Des. 2017, 17, 4336−4346

in the film the blue or green emissions could be finely tuned with very high PLQY (0.98−0.72). The inclusion of Tl into these systems does not improve the quantum efficiency; instead, the emission of **2B** resulted to be quenched because of the existence of weakly emissive ^{3}MMLCT [dσ*(Pt−Pt) → π*(NHC)] excited states, due to the strong Pt···Pt interactions in the extended metallic [Pt−Pt−Tl−Pt−Pt−] chain.

■ ASSOCIATED CONTENT

Supporting Information

The Supporting Information is available free of charge on the ACS Publications website at DOI: 10.1021/acs.cgd.7b00662.

General procedures and instrumentation, crystallographic and computational details; spectroscopic data, NMR spectra; X-ray crystallographic data and structures; UV−vis data and figures; DFT and TD-DFT calculations and emission spectra (PDF)

Accession Codes

CCDC 1541863−1541867 contain the supplementary crystallographic data for this paper. These data can be obtained free of charge via www.ccdc.cam.ac.uk/data_request/cif, or by emailing data_request@ccdc.cam.ac.uk, or by contacting The Cambridge Crystallographic Data Centre, 12 Union Road, Cambridge CB2 1EZ, UK; fax: +44 1223 336033.

■ AUTHOR INFORMATION

Corresponding Author

*E-mail: sicilia@unizar.es.

ORCID

Antonio Martín: 0000-0002-4808-574X

Violeta Sicilia: 0000-0002-0257-0483

Notes

The authors declare no competing financial interest.

■ ACKNOWLEDGMENTS

This work was supported by the Spanish Ministerio de Economía y Competitividad (MINECO)/FEDER (Project CTQ2015-67461-P led by Dr. Babil Menjón) and the Departamento de Industria e Innovación del Gobierno de Aragón and Fondo Social Europeo (Grupo Consolidado E21: Química Inorgánica y de los Compuestos Organometálicos led by Dr. José M. Casas). The authors thank the Centro de Supercomputación de Galicia (CESGA) for generous allocation of computational resources. A.C. acknowledges the support of a FPI grant from the Spanish government.

■ DEDICATION

This paper is dedicated to Prof. Dr. Juan Forniés on the occasion of his 70th birthday.

■ REFERENCES

(1) Collman, J. P.; Hegedus, L. S.; Norton, J. R.; Finke, R. G. *Principles and Applications of Organotransition Metal Chemistry*; University Science Books: Mill Valley, CA, 1987.

(2) Crabtree, R. H. *Organometallic Chemistry of the Transition Metals*, 3rd ed.; John Wiley & Sons: New York, 2001.

(3) Atwood, J. D. *Inorganic and Organometallic Reaction Mechanisms*, 2nd ed.; Wiley-VCH: Weinheim, 1997.

(4) Sculfort, S.; Braunstein, P. *Chem. Soc. Rev.* **2011**, *40*, 2741−2760.

(5) Moret, M.-E. *Top. Organomet. Chem.* **2011**, *35*, 157−184.

(6) Braunstein, P.; Oro, L. A.; Raithby, P. R., Eds. *Metal Clusters in Chemistry*; Wiley-VCH Verlag GmbH: Weinheim, Germany, 1999; *Vol 3*.

(7) Bauer, J.; Braunschweig, H.; Dewhurst, R. D. *Chem. Rev.* **2012**, *112*, 4329−4346.

(8) Diez, A.; Lalinde, E.; Moreno, M. T. *Coord. Chem. Rev.* **2011**, *255*, 2426−2447.

(9) Baya, M.; Belío, U.; Fernández, I.; Fuertes, S.; Martín, A. *Angew. Chem., Int. Ed.* **2016**, *55*, 6978−6982 and references therein.

(10) Forniés, J.; Giménez, N.; Ibáñez, S.; Lalinde, E.; Martín, A.; Moreno, M. T. *Inorg. Chem.* **2015**, *54*, 4351−4363 and references therein.

(11) Berenguer, J. R.; Lalinde, E.; Martín, A.; Moreno, M. T.; Sánchez, S.; Shahsavari, H. R. *Inorg. Chem.* **2016**, *55*, 7866−7878.

(12) Nagle, J. K.; Balch, A. L.; Olmstead, M. M. *J. Am. Chem. Soc.* **1988**, *110*, 319−321.

(13) Forniés, J.; Fuertes, S.; Martín, A.; Sicilia, V.; Gil, B.; Lalinde, E. *Dalton Trans.* **2009**, 2224−2234.

(14) Usón, R.; Forniés, J.; Tomás, M.; Garde, R.; Merino, R. I. *Inorg. Chem.* **1997**, *36*, 1383−1387.

(15) Jamali, S.; Ghazfar, R.; Lalinde, E.; Jamshidi, Z.; Samouei, H.; Shahsavari, H. R.; Moreno, M. T.; Escudero-Adán, E.; Benet-Buchholz, J.; Milic, D. *Dalton Trans.* **2014**, *43*, 1105−1116.

(16) Falvello, L. R.; Forniés, J.; Garde, R.; García, A.; Lalinde, E.; Moreno, M. T.; Steiner, A.; Tomás, M.; Usón, I. *Inorg. Chem.* **2006**, *45*, 2543−2552.

(17) Charmant, J. P. H.; Forniés, J.; Gómez, J.; Lalinde, E.; Merino, R. I.; Moreno, M. T.; Orpen, A. G. *Organometallics* **2003**, *22*, 652−656.

(18) Berenguer, J. R.; Fernández, J.; Lalinde, E.; Sánchez, S. *Chem. Commun.* **2012**, *48*, 6384−6386.

(19) Forniés, J.; García, A.; Lalinde, E.; Moreno, M. T. *Inorg. Chem.* **2008**, *47*, 3651−3660.

(20) Belío, U.; Fuertes, S.; Martín, A. *Dalton Trans.* **2014**, *43*, 10828−10843.

(21) Berenguer, J. R.; Forniés, J.; Gil, B.; Lalinde, E. *Chem. - Eur. J.* **2006**, *12*, 785−795.

(22) Berenguer, J. R.; Forniés, J.; Gómez, J.; Lalinde, E.; Moreno, M. T. *Organometallics* **2001**, *20*, 4847−4851.

(23) Chen, W.; Liu, F.; Xu, D.; Matsumoto, K.; Kishi, S.; Kato, M. *Inorg. Chem.* **2006**, *45*, 5552−5560.

(24) Fuertes, S.; Chueca, A.; Arnal, L.; Martín, A.; Botta, C.; Giovanella, U.; Sicilia, V. *Inorg. Chem.* **2017**, *56*, 4829−4839.

(25) Fuertes, S.; Chueca, A. J.; Perálvarez, M.; Borja, P.; Torrell, M.; Carreras, J.; Sicilia, V. *ACS Appl. Mater. Interfaces* **2016**, *8*, 16160−16169.

(26) Fuertes, S.; Garcia, H.; Peralvarez, M.; Hertog, W.; Carreras, J.; Sicilia, V. *Chem. - Eur. J.* **2015**, *21*, 1620−1631.

(27) Leopold, H.; Heinemeyer, U.; Wagenblast, G.; Münster, I.; Strassner, T. *Chem.—Eur. J.* **2016**, *22*, 1−12.

(28) Zhang, X.; Cao, B.; Valente, E. J.; Hollis, T. K. *Organometallics* **2013**, *32*, 752−761.

(29) Fuertes, S.; Chueca, A. J.; Sicilia, V. *Inorg. Chem.* **2015**, *54*, 9885−9895.

(30) Schildknecht, C.; Ginev, G.; Kammoun, A.; Riedl, T.; Kowalsky, W.; Johannes, H.-H.; Lennartz, C.; Kahle, K.; Egen, M.; Geßner, T.; Bold, M.; Nord, S.; Erk, P., Novel deep-blue emitting phosphorescent emitter. *Proc. SPIE*; doi:59370E **2005**, *5937*.

(31) Tronnier, A.; Metz, S.; Wagenblast, G.; Münster, I.; Strassner, T. *Dalton Trans.* **2014**, *43*, 3297−3305.

(32) Tronnier, A.; Nischan, N.; Metz, S.; Wagenblast, G.; Münster, I.; Strassner, T. *Eur. J. Inorg. Chem.* **2014**, *2014*, 256−264.

(33) Tronnier, A.; Nischan, N.; Strassner, T. *J. Organomet. Chem.* **2013**, *730*, 37−43.

(34) Hudson, Z. M.; Blight, B. A.; Wang, S. N. *Org. Lett.* **2012**, *14*, 1700−1703.

(35) Unger, Y.; Meyer, D.; Molt, O.; Schildknecht, C.; Münster, I.; Wagenblast, G.; Strassner, T. *Angew. Chem., Int. Ed.* **2010**, *49*, 10214−10216.

DOI: 10.1021/acs.cgd.7b00662
Cryst. Growth Des. 2017, 17, 4336−4346

(36) Catalano, V. J.; Bennett, B. L.; Muratidis, S.; Noll, B. C. *J. Am. Chem. Soc.* **2001**, *123*, 173−174.
(37) Yam, V. W. W.; Wong, K. M. C.; Zhu, N. *J. Am. Chem. Soc.* **2002**, *124*, 6506−6507.
(38) Kato, M.; Kosuge, C.; Morii, K.; Ahn, J. S.; Kitagawa, H.; Mitani, T.; Matsushita, M.; Kato, T.; Yano, S.; Kimura, M. *Inorg. Chem.* **1999**, *38*, 1638−1641.
(39) Buss, C. E.; Mann, K. R. *J. Am. Chem. Soc.* **2002**, *124*, 1031−1039.
(40) Dylla, A. G.; Janzen, D. E.; Pomije, M. K.; Mann, K. R. *Organometallics* **2007**, *26*, 6243−6247.
(41) Sun, Y.; Ye, K.; Zhang, H.; Zhang, J.; Zhao, L.; Li, B.; Yang, G.; Yang, B.; Wang, Y.; Lai, S. W.; Che, C. M. *Angew. Chem., Int. Ed.* **2006**, *45*, 5610−5613.
(42) Díez, A.; Fornies, J.; Larraz, C.; Lalinde, E.; López, J. A.; Martin, A.; Moreno, M. T.; Sicilia, V. *Inorg. Chem.* **2010**, *49*, 3239−3251.
(43) Holland, L.; Shen, W.-Z.; von Grebe, P.; Sanz Miguel, P. J.; Pichierri, F.; Springer, A.; Schalley, C. A.; Lippert, B. *Dalton Trans.* **2011**, *40*, 5159−5161.
(44) Bondi, A. *J. Phys. Chem.* **1964**, *68*, 441−451.
(45) Connick, W. B.; Marsh, R. E.; Schaefer, W. P.; Gray, H. B. *Inorg. Chem.* **1997**, *36*, 913−922.
(46) Charmant, J. P. H.; Forniés, J.; Gómez, J.; Lalinde, E.; Merino, R. I.; Moreno, M. T.; Orpen, A. G. *Organometallics* **1999**, *18*, 3353−3358.
(47) Aullón, G.; Alvarez, S. *Chem. - Eur. J.* **1997**, *3*, 655−664.
(48) Haneder, S.; Da Como, E.; Feldmann, J.; Lupton, J. M.; Lennartz, C.; Erk, P.; Fuchs, E.; Molt, O.; Münster, I.; Schildknecht, C.; Wagenblast, G. *Adv. Mater.* **2008**, *20*, 3325−3330.

DOI: 10.1021/acs.cgd.7b00662
Cryst. Growth Des. 2017, 17, 4336−4346

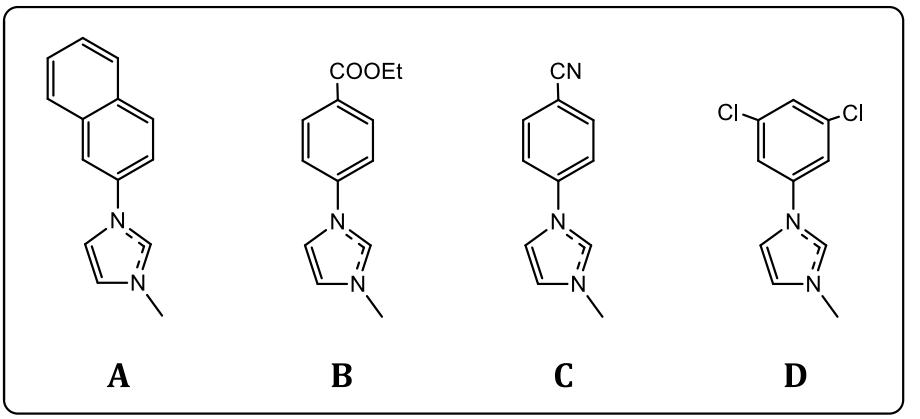

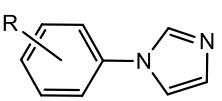

1A-D

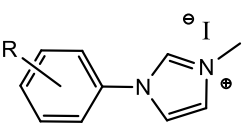

2A-D

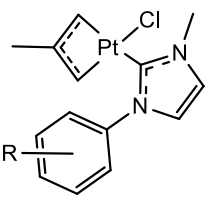

3A-D

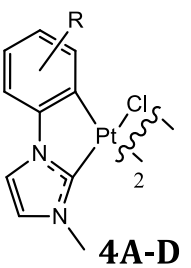

4A-D

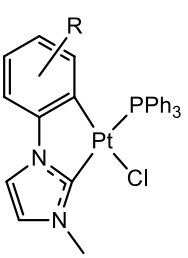

5C

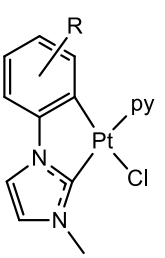

6C-*t*

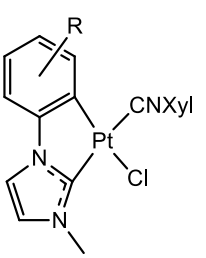

7C-*t*

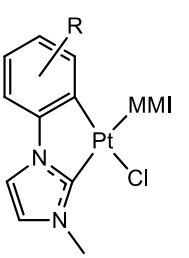

8C-*t*

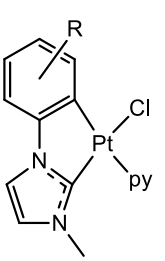

6C-*c*

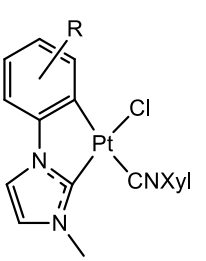

7C-*c*

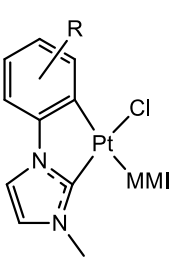

8C-*c*

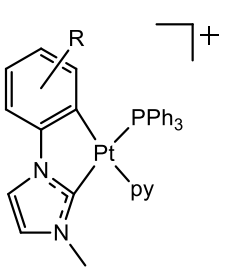

9A-C

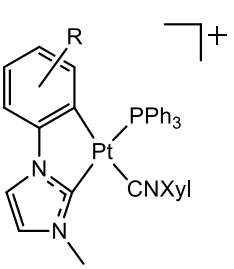

10C

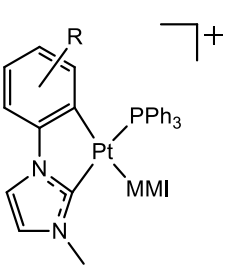

11C

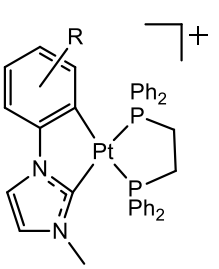

12C

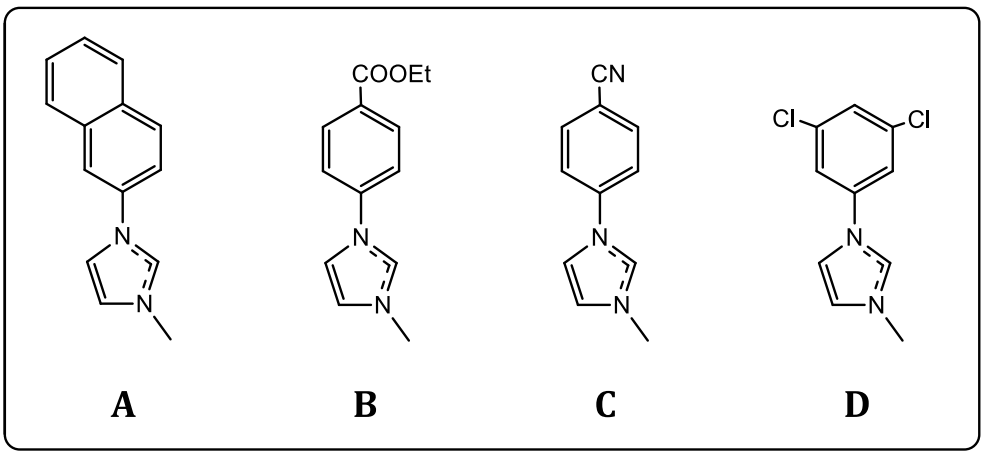

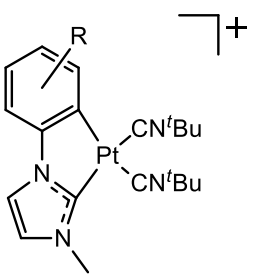

13A-C

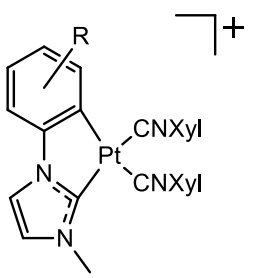

14A-C

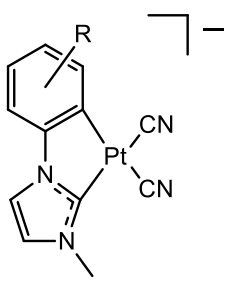

15A-D

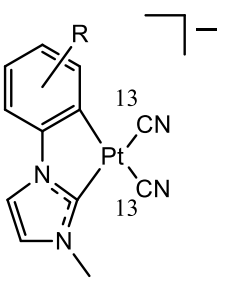

15A'-D'

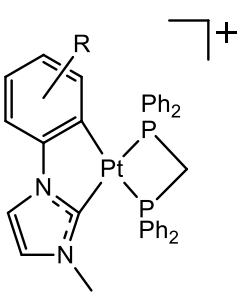

16A, C

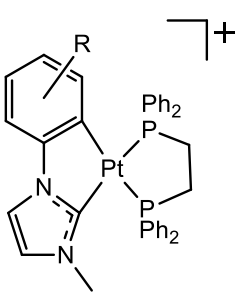

17A, C

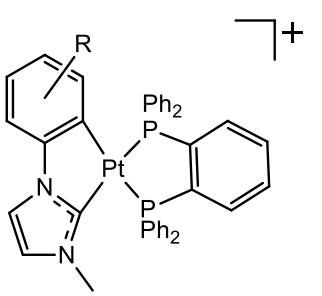

18A, C

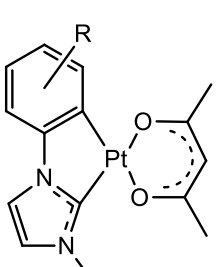

19B-D

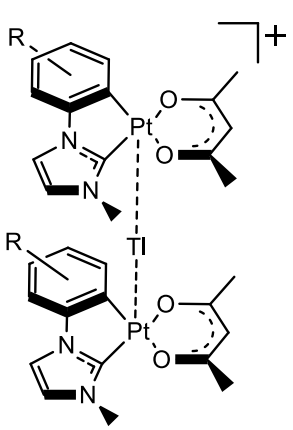

20B-D